INFORMATION TO USERS

This manuscript has been reproduced from the microfilm master. UMI films the text directly from the original or copy submitted. Thus, some thesis and dissertation copies are in typewriter face, while others may be from any type of computer printer.

The quality of this reproduction is dependent upon the quality of the copy submitted. Broken or indistinct print, colored or poor quality illustrations and photographs, print bleedthrough, substandard margins, and improper alignment can adversely affect reproduction.

In the unlikely event that the author did not send UMI a complete manuscript and there are missing pages, these will be noted. Also, if unauthorized copyright material had to be removed, a note will indicate the deletion.

Oversize materials (e.g., maps, drawings, charts) are reproduced by sectioning the original, beginning at the upper left-hand corner and continuing from left to right in equal sections with small overlaps. Each original is also photographed in one exposure and is included in reduced form at the back of the book.

Photographs included in the original manuscript have been reproduced xerographically in this copy. Higher quality 6" x 9" black and white photographic prints are available for any photographs or illustrations appearing in this copy for an additional charge. Contact UMI directly to order.

UMI

A Bell & Howell Information Company
300 North Zeeb Road, Ann Arbor MI 48106-1346 USA
313/761-4700 800/521-0600

The production of fullerenes

via

the thermal plasma dissociation of C_2Cl_4

Theodora Alexakis

Department of Chemical Engineering

McGill University

May 1997

Under the supervision of Prof. J.-L. Meunier and Dr. P.G. Tsantrizos

A thesis submitted to the Faculty of Graduate Studies and Research

in partial fulfilment of the requirements of the degree of Doctor of Philosophy

ABSTRACT

Fullerenes, the family of large, all-carbon, cage-like molecules, promise to launch an array of new products. However, the development of such products is hindered due to unavailability of large quantities of fullerenes and the present high cost of production. Fullerenes are produced commercially via the arc vaporization of graphite, a method which is limited to low production rates and low scale-up potential. In this work, a new process was developed in which fullerenes are produced via the thermal plasma dissociation of hydrocarbons. The process is attractive due to its potential for large scale fullerene production. Tetrachloroethylene (C_2Cl_4) was selected as the carbon source for fullerene synthesis, due to the instability of C-Cl bonds in the high temperature zone predicted for fullerene formation.

The effect of input electrical power, C_2Cl_4 feed rate and reactor pressure on fullerene formation and collection was studied. The temperature profile and its effect on the residence time of reactive species in the temperature zone required for fullerene formation was found to play a critical role in the production of fullerenes. With the present reactor configuration, an input power in excess of 55 kW was required for the treatment of up to 0.54 mol/min of C_2Cl_4. High C_2Cl_4 feed rates resulted in a lower conversion of C_2Cl_4 to fullerenes. Lower reactor pressures (200 and 300 torr) resulted in higher fullerene yields as compared to results obtained at 400 torr. The maximum concentration of fullerenes in soot was 5.3% and the maximum conversion of C_2Cl_4 to fullerenes was 2.8%, based on carbon input.

Fullerenes produced by the process were purified using conventional extractive

and chromatographic techniques. Although successful, purification by chromatography proved to be difficult due to the presence of perchlorinated, aromatic by-products. Some of these perchlorinated aromatic by-products were identified and were found to have structures reminiscent of fullerene precursors, and thus, may provide clues as to how fullerenes form in this plasma process.

RÉSUMÉ

Les fullerènes, famille de grosses molecules de carbone en forme de cages, est une source de toute une gamme de nouveaux produits. Malheureusement, le developement de ces produits est retardé en raison de la non-disponibilité de fullerènes en grande quantité et de leur coût de production elevé. Actuellement, les fullerènes sont produits commercialement par vaporisation du graphite à l'arc electrique, une methode qui est limitée par un taux de production tres faible et qui est difficile à rendre à grande échelle. Dans le cadre de cette thèse, un nouveau procédé a été mis au point pour produire les fullerènes par la dissociation d'hydrocarbures dans un plasma thermique. Ce procédé est avantageux grâce à son potentiel de production des fullerènes à grande échelle. Tetrachloroethylène (C_2Cl_4) a été choisi comme la source de carbone pour la production des fullerènes due à l'instabilité des liens de C-Cl dans la zone de temperature où les fullerènes devraient se former.

L'effet de la puissance électrique dans le plasma, du débit de C_2Cl_4 et de la pression du gaz sur la formation et la récupération des fullerènes a été étudié. Le profile de température dans le réacteur ayant un effet sur le temps de residence des réactifs dans la zone de température prévue pour la formation des fullerènes, joue un rôle important dans la production des fullerènes. Etant donnée la géométrie de réacteur utilisée dans ce travail, une puissance électrique de 55 kW est requise pour le traitement de 0.54 mol/min de C_2Cl_4. Les hauts débits de C_2Cl_4 donnent de faibles conversions de C_2Cl_4 en fullerènes. Les basses pressions (200 et 300 torr) donnent un taux de production de fullerènes superieur à celui obtenu à 400 torr. La concentration maximum de fullerènes dans la suie est de 5.3% et la conversion maximum de C_2Cl_4 en fullerènes est de

2.8% par rapport au carbon injecté. Les fullerènes produits par le procédé sont purifiés à l'aide de techniques chromatographiques conventionnelles. Quoique réussie, la purification par chromatographie est difficile en raison de la présence de sous-produits aromatiques chlorés. Certains de ces sous-produits ont été identifié comme ayant une structure voisine de celles des précurseurs menant à la formation des fullerènes; cette observation peut suggérer comment les fullerènes sont formés dans notre réacteur à plasma.

ACKNOWLEDGEMENTS

The undertaking of this work has not only been a challenging scientific endeavour for me, but also a fulfilment of personal achievement and growth. There are so many people that contributed to my life during this period, my family, friends and colleagues, so I will therefore limit my acknowledgements of those whose contribution was directly related to the carrying out of this work.

To Dr. Peter G. Tsantrizos, for not only giving life to the *PyroGenesis* process, but for giving me the opportunity to work on such a challenging and exciting project at PERMA under his supervision.

To Jean-Luc Meunier, my thesis supervisor for the many useful discussions, valuable advice and support.

To Prof. Youla Tsantrizos (Concordia, Dept. of Chem.), for her ongoing advice on chemistry matters and her valuable contribution to the work.

To Jean-François Bilodeau, for developing a very useful mathematical model of the *PyroGenesis* reactor.

To Irina Grigore and Jacques Potvin, at PERMA, who made working on this project a thrill. (We made a great team!) My thanks also goes out to Jocelyn Remillard for designing such an "inspiring" reactor, to Platon Manoliadis for his "toy-making" skills and valuable discussions, to Kosta Manoliadis and Bill Kreklewetz for their artistic abilities using Autocad and to Michel Drouet and Peter Pascali, for their encouragement and humour. To my colleagues at PERMA, who are too many to name, I extend my appreciation for their support

and friendship.

To Jim Kolokotronis for his great efforts during the GC/MS experiments, Aline Beyrouti, Angelo Filosa and Robert Langlois, for their assistance in the development of extraction and analytical methods, and Warren Chew, for useful discussions on chemistry.

To Sylvain Coulombe, Tony Addona, Karen Sum and Munther Kandah of the McGill Plasma Group for their help during my time of need and for assistance with the model. To Prof. Munz and the rest of the plasma group for the useful exchange of ideas and advice.

To my brother George Alexakis, Irene, Bill and little Jasmine Vryonis, Despina and Spyros Montzenigos, and Gina Nasra their love and support.

To my husband, Thomas Montzenigos, for his never-ending encouragement, eternal optimism, and most of all, love. And, of course, for his superb talent and dedication to the art of "cutting and pasting"! (What a year!)

I wish to extend my special thanks to my parents, Chrisoula and Kostantinos Alexakis, whose unconditional love and support has been the guiding light of my life. Thank you for always believing in me!

Finally, I wish to extend my appreciation to the National Science and Engineering Research Council (NSERC), Industry Canada, Ministère de l'Industrie du Québec and the National Research Council of Canada for their financial support.

TABLE OF CONTENTS

LIST OF TABLES

LIST OF FIGURES

INTRODUCTION

Fullerenes are large, all-carbon, cage-like molecules, named after the American architect of the geodesic dome structure, Buckminster Fuller. The molecules containing 60 and 70 carbon atoms are the most abundant among the fullerenes.

Because of their extraordinary properties, fullerenes promise to launch an array of new compounds, with possible uses in electronics, polymers, catalysts, diamond film production, optical sensors and pharmaceuticals. However, many of the potential applications will remain untapped due to the exorbitant prices for pure fullerenes. In 1996, C_{60} and C_{70} sold between \$45-\$180 (U.S.) and \$350-\$375 (U.S.) per gram, respectively, depending on the purity and quantity purchased. At such high prices, it is doubtful whether fullerenes will ever become industrial commodities. Fullerenes are presently produced commercially in two steps, both of which lead to high production costs. The first step consists of the production of a fullerene-bearing soot by the arc-vaporization of graphite and the second step involves the purification of fullerenes by column chromatography.

In 1992, research at PERMA, a division of PyroGenesis Inc., led to a novel process in which fullerenes are produced via the thermal plasma dissociation of

hydrocarbons. This process was named *PyroGenesis*. In a preliminary investigation, a variety of hydrocarbons, including CH_4, C_2H_2, CF_3Br, and CCl_2F_2 were investigated. Although, at the time, the concentration of fullerenes in the soot was extremely low, less than 0.5%, the process was still considered very promising. Because thermal plasma technologies have been demonstrated in industrial processes for the production of chemicals, such as acetylene [Gladisch, 1962] and TiO_2 [Orfeuil *et al.*, 1988], it became the Company's vision that the *PyroGenesis* process could potentially be capable of producing industrial quantities of fullerenes at a fraction of the present price. However, much work was required in order to understand the effect of the process parameters on fullerene production and to characterize the *PyroGenesis* soot.

The work undertaken as part of this PhD thesis focusses on the following goals:

- to perform a thermodynamic analysis of potential hydrocarbon precursors for fullerene synthesis via the *PyroGenesis* process;
- to study the effect of operating parameters on fullerene production;
- to investigate the temperature profile within the reactor for various operating conditions, using the model developed by Bilodeau *et al.* [1996]; and, finally,
- to characterize the *PyroGenesis* soot via conventional extractive and chromatographic techniques.

LITERATURE REVIEW

CHAPTER 1: FULLERENES

1.1 Introduction to Carbon Structures

When they were first discovered in 1985, fullerenes were described as the third allotrope of carbon, the other two well known forms of carbon being graphite and diamond. As described herein, each carbon form has a characteristic molecular geometry which is responsible for the unique properties of each allotrope.

Graphite, is an all-carbon material consisting of a two-dimensional network of fused six-membered rings, similar to benzene rings, as can be seen in Figure 1. The individual carbon atoms in graphite are held together by rigid sigma, σ, bonds, giving graphite its overall flat structure. However, graphite, like other aromatic compounds, also possesses pi, π, electrons, which are shared by neighbouring carbon atoms. This type of bonding configuration is known as sp^2 bonding. The layers in graphite are held together by Van der Waals forces, thus the energy required to slide the layers over one another is low. This feature makes graphite a soft material which can be used as a lubricant. Graphite is also a good conductor of heat and electricity.

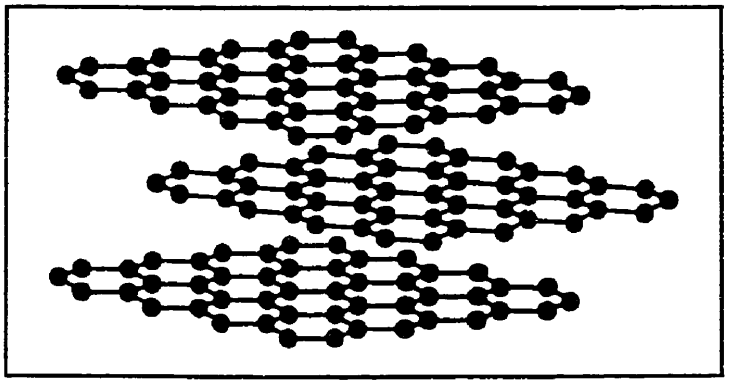

Figure 1: Structure of graphite.

Diamond is a crystalline material having an sp^3 bonding configuration, resulting in a regular three-dimensional network of σ-bonds. The structure of diamond can be seen in Figure 2. The configuration of the carbon atoms in diamond provides a rigid, stable structure resulting in a material which possesses high strength, hardness and resistance to chemical attack. Diamond also exhibits high heat conductivity and excellent electrical insulation.

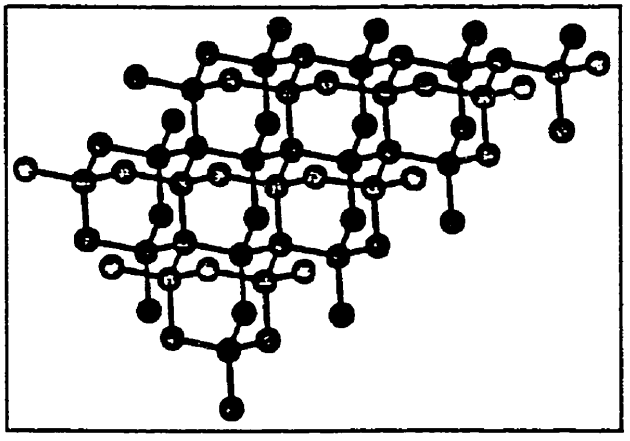

Figure 2: Structure of diamond.

In 1985, a new class of carbon compounds, the **fullerenes**, was welcomed into the history of carbon science. Fullerenes are essentially hollow carbon caged molecules which may contain as few as 32 and as many as 600 carbon atoms [Maruyama *et al*, 1991]. The first of such molecules to be discovered was carbon sixty, C_{60}, named buckminsterfullerene, after the geodesic domes of the famous American architect and engineer R. Buckminster Fuller.

The molecules containing 60 and 70 carbons, shown in Figure 3, have received the most attention due to their higher abundance and relative ease of isolation. Support for the shape and structure of C_{60} and C_{70} has been given mostly by mass spectroscopy and ^{13}C nuclear magnetic resonance [Kroto *et al.*, 1985].

C_{60} has a shape reminiscent of a soccer ball. The carbon atoms of C_{60} are arranged in an array of 12 pentagons and 20 hexagons; each atom existing at the juncture of two six-membered rings and one five-membered ring. C_{60} has a diameter of about 7Å [Kroto *et al.*, 1985]. C_{70} has an oblong shape which is reminiscent of a rugby ball and has dimensions of 7Å x 7Å x 9Å [Diederich and Whetten, 1992].

Fullerenes have been described as being halfway, structurally , between diamond

and graphite. The bonding of fullerenes is neither sp^2, like graphite, nor sp^3 like diamond, but an intermediate between these two hybridizations. As a result, this characteristic would strongly affect chemical reactivity, thermal and electrical conductivity, superconductivity and optical properties of fullerenes.

Larger fullerenes have also recently been isolated and characterized. These include C_{76}, C_{78}, C_{82}, C_{84}, C_{90} and C_{96} [Kikuchi *et al.*, 1992] and are shown in Figure 4. Furthermore, microtubules comprising of graphite sheets terminated with fullerene end caps have also been discovered and are also shown in Figure 4 [Iijima, 1991]. These microtubules are often referred to as buckytubes. Microtubules having diameters and lengths in the order of microns have been synthesised in 1960 [Bacon], however tubes with diameters of a single C_{60} molecule have only recently been reported [Ajayan and Iijima, 1992].

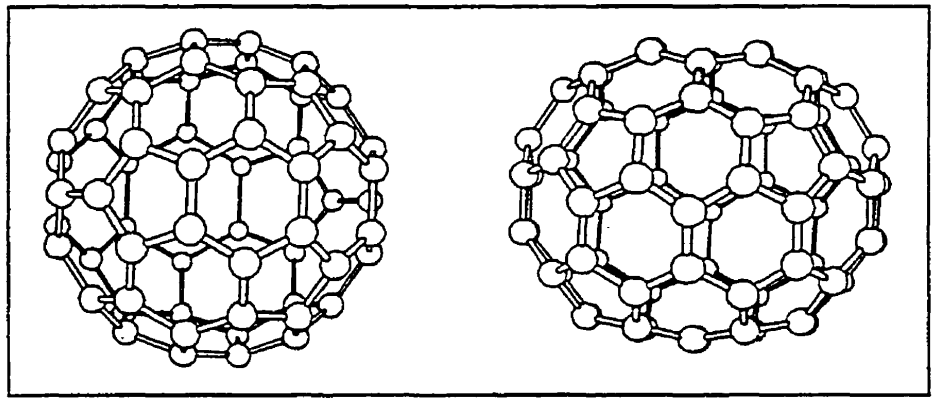

Figure 3: Structures of C_{60} (left) and C_{70} (right).

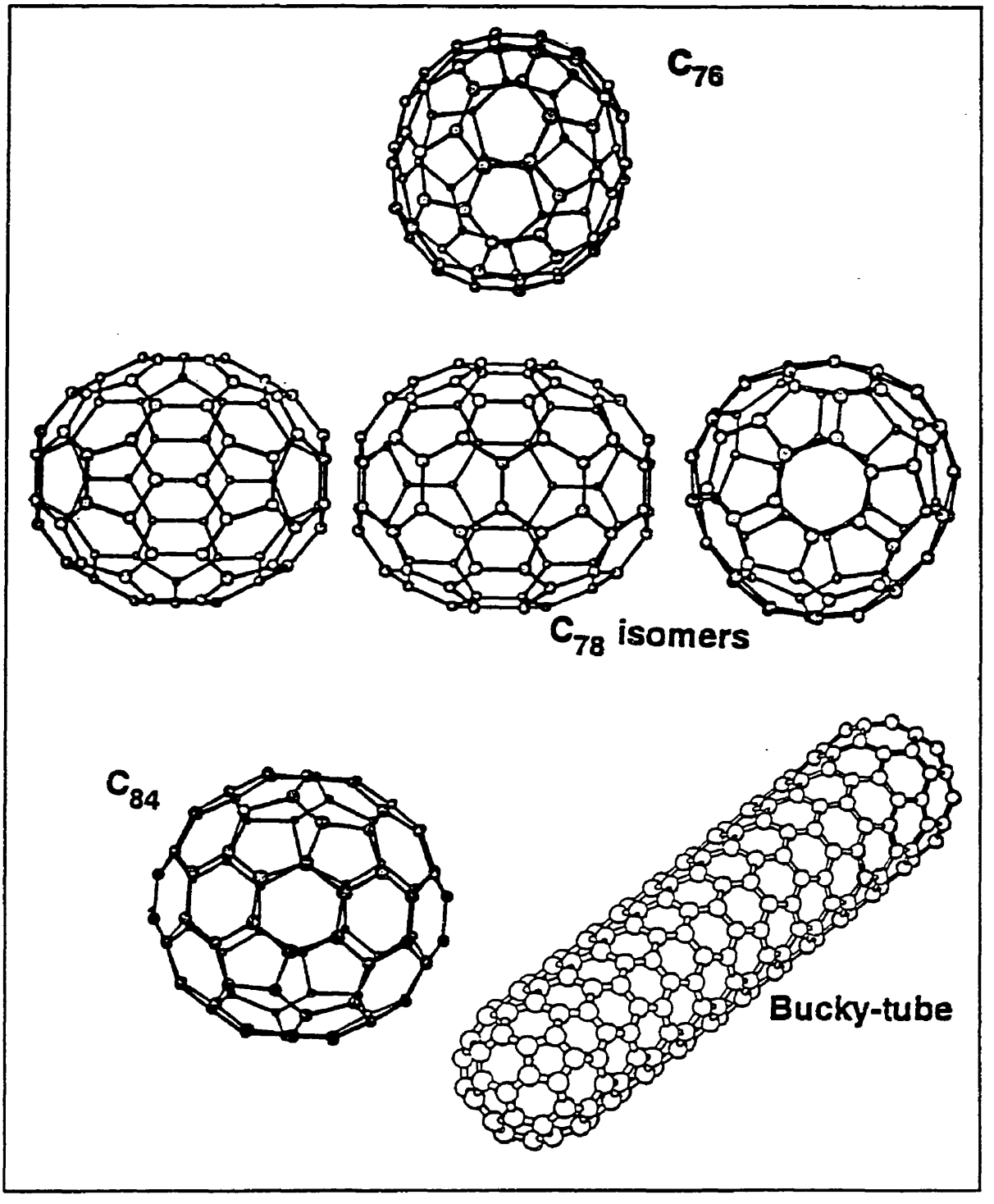

Figure 4: Structures of higher fullerenes and buckytubes.

1.2 Properties of Fullerenes

Due to the higher relative abundance of C_{60}, most work on characterization of fullerenes has been done on C_{60}. As a result, most of the information presented in this section is based on C_{60}.

Solid C_{60} is a molecular solid held together by van der Waals forces. The mass and molecular densities are listed in Table 1. Because of the weak intermolecular forces, C_{60} solids are highly compressible [Fisher *et al.*, 1991], although the molecular cage structure itself is highly incompressible [Duclos *et al.*, 1991]. The bulk modulus has been measured to be 14-18 GPa [Fisher *et al.*, 1991, Duclos *et al.*, 1991], a factor of 40 smaller than diamond. The Vickers hardness has also been measured to be 14.5-17.5 kg/mm^2 compared to 7,000-10,000 kg/mm^2 for diamond [Li *et al.*, 1992].

Because diamond and graphite are infinite lattices, the breaking of covalent bonds is required to release atoms or molecules. By contrast, fullerene crystals consist of molecular solids held together by van de Waals forces. As a result, dissolution and evaporation processes are simplified since they do not require the cleavage of covalent carbon-carbon bonds to release molecules. Thus, fullerenes are soluble in organic solvents and have a relatively high vapour pressure for a pure

carbon material. The solubility of C_{60} in various organic compounds is summarized in Table 1. The heat of sublimation and vapour pressure of C_{60} as a function of temperature is also presented in Table 1.

Table 1: Selected properties of C_{60}

Mass Density	1.65 ± 0.05 g/ml		Kratschmer *et al.* [1990]
Solubility in	mg/ml	colour	Ruoff *et al.* [1993]
hexane	0.04	magenta	
dichloromethane	0.26	magenta	
toluene	2.8	magenta	
CS_2	7.9	magenta	
1,2,3,5-tetramethylbenzene	20.8	yellow	
1-methylnaphthalene	33.2	olive green	
Heat of Sublimation	33.1-43.3 kcal/mol		Mathews *et al.* [1992] Pan *et al.* [1991, 1992]
Vapour Pressure at:			
500 K	1.2×10^{-10}	torr	Mathews *et al.* [1992]
600 K	1.8×10^{-7}	torr	
800 K	1.6×10^{-3}	torr	
1200 K (extrapolated)	15	torr	

The hybrid bonding pattern of fullerenes, as mention is Section 1.1, is partially responsible for the reactivity of C_{60} [Taylor and Walton, 1993]. C_{60} has been modified to give halogenated materials, alkylated C_{60}, C_{60} epoxide, C_{60} ethers and other interesting compounds.

Researchers have also studied the oxidative behaviour of fullerenes compared with graphite and diamond. In an atmosphere of air, fullerenes decomposed at 444 °C, whereas the decomposition of diamond and graphite occurred at 629 °C and 644°C, respectively [Saxby *et al.*, 1992]. Other researchers have found that in the presence of oxygen, C_{60} powder decomposes at 200 °C into an amorphous carbon-oxygen compound [Chen *et al.*, 1991].

In the bulk solid, fullerenes are black, but thin films are coloured. C_{60} and C_{70} thin films are a yellow and red, respectively. Solutions of fullerenes in organic solvents are also coloured, for instance magenta (C_{60}), wine red (C_{70}), greenish yellow (C_{76}), brown (C_{78}) and greenish yellow (C_{84}) [Kikuchi *et al.* 1992].

1.3 Methods of Fullerene Soot Production

1.3.1 Vaporization of graphite

1.3.1.1 Laser vaporization of graphite

The discovery of C_{60} in 1985 resulted from experiments by Kroto (University of Sussex) and Smalley (Rice University) in which graphite was subjected to a pulsed laser for the purpose of studying carbon clusters [Kroto *et al.*, 1985]. In pulsed laser vaporization, all of the energy is deposited onto the surface of a target in

a short period of time. For the typically used lasers, such as Q-switched Nd:YAG and excimer, this period of time ranges from 5 to 25 nanoseconds. Typical pulse energies vary from 0.1 to 1 Joules. The production of fullerenes via laser vaporization of graphite resulted in a soot containing up to 40% fullerenes. However, this technique is limited to the production of milligram quantities of fullerenes. As such, the Kroto-Smalley apparatus holds its place in fullerene history for contributing to the discovery of fullerenes, however such a technique is used only for fundamental research in studying the formation of fullerenes and for the production of milligram quantities of endohedral fullerenes, such as $La@C_{60}$.

1.3.1.2 Arc vaporization of graphite rods

Various methods used to vaporize carbon for the production of fullerenes include resistance heating [Kratschmer *et al.*, 1990], and a.c. or d.c. arc discharge [Haufler *et al.*, 1990 and 1991, Koch *et al.*, 1991, Pang *et al.*, 1991]. Currently, fullerenes are produced commercially using the carbon arc discharge method.

Figure 5 presents a cross-sectional view of a typical carbon arc C_{60} generator [Haufler *et al.*, 1990]. The electrodes are two graphite rods, 6 mm in diameter, which are usually screw-fed to maintain a constant arc distance and turn in

opposite directions to help maintain even erosion as the ends of the rods are vaporized in the arc. When sufficient current is applied, a sudden increase in power dissipation at the anode results in the vaporization of the anode material, resulting in the production of a cloud of volatile carbon species. As the carbon cloud cools by radiation and through the introduction of a carrier gas, the condensation of carbon species results in a soot which contains fullerenes. In fullerene production experiments by Haufler *et al.* [1991], the arc voltage maintained at 10-20 V and the range of current used was 100-200 A. The surface temperature of the electrodes was measured to be 3,150-3,700 K, depending on the arc current [Huczko *et al.*, 1995].

The first version of the reactor shown in Figure 5 did not have a water-cooled shroud. The weight percent of fullerenes in the soot produced via this device was 6-8%, whereas when a chimney was added, the weight percent of fullerenes in soot increased to 15-22%. The authors did not fully understand why the overall weight percent of fullerenes in the dust increased upon addition of the water cooled chimney. The authors believed that reducing the ambient temperature may be beneficial to fullerene formation or perhaps that beneficial flow patterns were created. The convection patterns in the reactor, as suggested by Huczko *et al.* [1995], play a major role in explaining the differences in fullerene yields as a

function of location.

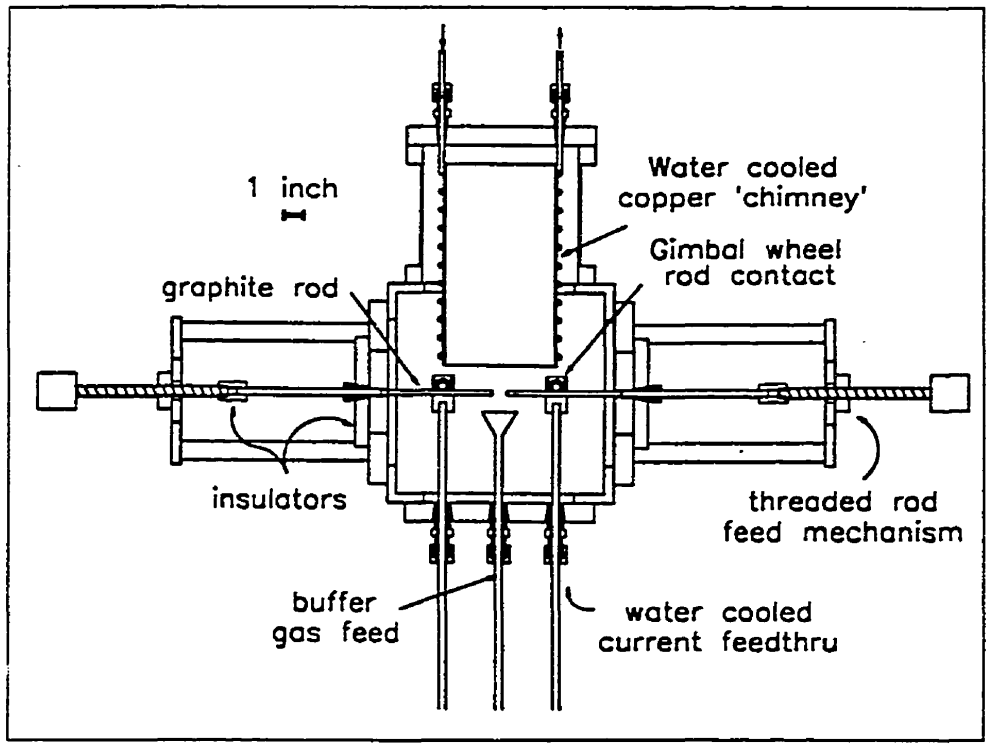

Figure 5: Apparatus for producing fullerenes via the arc vaporization of graphite [Haufler *et al.*, 1990].

The first step in optimizing fullerene production was in the determination of the optimal pressure of the buffer gas. With the apparatus in Figure 5, the optimum pressure in the chamber was found to be between 100-200 torr, when helium, argon or nitrogen were used as the carrier gas. However, the nature of the carrier gas seems to be an important parameter. When helium was used as the

carrier gas, the yield of C_{60} in the soot was between 10 and 15%, whereas argon and nitrogen resulted in maximum yields of 5% and 0.8%, respectively. Since the purpose of the carrier gas is primarily to adjust the rate of diffusion of the small carbon radicals away from the point of vaporization, it has been suggested that the optimum gas pressure should depend on the nature of the carrier gas and the rate of its hydrodynamic flow past the carbon vapour [Haufler *et al.*, 1991].

Using variations of the apparatus shown in Figure 5, researchers have reported the percentage of fullerenes in soot to vary from 0.5% to 30%, however typical production runs yield 12-15% fullerenes [Koch *et al.*, 1991]. The fullerene content in the soot is typically 80-85% C_{60}, 15-20% C_{70} and 0.5-2.5% higher fullerenes. The ratio of C_{70}/C_{60} ranges from 0.02 to 0.18 [Ajie *et al.*, 1990].

Attempts have been made to scale up the device shown in Figure 5 by increasing the electrode diameter and the input power. When the electrode diameter was increased from 6 mm to 13 mm, the maximum percent of fullerenes in the soot was found to be 5% [Haufler, 1994]. Chibante *et al.* [1993] speculated that the decrease of fullerene content with increasing electrode diameter is due to the higher UV and radiation flux resulting from the higher power consumption. It was thought that the fullerene yield in soot decreases due to photochemical

destruction of fullerenes by reactions of electronically excited fullerenes. In contrast, Haufler *et al.* [1994], argue that the effect of temperature and residence time are critical in the formation of fullerenes. Growing carbon clusters must experience a sufficient period of time in an appropriate temperature zone in order to facilitate bonding rearrangement and annealing. The temperature range has been predicted to be 2,000-3,000 °C [Haufler *et al*, 1990]. If growing clusters are kept at this temperature too long, polymerization and continued growth to large, unextractable species occurs. As a result, as the power consumption increases approximately to the square of the electrode diameter, it is possible that larger electrodes resulted in a undesired increase in residence time of the growing carbon cluster in a "hot" zone.

The temperature profile and residence time of carbon clusters in the "hot zone" are controlled by the arc current, pressure and type of buffer gas. Higher pressures and buffer gases with high molecule weights increase the residence time. Increasing the arc current increases the overall temperature.

Researchers at MER Corp. investigated the effect of arc current from 70-250 A on fullerene production using a ¼ inch rod. They reported that the lowest current resulted in a higher yield of fullerenes in soot but in very low production

rates of soot [Koruga *et al.*, 1993]. Thus, there seem to be an inverse relationship between the rate of soot production and fullerene yield, which was not explained by the authors. Furthermore, the use of a d.c. current, rather than a.c., seems to increase the yield of fullerenes [Huczko *et al.*, 1995]. This result may be due to the more stable arc obtained when d.c. is used, resulting in very low rates of spallation of the electrodes.

Although the production rate of soot is not reported in the papers reviewed, some information on the soot production rate was obtained from patent No. 5,227,038 [Smalley, 1993]. Using electrodes 6 mm in diameter and arc current and voltage of 150 A and 26 V, respectively, soot, having a fullerene concentration of 13%, was produced at a rate of 0.5 g/min. The reported data seems to suggest that an equivalent of 0.92 grams of fullerenes may be produced per kWh of energy input, via the arc vaporization of graphite method. However, an important disadvantage of this process, as expressed by Haufler [1994], is its difficulty to scale up due to the adverse effect of electrode diameter on fullerene production yields.

1.3.2 Arc vaporization of other solid carbonaceous materials

Pang *et al.* [1991] attempted to produced fullerene soot by replacing graphite rods

by demineralized coal formed into electrically conducting rods, 18 mm in diameter. The arcing of demineralized coal resulted in a soot containing 2-8.6 % fullerenes. The presence of minor mineral matter and hydrogen does not inhibit fullerene formation but does have an adverse effect on the total yield of fullerenes in soot when compared to vaporization of pure graphite. Other researchers [Koruga *et al.*, 1993, Tohji *et al.*, 1994] attempted to use a variety of carbon materials, including low quality coke, carbon black and spent soot for fullerene synthesis, however, as expected, higher quality of carbon precursor resulted in higher yields of fullerenes.

1.3.3 Fullerenes via combustion of hydrocarbons

The first attempt at producing fullerenes from a gaseous carbon source was performed by researchers at the Massachusetts Institute of Technology studying benzene flames [Howard *et al.*, 1992]. It was found that fullerenes could be produced from flames of premixed benzene and oxygen with argon as a diluent. Reactor conditions such as temperature, pressure, carbon/oxygen ratio and residence time were the key parameters affecting the production of fullerenes. With this process, up to 0.26% of the fuel carbon was converted into fullerenes. The authors have predicted this value to be as high as 0.5%. The low conversion of carbon to fullerenes is expected, from thermodynamic calculations, since

approximately 5/6 of the carbon input forms CO, leaving a maximum of 1/6 of the carbon for fullerene and soot formation [Pope and Howard, 1996]. The fullerene content in soot ranged from 0.003% to 20%. The largest yields of fullerenes occurred when the C/O ratio was maximized. However, when using a combustion process, there is an upper limit in the C/O ratio which may be possible since an adequate amount of O_2 must be supplied in order to maintain the temperature at a desired level. McKinnon [1991] proposed that fullerenes form between 2,200 K and 2,600 K from the combustion of C_2H_2. Using this method, the highest production rate of fullerenes was 0.45 g/hr, corresponding to a soot having a fullerene content of 12.2%. The fullerene yield increased with increasing temperature and decreasing pressure [Howard *et al.*, 1992].

One important characteristic of this process compared to the vaporization of graphite technique is the ability to vary the ratio of C_{70} to C_{60} . The C_{70}/C_{60} ratio varied from 0.26 to 8.8 [Howard *et al.* 1992], compared to 0.02-0.18 for graphite vaporization [Ajie *et al.*, 1990]. The relative abundance of C_{70} increases with increasing pressure in the combustion experiments. In addition, isomers of C_{60} having adjacent five membered rings in their structure were observed in soot produced by the combustion of benzene. Such isomers of C_{60} have not been reported to exist in the soot produced by vaporization of graphite.

1.3.4 Plasma pyrolysis of hydrocarbons

1.3.4.1 Plasma pyrolysis of carbon black and acetylene

Yoshie *et al.* [1992] developed an alternative process for fullerene production involving the vaporization of carbon black in an r.f.-d.c. plasma reactor. In this process, carbon black (less than 10 μm) was introduced into a plasma flame. It was found that when commercial grade carbon black, which contains 2 mol% hydrogen and 3 mol% oxygen was used as the starting material, the fullerenes weight percent in soot was 4%. However, when a purer grade of carbon black was used, with no hydrogen present, the weight percent of fullerenes in soot increased to 7%. It was suggested that the presence of hydrogen and/or oxygen reduces the yield of the fullerenes. An attempt was also made to use C_2H_2, as the carbon source, however, no fullerenes were found in the soot. It was also found that decreasing the pressure in the reactor chamber from 760 torr to 260 torr reduced the yield of fullerenes from 7% to 3%. Such a pressure dependence is different from that in the carbon arc C_{60} generator, where the optimal pressure was found to be 100-200 torr [Haufler *et al.*, 1990].

1.3.4.2 Pyrolysis of aromatic hydrocarbons

The formation of C_{60} and C_{70} by pyrolysis of naphthalene at 1,000 °C has been reported [Taylor *et al.*, 1993]. C_{60} and C_{70} are formed by the "patching together"

of six and seven naphthalene molecules ($C_{10}H_8$), respectively. The reaction was carried out in a silica tube, 1 cm in diameter and 40 cm in length. Two plasma torches were used to evaporate and subsequently pyrolyse naphthalene. The mass percent of fullerenes in the soot collected at the exit of the tube was less than 0.5%. The proposed mechanism of fullerene formation via the addition of naphthalene molecules is shown in Figure 6.

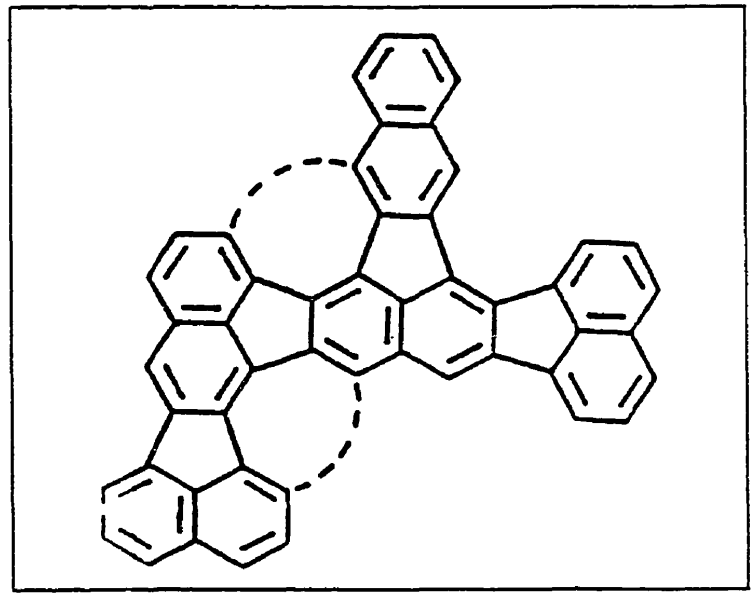

Figure 6: Possible route to C_{60} formation via addition of naphthalene molecules [Taylor *et al.*, 1993].

The production of fullerenes via the use of benzene or naphthalene in a low temperature plasma chemical vapour deposition apparatus was reported by Inomata *et al.* [1994]. In their work, benzene or naphthalene vapour was fed into an Ar-He plasma. A low temperature plasma was generated by applying r.f. voltage across two electrodes. The temperature of the plasma was measured during the experiments and it was found that the electron temperature was 1.4-2.2 eV, whereas the gas temperature was 255-455 °C. The authors suggest that due to the low temperatures of the plasma, thermal decomposition of the aromatic compounds is not required for the formation of fullerenes. Instead, high energy electrons in the plasma contribute to the synthesis of fullerenes from the hydrocarbons. The production rate of fullerene soot and the concentration of fullerenes in the soot obtained during this study were not reported.

1.3.4.3 Plasma pyrolysis of halogenated hydrocarbons

A thermal plasma process, named *PyroGenesis*, was developed at PERMA, a division of PyroGenesis Inc. (Montreal, Canada), for the synthesis of fullerenes via the dissociation of hydrocarbons [Tsantrizos and Grenier, 1992]. A plasma reactor, equipped with a non-transferred d.c. plasma torch, was used to dissociate hydrocarbons. The hydrocarbons investigated include CH_4, C_2H_2, $CBrF_3$ and CCl_2F_2. By controlling the reactor conditions, some carbon atoms recombine to

form fullerenes in a soot which condenses on the water-cooled reactor wall. When CH_4 and C_2H_2 were each used as feed materials, the resulting soot did not contain a significant amount of C_{60} (less than 0.05%). C_{70} was not detected in the samples produced during these experiments. However, when $CBrF_3$ and CCl_2F_2 were investigated as starting materials, both C_{60} and C_{70} were present in the soot produced. The pyrolysis of CCl_2F_2 provided higher yields of fullerenes, resulting in a soot containing up to 0.5% C_{60} and a small quantity of C_{70}. As part of this PhD thesis, the *PyroGenesis* process was further developed through the use of tetrachloroethylene, C_2Cl_4, as the carbon source.

1.4 Theories of Formation

Of the many interesting scientific questions raised by the discovery of fullerenes, the most intriguing remains that which concerns the mechanism by which small carbon molecules combine to form large hollow cages. Despite the great progress in experimental research on fullerenes, there still exists no generally accepted theory on the formation of fullerenes. The main reason for this is the extreme complexity of the composition of carbon gas at high temperatures.

Since the discovery of fullerenes, many mechanisms for fullerene formation have been proposed. Among the earlier steps in defining a mechanism of formation

was the determination of the nature of the carbon species initially expelled from the graphite rods during arc vaporization. Initially, it was thought that fullerenes were formed from graphitic fragments derived from the graphite rods. These graphite fragments would have to undergo structural rearrangement in order to include pentagons, which are required for curvature of the structure. This hypothesis was put to the test by isotopic scrambling experiments [Meijer and Bethune, 1990, Ebbesen *et al.*, 1992]. In these experiments, the graphite rods used for fullerene synthesis were constructed so as to have regions of pure ^{13}C and regions of naturally occurring ^{13}C. If the results of these experiments were to show that the ^{13}C atoms are randomly distributed throughout the C_{60} network, then this would suggest that a small-molecule synthesis of fullerenes is most-likely occurring, rather than the synthesis via large graphitic sheets. A mechanism based on the formation of fullerenes from large graphitic fragments would result in two distinct groups of C_{60} molecules, one group having a higher proportion of ^{13}C atoms than the other group. The results for the isotopic scattering experiments provided strong evidence that carbon-arc fullerene synthesis originates from atoms or, at most, from very small carbon clusters (C_2, C_3).

A four-step chemical model for fullerene synthesis has been proposed [Smalley, 1992, Heath, 1992]. A general diagram of this type of chemical model is shown

in Figure 7. It has been suggested that the growth process which generates fullerenes begins with an initial condensation process resulting in the formation of linear chains of carbon (C_n, $n<10$). The next step involves the formation of monocyclic rings, which are predicted to be the most dominant intermediates for species in the size range of C_{10} to C_{20}. The two-dimensional monocyclic rings then undergo a rearrangement of atoms to form three-dimensional structures (C_{21}-C_{31}). Since these open graphite-like sheets would have many peripheral "dangling bonds", or unsatisfied valances, the graphitic sheets would rearrange to incorporate pentagons as well as hexagons in the bonding pattern. The pentagons would cause the sheet to curl and enable some of the peripheral bonds to join. Such species are predicted to be unstable due to these "dangling bonds" and as a result, these species are expected to readily react with carbon atoms and clusters until a relatively stable closed fullerene structure is reached. Haufler *et al.* [1991], suggest that the energetically most favoured form of any open graphitic sheet is one which i) is made solely of pentagons and hexagons, ii) has as many pentagons as possible, while iii) avoiding adjacent pentagons. This is referred to as the pentagon rule, and C_{60} is the first pentagon rule structure that forms a closed structure.

Another model, proposed by Goeres and Sedlmayr [1991], suggests that the

formation of fullerenes occurs via the addition of elementary bricks of clustered carbon compounds, C_n, which are already two-dimensional structures. Based on the evidence that carbon chains tend to form monocyclic rings and that C_{10} is the most prominent structure in a carbon gas [Raghavachari and Binkley, 1987], C_{10} is assumed to be the elementary brick. During addition reactions of C_{10} rings with intermediates, it is predicted that the monocyclic C_{10} rings collapse to form a naphthalenoctyl structure, thus favouring the formation of a connecting pentagon which produces the curvature of the intermediates.

Using experimental techniques, Chang *et al.* [1992] attempted to trap some possible intermediates responsible for the synthesis of fullerenes. The standard arc vaporization procedure was modified to allow for the introduction of hydrogen donors to saturate the carbon clusters, thus trapping possible intermediate species. Intermediates included $C_{12}H_8$, C_nH_{10} ($12<n<18$). The authors describe a number of possible synthetic routes for fullerene formation. Other authors [Brabec *et al.*, 1992, Lafleur *et al.*, 1993] have identified corannulene as a precursor for fullerene formation.

Although theoreticians are actively searching for answers relating to the mechanism by which fullerenes form, the mechanism of fullerene formation still

remains a controversial area in fullerene research.

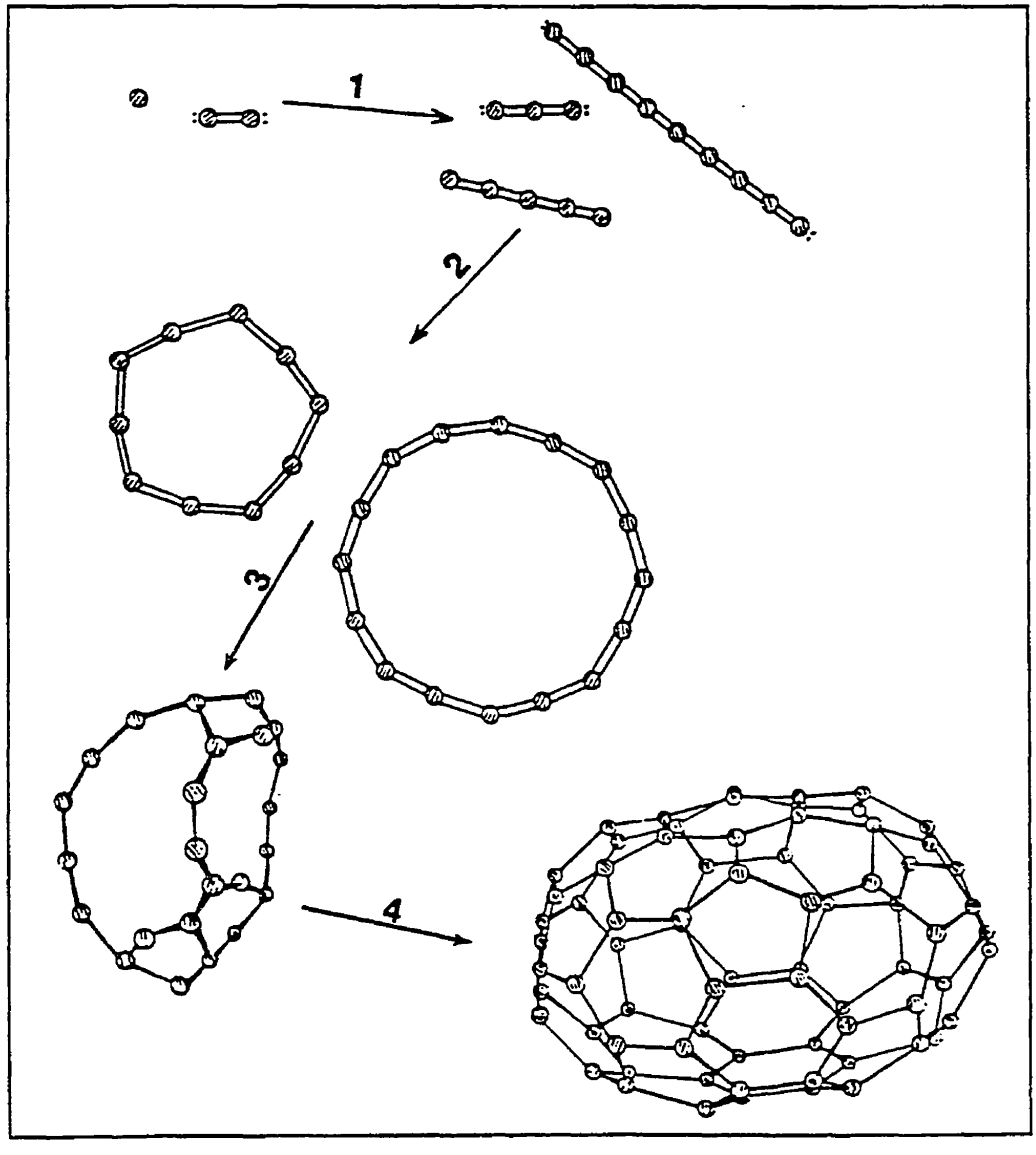

Figure 7: A chemical model for the generation of fullerenes from atomic and dimeric carbon vapour [Heath, 1992].

1.5 Purification of fullerenes

1.5.1 Extraction of fullerenes from soot

The first step required in virtually all types of fullerene purification methods involves the extraction of soluble fullerenes from the insoluble carbon soot. The solubility of fullerenes in different solvents was presented in Table 1 (Section 1.2). Solvents which are typically used for the extraction of fullerenes are toluene, benzene and CS_2. Various techniques may be used for extraction, two of which are described herein.

In a SOXHLET extraction apparatus, as shown in Figure 8, the carbon soot is placed in a "thimble" or filtering cup and solvent is evaporated from the holding flask. The solvent vapour travels to the condenser, where the solvent recondenses and is allowed to percolate through the carbon soot, resulting in the dissolution, or extraction, of soluble compounds including fullerenes. The extract solution is then returned to the boiling solvent vessel where the solvent is re-evaporated and recycled in the extraction process. This type of extraction is used because it permits continuous extraction of material using a very small volume of solvent. Such a process is desired for the extraction of fullerene due to their very low solubility in organic solvents. The SOXHLET extraction is typically run for 24-48 hours. It should also be noted, that this step does not preferentially dissolve

fullerenes over any other soluble compounds present in the soot, and as a result the extract may contain a variety of by-products depending on the process used to produce the fullerene soot.

A simpler approach for the extraction of fullerenes involves the dispersion of carbon soot in solvent through the use of a sonication bath. Sonication of the mixture enhances the dissolution of the fullerenes in the solvent. This process requires the use of more solvent than in SOXHLET extraction, however, the extraction process using sonication may be completed in less than 30 minutes, depending on the quantity of solvent used. Following the extraction process, the mixture is filtered to yield a fullerene rich filtrate.

The crude extracts vary in composition, depending on the soot production process employed. Crude extracts from soot produced via the arc vaporization of graphite consist of: 80-85%C_{60}, 15-20% C_{70} and up to 2.5% higher fullerenes [Ajie *et al.*, 1990]. The crude extract must then be further purified to yield pure C_{60} and C_{70}.

1.5.2 Purification of fullerenes by chromatography

C_{60} and C_{70} are presently purified commercially by column chromatography. In

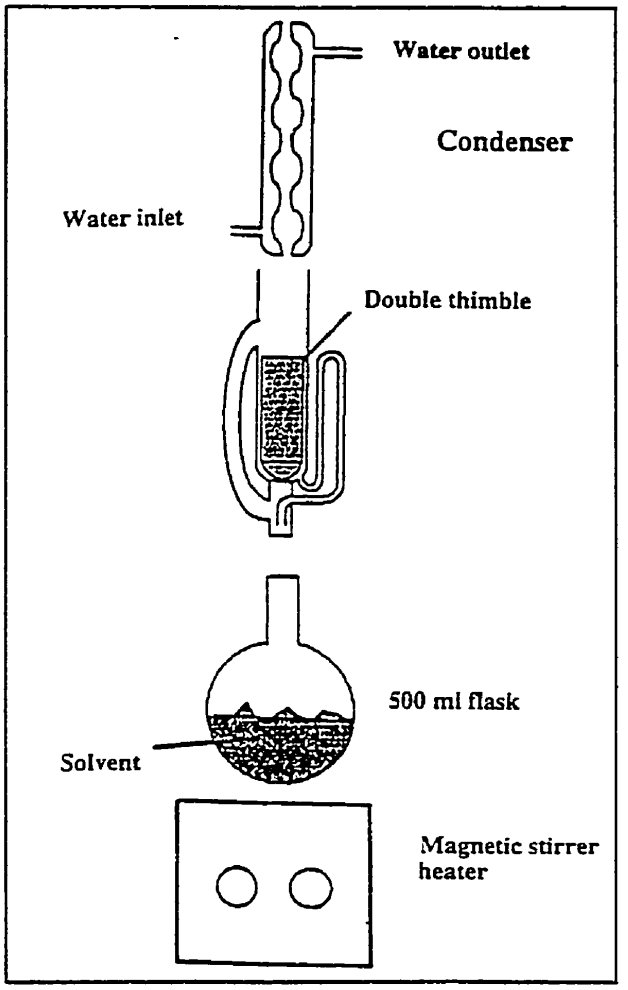

Figure 8: SOXHLET apparatus for the extraction of fullerenes.

chromatography, a solution containing several solutes is eluted through a packed column. The solutes interact with the column packing to varying degrees depending on their polarity, molecular size, ionization energy, adhesion and other properties [Hamilton and Sewell, 1977]. Solutes having a greater interaction with the packing material move more slowly down the column than the solutes that interact to a lesser degree. If the column is long enough, the zones for each individual solute will draw apart from one another sufficiently to be recovered in the effluent as separate solutions. Chromatography can be performed either in *bulk mode* or *trace mode*. In the bulk mode, a mixture of compounds is fed in a relatively large amount onto a packed column. In the trace mode, used for analytical purposed, only a minute amount of solute is admitted to the column.

In a standard, bulk-mode chromatography used for the purification of C_{60} and C_{70}, a small sample of crude extract is eluted with hexane, or a mixture of hexane and toluene (95:1) through a chromatography column packed with neutral alumina. As fullerenes are separated within the column, the coloured bands move down the column and spread apart. C_{60} yields a violet band while C_{70} gives a wine-red coloured band. Solvent is added to the top of the column manually. The column is run until each band reaches the bottom of the column and is collected in separate flasks. The process takes about 8-12 hours.

Alternatively, a SOXHLET type chromatographic column, using alumina as the stationary phase, may be used [Khemani *et al.,* 1992] in which the solvent is recirculated by evaporation and condensation. This method is similar to that used for extracting the mixed fullerenes from the soot (Section 2.7.1). Although this type of column requires minimal supervision, it takes several days for purification. For example, this technique takes 20 to 30 hours to elute pure C_{60} and another 50-70 hours to elute C_{70}.

Recently, purification of C_{60} and C_{70} has been achieved on chromatography columns packed with graphite [Vassallo *et al.,* 1992] or a mixture of activated carbon and silica gel [Scrivens *et al.,* 1992], using toluene as the mobile phase. These methods offer significant improvements over purification on alumina since the time required for purification is greatly reduced due to the higher solubility of fullerenes in toluene. Furthermore, the packing material is much less expensive than alumina. To improve the elution rate, the columns may be run under N_2 or air, referred to as flash chromatography. Although flash chromatography reduces processing time, the purity of the samples is sometimes compromised.

For the analysis of C_{60}, C_{70} and higher fullerenes, trace-mode chromatography

is performed using a high pressure (or performance) liquid chromatograph. In high pressure liquid chromatography (HPLC), only milligram quantities of crude extract are injected into the column. HPLC differs from standard chromatography in two ways: (1) the type and mesh of the packing material and (2) the feed pressure [Hamilton and Sewell, 1977]. There are various alternative types of HPLC packing materials that can be used: alumina, silica gel, reverse phase silica gel, activated carbon, ion exchange resin, permeation gels, and others. The main advantage, however, of HPLC is the density with which the stationary phase material are packed and the effective surface area/gram of packing material. HPLC has a much denser packing, resulting in a high surface area/gram of packing material. As a result, the pressure drop through the HPLC packed bed is much higher, thus requiring a high pressure pump to deliver the mobile phase. The advantage of having a denser packing with a higher effective surface area is that the resolution of separation is greatly improved using a very short column.

1.5.3 Purification of fullerenes by sublimation

Another possible method for separation of fullerenes from soot is sublimation. Fullerenes are known to sublimate at temperatures as low as 400 °C under vacuum and the sublimation temperature seems to increase with molecular weight. Since the raw soot contains several different types of fullerenes having

very close sublimation temperatures, fractional sublimation may be useful in purifying the fullerenes.

Averitt *et al.* [1994] report of a purification method in which fullerene extract is introduced into one end of a distillation column, lined with a series of evenly spaced baffles with circular perforations. The starting materials are heated under high vacuum to 970 K while a linear temperature gradient is established along the length of the column. C_{60} having a purity of 99.97% has been obtained, however the recovery of C_{60} in the pure fraction was only 16.2%.

A thin film fractional sublimation, developed by Gillot and Goldberger [1969] for the separation of zirconium tetrachloride and hafnium tetrachloride, was adapted as a batch process for the purification of fullerenes in a research study at Pegasus Refractory Materials [Manoliadis, 1995].

In this process, inert, non-volatile solids are fed in the top of a heated column and move down, counter-currently to the saturated fullerene vapours. Since the solids enter at a temperature below the condensation temperatures of the vapours, a thin film of volatile solids condenses on the surface of the inert solids. This coating acts as a reflux for the enriching section of the condenser and is

carried down along with the solid packing. A carrier gas is fed from the bottom to keep the flow of gas moving up, counter-current to the solid phase. Best results provided a fraction of C_{60} with a purity of 95%, however the recovery of C_{60} in this fraction is very low. This process is promising since continuous operation would result in a higher recovery of C_{60}, since pure C_{60} would be removed from the top of the column continuously.

Although research in the use of fractional sublimation for the purification of fullerenes is on-going, there is no process available at this time which is capable of purifying fullerenes commercially.

1.5.4 Purification of fullerenes via reactive techniques

A number of reactive techniques have been developed to selectively and reversibly react with either C_{60} or C_{70}, thereby providing a means for purification [Huang *et al.*, 1993, Atwood *et al.*, 1994]. Only the reactive technique based on complexation with calixarene compounds is described briefly below.

Fullerenes can be separated from crude mixtures by selective complexation with calixarenes, bowl-shaped macromolecules with hydrophobic cavities [Atwood *et al.*, 1994]. The researchers used 1-tert-butyl-calix[8]arene to selectively react with

C_{60}. The calixarene-C_{60} complex precipitates out of the toluene solution and thus can be isolated by crystallization and filtration. Once isolated, the complex is decomposed in chloroform, yielding purified C_{60} as the final product. The authors claim that a high recovery of C_{60} having a purity of 99.9% may be obtained after several recrystallization and filtration steps.

1.6 Applications

Despite its fame as the "Molecule of the Year" on the cover of Science Magazine in 1990 and the "Most beautiful molecule", in the book by Aldersey-Williams [1994], C_{60} has yet to find any commercial applications. However, since the commercial availability of C_{60} in 1990, researchers worldwide have been focussing on the development of fullerene-based products. Fullerenes promise to launch an array of new compounds, with possible uses in electronics, polymers, catalysts, diamond film production, optical sensors and pharmaceuticals.

Currently, the most commercially important properties of fullerenes relate to electronics applications. C_{60} molecules readily accept electrons and thus can easily be doped with alkali metals or other atoms to form fullerides. Different fullerides act as conductors, semiconductors and superconductors [Hebard, 1992]. AT&T Bell Laboratories discovered that when C_{60} is doped with potassium to

produce the metallic salt, known as K_3C_{60} or potassium buckide, the buckide becomes superconductive when cooled below 18 K. When rubidium is substituted for potassium, the critical temperature (T_c) for superconductivity was found to be 29 K [Rosseinsky *et al.*, 1991]. At present, the organic superconductors having the highest T_c is Cs_3C_{60} with a T_c of 40 K [Palstra *et al.*, 1995]. Although the superconductive limits of doped fullerenes have not yet been established, it is hoped that they will be as good as, or better than superconductive ceramics (oxides of thallium, calcium, barium and copper), whose critical temperature for superconductivity may be as high as 160 K under pressure [Calestani, 1994].

Researchers at Japan's Institute for Molecular Sciences were first to detect the non-linear optical properties of fullerenes. A material exhibiting non-linear optical properties demonstrates a non-linear change in its refractive index as the intensity of light changes, and becomes opaque above a critical intensity. A number of research groups have demonstrated that fullerenes are excellent optical limiters in solution [Heflin and Garito, 1992, Tutt and Kost, 1992] and as thin films [Diehl *et al.* 1993]. To date, the optical limiting effects of fullerenes have only been demonstrated against laser light, however, if the optical limiting behaviour of fullerenes is general for all wavelengths, fullerenes could find applications as light shields for electronic devices, light-activated sensors and in

eye wear.

The use of thin films of C_{70} for the synthesis of diamond coatings may become a very important application of fullerenes. Researchers at Northwestern University [Meilunas *et al.*, 1991] have recently reported that diamond films grow readily on a specially prepared layer of C_{70}. The substrate is first coated with a film of C_{70} and then bombarded with carbon and hydrogen atoms. This pretreatment results in breaking the cage structure and exposing the free ends of the fullerene network. These free ends seem to provide ideal templates for nucleating diamond growth.

C_{60} crystals may also be transformed into diamond at room temperature by being subjected to high pressures, as reported by Regueiro *et al.* [1991]. The energy barrier inhibiting a C_{60}-diamond transformation is evidently low enough to allow this conversion by non-hydrostatic compression of C_{60} at pressures of 50 ± 5 GPa at room temperature.

The chemical modification of fullerenes will be the source of many long-term applications. Fullerenes have been modified to give halogenated materials, alkylated fullerenes, fullerene epoxides, fullerene ethers and fullerene-based

polymers [Taylor and Walton, 1993]. The chemistry of metal complexes, especially endohedral complexes is also an area of great interest, since these materials are predicted to have interesting electronic and optical properties [Taylor and Walton, 1993]. In addition, a water soluble derivative of C_{60} was found to be active against the HIV viruses which cause AIDS [Friedman *et al.*, 1993]. Potential commercial applications of chemically modified fullerenes are fullerene-based composite materials, photoconducting polymers, medical diagnostics and therapeutics, catalysts, and conductive plastics.

Despite the extraordinary properties of fullerenes, many of the potential applications will remain untapped due to the exorbitant prices for pure fullerenes. In 1996, the prices for C_{60} and C_{70} were between \$45-\$180 (U.S.) and \$350-\$375 (U.S.) per gram, respectively, depending on the purity and quantity required.

1.7 Market

C_{60} was first introduced into the marketplace in 1991 at a price of \$1,200 U.S. per gram. As can be seen in Figure 9, the price of C_{60} has steadily decreased from \$1,200 to less than \$100 U.S. per gram. The decreases in the price of fullerenes is due partly to automation of fullerene soot production and purification processes and partly to direct competition between suppliers. The

selling price of pure C_{70} has remained quite high due to the difficulty relating to the purification of C_{70}. The present selling price of C_{70} is $800 U.S. per gram.

In Figure 10, the current fullerene consumption worldwide is shown. Although there is a significant increase in the consumption of fullerenes since 1991, the present market is only 10 kilograms per year.

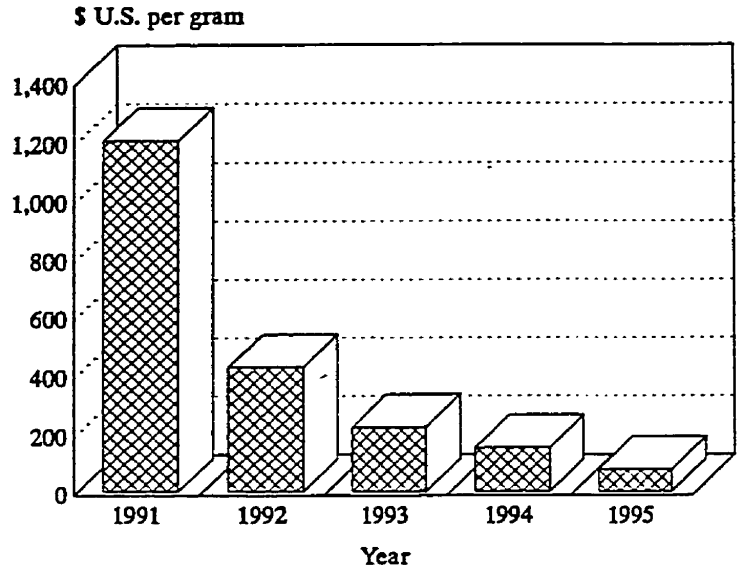

Figure 9: Selling price of C_{60} from 1991-95.

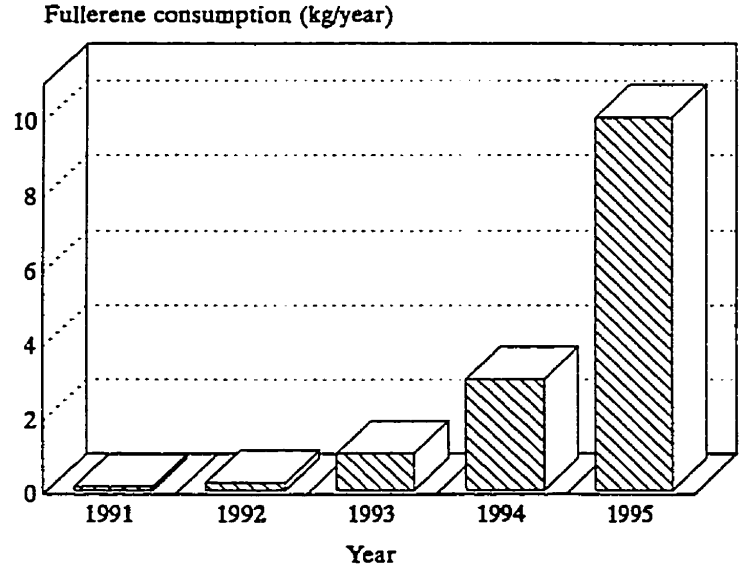

Figure 10: Global fullerene consumption from 1991-95.

CHAPTER 2: PLASMA PYROLYSIS OF HYDROCARBONS

2.1 Properties of Plasmas

2.1.1 Definition of plasma

Plasma is a physical state of matter obtained when a gas is ionized. A plasma consists of positively charged ions, free electrons, as well as neutral atoms and molecules. In a plasma, the electrons produced by the partial ionization of the gas act as the chief agent for transferring energy from the electric field to the gas. This transfer process is effected through electron-molecule collisions. Most plasmas are only partially ionized, where ionization may approach 5%.

Plasmas have been divided into two categories, cold plasmas and thermal plasmas. In cold plasmas, the temperature of the heavy particles forming the gas (T_g) is significantly lower than that of the electrons (T_e). The ratio of T_g to T_e is between 10 and 100, with an electron temperature of about 10,000 K. Cold plasmas operate at low pressures, typically less than 100 torr. In thermal plasmas, the electrons and heavy particles (ions, atoms) are at the same temperature, which may be as high as 20,000 K. Gas enthalpy is the main factor in applications for thermal plasmas [Boulos *et al.*, 1983].

The remainder of the discussion on plasmas will be focussed on thermal plasmas since this work relates to the thermal plasma production of fullerenes.

2.1.2 Thermodynamic properties of thermal plasmas

Specific enthalpy and specific heat

The specific mass enthalpy and specific heat of Ar, H_2 and He as a function of temperature are shown in Figure 11. For Ar and He, the variation in enthalpy with temperature is linear up to the point when ionization occurs (above 14,000 K for Ar and 18,000 K for He). For H_2, there is a steep variation in enthalpy occurring between 2,000 and 5,000 K due to dissociation. The specific heat at constant pressure, c_p, of Ar and He is constant below their respective ionization temperatures. For H_2, the c_p is not constant due to dissociation which occurs at approximately 4,000 K and ionization at 16,000 K.

2.1.3 Transport properties of thermal plasmas

Viscosity

The viscosity of plasmas are significantly higher than the viscosity of the same gases at room temperature, approximately ten times higher. The consequences of this fairly high viscosity is the difficulty to introduce products into thermal plasmas [Boulos *et al.*, 1983].

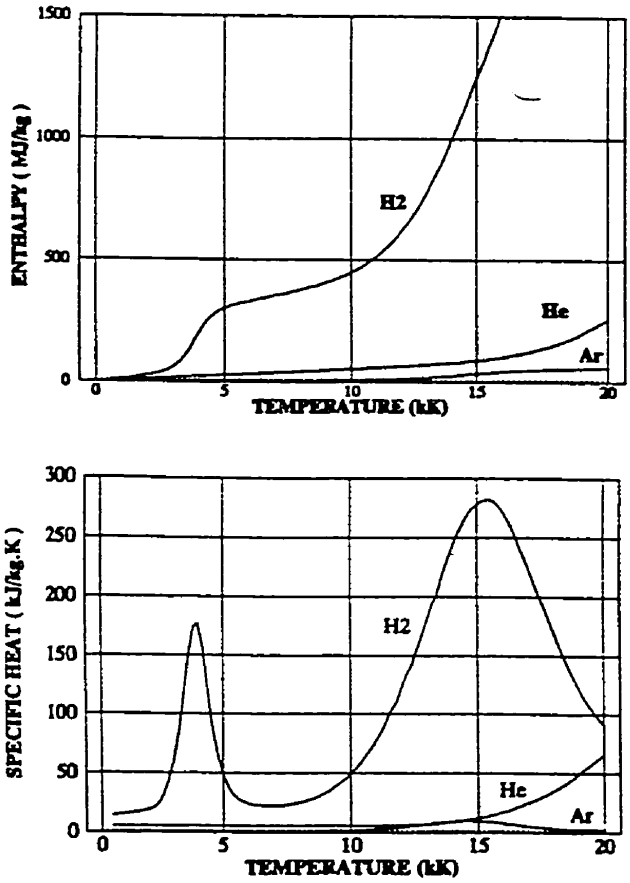

Figure 11: Specific mass enthalpy (top) and specific heat (bottom) of argon, hydrogen and helium as a function of temperature [Pateyron *et al.*, 1992].

The dependence of the viscosity of argon, hydrogen and helium on temperature is shown graphically in Figure 12. The viscosity of plasmas increases with temperature, up to a maximum at the ionization temperature. Above the ionization temperature, the viscosity decreases as a function of temperature.

Figure 12 also demonstrates that He has a higher viscosity that Ar and H_2, especially at higher temperatures.

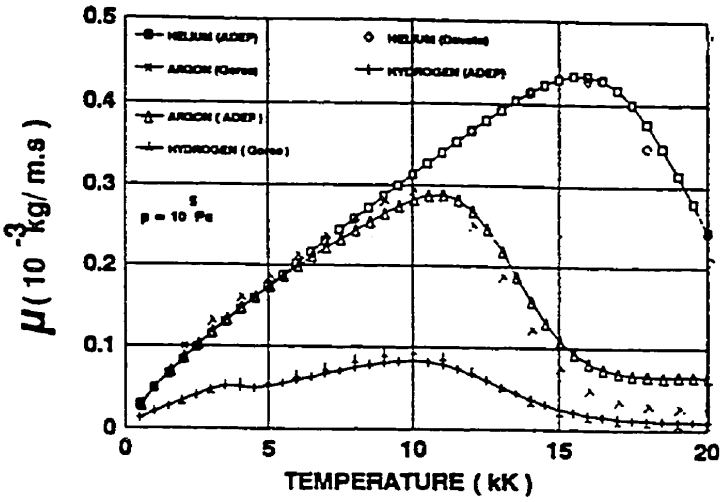

Figure 12: Molecular viscosity, μ, of Ar, H_2 and He as a function of temperature [Pateyron *et al.*, 1992].

Electrical Conductivity

In the presence of an electric field, transport within a plasma occurs by electric charges which constitute an electric current. The electrical conductivity of a gas is influenced by its ionization energy. Since Ar and H_2 have similar ionization energies, they consequently have comparable electrical conductivities, in the order of 30 $(\Omega \cdot cm)^{-1}$ at 10,000 K. At the same temperature, He has a low electrical conductivity of 5 $(\Omega \cdot cm)^{-1}$ due to its high ionization energy [Pateyron *et al.*, 1992].

Thermal Conductivities

At high temperatures, dissociation and ionization phenomena occur, resulting in a large contribution to energy transport. When a diatomic gas is dissociated and ionized in a high temperature zone, resulting species diffuse to the cooler regions. This results in a transport of chemical energy which is accounted for as reaction conductivity. In addition to the reaction conductivity, thermal conductivity is also comprised of the internal thermal conductivity of the gas (vibrational, rotational, electronic excitation) and the translational thermal conductivity. The thermal conductivities of pure Ar, H_2 and He are shown in Figure 13. It can be seen that the thermal conductivity of H_2 is by far the highest due to dissociation at 3,700 K.

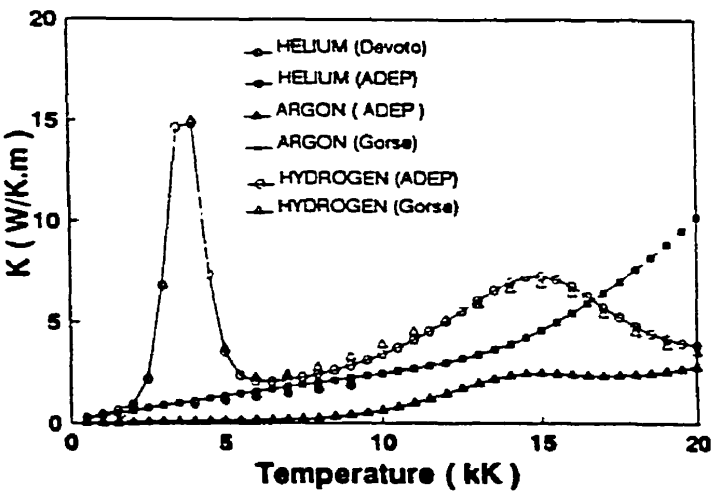

Figure 13: Thermal conductivity of Ar, H_2 and He as a function of temperature [Pateyron *et al.*, 1992].

2.2 Plasma Dissociation of Halogenated Hydrocarbons

As seen in the previous chapter, the synthesis of fullerenes is essentially accomplished via the utilization of plasma. Fullerenes have been produced through the vaporization of graphite in electric arcs and by the plasma pyrolysis of acetylene, benzene or naphthalene. In this section, recent work relating only to the plasma dissociation of halogenated hydrocarbons will be discussed since such information is of value for understanding possible reactions which may occur in the *PyroGenesis* process.

2.2.1 Pyrolysis of chlorofluorocarbons

The pyrolysis of chlorofluorocarbons (CFC's) has become an area of intense scientific research due to their prevalence in toxic wastes emitted by high-temperature incinerators. The thermal plasma approach for the decomposition of CFC's is very attractive since plasmas provide very high temperatures, high energy densities, along with an ionized and reactive medium which can increase the kinetics of some reactions.

The plasma decomposition of CCl_2F_2 has been actively investigated by Sekiguchi *et al.* [1991], using a thermal argon plasma generated by a d.c. discharge. The authors performed a thermodynamic analysis for several reaction systems,

including C-Cl-F-Ar (0.3 mol CCl_2F_2, 10 mol Ar). According to their calculations, CCl_2F_2 is decomposed into atomic species, C, F and Cl, above 5,000 K. CF_4, CF_2 and solid carbon were found to be major products below 2,000 K. When H_2 and O_2 were added to the reaction system, there was no solid carbon formation and no halocarbon (CF, CF_2 and CF_4) formation. As part of the same work, experimental evidence confirmed that when H_2 and O_2 were added to the reactor, soot was not produced. CO and CO_2 were the dominant carbon species at lower temperatures.

In 1989, Wakabayashi *et al.* studied the decomposition of CCl_3F by r.f. plasma. The decomposition of CCl_3F was greatly improved at elevated power levels, resulting in the production of fine particles of soot, which deposited on the reactor wall. The addition of water also resulted in an increase of CCl_3F decomposition, however CO and CO_2 were produced instead of solid carbon, as confirmed by Sekiguchi *et al.* Based on the information revealed by the *PyroGenesis* process for fullerene formation, it is quite likely that fullerenes were present in the soot produced by Wakabayashi *et al.* in the absence of H_2O.

2.2.3 Pyrolysis of tetrachloroethylene (C_2Cl_4)

The pyrolysis of tetrachloroethylene was investigated by Ballschmiter *et al.* [1986].

A multitude of organic compounds were found, including mostly aromatic compounds such as, hexachlorobenzene, octachlorostyrene, octachloronaphthalene and octachloro-acenaphthene. The authors state that the formation of such compounds occurs via a free radical mechanism, resulting from the cleavage of C-Cl bonds. Furthermore, it seems that the formation of complex mixtures, even when starting with only one precursor, is typical for the high temperature chemistry of organohalogen compounds.

Tirey *et al.* [1990] have also studied the formation of chlorinated aromatic compounds resulting from the pyrolysis of tetrachloroethylene. Tetrachloro-ethylene was chosen for this study because it has been identified as a common intermediate in all previous studies in which chlorinated aromatic species were observed.

Tirey *et al.* observed minimal decomposition of tetrachloroethylene below 800 °C. The observed reaction intermediates were divided into three classes:

(I) Low yield C_1-C_4 chlorocarbons, such as carbon tetrachloride (CCl_4), hexachloropropene (C_3Cl_6) and C_4Cl_6, which formed and decomposed between 700-900 °C.

(II) High yield, very stable aromatic species, such as hexachlorobenzene (C_6Cl_6) and octachloroacenaphthalene ($C_{12}Cl_8$).

(III) Very low yield, stable aromatic species, such as octachlorostyrene (C_8Cl_8) and octachloronapthalene (C_8Cl_{10})

Figure 14 summarizes the concentration of reaction products as a function of temperature.

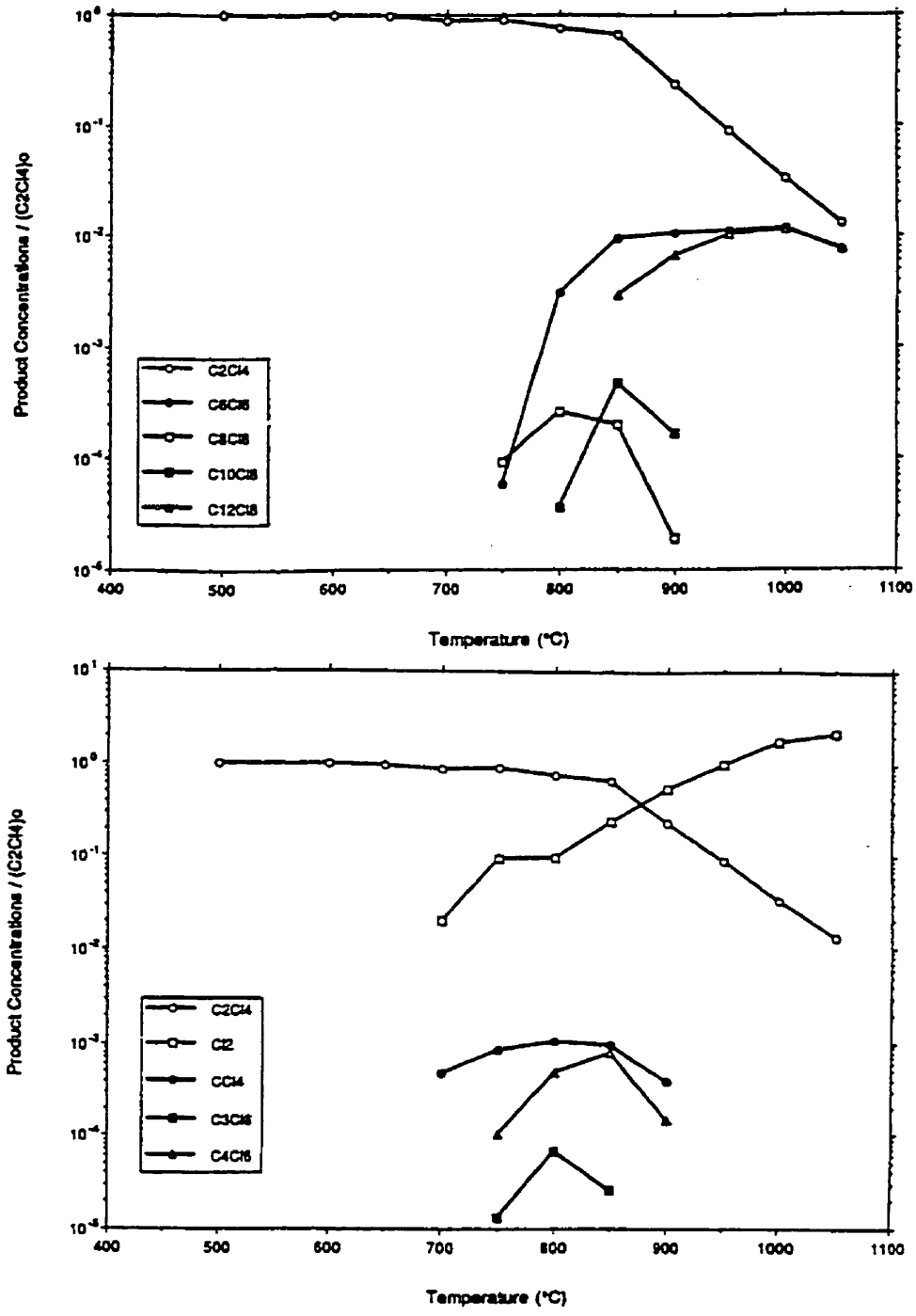

Figure 14: Reaction yields of pyrolysis products as a function of temperature.

EXPERIMENTAL

CHAPTER 3:
APPARATUS AND INSTRUMENTATION

3.1 Fullerene Soot Production

Figure 15 presents a schematic of the overall soot production system. Fullerene soot was produced in a spherical, water-cooled reactor equipped with a non-transferred d.c. plasma torch. Using helium as the inert plasma-forming gas, the plasma torch was operated between 35 and 70 kW. The carbon-bearing gas was introduced into the plasma at the torch exit through a nozzle. A condenser [not shown], referred to as the quench zone in the text, is located below the reactor. The quench zone consists of a water cooled coil onto which additional products are removed from the exhaust gas prior to entering the vacuum pump. Leaving the vacuum pump, the exhaust gas enters a burner where remaining soot particles or other organic material present in the exhaust gas are combusted. The exhaust gas from the burner enters a scrubber where HCl is removed. The system is equipped with a control console from which the plasma gas flow rate, current, torch cooling water flow rate, and reactor pressure are monitored and controlled. The hydrocarbon flow rate is controlled by a rotameter connected to a peristaltic pump. A data acquisition system is in place to monitor all of the process

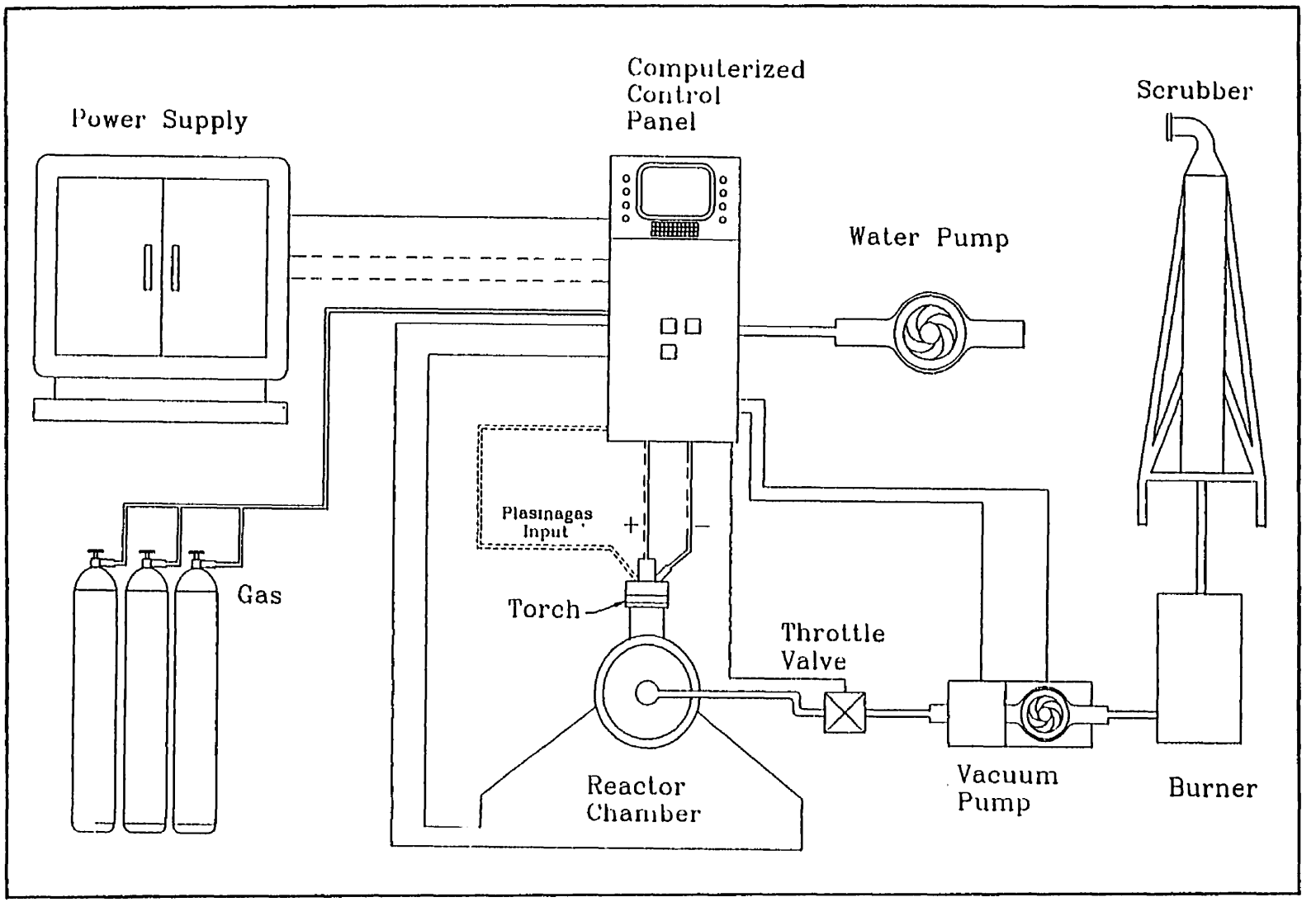

Figure 15: Schematic of the overall fullerene soot production system.

parameters during operation.

3.1.1 Reactor Assembly

A schematic of the reactor assembly is shown in Figure 16. The reaction chamber, or *reactor* as referred to in the text, is a spherical, double-walled stainless steel vessel with an internal diameter of 12 inches. The gas leaving the reactor then enters the *quench zone*; a stainless steel receptacle consisting of water-cooled coils, where the products remaining in the exhaust gas condense. The reactor has an extended neck on its lower hemisphere, where the plasma torch was mounted. Seven ports (0.5 in. ID), used for thermocouples, were located throughout the surface of the reactor wall. During soot production experiments (Chapter 6), thermocouples were inserted in ports A and B, whereas all ports were used during the temperature mapping experiments (Chapter 9). A view port is located on the top hemisphere, but unfortunately the location of this port was not appropriate for viewing the plasma flame. A photograph of the system is shown in Figure 17.

3.1.2 Plasma torch

A non-transferred d.c. plasma torch was used for the dissociation of the hydrocarbon gas. The hydrocarbon was introduced into the plasma at the torch

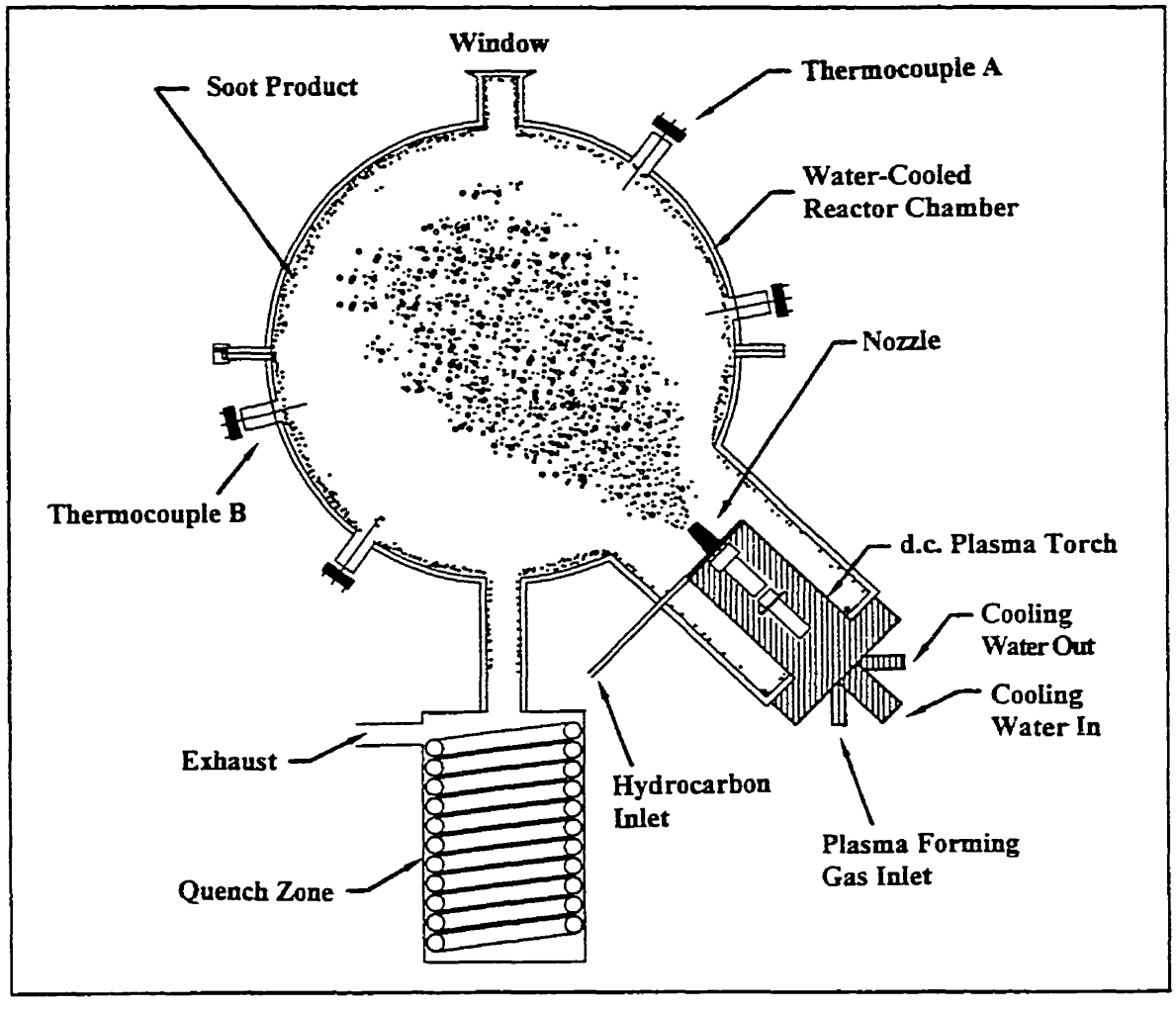

Figure 16: Schematic of *PyroGenesis* reaction vessel.

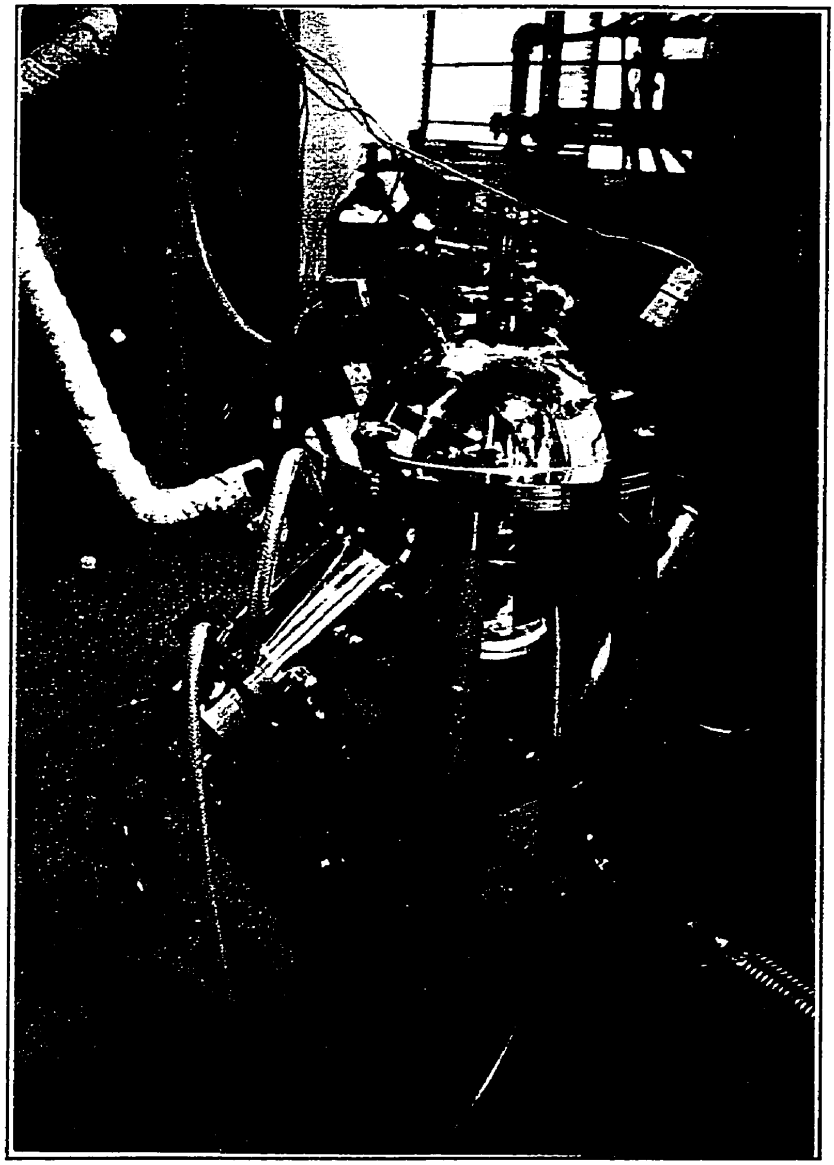

Figure 17: Photograph of *PyroGenesis* reactor assembly.

exit through a nozzle. A cross-sectional view of the plasma torch and nozzle is shown in Figure 18. The torch, consisting of tubular type electrodes, was operated in reverse polarity such that the cathode, instead of the anode as in many other torches, is located at the torch exit. The anode and cathode were made of molybdenum and thoriated tungsten, respectively. The arc was stabilized aerodynamically by introducing the plasma forming gas through a perforated annular ring, located between the two electrodes. Using helium as the inert plasma-forming gas, the plasma torch was operated between 35 and 70 kW. The nozzle, made of thoriated tungsten, was 2.6 cm in length with an exit opening of 1 cm in diameter. The hydrocarbon gas was introduced into the nozzle through an annular ring having 3 openings, each having a diameter of 2 mm.

3.1.3 Hydrocarbon feed system

The hydrocarbon feed system consisted of the following components:

- a peristaltic pump for C_2Cl_4 delivery
- a rotameter
- a liquid vaporizer
- a gas heating line for the inert carrier gas
- a heated, insulated line introducing the mixture of inert gas and hydrocarbon to the torch nozzle

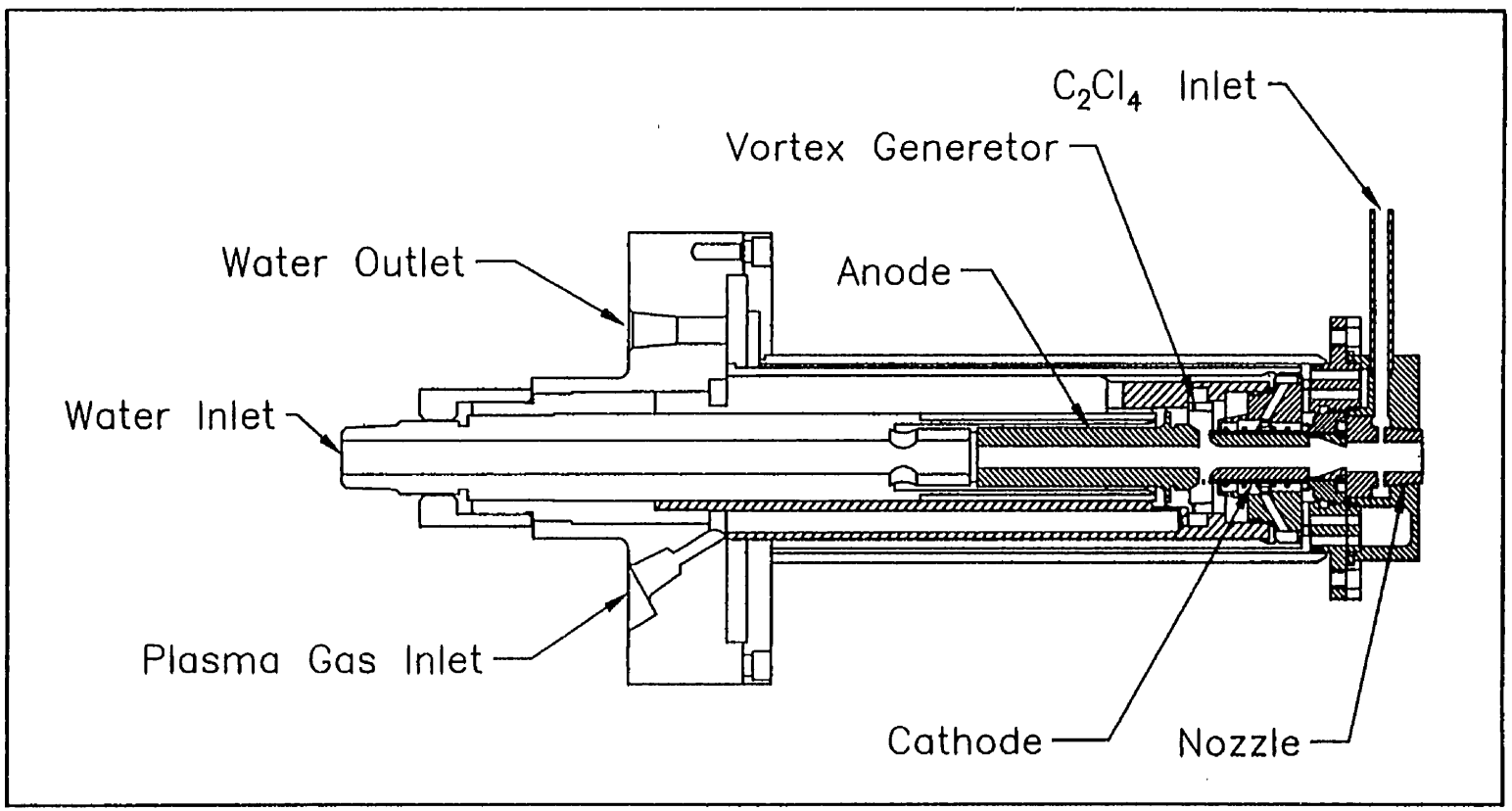

Figure 18: Cross-sectional view of plasma torch.

C_2Cl_4 was delivered to the liquid vaporizer, or hot box, by a peristaltic pump, through a rotameter, which controlled the flow rate from 15 to 54 ml/min. The temperature of the vaporizer was approximately 200 °C. Upon exiting the vaporizer, the C_2Cl_4 vapour was diluted with preheated inert gas prior to being introduced into the torch through a nozzle. The flow rate of the carrier gas (helium) was maintained at 20 slpm for all experiments. The temperature of the hydrocarbon gas mixture was maintained at 172 ± 11 °C.

3.1.4 Exhaust gas clean-up system

A tubular vessel approximately 46 cm in length and 10 cm in diameter, lined with refractory, was used as an after burner for the treatment of chlorinated aromatic compounds which may have been present in the off-gas. A Honeywell flame ignition and detection system (Model No. 7795) was used for this application. The CH_4 and O_2 flow rates were controlled by calibrated rotameters.

A scrubber, packed with Intalox ceramic saddles (25 mm), was used to remove HCl from the off-gas stream prior to exhausting the off-gas. The water from the scrubber was neutralized with NaOH prior to discharge. During normal operation, the exhaust gas was colourless and did not smell of chlorine gas and thus the operation of the exhaust gas clean up system was assumed to be satisfactory.

3.1.5 Auxiliary Equipment

3.1.5.1 Power Supply and Arc Ignition

Power was supplied to the non-transferred plasma torch by a Hypertherm (H-601) six-pulse thyristor controlled rectifier. The arc was ignited by providing the arc gap momentarily with a high frequency pulse from a Miller (2000) spark inductor. The power supply operates at constant current and has the following electrical specifications:

open circuit voltage:	400 V
maximum current:	1,000 A (600 A @ 100% duty)
maximum power:	120 kW (100% duty, 200 V, 600 A)

In order to avoid problems during start-up and operation, the torch body was well grounded and a contact block disconnected the voltage and ampere signals going from the power supply to the data acquisition system.

3.1.5.2 Cooling Systems

De-ionized cooling water for the torch, reaction system and burner was delivered by a Gould's 3196 pump. The torch cooling water flow rate was fixed at 32.3 l/min. The reactor cooling water flowed through the coil of the quench zone first and then entered the reactor wall following a spiral path around the reactor. The flow of the reactor cooling water was maintained at 25.3 l/min. The flow rate

of each cooling water circuit was regulated by valves and monitored by calibrated rotameters. Calibration of the rotameters was made using the "bucket and stopwatch" method.

3.1.5.3 Control Console and Data Acquisition System

The rectifier was connected to a control console from which the power input was controlled by varying the arc current through a regulator. The high-frequency generator was also activated through the control console. The control console also consisted of a voltmeter, an MKS mass flow meter for controlling the plasma gas, a pressure controller (VAT, PM-3), and rotameters for monitoring the torch cooling water and inert carrier gas flow rates. All data, including voltage, current, pressure, gas flow rate, cooling water temperatures and reactor temperatures were recorded by a data acquisition system, consisting of a DAS-8 plug-in board with 2 EXP-16 multiplexers for the thermocouples.

3.1.5.4 Thermocouples

During soot production experiments, the temperature near the reactor wall (4 mm from the surface), was measured by two stainless steel, K-type thermocouples (Ni-Cr, Ni-Al), protected by a ceramic sheath. The ceramic sheath was required because Cl_2 produced during experiments was detrimental to stainless steel sheaths. The location of the thermocouples is shown in

Figure 16.

For the temperature mapping experiments (Chapter 8), when no hydrocarbon was injected into the system, the temperature of the surface was measured by six, stainless steel, K-type thermocouples. The thermocouples were bent and securely tightened to make contact with the surface. When tightened securely, the thermocouples did not detach from the surface during operation.

3.1.5.5 Vacuum pump

A Kinney Liquid Ring Pump (KLRC-75) water ring vacuum pump, coupled with a VAT Adaptive Pressure Controller, was used to automatically control the pressure in the reaction chamber from 100 to 400 torr. The pressure was constant within 12 torr during operation

3.2 Extraction and Purification of fullerenes

For the extraction and purification of fullerenes, the following equipment and instruments were used:

- a Bransonic 8210R-MT (VWR Scientific) ultrasonic bath, for promoting mixing of the soot particles with toluene during the extraction process;

- a Caframo VV2000 rotary evaporator, for the evaporation of solvents;
- a standard glass chromatography column (3.8 cm ID) with pressure adapter, for the purification of C_{60};
- a SOXHLET type chromatography column (3 cm ID) for the purification of C_{70};
- a high vacuum manifold (10^{-3} torr), equipped with a Balzers Rotary Vane Pump, for drying solid samples in analytical work;
- an alumina, vacuum furnace used for the by-product removal experiments; and,
- a Mettler AE200 analytical balance having a precision of 0.1 mg and accuracy of ± 0.3 mg, used for measuring the weight of samples.

3.3 Quantification of Fullerenes via HPLC

For the quantification of fullerenes, High Performance Liquid Chromatography (HPLC) was carried out on a Waters 600EP multisolvent system equipped with a UV/VIS detector. For the quantification of C_{60} and C_{70}, an analytical μBondapak reverse-phase silica gel column (Waters) was used for the stationary phase with a mixture of toluene and methanol as the mobile phase. The

quantification of higher fullerenes required the used of a Buckyclutcher analytical column (Regis) as the stationary phase with a mixture of toluene/hexane as the mobile phase. The system was equipped with a manual sample injector. A computer was used to run the Millennium 2000 software program, which was used to control the operation of the HPLC.

3.4 Identification of by-products via GC/MS

A Hewlett Packard 5890 Series 2 gas chromatograph (GC) coupled with a Hewlett Packard 5970B Electron Impact Mass Spectrometer (MS) was used for the identification of the by-products present in the *PyroGenesis* soot. The gas chromatograph was equipped with an HP1 capillary column (0.2 mm ID, 29 m L) having a film of cross-linked methyl silicon gum phase, 25 μm in thickness.

Data acquisition and analysis was accomplished with the aid of an HP 59970 ChemStation and the accompanying system software which includes on-line NIH-EPA mass spectral library. Only species with molecular weights between 16 and 450 were detected by this system

CHAPTER 4:
PROCEDURES AND ANALYSIS

4.1 Operation of Soot Production System

Before each soot production run, the reaction system was evacuated by reducing the pressure to approximately 10 torr and backfilling with argon [Cannox, HP]. The burner was then ignited and the flows of the torch and reactor cooling water, scrubber water and NaOH solution were initiated. The pressure in the reaction system was set to the desired value. A flow of 60 slpm of argon was used for torch ignition. Once an arc was generated by the high-frequency generator and a stable arc attachment was obtained, the plasma gas was switched to helium [Cannox, UHP] and the flow rate was adjusted to 225 slpm. After the temperature in the reactor stabilized, preheated C_2Cl_4 [BDH, >99.%] vapour diluted with 20 slpm of helium was introduced into the plasma flame by opening the appropriate valves. The fixed operating parameters are listed in Table 2.

The duration of each experiment was between 1 and 8 minutes, depending on the purpose of the experiment. Once each experiment was completed, the reactor was re-pressurised, the C_2Cl_4 flow was terminated and the torch was turned off. The plasma gas flow was terminated and the burner was shut off. The system was then allowed to cool before the reactor was opened for inspection. The soot

deposit on the reactor wall and quench zone was brushed into pre-weighed containers for extraction and analysis. The soot in the reactor and quench zone was collected and analyzed separately for all experiments.

Table 2: Fixed parameters during experimental soot production runs

Plasma forming gas	Helium
Plasma forming gas flow rate	225 slpm
Carrier gas	Helium
Carrier gas flow rate	20 slpm
Torch cooling water flow rate	32.3 l/min
Reactor cooling water flow rate	25.3 l/min
Run duration	4 min

4.2 Extraction of Fullerenes from Soot

The fullerenes were extracted from the soot by placing a suspension (1 mg/ml) of soot in toluene [BDH, ACS] into a sonication bath for 30 minutes. The resulting mixture was then filtered over a filtering agent [Celite 521, Aldrich], in a sintered glass funnel, to obtain a red-brown solution of crude extract. During the filtration process, additional solvent was added until the droplets of filtrate were clear, thus ensuring complete extraction. The solvent was then evaporated

via rotary evaporation to yield a brown-black solid of crude extract.

The weight of soot produced during each experiment was measured. All samples of crude extracts were dried under high vacuum prior to taking the weight. The percent extraction was calculated as follows:

$$\%Extraction = \frac{Weight\ of\ crude\ extract}{Weight\ of\ soot} * 100$$

4.3 Quantification of Fullerenes via HPLC

4.3.1 Quantification of C_{60} and C_{70}

Once the crude extract was obtained from the extraction process, a known concentration of extract in toluene was prepared for analysis by HPLC. The following operating conditions were used for the quantification of C_{60} and C_{70}.

Solvent system:	methanol/toluene [BDH, Onmisolv]
Injection volume:	20 μl
Flow rate:	2 ml/min
Detection wavelength:	330 nm

The instrument was calibrated for the quantification of fullerenes using standards of C_{60} and C_{70} [SES, 99.9%]. A typical chromatogram for extract produced via

this process is shown in Figure 19. Under the HPLC operating conditions listed above, C_{60} and C_{70} elute at 7.4 and 10.4 minutes, respectively. The area under each peak in the chromatogram, expressed in units of $\mu V \cdot s$, is proportional to the concentration of a particular compound in the injected sample.

4.3.2 Error Analysis

An estimation of the sampling, analytical and experimental errors was made and may be found in Appendix A. Because only a representative sample of the soot produced in each experiment underwent solvent extraction and analysis by HPLC, there was the possibility that sampling error exists. To avoid sampling error, the soot collected from each experiment was mixed thoroughly before a sample of soot was taken for analysis. From the statistical analysis of variance, shown in Table A (Appendix A), the sampling error does not seem to be significant within a confidence interval of 99%. The analytical error, which includes sampling error, was evaluated in Table B (Appendix A), using three samples of soot taken from the same experiment. The analytical error was determined to be 3.5% The experimental error was determined from three different experiments performed under the same operating conditions. The error was found to be 6.8%, as seen in Table C (Appendix A). Therefore, the maximum total error was estimated to be 10.3%.

Millennium Sample Information

Project Name:	**Production**		
Sample Name:	**B39 R 500 5**		
Vial:	**1**	**Sample Type:**	**Unknown**
Injection:	**1**	**Volume:**	**20.00**
Channel:	**486**	**Run Time:**	**15.0 min**
Date Acquired:	**07/10/95 09:05 AM**	**Date Processed:**	**07/10/95 09:47 AM**
Scale Factor:	**1.00**	**Dilution:**	**1.00000**
Acq Meth Set:	**330 55 45 0 av mst set**		
Processing Method:	**330 55 45 0 av proc mst**		

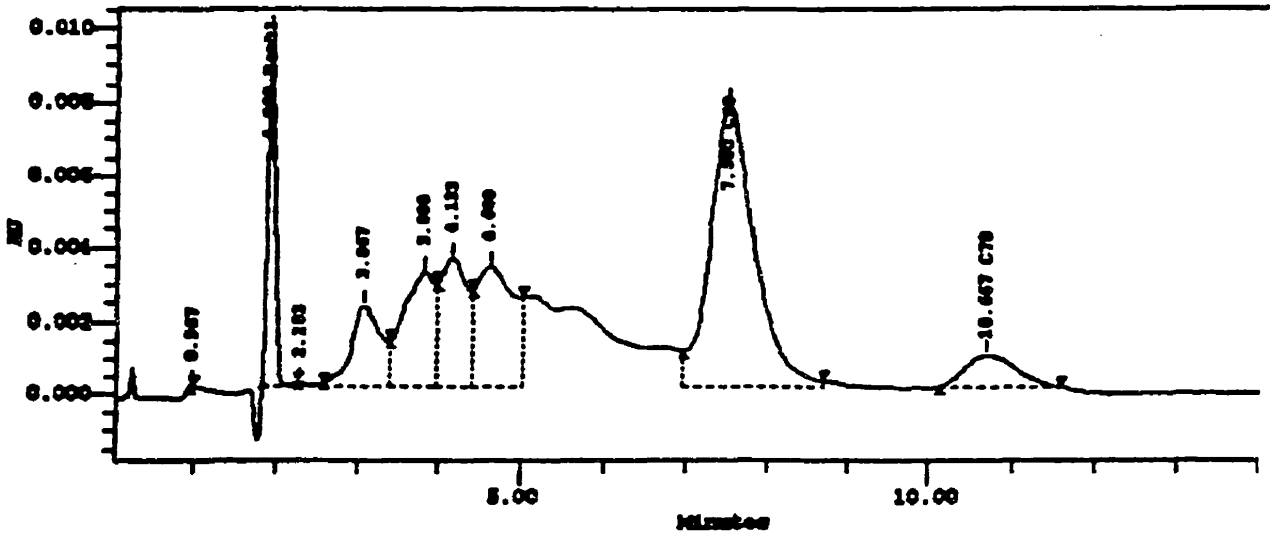

Peak Results

#	Name	Ret Time (min)	Area (mV*sec)	Height (mV)	Amount	Int Type
1		0.967	26	16		BB
2	Peak1	1.900	61819	9701		BV
3		2.283	1318	102		VV
4		3.067	57028	2190		VV
5		3.800	82800	3106		VV
6		4.133	79702	3478		VV
7		4.600	104810	3245		VB
8	C60	7.500	297332	7766	0.008	BB
9	C70	10.667	38512	899	0.002	BB

Figure 19: Typical chromatogram of *PyroGenesis* crude extract (reverse-phase C_{18} column).

4.4 Purification of C_{60} and C_{70}

To facilitate purification by chromatography, a number of techniques were investigated for the removal of by-products from the fullerene crude extract prior to column chromatography. These techniques are described in detail in Appendix B.

The purification method developed by Scrivens *et al.* [1992] was used during this work, for the purification of C_{60} from *PyroGenesis* soot. A mixture of activated carbon [Norit® SA3, 100 mesh, Aldrich] and silica gel 60 [40-63 μm, Caledon], in a ratio of 2:1 was used as the stationary phase and toluene was used as the mobile phase. A glass column (3.8 cm ID) was used for this work. A slight pressure of argon above the solvent was used to control the flow of toluene at 1.4 cm/min. The column height was varied from 20 to 30 cm. Approximately 4 grams of crude extract was added to the column as a saturated solution in toluene.

For the purification of C_{70}, the red fraction obtained from the Norit A/Silica Gel column was loaded onto a SOXHLET chromatography column packed with neutral alumina [63-150 μm, Selecto Scientific]. Hexane was used as the mobile phase. The C_{70} enriched fraction was added to this column by adsorbing the

sample onto alumina through the use of rotary evaporation.

4.5 Confirmation of C_{60} and C_{70} structures

Mass spectrometry and C^{13} Nuclear Magnetic Resonance (^{13}C NMR) were the selected analytical methods used to determine, with certainty, the presence of C_{60} and C_{70} in the soot produced during this work.

4.5.1 Mass Spectrometry

The presence of C_{60}, C_{70} and higher fullerenes was first detected by Fast Atom Bombardment (FAB) Mass Spectrometry. A typical mass spectrometry scan of *PyroGenesis* crude extract is shown in Figure 20. The peaks at atomic masses of 720 and 840 correspond to C_{60} and C_{70}, respectively. The higher fullerenes ranging from C_{74}-C_{98} are also present in the soot as can be seen by the atomic mass peaks ranging from 888 to 1176.

4.5.2 C^{13} Nuclear Magnetic Resonance (^{13}C NMR)

C^{13} Nuclear Magnetic Resonance (^{13}C NMR) measurements were made on sample of C_{60} and C_{70} dissolved in benzene. C_{60} was purified by column chromatography as described later in Section 9.3.1, and was over 99% pure. The NMR spectrum of C_{60} is Shown in Figure 21. The signal at 143.6 ppm is

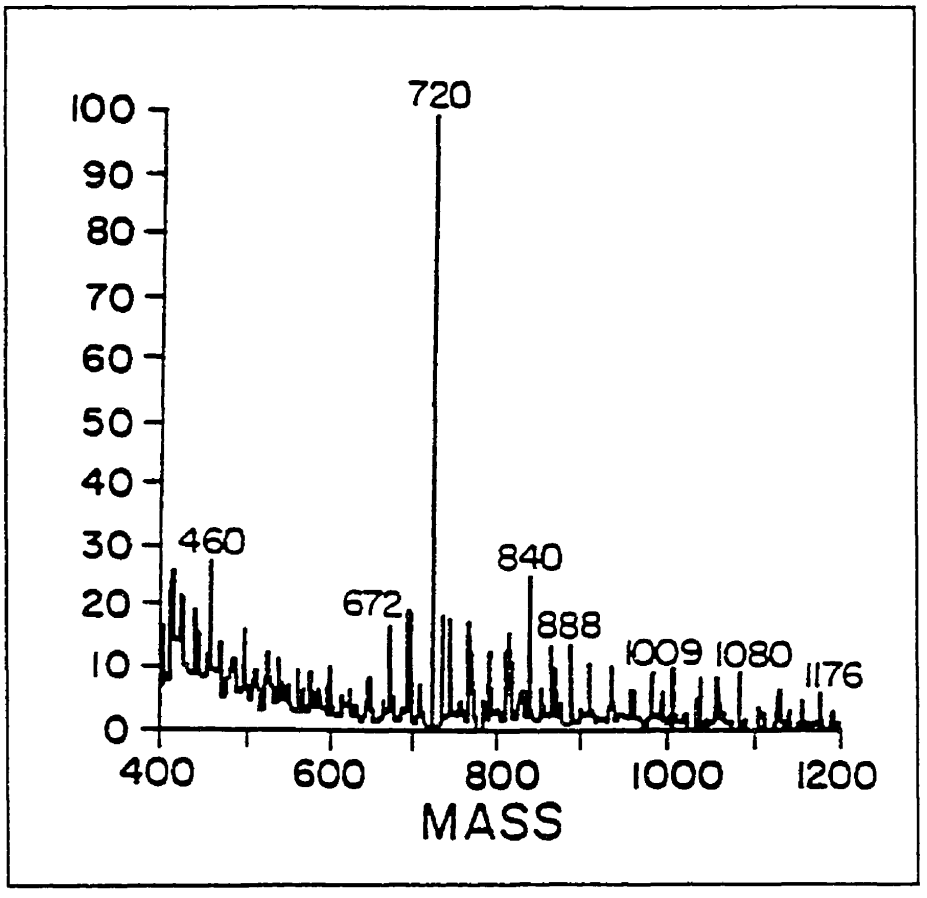

Figure 20: FAB Mass Spectrum of *PyroGenesis* soot.

assigned to C_{60} and is in good agreement with other NMR studies [Ajie *et al.*, 1990]. The peak at 128.4 ppm corresponds to the solvent, benzene. The signal at 30.6 ppm possibly corresponds to a chlorinated by-product or an impurity.

The NMR spectrum for C_{70} is shown in Figure 22. The purity of the C_{70} sample was 92%, as purified by the methods described in Section 4.4. Five weak lines at 151.0, 148.5, 147.8, 145.8 and 131.2 ppm are in good agreement with the 10, 20, 10, 20, 10 intensity ratio published by Ajie *et al.* [1990]. The peak at 143.6 ppm corresponds to C_{60}, which is an impurity in the C_{70} solution.

The NMR measurements in addition to the mass spectral data confirm that the products produced by the *PyroGenesis* process, C_{60} and C_{70}, are identical in structure as the molecules produced via the arc vaporization of graphite method.

4.6 Identification of by-products via GC/MS

For the identification of some of the by-products produced during the *PyroGenesis* process, fractions of products were collected during chromatographic purification by HPLC. Several injections of the same sample of crude extract were made in order to collect sufficient quantities of each fraction for analysis by gas chromatography coupled with mass spectrometry. The fractions collected were

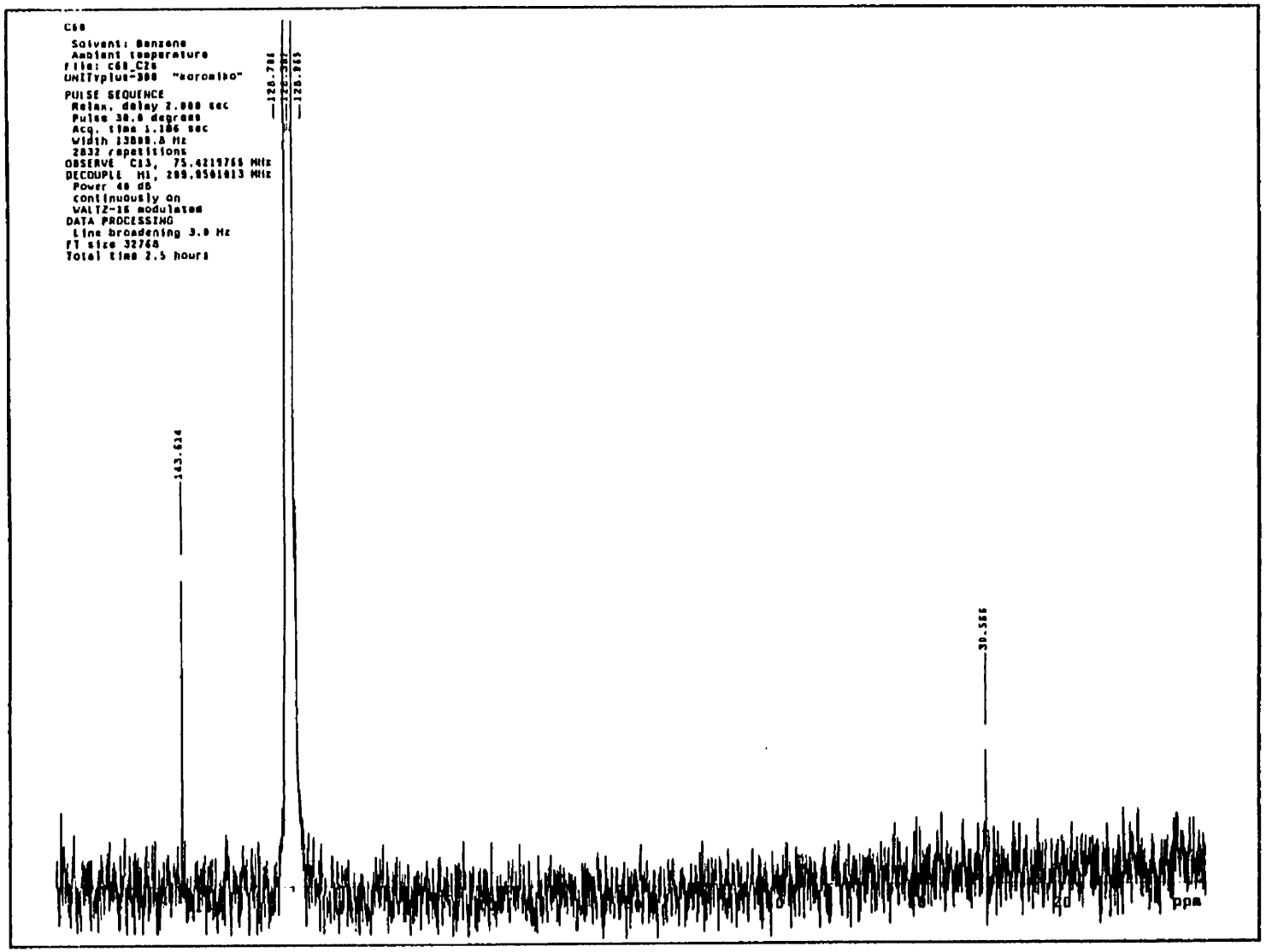

Figure 21: ^{13}C NMR Spectrum of C_{60} in benzene.

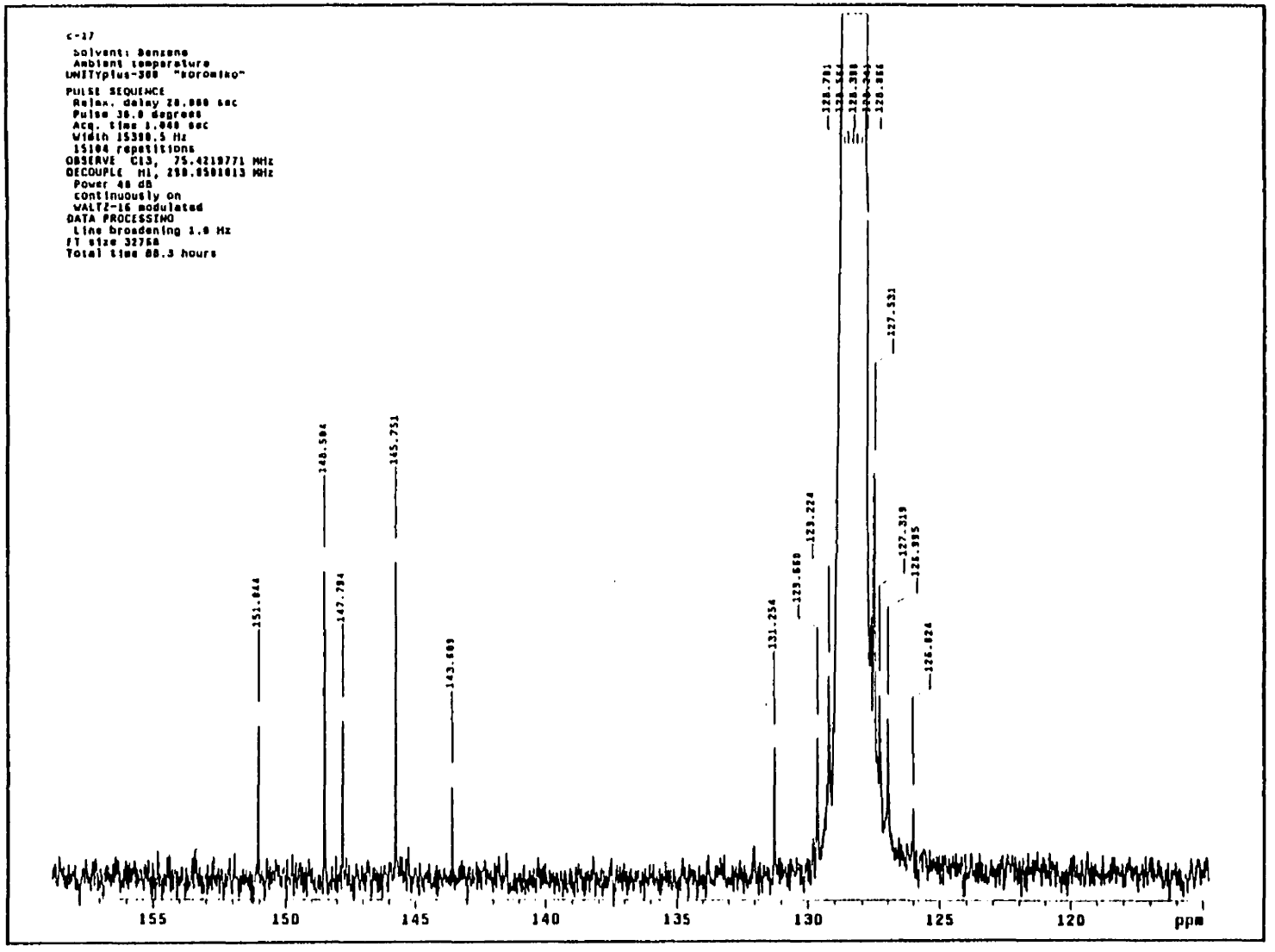

Figure 22: ^{13}C NMR Spectrum of C_{70} in benzene.

concentrated via rotary evaporation. Because of the small quantities of samples collected, this work could only produce qualitative results.

Mass spectral acquisition was initiated from the moment of injection of each sample. Because standards for the "observed" compounds could not be obtained for calibration of the instrument, the database and manual determination of the structure of potential compounds was considered adequate. As a result, this work only provides a qualitative analysis of the types of products obtained via the thermal pyrolysis of C_2Cl_4 and cannot be used to quantify or conclusively determine the existence of these products in the soot produced.

RESULTS and DISCUSSION

CHAPTER 5: SELECTION OF HYDROCARBON FOR FULLERENE SYNTHESIS

A thermodynamic analysis was performed in an attempt to understand the dissociation pattern of hydrocarbons at high temperatures. A good understanding of high temperature chemistry allows one to predict the starting chemistry which would most likely favour fullerene formation. The thermodynamic analysis was made using a Gibbs free energy minimization method. Calculations were made using the computational program HSC Chemistry for Windows Version 2.03 (Outokumpu Inc.).

In thermal plasma chemistry, equilibrium calculations are usually insufficient for predicting the composition of products, due to the short residence time of the reactants in the plasma. Furthermore, the calculation of equilibrium concentrations implicitly disregards any kinetic limitations which may play a key role in the formation of certain compounds. As a result, the equilibrium calculations in this work serve as a guide to understanding the chemistry of hydrocarbons at high temperatures, rather than providing an accurate prediction

of product concentrations.

CCl_2F_2 and C_2H_2 were selected as two representative compounds since these materials were previously investigated experimentally as precursors for fullerene production via the *PyroGenesis* process, as described in Section 1.3.4.3. The equilibrium products resulting from the dissociation of CCl_2F_2 and C_2H_2 are shown graphically in Figures 23 and 24, respectively. A list of the species considered in the thermodynamic calculations is shown below each figure. Although helium was considered in the calculations, the equilibrium concentration of helium was omitted in the figures.

Thermodynamic data for C_{60}, obtained from the work of McKinnon [1991] was added to the database of the program. However, as will be seen from the results, equilibrium calculations only predict the formation of solid graphite. Diamond was also excluded in the calculations since it is known that diamond is not produced under the conditions used in the *PyroGenesis* process. The production of diamond is a non-equilibrium process requiring a large quantity of hydrogen for nucleating diamond growth [Martin, 1992].

Figure 23 shows the equilibrium composition, as a function of temperature, of a

mixture of 1 mol CCl_2F_2 and 10 mol He at 760 torr. At 5,000 °C, CCl_2F_2 is almost completely decomposed into atomic species, namely C(g), F(g) and Cl(g). Carbon atoms recombine at temperatures below 5,000 °C to form C_2 and C_3. Recombination of carbon and fluorine species occurs in the temperature range from 1,600 °C to 3,600 °C, with the major products being CF, CF_2 and CF_4. Further recombination occurs below 1,500 °C, resulting in the formation of $CClF_3$.

In Figure 24, the equilibrium products resulting from the decomposition of 0.5 mol C_2H_2 in an atmosphere of 10 mol of He are shown for the temperature range from 1,000 °C to 5,000 °C. Once again, the hydrocarbon molecules are shown to almost completely decompose at 5,000 °C. C_2H and C_2H_2 are stable species at temperatures between 2,200 °C and 4,300 °C. At temperatures below 2,000 °C, polyaromatic hydrocarbons (PAH's) have been reported to be dominant equilibrium products, along with graphite [McKinnon, 1991]. However, PAH compounds were not included in these calculations since such compounds were not listed in the database of the program used.

Using thermodynamic calculations, McKinnon [1991] proposed that fullerenes form between 2,200 K and 2,600 K (1,927-2,327°C) from the combustion of C_2H_2.

Haufler [1994] reports that the temperature range for fullerene formation is 2,200 K to 3,200 K. In the work of McKinnon, it was shown that the C/H and C/O ratios have an important effect on the computed equilibrium concentration of C_{60}. The highest concentrations were predicted when a maximum C/H ratio of 2 was used. Furthermore, the maximum C/O ratio resulted in the highest equilibrium concentration of C_{60}, suggesting the pyrolysis of hydrocarbons should yield higher concentrations of C_{60} than the combustion of hydrocarbons.

In the *PyroGenesis* process, it is conceivable that the presence of hydrogen and fluorine atoms, when using CCl_2F_2 and C_2H_2 as starting materials, would not be favourable for fullerene formation due to the stability of C-F and C-H bonds near the temperature range required for fullerene formation. In fact, experiments using CH_4, C_2H_2, $CBrF_3$ and CCl_2F_2 as starting materials resulted in very low concentrations of fullerenes in soot, as described in Section 1.3.4.3. The highest concentration of fullerenes in soot was obtained when CCl_2F_2 was used as the carbon source. From the thermodynamic results for CCl_2F_2, shown in Figure 23, it seems that although Cl is present in CCl_2F_2, C-Cl bonds are not stable at temperatures above 2,000 °C. As a result, the equilibrium products resulting from the dissociation of chlorinated hydrocarbons at high temperatures was explored.

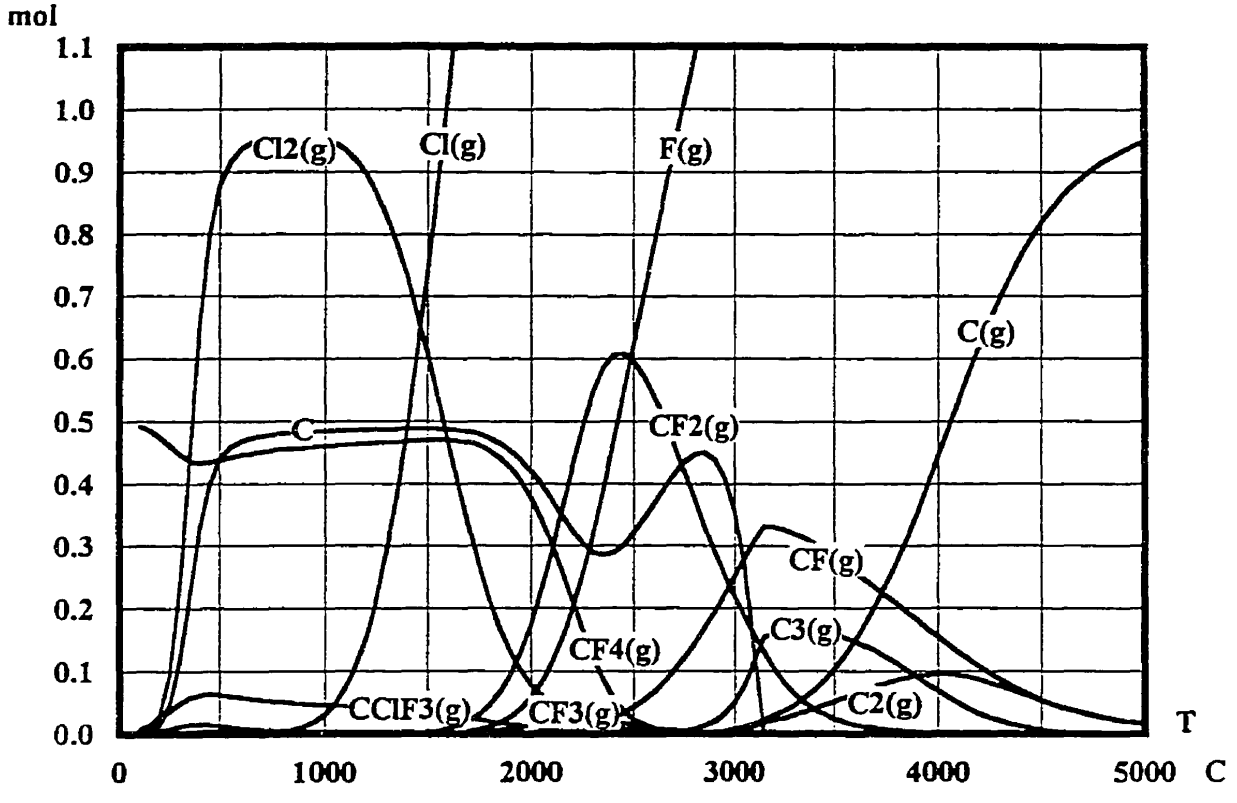

Figure 23: Computed equilibrium concentrations resulting from dissociation of CCl_2F_2 as a function of temperature at 760 torr.

C, C_2, C_3, C_4, C_5, CCl, CCl_2, CCl_3, CCl_4, C_2Cl_2, C_2Cl_4, C_2Cl_6, $CClF_3$, CF, CF_2, CF_3, CF_4, C_2F_2 C_2F_4, C_2F_6, C_6F_6, CF, Cl_3, CCl_2F_2, CF_3Cl, Cl, Cl2, ClF, ClF3, $ClClF_5$, F, F_2, He, C_{60}, C(s)

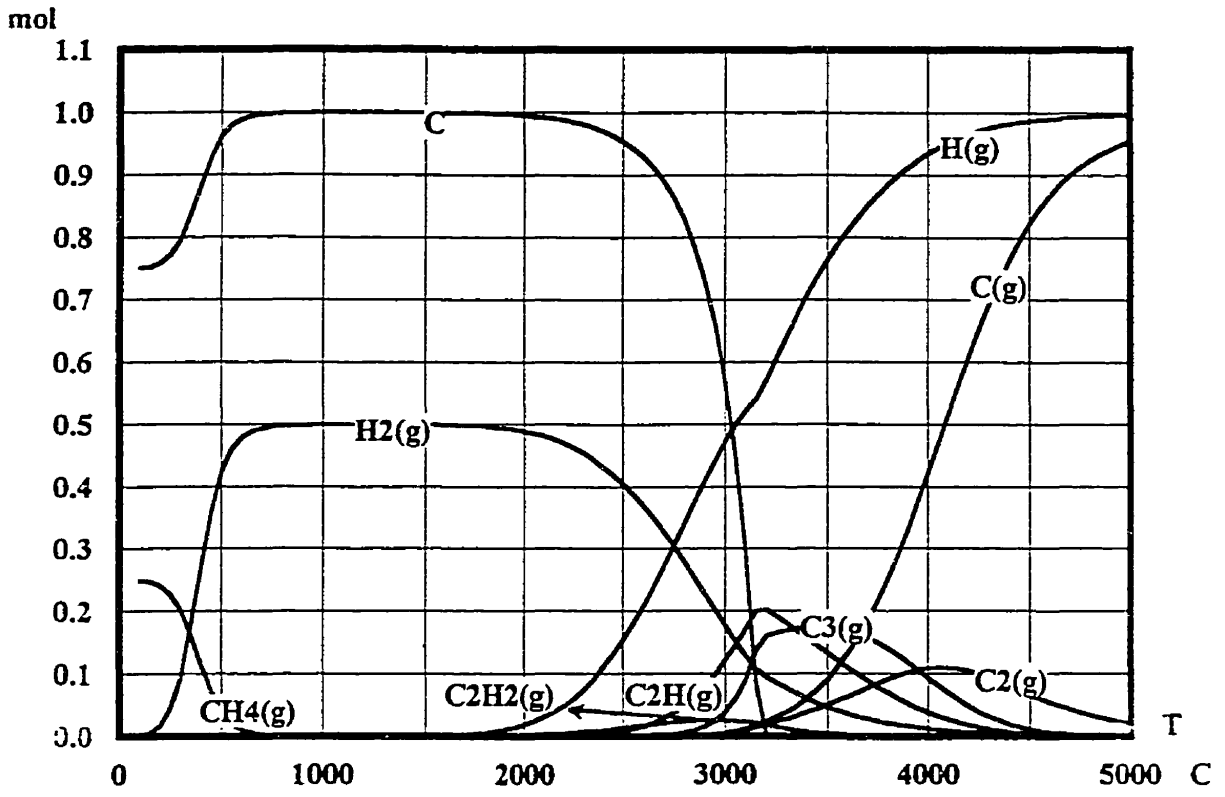

Figure 24: Computed equilibrium concentrations resulting from dissociation of C_2H_2 as a function of temperature at 760 torr.

C, C_2, C_3, C_4, C_5, CH, CH_2, CH_3, CH_4, C_2H, C_2H_2, C_2H_4, C_2H_6, C_3H_4, C_3H_6, C_3H_8, H, H_2, He, C_{60}, C(s)

Tetrachloroethylene, C_2Cl_4, was chosen as a representative compound for predicting the equilibrium products formed in an atmosphere of C and Cl atoms. The equilibrium products formed from the mixture of 0.5 mol C_2Cl_4 and 10 mol He are shown in Figure 25. As seen in the figure, only C-C bonds seem to be stable at high temperatures. As a result, chlorinated hydrocarbons are attractive precursors for fullerene formation via the *PyroGenesis* process since C-Cl bonds are not predicted to be stable in the temperature range required for fullerene formation.

Since the properties of C_{60} were added to the database, an attempt was made to reproduce the results of McKinnon [1991], which predict the temperature range required for fullerene formation. In order to perform these calculations, solid graphite had to be excluded from the list of species, as in McKinnon's work. As was seen in the previous graphs, when graphite is included, equilibrium predicts that all carbon goes to this state. As such, McKinnon suggests that the removal of graphite from the calculations may be seen as the implicit application of a kinetic constraint.

The result of these calculations may be seen in Figure 26. C_{60} is present in the temperature range between 1,500 °C and 2,400 °C. Interestingly, the formation

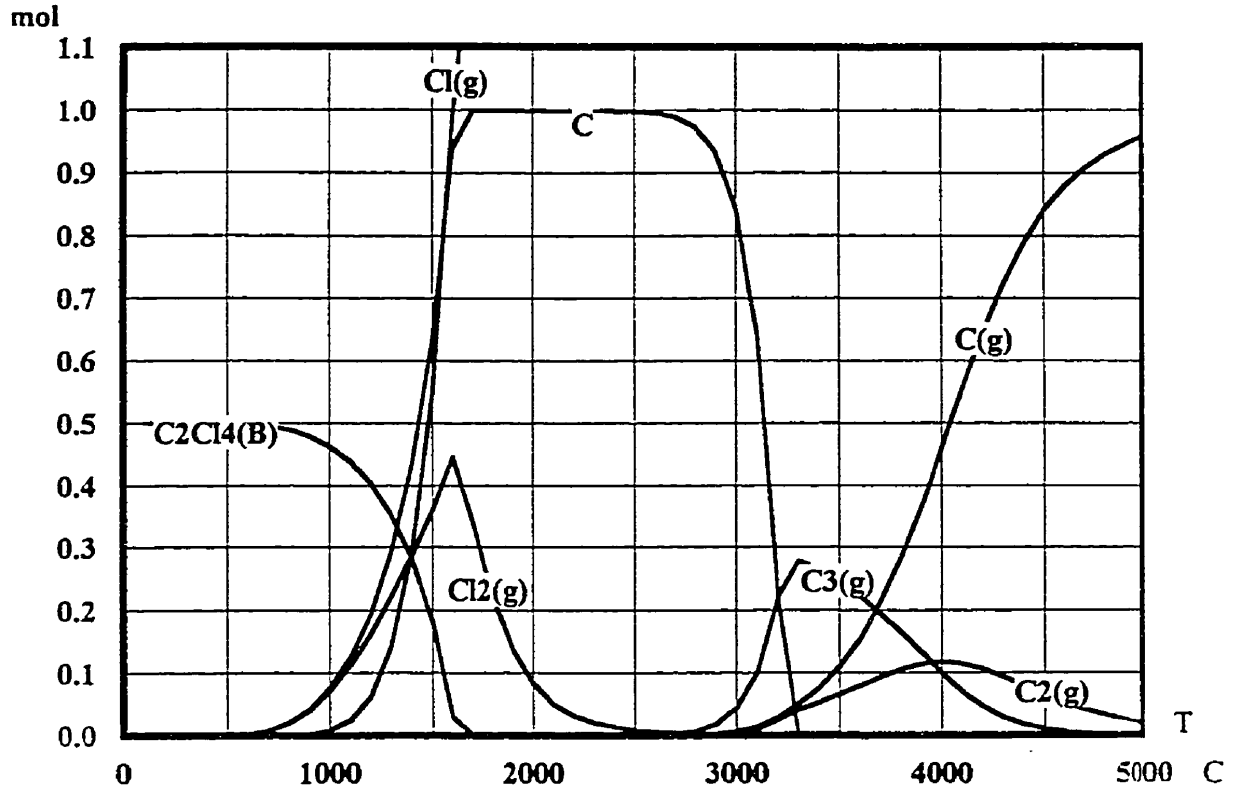

Figure 25: Computed equilibrium concentrations resulting from dissociation of C_2Cl_4 as a function of temperature at 760 torr.

C, C_2, C_3, C_4, C_5, CCl, CCl_2, CCl_3, CCl_4, C_2Cl_2, C_2Cl_4, C_2Cl_6, Cl, Cl_2, He, C_{60}, C(s)

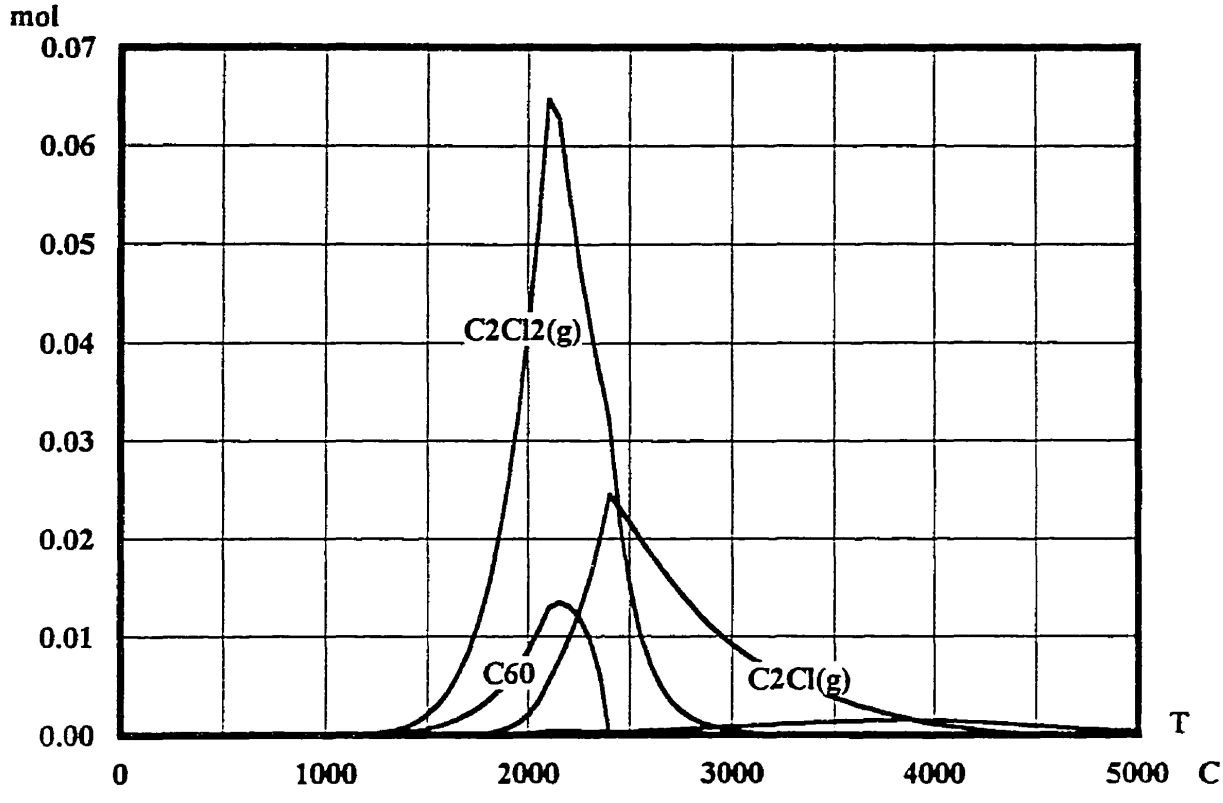

Figure 26: Computed equilibrium concentrations of C_{60} CCl, C_2Cl and C_2Cl_2 as a function of temperature at 760 torr.

of C_2Cl and C_2Cl_2 radicals is seen in the temperature range from 1,500 K to 4,000 K.

The presence of the C_2Cl_2 radical in the temperature range where fullerenes are predicted to form raises the question as to whether fullerenes form through a series of C-C reactions, as in the arc vaporization of graphite process (Section 1.4), or alternatively through free radical addition reactions involving C_2Cl_2. In the work of Howard *et al.* [1992], the formation of fullerenes from the combustion of hydrocarbons is speculated to occur through a series of reactions in which C_2H_2 plays an active role in the growth of clusters into fullerene structures. Is it possible that in the *PyroGenesis* process, the C_2Cl_2 radical plays a key role in the formation of fullerenes? Although such a hypothesis is difficult to confirm from the results obtained from this work, a discussion of the mechanism of fullerene formation has been included in Chapter 9.

CHAPTER 6:
MASS AND ENERGY BALANCES

6.1 Overall Mass Balance

Samples of soot produced under three different operating conditions were analyzed for their carbon and chlorine content (Guelph Chemical Laboratories). Experiments were performed at 45, 55 and 65 kW to determine the effect of input power on the overall mass balance. The C_2Cl_4 feed rate was 0.29 mol/min and the pressure was 300 torr except for the experiment at 45 kW, when the pressure was 200 torr. As will be discussed in Chapter 7, the variation in pressure between 200 and 300 torr did not have an effect on soot and fullerene production and thus does not affect the overall mass balance.

Carbon and chlorine accounted for 95.5 - 97.9% of the total weight of samples. Adsorbed oxygen, nitrogen and other contaminants presumably account for the remainder. The carbon content of the soot collected in the reactor chamber, as seen in Figure 27, increased from 65% at 45 kW to 82% at 65 kW. The increasing carbon content of the soot with increasing input power is also evident in the soot collected in the quench zone. At higher power levels, reacting species have a longer residence time at elevated temperatures, thus favouring the growth of large molecules, including graphite, fullerenes and large, polychlorinated

hydrocarbons. Therefore, at high power levels, the carbon content in the soot collected in the reactor is expected to be relatively high. The molar ratio of C to Cl is shown in Figure 28, as a function of input power. At 65 kW, the C/Cl molar ratio is 18, compared to a ratio of 6 obtained at 45 kW.

The soot collected in the quench zone has a substantially higher concentration of Cl as is seen by the relatively low weight percent of C in Figure 27 and the low C/Cl molar ratio in Figure 28. The maximum concentration of carbon in the soot of the quench zone was 62%, compared to 82% in the reactor. The distinct difference in the composition of the soot in the quench zone may be explained as follows:

(i) Chlorinated, organic compounds which may have been formed in the reactor did not condense in the reactor due to the elevated collection temperatures and thus were carried by the exhaust gas to the quench zone, where they condensed on the water-cooled coil.

(ii) Lower temperatures may favour C-Cl reactions which may lead to the formation of additional chlorinated compounds in the quench zone.

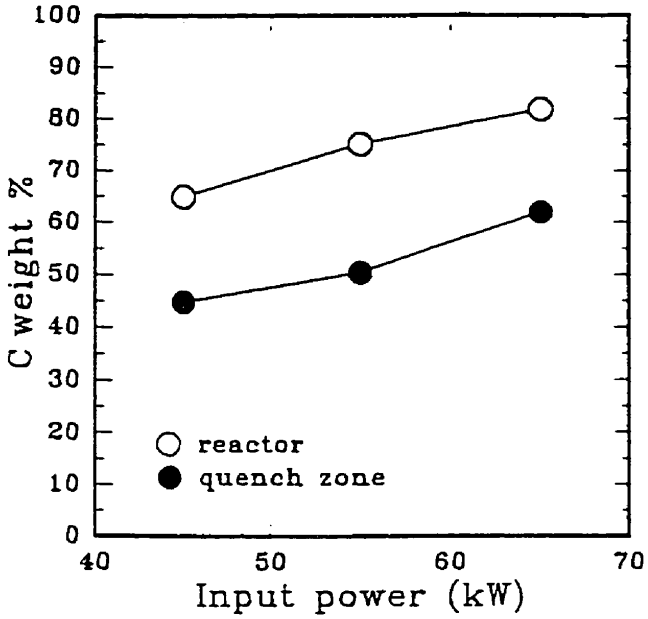

Figure 27: Carbon content in soot collected in the reactor and quench zone.

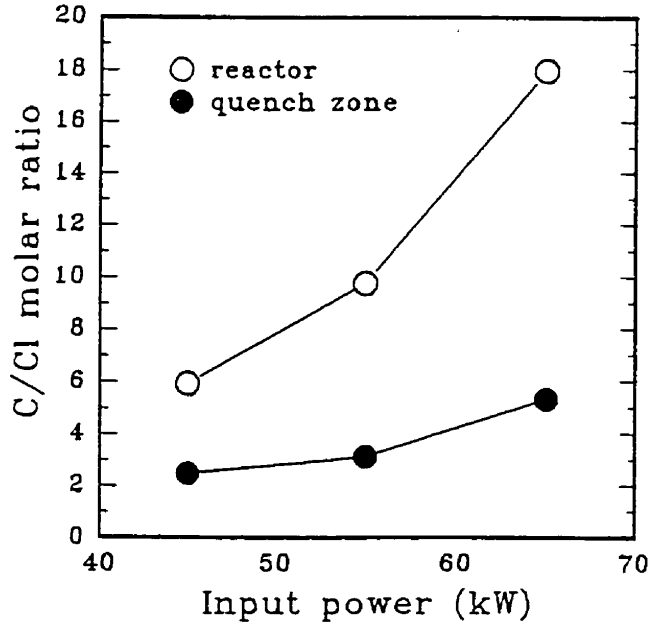

Figure 28: C/Cl molar ratio of soot collected in reactor and quench zone.

The total carbon and chlorine recovery in the soot collected in the reactor and quench zone, expressed as a percentage of the initial amounts introduced as C_2Cl_4, are summarized in Table 3. The maximum carbon recovery was 50.8%, which was obtained at 65 kW. Only up to 2.6% of the chlorine was recovered in the soot as chlorinated hydrocarbons. Most of the chlorine presumably leaves the reactor system as Cl_2 with some portion of the chlorine leaving as volatile organic compounds such as CCl_4, C_2Cl_4, C_6Cl_6 etc...

Table 3: Summary of carbon and total mass recovery

Input Power (kW)	Carbon Recovery	Chlorine Recovery	Total Mass Recovery
45	24.6%	2.5%	27.1%
55	38.2%	2.6%	40.8%
65	50.8%	1.2%	52.0%

6.2 Overall Energy Balance

The overall energy balance may be expressed by the following equation:

$$Q_{Accumulation} = Q_{Input} - Q_{Torch\ Water} - Q_{Reactor\ Water} - Q_{Exhaust\ Gas}$$

Calorimetric measurements were performed under the operating conditions listed in Table 2 (Chapter 4). It should be noted that these measurements were made in the absence of C_2Cl_4 injection into the system since steady state is not achieved during soot formation, due to the accumulation of soot on the reactor wall, as will be seen in Section 7.2. Therefore, there was no accumulation of products in the reactor during these calorimetric measurements, resulting in no accumulation of energy in the reactor ($Q_{Accumulation} = 0$). The temperature of the cooling water was 22.9 ± 2.8 °C. The results of the calorimetric study are summarized in Table 4.

Table 4: Summary of results from calorimetric measurements

Input Power (kW)	$Q_{(Torch\ Water)}$ (kW)	$Q_{(Reactor\ Water)}$ (kW)	Fraction of energy recovered in cooling water
45	11.4 ± 0.6	26.7 ± 0.5	84.5%
55	13.0 ± 0.5	31.5 ± 1.3	80.8%
65	15.3 ± 0.5	36.8 ± 1.5	79.7%

Based on the energy balance, up to 20.3 % of the energy leaves with the off-gas and the remainder is transferred to the torch and reactor cooling water. From the energy balance calculations, the torch efficiency was determined by the

following equation:

$$Torch\ \epsilon\ \% = \frac{Q_{INPUT} - Q_{TORCH\ WATER}}{Q_{INPUT}}$$

The torch efficiency was found to vary from 73-77%, as is shown in Figure 29.

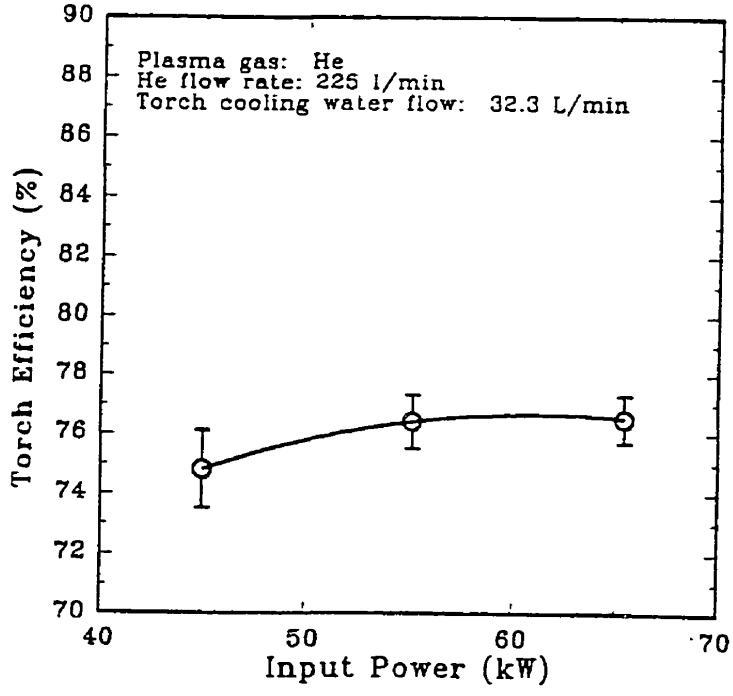

Figure 29: Torch efficiency as a function of input power [200 torr].

CHAPTER 7: EFFECT OF PROCESS PARAMETERS ON FULLERENE PRODUCTION

7.1 Verification of C_2Cl_4 mixing with plasma

The effect of nozzle length was evaluated in order to assess whether there was adequate mixing of C_2Cl_4 with the plasma. C_2Cl_4 vapour, diluted with helium, entered the nozzle through an annular ring, having 3 openings. The openings had an internal diameter of 2 mm. The C_2Cl_4 mixture entered the nozzle at 172 ± 11 °C. For a C_2Cl_4 feed rate of 0.29 mol/min, the vapour flow rate at 172 °C was 10.6 l/min, resulting in a total flow of 43.2 l/min of C_2Cl_4 in helium at this temperature. The estimated velocity of the mixture through each opening is 77 m/s. Due to the high viscosity of plasmas, there was a concern whether C_2Cl_4 was being properly mixed with the plasma. To verify the mixing of C_2Cl_4 with the plasma, experiments were performed with 2 nozzles, each identical in all aspects except their length. The longer nozzle had a length of 4 cm, whereas the smaller nozzle was 2.6 cm in length.

The data for this test was obtained during a fullerene soot production run and not as part of the experimental program. The conditions of the production run are listed below and the results from the test are presented in Table 5.

Plasma gas:	helium
Plasma gas flow:	225 slpm
Pressure:	200 torr
C_2Cl_4 feed rate:	0.29 mol/min
Carrier gas flow rate:	20 slpm
Power:	65 kW for 2 min, 50 kW for 5 min
Run duration:	7 minutes

Table 5: Effect of nozzle length on fullerene production

Nozzle Length (cm)	Soot prod. rate (g/min)	C_{60} prod. rate (mg/min)	C_{70} prod. rate (mg/min)
4	2.9	24.4	8.4
4	3.1	23.3	7.16
2.6	3.3	24.0	8.9

The results obtained during this test indicated that there was no significant difference in the soot and fullerene production rates when the nozzle length was changed, suggesting that it is likely that good mixing of C_2Cl_4 with the plasma was achieved. As a result, the shorter nozzle was used in all subsequent experiments. Although these experimental results were convincing, the evaluation of mixing of

C_2Cl_4 with the plasma was investigated further using theoretical modelling.

The mathematical model, developed by J.F. Bilodeau, was used to confirm some of the experimental findings on C_2Cl_4 mixing [Bilodeau *et al.*, 1996]. The assumptions and equations used in the model and the results from the model are included in Appendix C. Figure 30 shows the isocontours of the mass fraction of C_2Cl_4 in the plasma jet regions, as predicted by the model. According to these results, at an axial distance of 0.08 m from the torch exit, the mass fraction of C_2Cl_4 at temperatures less than 2,000 K is very low, approximately 0.04. As such, it is evident that C_2Cl_4 is well heated by the plasma jet since most of the hydrocarbon is heated to temperatures in excess of 2,000 K. Since C_2Cl_4 decomposes completely above 1,000 °C [Tirey *et al.*, 1990], it is concluded that in the present reactor configuration, good mixing occurs between the plasma and C_2Cl_4, thus favouring complete dissociation of C_2Cl_4.

7.2 Study of temperature within the reactor surface

7.2.1 Measurement of temperature near the reactor surface

The temperature near the reactor surface was measured during soot production runs to determine if the temperature inside the reactor changes with time. The effect of process variables on temperature was also evaluated. The fixed

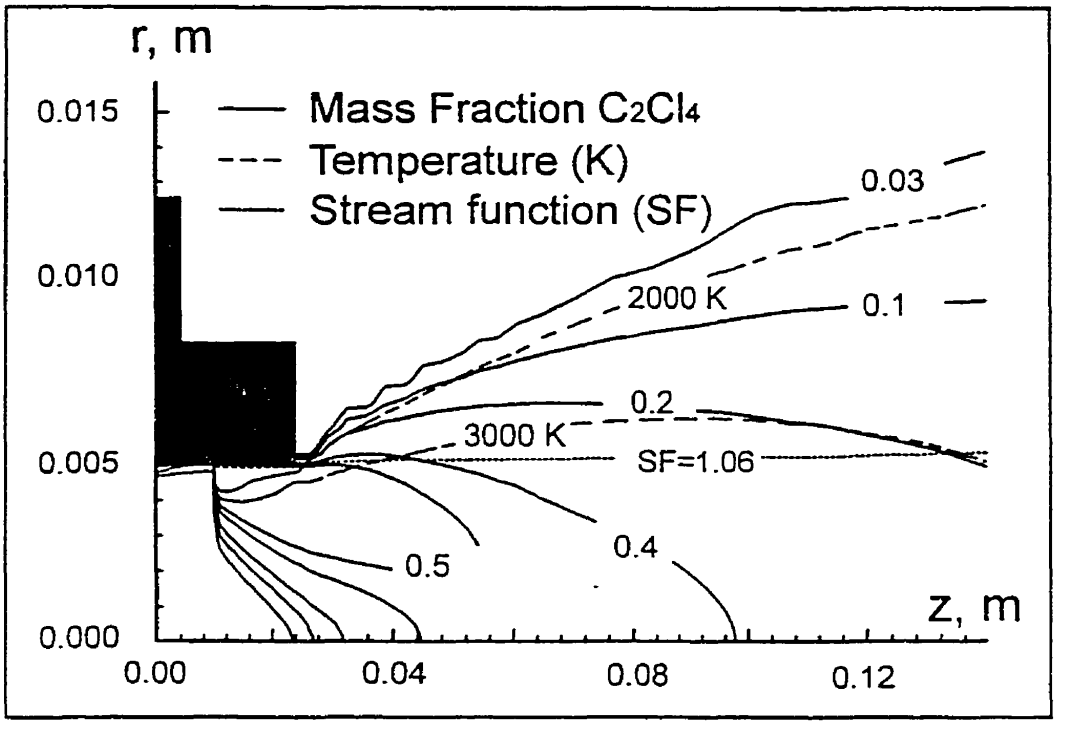

Figure 30: Mathematical modelling of mass fraction of C_2Cl_4 in the plasma jet region [Bilodeau, 1996].

operating parameters used in the experiments are listed in Table 2 (Chapter 4).

The temperature near the reactor surface was first measured for different torch power levels. The C_2Cl_4 flow rate and pressure were kept constant at 0.29 mol/min and 200 torr, respectively. The temperature was measured over a period of 4 minutes during which C_2Cl_4 was fed into the plasma at a steady rate. As expected, higher temperatures were obtained at higher power levels, as seen

in Figure 31. However, the temperature near the reactor wall did not stabilize during the run, but increased almost linearly with time, revealing that during the soot production process, the temperature near the reactor wall does not reach a steady value.

The effect of C_2Cl_4 feed rate on the temperature of the reactor surface is summarized in Figure 32. The temperature inside the reactor was measured for three different experimental conditions: no C_2Cl_4 flow, 0.29 mol/min C_2Cl_4 and 0.44 mol/min C_2Cl_4. The power level and pressure were fixed at 55 kW and 200 torr, respectively. When the plasma torch operated, under the conditions indicated above, without C_2Cl_4 injection, the temperature near the reactor wall stabilized at 350°C. However, when 0.29 mol/min of C_2Cl_4 was introduced into the plasma, the temperature quickly increased, reaching 580°C after 4 minutes. When the C_2Cl_4 feed rate was increased to 0.44 mol/min, a temperature of 690°C was reached after 4 minutes. Two plausible explanations for this trend are:

(i) As the C_2Cl_4 feed rate is increased, there is a significant increase in the thickness of the soot layer, which may be acting as an insulator, thus increasing the temperature near the surface.

(ii) It is also possible that reactions occurring near the reactor surface are exothermic, thus as more C_2Cl_4 is fed into the system, the

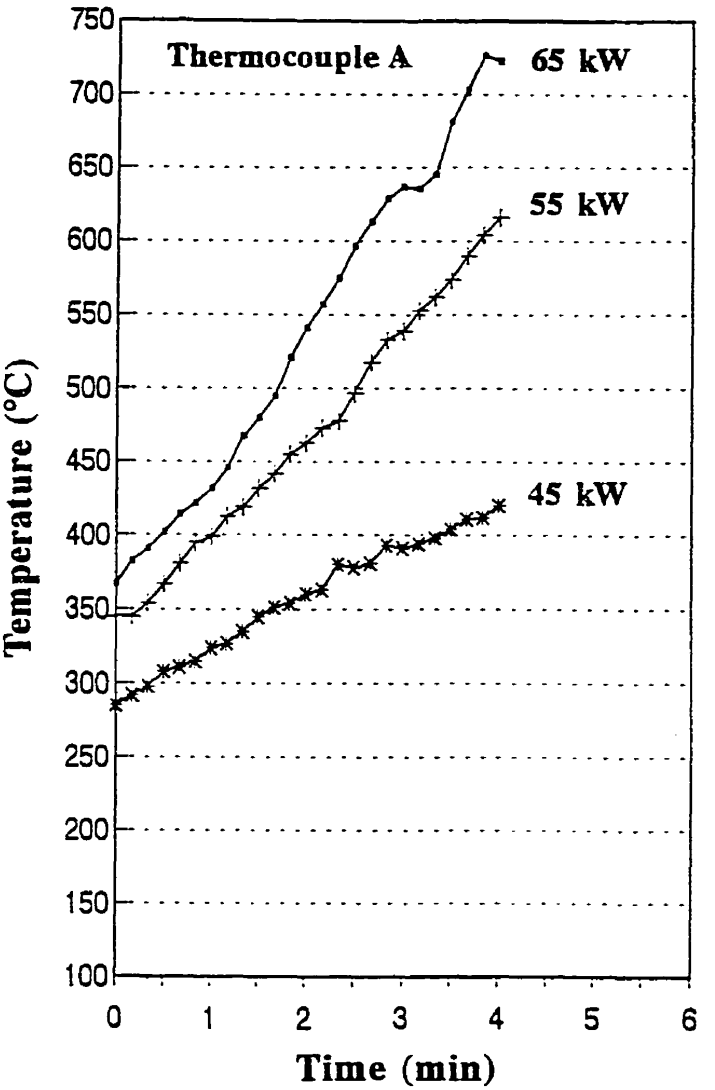

Figure 31: Temperature near reactor wall (T_A) for different torch power levels [0.29 mol/min C_2Cl_4, 200 torr].

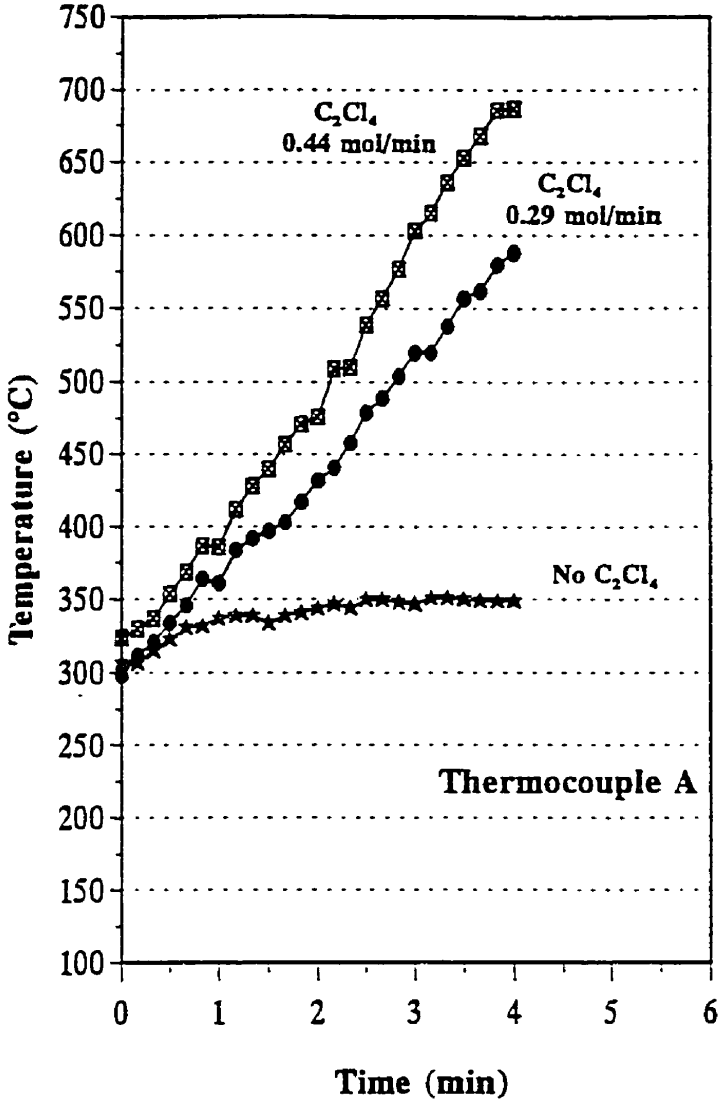

Figure 32: Temperature near reactor wall for different C_2Cl_4 feed rates [55 kW, 200 torr].

temperature near the reactor surface may increase.

Temperatures measurements obtained near ports A and B (Figure 16) are shown in Figure 33 for different C_2Cl_4 feed rates (65 kW, 200 torr). At 65 kW, the rise in temperature near the reactor surface becomes more alarming, since it exceeds 1,100 °C. At 1,100 °C, the vapour pressure of C_{60} is expected to be quite significant [Table 1, Chapter 1], thus it is possible that after some time, C_{60} no longer condensed in the high temperature zones of the reactor, such as the location near port B.

The effect of reactor pressure on the temperature near the reactor surface was also evaluated as part of this study and is shown in Figure 34. At 400 torr, the temperature near the surface seems to be stable at 180-200 °C. It should be noted that under these experimental conditions, very little soot was formed, as will be discussed in Section 7.5. The temperature near the surface was highest at the lowest pressure investigated, 200 torr. In thermal plasmas, a reduction in pressure results in the generation of a substantially longer plasma jet, and therefore, in the present reactor, would result in heating of the reactor surface.

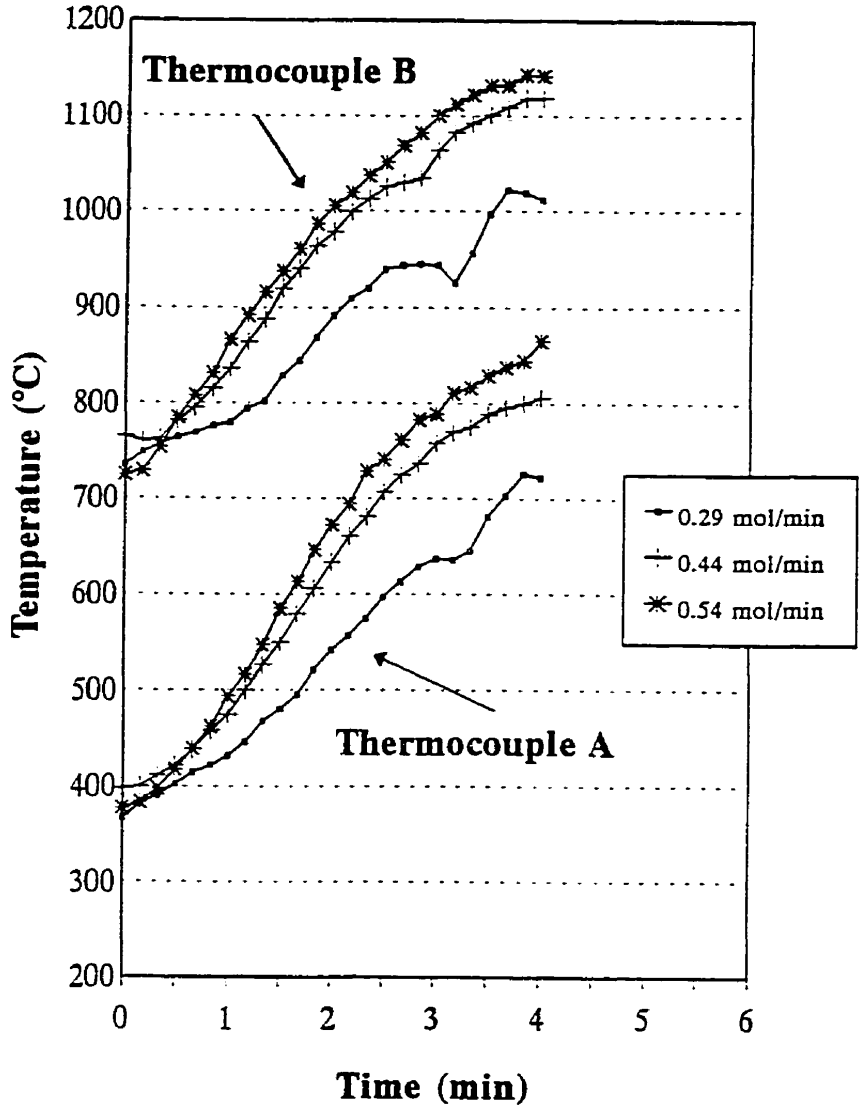

Figure 33: Temperature near reactor wall for different C_2Cl_4 feed rates [65 kW, 200 torr].

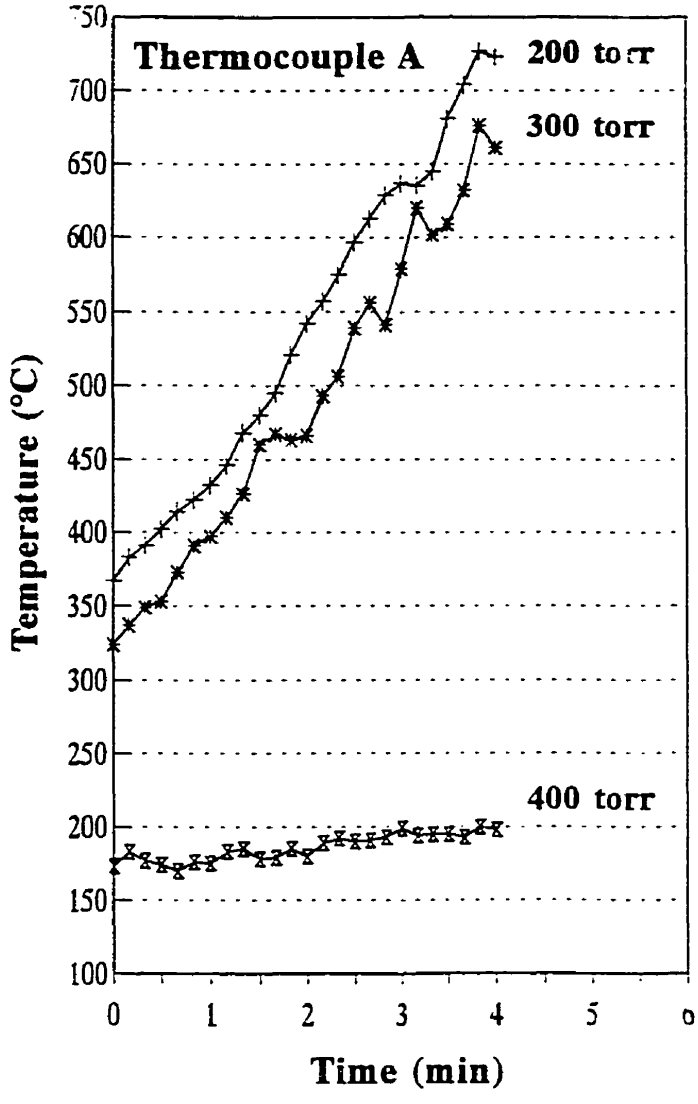

Figure 34: Temperature near reactor wall (T_A) for different reactor pressures [65 kW, 0.29 mol/min C_2Cl_4].

7.2.2 Verification of insulating effect of soot layer

To substantiate the concept of the thermal resistance resulting from the growing soot layer, the first derivative of the temperature versus time curves, shown in Figures 31-34, was calculated and plotted against the average soot collection rate obtained from the corresponding experiments. The plot of dT/dt versus the soot collection rate is seen in Figure 35. Although each point corresponds to different operating conditions, it is quite evident that dT/dt is strongly influenced by the soot collection rate and thus the soot layer thickness.

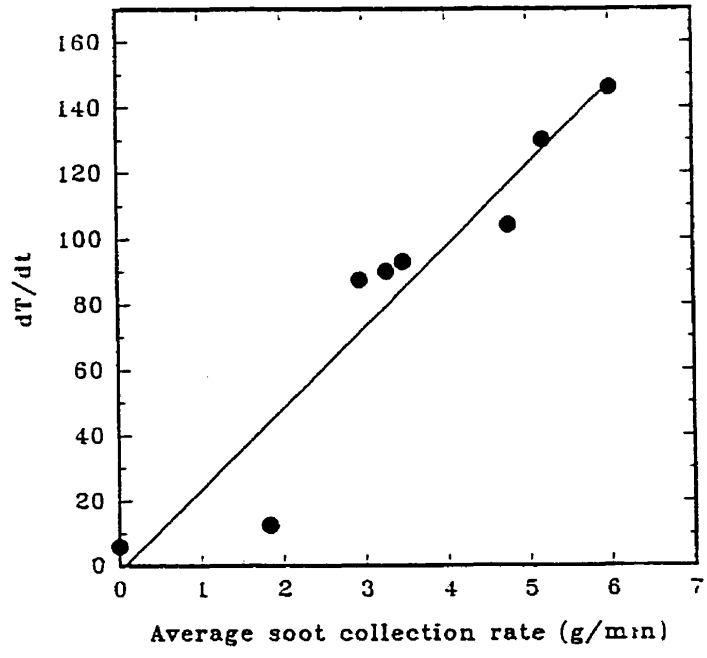

Figure 35: dT/dt as a function of soot collection rate.

As observed experimentally, the soot layer which accumulates on the surface of the reactor wall seems to have an important effect on the temperature near the reactor surface and consequently, on the temperature of the collection site. Such differences in temperature during the course of the runs may affect the chemical reactions occurring near the reactor surface, the types of products which condense on the surface, as well as their rate of condensation. In order to substantiate the claim that the soot deposit acts as an insulating layer inside the reactor, calorimetric measurements of the reactor cooling water were performed. The data was obtained from the experiment corresponding to the highest energy input (65 kW) and highest insulating effect (0.54 mol/min of C_2Cl_4). The energy transferred to the reactor cooling water as a function of time is shown in Figure 36.

If the soot deposit does in fact act as an insulating layer on the inner surface of the reactor, the temperature rise and consequently the energy transferred to the reactor cooling water should decrease with time. Although there is a relatively large degree of scatter in the data shown in Figure 36, a decrease in the energy transferred to the cooling water as a function of time is observed, hence confirming the insulating effect of the soot layer of the reactor surface.

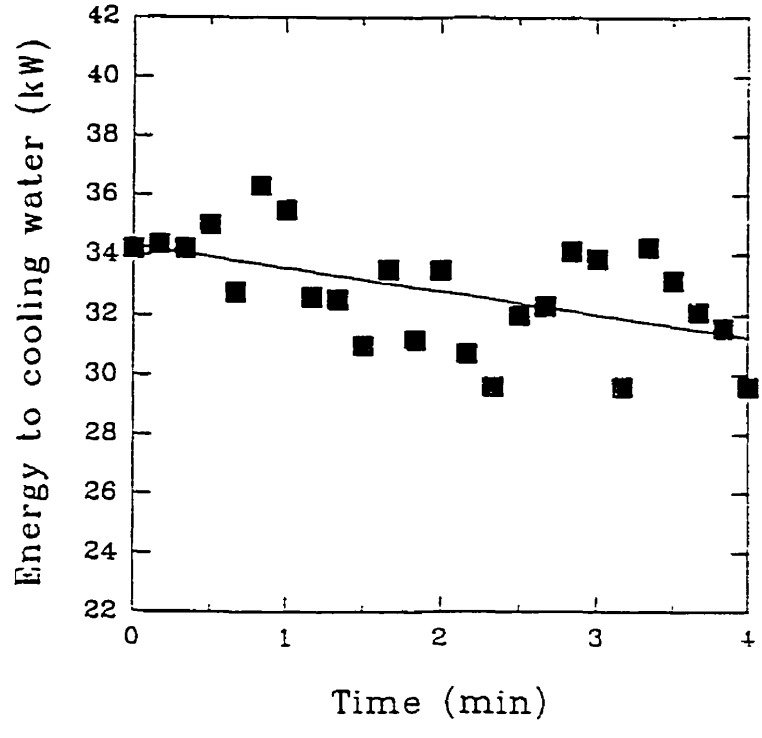

Figure 36: Energy transferred to reactor cooling water as a function of time [65 kW, 0.54 mol/min C_2Cl_4, 200 torr].

7.2.3 Prediction of reactor temperature profiles through modelling

As seen in Figures 31-34, process variables in addition to run duration strongly influence the temperatures inside the reactor. The model developed by Bilodeau [1996] was run for the different operating conditions used in the experimental work in an attempt to determine the effect of operating parameters on the temperature profile within the reactor.

Figure 37 shows the temperature profiles with the reactor at three levels of input power (45, 55 and 65 kW). As expected, high input power results in high temperatures within the reactor. At 45 kW, the reactor temperatures are significantly lower than those computed at 55 kW and 65 kW, and as a result, the temperature zone required for fullerene formation, 2,200-2,600 K, as proposed by McKinnon [1991], seems to be very small under such low power input conditions.

The effect of the C_2Cl_4 feed rate on the temperature profile in the reactor was computed and is shown graphically in Figure 38. As the C_2Cl_4 feed rate is increased, at constant input power and pressure, the temperature of the plasma jet is expected to decrease due to the endothermic energy requirements of C_2Cl_4 for dissociation and heating of its products. The decrease of the reactor

temperatures with increasing C_2Cl_4 feed rate is evident in Figure 38 for three C_2Cl_4 feed rates (0.15, 0.29 and 0.44 mol/min C_2Cl_4). It should be noted that the validity of these temperature profiles is limited since the model does not take into account any chemical reactions which may greatly affect the temperature profile within the reactor. Furthermore, as was determined experimentally (Section 7.2.1), as more soot deposits on the reactor surface as a result of higher C_2Cl_4 feed rates, the thermal resistance of the soot layer increases, thus increasing the temperature near the reactor surface. The growing insulating layer of soot was also not taken account by the model.

The effect of reactor pressure on the temperature profile, as predicted by the model, is shown in Figure 39. As the reactor pressure is decreased from 300 torr to 200 torr, with a fixed C_2Cl_4 feed rate and input power, the plasma zone is extended as can be seen by the longer isotherm at 2,000 K. Therefore, as the pressure is increased, the temperature near the reactor surface is expected to decrease, as was also shown experimentally in Figure 34.

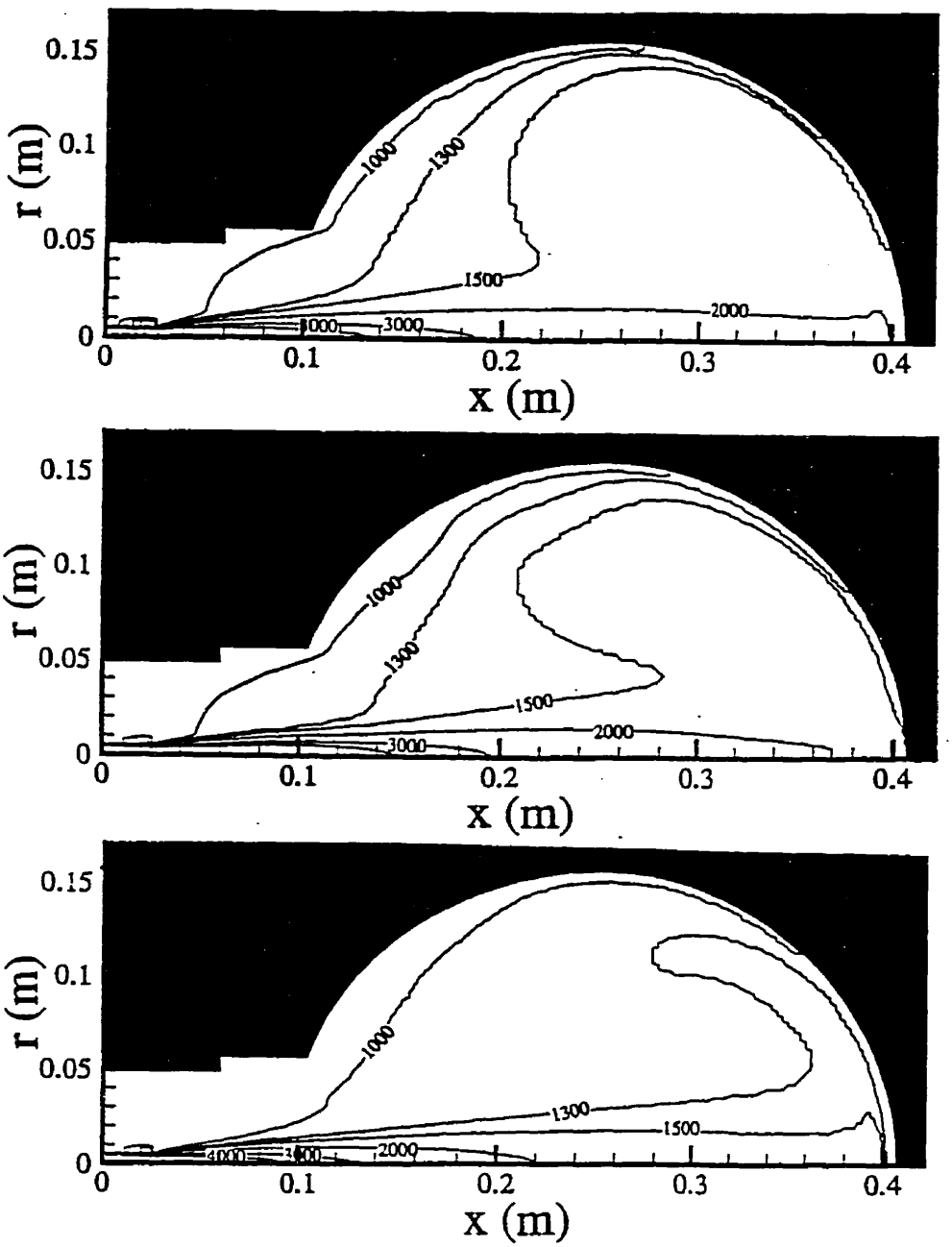

Figure 37: Temperature profiles within reactor for different levels of input power: 65 kW (top), 55 kW (middle), and 45 kW (bottom) [0.29 mol/min C_2Cl_4, 200 torr].

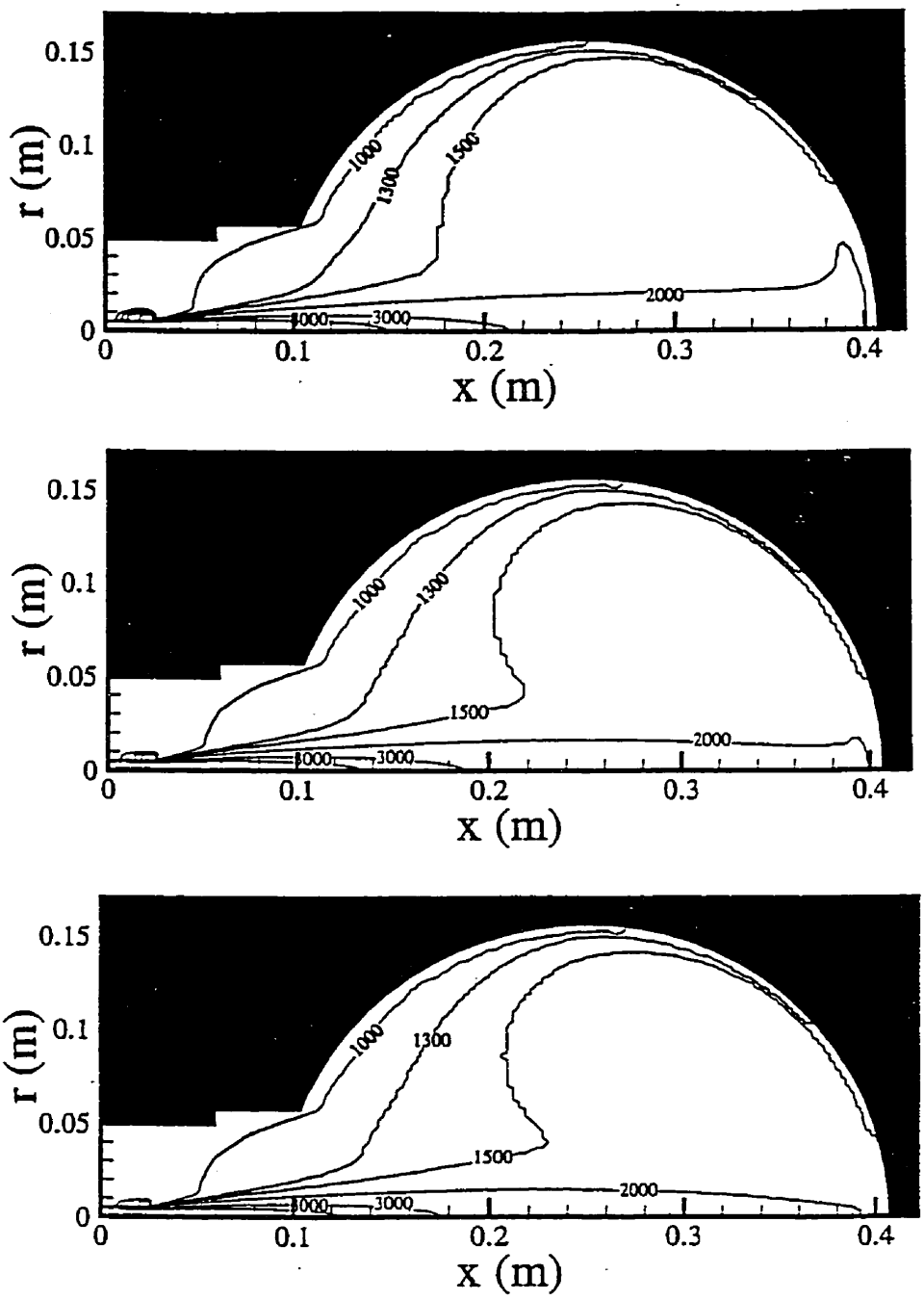

Figure 38: Temperature profiles within reactor for different C_2Cl_4 feed rates: 0.15 mol/min (top), 0.29 mol/min (middle), and 0.44 mol/min (bottom) [65 kW, 200 torr].

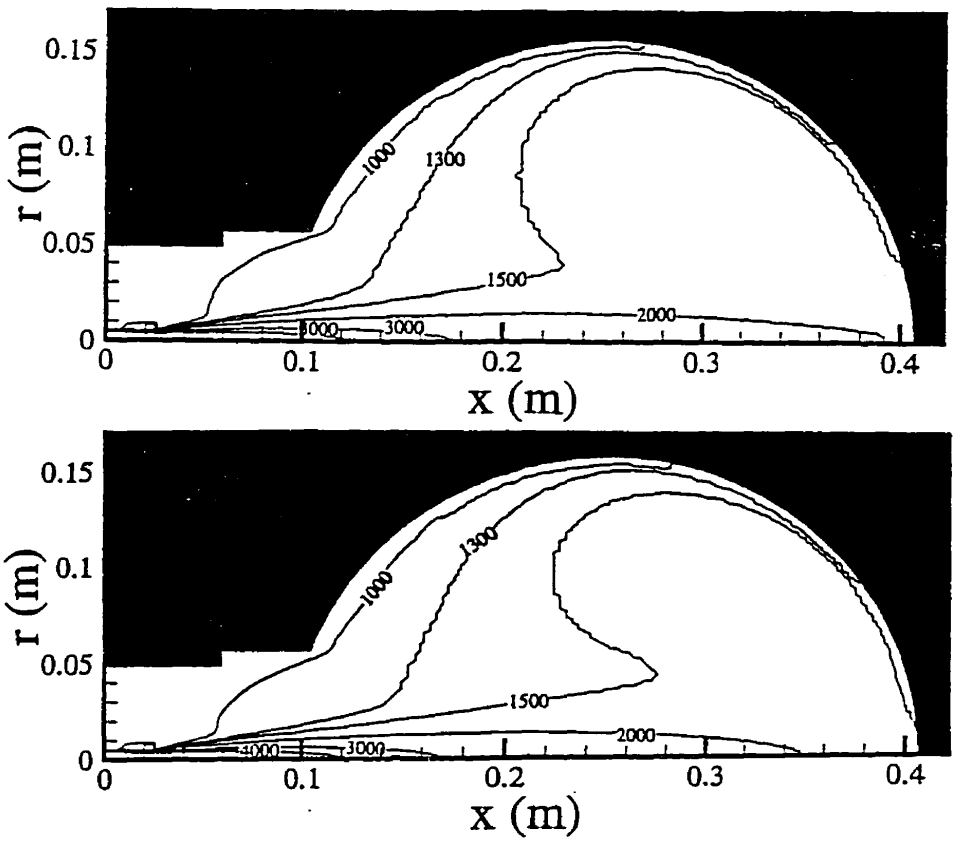

Figure 39: Temperature profiles within reactor for different pressures: 200 torr (top) and 300 torr (bottom) [65 kW, 0.44 mol/min C_2Cl_4].

7.3 Effect of run duration on fullerene collection

7.3.1 Average soot collection rate and soot composition

The variations in soot collection rate and soot composition as a function of run duration were studied in order to assess the operating consistency of the reaction system. For this study, the torch power, C_2Cl_4 feed rate and pressure were fixed at 55 kW, 0.29 mol/min, and 200 torr, respectively. A complete list of all of the fixed variables may be found in Chapter 4 (Table 2). The soot collected in the reactor and quench zone was analyzed separately.

Figure 40 shows the average soot collection rate in the reactor and quench zone, as a function of run duration. Each experiment is represented by one data point in the reactor and one point in the quench zone. The average soot collection rate was determined by dividing the mass of soot collected in each experiment by the run duration. Approximately 70% of the total soot collected condensed on the water-cooled reactor wall, while the remaining 30% of the soot condensed in the quench zone. After an initial transition period of 2 minutes, the average soot collection rate was constant at 3.2 g/min. The soot collection rate in the quench zone reaches a maximum value of 0.7 g/min during the 8-minute run.

Since the temperature in the reactor increases during the run, as seen in the

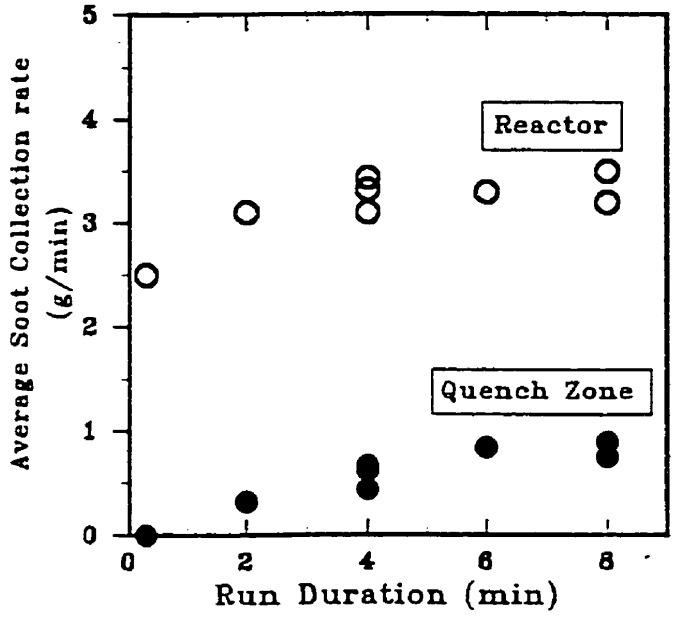

Figure 40: Average soot collection rate as a function of run duration [55 kW, 0.29 mol/min C_2Cl_4, 200 torr].

previous section, long experimental runs are associated with high reactor temperatures. As a result of higher reactor temperatures, it is expected that the formation of graphitic networks will be favoured since carbon species are allowed to grow into large graphitic-like compounds at high temperatures. These graphite-like precursors may either form graphite, polychlorinated aromatic hydrocarbons or fullerenes. When the temperature in the reactor is relatively low, as in short runs, the residence time of the carbon species in a high

temperature zone is lower, thus favouring the formation of small, chlorinated compounds.

The importance of run duration on the chemistry of the reactor is emphasized by the data in Figure 41, where the concentration of soluble by-products in soot is plotted as a function of run duration. The concentration of soluble material was determined by subtracting the fraction of fullerenes from the weight of crude extract, which represents the total soluble material, and dividing by the total weight of soot.

For short runs, more than 50% of the soot collected in the reactor consisted of chlorinated by-products, whereas in longer runs, the concentration of these by-products in the soot collected dropped to 10%. The drastic difference in the composition of the soot during the course of the run is further demonstrated in Figure 42, where the HPLC chromatograms of the crude extract derived from the experiments run during 2, 4 and 8 minutes are shown. The peaks at 7.3-7.6 minutes and 9.9-10.3 minutes on the chromatogram correspond to C_{60} and C_{70}, respectively. The soot produced during the 2-minute run contained a significant amount of by-products which elute before 7 minutes during the HPLC run. As the run duration was increased, the relative height of the by-product

peaks to fullerene peaks decreases, as can be seen by comparing the different chromatograms in Figure 42. In fact, the by-product peaks observed in the soot produced during the 8-minute experiment were significantly lower than those observed in the soot produced during the 2-minute experiment.

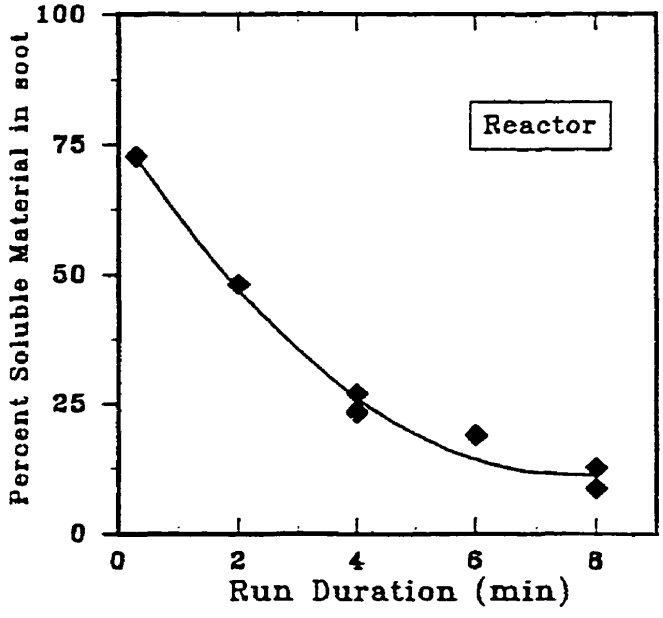

Figure 41: Concentration of soluble chlorinated by-products in the reactor soot, plotted as a function of run duration [55 kW, 0.29 mol/min C_2Cl_4, 200 torr].

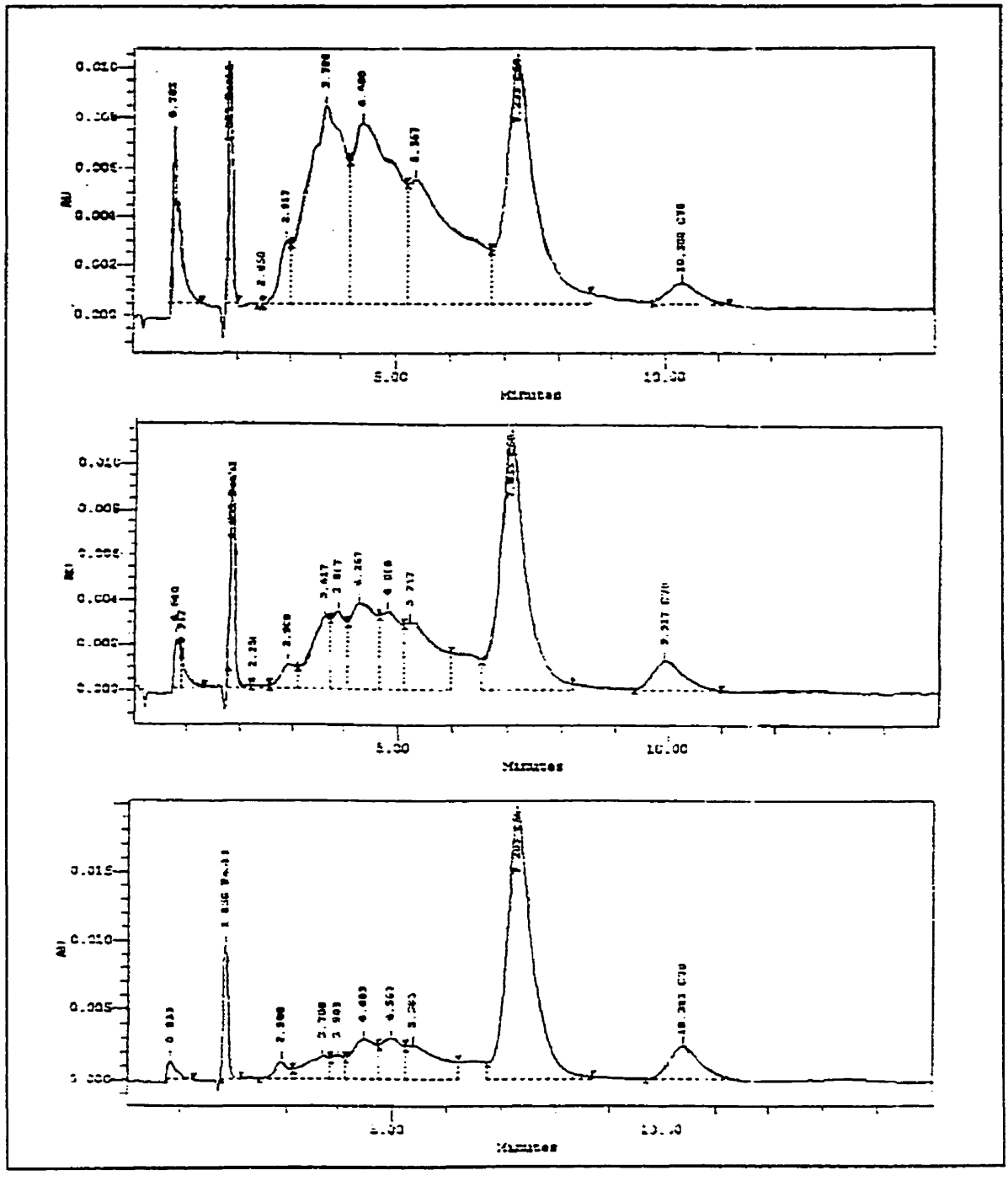

Figure 42: HPLC chromatograms of crude extracts derived from experiments run for 2 minutes (top), 4 minutes (middle), and 8 minutes (bottom) [55 kW, 0.29 mol/min C_2Cl_4, 200 torr].

7.3.2 Average C_{60} and C_{70} collection rate

The average collection rate of C_{60} in the reactor and quench zone is plotted versus run duration in Figure 43. The average C_{60} collection rate in the reactor increased up to 2 minutes at which point the collection rate remained constant until 6 minutes. After 6 minutes, a drop in the C_{60} collection rate was observed.

As already discussed in Section 7.2, the temperature near the reactor surface increases with run duration, possibly approaching and even surpassing the sublimation temperature of C_{60}, depending on the reactor conditions. As such, it is conceivable that newly formed C_{60} would not condense on the reactor surface if the surface temperature exceeds the sublimation temperature. As a result of such elevated collection site temperatures, a decrease in the average C_{60} collection rate may be seen with time. If the C_{60} formed is prevented from condensing in the reactor due to elevated temperatures, an increase in the C_{60} collection rate in the quench zone should be seen, since C_{60} leaving the reactor would condense in the quench zone.

This behaviour seems to be confirmed by the two data points obtained during the 8-minute experiments, labelled as 1 and 2 in Figure 43 (top). The collection rate of C_{60} in the reactor was higher for Experiment 1 than Experiment 2. However,

in the quench zone, the collection rate was higher for Experiment 2. Differences in the reactor cooling water temperature may explain the discrepancy between the two replicate experiments.

The total collection rate of C_{60}, which is the sum of the collection rate in the reactor and quench zone is also plotted as a function of run duration in Figure 43. The total collection rate from the two highlighted experiments is equal, as is seen by the superposition of the two points at 8 minutes, thus suggesting that the overall C_{60} production was not affected by the elevated reactor temperatures after 8 minutes. The total collection rate of C_{60} increased during the run, reaching a maximum average value of 112 mg/min after 4 minutes.

The collection rate of C_{70}, as a function of run duration, is plotted in Figure 44. The C_{70} collection rate in the reactor stabilized at 22 mg/min after 4 minutes, whereas an increasing trend in the C_{70} collection rate as a function of run duration was noted in the quench zone. The total collection rate of C_{70} is also shown in Figure 44. It is difficult to determine whether the total collection rate of C_{70} stabilized after 4 minutes or wether there is a slight increase in the collection rate with run duration. A slight increase would suggest that higher reactor temperatures, associated with longer runs, favour C_{70} production,

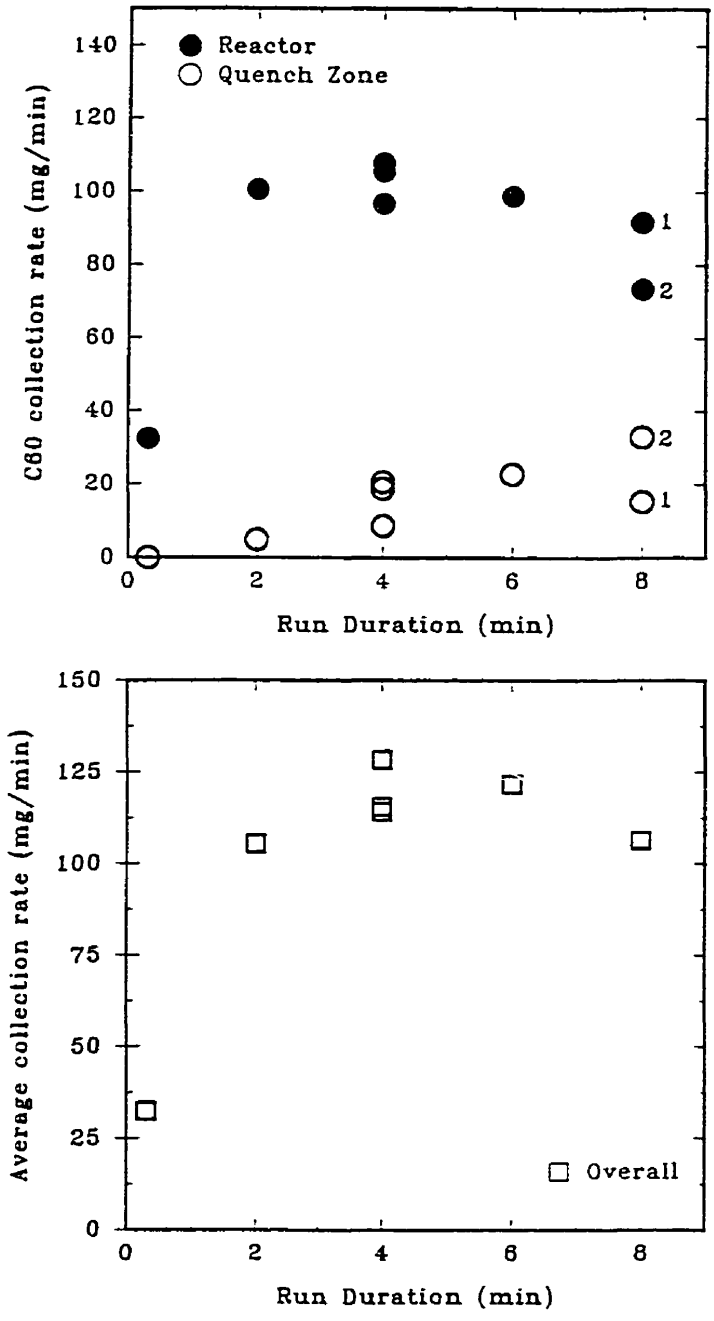

Figure 43: Average C_{60} collection rate as a function of run duration in reactor and quench zone (top), and overall (bottom) [55 kW, 0.29 mol/min C_2Cl_4, 200 torr].

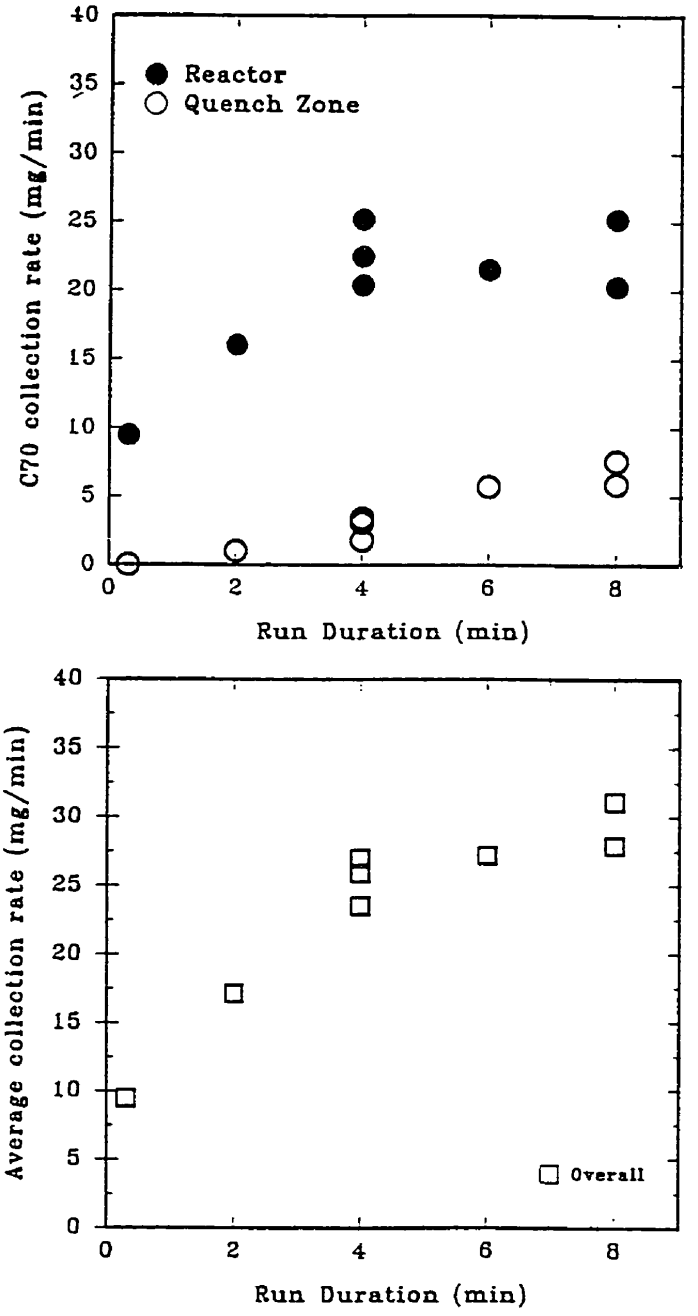

Figure 44: Average C_{70} collection rate as a function of run duration in reactor and quench zone (top), and overall (bottom) [55 kW, 0.29 mol/min C_2Cl_4, 200 torr].

although this conclusion cannot be made based on the experimental data shown in Figure 44.

Based on the results presented in this section, it is evident that in the present reactor configuration, run duration has an influence on the collection rate of soot, fullerenes and by-products due to the effect of run duration on reactor temperatures. Longer runs result in high reactor temperatures which, consequently, affect the quantity and type of products collected on the reactor wall. A decrease in the collection rate of C_{60} and by-products occurred as a result of high collection temperatures, whereas C_{70} was less affected due to its higher sublimation temperature. The collection rate of products should not be affected by run duration, and thus, a more suitable reactor design should provide for a collection zone which is not affected by the high temperature reaction zone, so as to maintain a better control of the condensation of products.

7.4 Effect of input power and C_2Cl_4 feed rate

7.4.1 Soot collection yield

The soot collection yield, expressed as grams of soot per mole of C_2Cl_4, is plotted in Figure 45 for different levels of torch power. In these experiments, the soot collected in the reactor represented 78% to 93% of the total soot collected,

depending on the reactor conditions. According to Figure 45, the soot yield was significantly reduced at 45 kW. At 55 kW and 65 kW, the soot yield was approximately 12 grams per mole of C_2Cl_4 fed, whereas at 45 kW, the soot yield dropped to 7 grams per mole C_2Cl_4. As was already discussed in Chapter 6, (Section 6.1), lower power levels result in the formation of C-Cl compounds. Small chlorinated compounds tend to have relatively lower boiling or sublimation points and, thus, would not condense in the reactor due to the elevated collection temperatures. However, high power levels result in the formation of graphite,

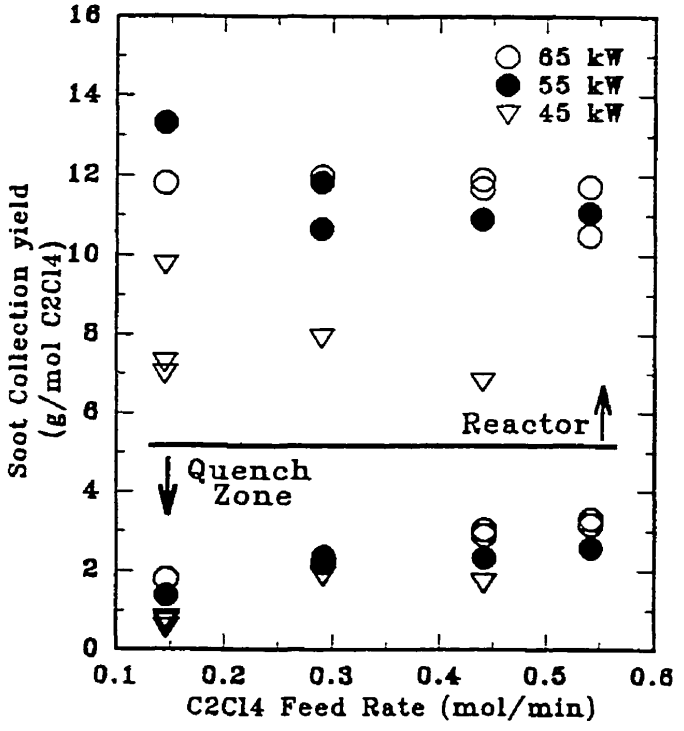

Figure 45: Soot collection yield as a function of C_2Cl_4 feed rate and torch power [200 torr].

fullerenes and large PAH's, which have relatively high sublimation temperatures and, thus, would tend to condense in the reactor.

Based on the data generated during this study, it is not possible to conclusively determine the effect of C_2Cl_4 feed rate on the soot collection yield, due to the complex chemical composition of the soot. However, despite the scatter in the experimental data, the soot collection yields in the reactor and quench zone seem to be constant as the C_2Cl_4 feed rate is increased from 0.15 mol/min to 0.54 mol/min, for experiments at 55 kW and 65 kW.

7.4.2 Concentration of C_{60} and C_{70} in soot

Figure 46 shows the concentration of C_{60} and C_{70} in the reactor soot, as a function of C_2Cl_4 feed rate and torch power. It is quite evident from Figure 46 that higher power levels result in higher concentrations of C_{60} and C_{70} in the soot, especially at low C_2Cl_4 feed rates. The richest soot, in terms of fullerene content was obtained when 0.15 mol/min of C_2Cl_4 was fed into a plasma operating at 65 kW. The soot produced under these conditions contained 4.5% C_{60} and 0.83% C_{70}.

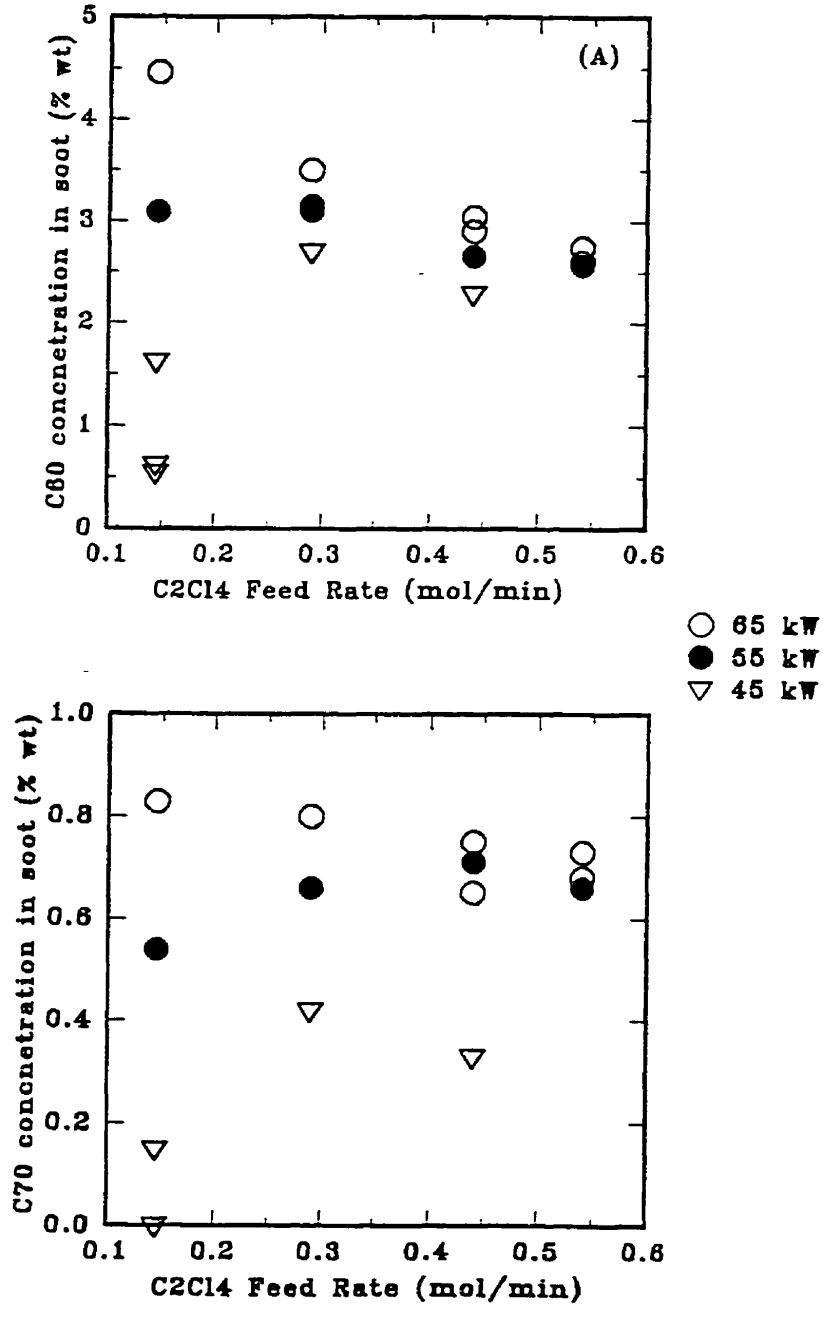

Figure 46: C_{60} (top) and C_{70} (bottom) concentrations in reactor soot as a function of C_2Cl_4 feed rate and torch power level [200 torr].

Knowledge of the concentration of C_{60} and C_{70} in the soot is useful when comparing the "quality" of fullerene soot produced by the *PyroGenesis* process with the soot produced by other processes. The value of the concentration of fullerenes in the soot, however, does not give a good basis for comparison of the technologies, since this point of comparison does not take into account the production rate of fullerenes and the conversion based on carbon feed. Furthermore, in the present reactor configuration, the concentration of fullerenes in the soot is influenced by the collection site temperature, and, thus, this value cannot be used to evaluate the technology since a different reactor design would alter the fullerene concentration in the soot.

7.4.3 Collection yield of C_{60} and C_{70}

The overall yield of C_{60} and C_{70}, expressed in milligrams per mole of C_2Cl_4, is plotted in Figure 47, for different levels of power and C_2Cl_4 feed rates. The overall yield of fullerenes was determined by dividing the sum of the fullerenes collected in the reactor and quench zone (mg/min) by the C_2Cl_4 feed rate (mol/min). It is evident from Figure 47 that higher power levels result in higher fullerene yields, especially at low C_2Cl_4 feed rates. At 45 kW, there is a drastic drop in fullerene production, suggesting that at this power level, the temperature profile is inadequate for fullerene synthesis, since it is likely that the residence

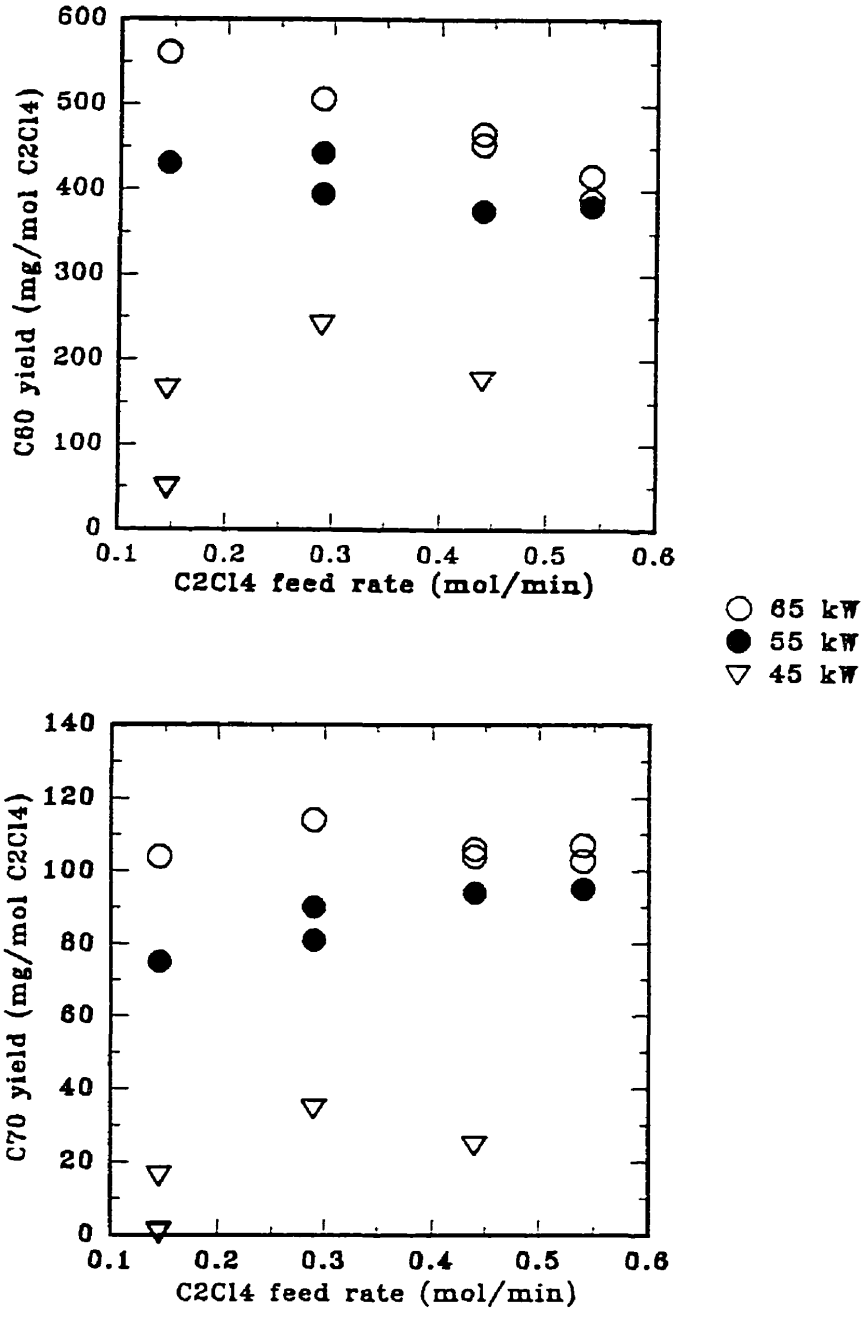

Figure 47: Overall C_{60} (top) and C_{70} (bottom) yields as a function of C_2Cl_4 feed rate and torch power level [200 torr].

time of reactive species in the fullerene formation zone, 2,200 K to 2,600 K, is probably very short.

There are also distinct trends in the C_{60} collection yield, as a function of C_2Cl_4 feed rate. At 65 kW, C_{60} collection per mole of C_2Cl_4 decreases, whereas the C_{70} yield remains constant, with increasing C_2Cl_4 feed rate. At 55 kW, however, the C_{60} yield seems to remain constant while the C_{70} yield increases slightly with increasing C_2Cl_4 feed rate. This finding suggests that the formation of C_{60} and C_{70} is optimal under different conditions.

The decrease of the C_{60} collection yield with increasing C_2Cl_4 feed rate at 65 kW, suggests that the residence time of growing carbon species in the temperature zone which favours C_{60} formation may be adversely affected by variations in the C_2Cl_4 feed rate. It may be speculated that the residence time of reactive species in the fullerene formation zone may decrease as the C_2Cl_4 feed rate is increased, due to quenching effects, caused by the introduction of a cold gas into the plasma, as seen by the modelling results in Figure 38. However, such a decrease in the residence time of carbon species in the hot zone would not explain why the yield of C_{70} is unaffected at the same power level by increasing C_2Cl_4 feed rates. Experimental measurement of the temperature near the reactor surface

(Chapter 7, Figures 32 and 33) showed that in fact the temperature near the reactor surface increases with increasing C_2Cl_4 feed rates, due to the increasing thickness of the thermally insulating layer of soot on the reactor wall and possibly exothermic reactions. As a result, it seems more likely that the residence time of reactive species in the high temperature zone increases, rather than decreases, with increasing C_2Cl_4 feed rates.

Therefore, it seems plausible that the decreasing trend of the C_{60} yield with increasing C_2Cl_4 feed rate may be explained by the fact that C_{60} formation is less favoured by the higher residence time of reactive species in the hot zone, associated with the higher feed rates of C_2Cl_4. The difference in the behaviour of C_{60} and C_{70} formation seems to reinforce the importance of residence time of reacting species in the high temperature zone. The importance of residence time on fullerene formation is also reported by Haufler [1994]. According to Haufler, growing fullerenes must be exposed to sufficient temperatures for a sufficient period of time to facilitate bonding rearrangement and annealing, to increase the fraction of structures possessing the lowest energy. In Haufler's work, the temperature range favouring the growth of fullerenes was reported to be 2,000-3,000 °C. If growing clusters are kept in this temperature range for too long, polymerization and continued growth to species of sizes too large to be

extractable occurs. Thus, there is a balance between "hot-enough-long-enough" and "too-hot-too-long". At the maximum feed rate of C_2Cl_4, 0.54 mol/min, C_{60} formation seems to be on the "too-hot-too-long" end of the spectrum.

Other possible explanations for the decrease in the total C_{60} collection yield as a function of C_2Cl_4 feed rate are:

(i) C_{60} may be carried out of the quench zone with the off-gas; and/or,

(ii) C_{60} may decompose or react with the soot or other by-products, as the temperature near the reactor wall increases with increasing C_2Cl_4 feed rate, resulting in the formation of new, unidentifiable fullerene products.

These factors may be contributing to the decreasing yield of C_{60} with increasing C_2Cl_4 feed rate to a varying degree. Some C_{60} and C_{70} has in fact been detected on the inner surface of the tube leaving the quench zone, however, the quantity of soot collected at this location was only a few milligrams, thus it is not likely that the sublimation or carry-over of C_{60} from the quench zone would explain the decreasing trend observed. The reaction of C_{60} with soot and other by-products during the course of the run is quite possible, and has been confirmed in sublimation experiments, described in Appendix B. During these sublimation

experiments, it was found that C_{60} and C_{70} react with soot and other by-products when heated to 400 °C, in the absence of air. As a result, it is possible that some reactions do take place on the surface of the reactor during the course of the run. However, in the sublimation experiments, the duration of the experiment was 2.5 hours compared with 4 minutes in the soot production experiments. Furthermore, the reactions in the sublimation experiments were not found to be selective to C_{60}, as seems to be the case in the fullerene production experiments. It is therefore, evident that in the present reactor configuration, the proximity of the water-cooled reactor wall to the high temperature reaction zone results in the simultaneous influence of the operating parameters and the growing insulating layer of soot on fullerene synthesis. In an optimal reactor configuration, fullerene formation and condensation should be controlled independently.

7.4.4 Concentration of C_{60} and C_{70} in crude extract

When chromatographic techniques are used for purification of fullerenes, the concentration of C_{60} and C_{70} in the crude extract is a critical factor influencing purification performance. Crude extracts obtained by the procedure described in Section 2.2.2 were analyzed for C_{60} and C_{70} concentration. The percent of extractable material from soot, and the concentration of C_{60} and C_{70} in the crude extract are presented in Figure 48, as a function of torch power and C_2Cl_4 feed

rate. Extractable material refers to fullerenes and chlorinated polyaromatic hydrocarbons, whereas unextractable material consists primarily of graphitic carbon soot. It is evident that at 65 kW compared to 55 kW, less extractable material is collected, confirming that as more energy is introduced into the plasma, more carbon soot is formed. Furthermore, the percent of extractable material in the reactor soot decreases with increasing C_2Cl_4 feed rate. Because chlorinated organic compounds form at lower temperatures, as confirmed by the high concentration of chlorine in the soot produced under low temperature conditions (Section 6.1), these products form near the water-cooled reactor wall. Low C_2Cl_4 feed rates result in lower temperatures near the reactor wall, thus lead to higher yields of soluble chlorinated organic compounds.

The C_{60} and C_{70} concentrations in the crude extract, as seen in Figure 48, increase with increasing power and C_2Cl_4 feed rate. These conditions correspond to the highest collection temperature observed. At these operating conditions, a relatively "clean extract", which can be more easily purified by chromatography is obtained. However, under such conditions, the collection yield of C_{60} is reduced due to the elevated collection site temperatures associated with high C_2Cl_4 feed rates (Figure 47).

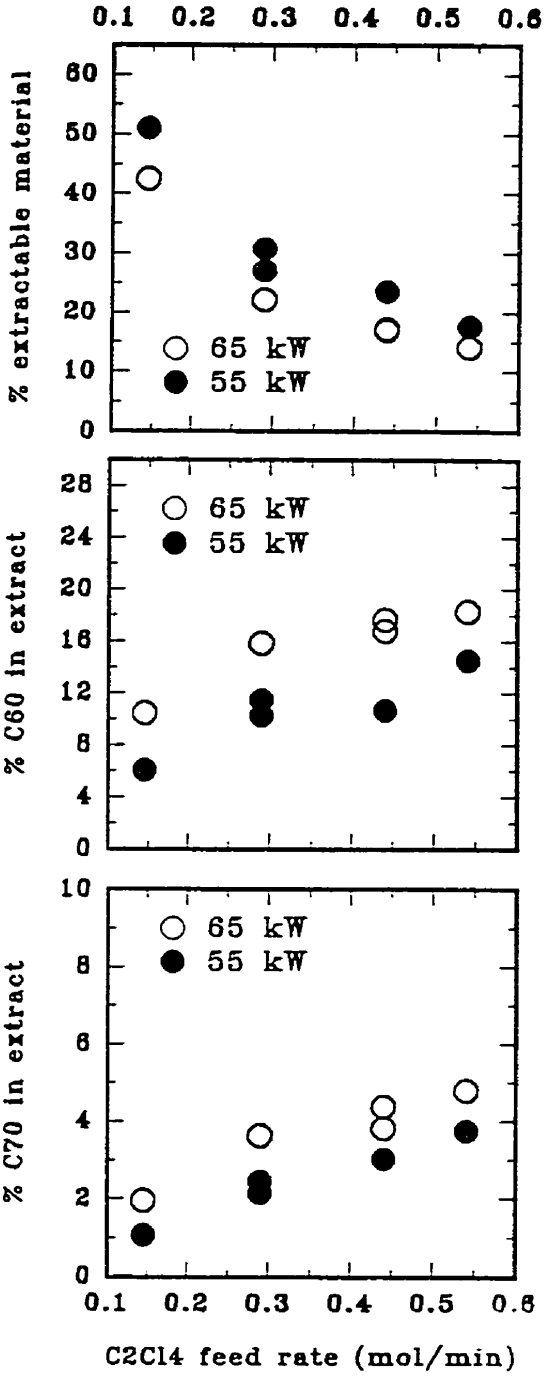

Figure 48: % extractable material (top), % C_{60} in extract (middle), and % C_{70} in extract (bottom), as a function of C_2Cl_4 feed rate and torch power level.

As will be discussed in Chapter 9, efficient purification of *PyroGenesis* soot requires that the crude extract be relatively rich in fullerenes. However, in the reactor design used in this study, conditions resulting in a relatively "clean" extract do not produce a high yield of fullerenes in the collected soot. For example, to obtain an extract which contains 23% fullerenes, a yield of 524 mg fullerenes per mole of C_2Cl_4 is obtained. However, when the yield of fullerenes is higher, such as 688 mg fullerenes per mole C_2Cl_4, the crude extract contains only 12% fullerenes. Soot resulting in a high quality extract can only be obtained under operating conditions offering high reactor temperatures. Under such conditions, there are losses of C_{60}, due to the collection site temperatures which exceed the sublimation temperature of C_{60}.

7.5 Effect of reactor pressure

The effect of reactor pressure on soot collection yield is shown graphically in Figure 49 for experiments run at 55 kW and 65 kW. The C_2Cl_4 feed rate was kept constant at 0.29 mol/min during these experiments. The soot collection yield was drastically reduced above a pressure of 300 torr. The collection yields of C_{60} and C_{70} also dropped significantly above 300 torr, as is shown in Figure 50. Several factors may play a role in the reduced collection rate of soot and fullerenes at higher operating pressures. Firstly, as shown previously in Figure 33,

higher pressure results in lower reactor temperatures, which in turn favour the formation of small chlorinated species. Secondly, higher pressures may adversely affect the mixing of C_2Cl_4 with the plasma, thus resulting in incomplete pyrolysis or in the formation of small chlorinated compounds. In fact, in the experiment performed at 55 kW and 400 torr, the soot was composed of 47% non-fullerene, organic compounds. At 200 torr, at the same input power level, the soot produced contains only 32% non-fullerene, organic compounds.

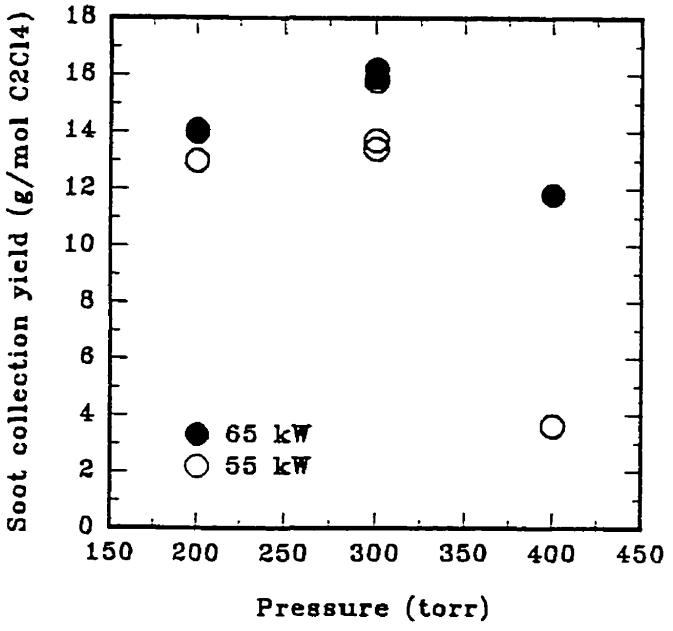

Figure 49: Soot collection yield as a function of reactor pressure [0.29 mol/min C_2Cl_4].

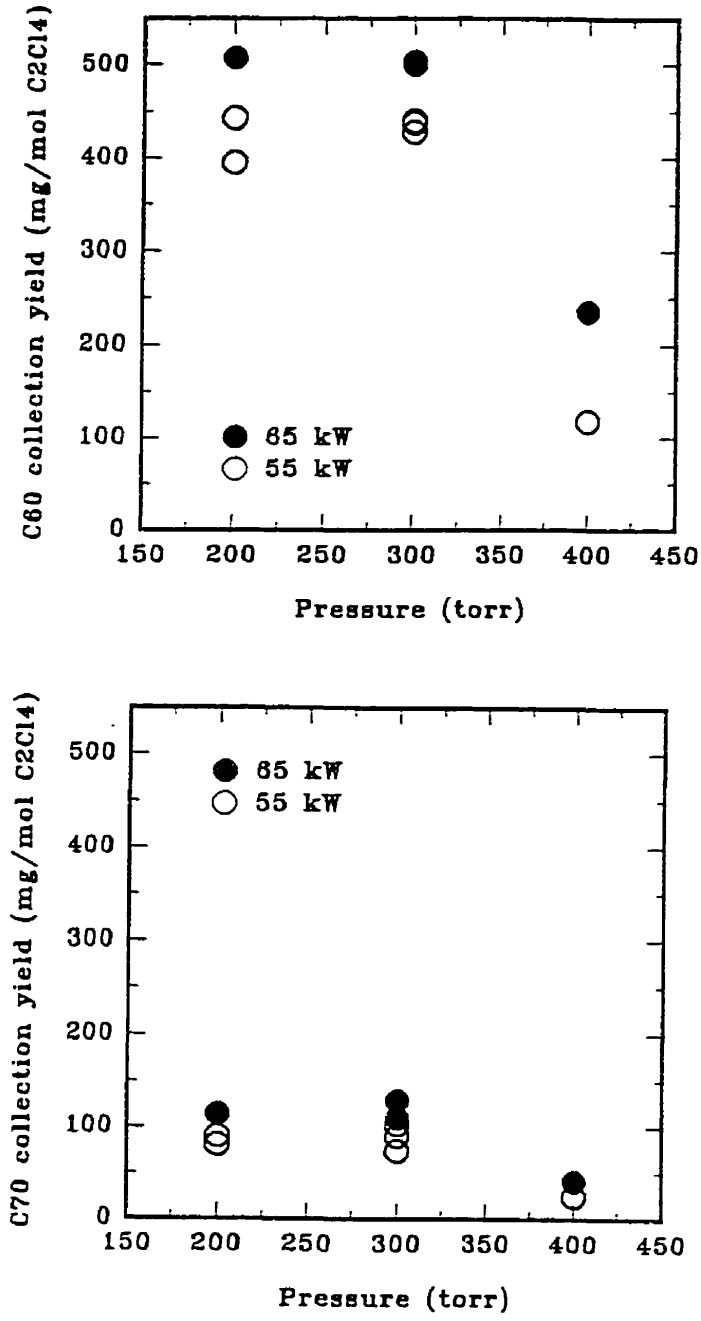

Figure 50: Overall C_{60} (top) and C_{70} (bottom) yields, as a function of reactor pressure [0.29 mol/min C_2Cl_4].

7.6 Theoretical determination of residence time in fullerene formation zone

Since the residence time of reacting species in the temperature zone required for fullerene formation is important in explaining the trends observed experimentally, the residence time in the temperature zone from 2,200 K to 2,600 K was estimated using the model of Bilodeau [1996] for different operating conditions. A plot of the axial velocity of the mainstream (r=0) as a function of location in the axial direction is shown in Figure 51, for different levels of power, C_2Cl_4 feed rate and pressure, respectively. The velocities were determined at location r=0 between the 2,200 K and 2,600 K isotherms of the temperature profile curves presented earlier in Section 7.2.3. The residence time of the mainstream between two isotherms, T_1 and T_2, was approximated by the following equation:

$$rt_{(T_2 - T_1)} = \frac{x_2 - x_1}{v}$$

where,

x_1 = axial distance of first point

x_2 = axial distance of second point

v = average velocity between two points

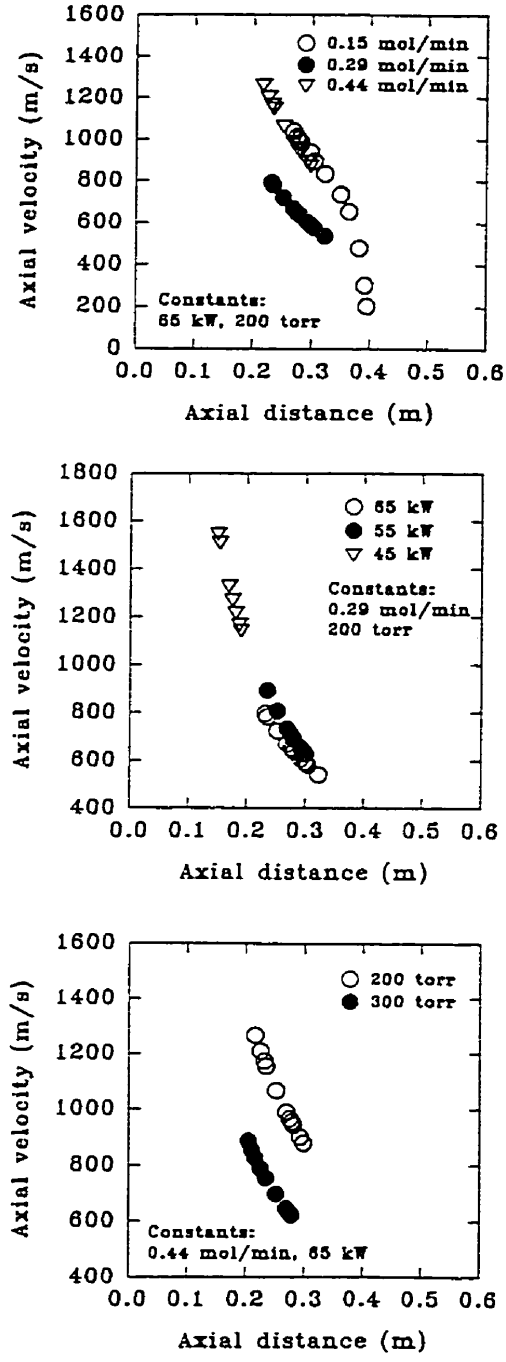

Figure 51: Computed axial velocity as a function of axial location in the 2,200-2,600 K zone.

The total residence time was estimated as the sum of the residence times measured incrementally over the whole distance, for each operating condition. The residence time of the mainstream in the 2,200-2,600 K temperature zone for the different operating conditions is are summarized in Table 6.

Table 6: Theoretical estimation of residence time in 2,200-2,600 K zone

Power (kW)	C_2Cl_4 feed rate (mol/min)	Pressure (torr)	Residence time in 2,200-2,600 K (s)
45	0.29	200	3.0×10^{-5}
55	0.29	200	9.1×10^{-5}
65	0.29	200	14.1×10^{-5}
65	0.15	200	19.0×10^{-5}
65	0.29	200	14.1×10^{-5}
65	0.44	200	7.9×10^{-5}
65	0.44	200	7.9×10^{-5}
65	0.44	300	9.9×10^{-5}

According to the results shown in Table 6, higher power levels result in longer residence time in the specified high temperature zone. This result correlates well with the experimental findings in which high power level resulted in higher soot

and fullerene production yields.

According to the model, higher C_2Cl_4 feed rates result in a shorter residence time in the 2,200-2,600 K temperature zone. Based on the experimental work, presented in Section 7.4.3, it was speculated that increasing the C_2Cl_4 feed rate, in the present reactor configuration, may increase the residence time of the reactive species in the specified hot zone due partly to the increase in reactor temperatures caused by the growing, thermally insulating layer of soot and possibly by exothermic reactions. Since the model does not take into account these two important factors which would greatly contribute to the temperature profile within the reactor, the model does not seem to accurately predict the trends observed experimentally for the effect of C_2Cl_4 feed rate on fullerene production.

The residence time of reacting species in the 2,200-2,600 K zone is also affected by the operating pressure. Lower pressures result in longer plasma jets having higher velocities, as compared to plasmas at higher pressures. In this study, the computed residence time of reactive species in the 2,200-2,600 K zone for pressures of 200 torr seem to be slightly lower that the residence time computed at 300 torr. This slight difference in residence times does not seem to be evident

in the experimental results, which showed that the fullerene production did not vary when the pressure was increased from 200 torr to 300 torr (Figure 50). Although not computed by the model, a significant drop in the residence time of reacting species in the hot zone may occur at 400 torr, since there is an important drop in fullerene yields.

CHAPTER 8: TEMPERATURE MAPPING AND LOCAL SAMPLING OF REACTOR SURFACE

A preliminary mapping of the collection temperatures inside the reactor was made by measuring the surface temperature at several locations in the reactor, according to the procedure described in Section 3.1.4.4. Sampling of soot from different locations within the reactor was also performed, as a first step to predicting the deposition patterns within the reactor. The mathematical model developed by Bilodeau [1996] was compared to the experimental results.

Experiments were performed at 55 kW and 65 kW under the conditions specified in Chapter 4 (Table 2). The C_2Cl_4 feed rate and pressure were fixed at 0.29 mol/min and 300 torr, respectively. The temperatures of the reactor surface reported in this chapter were measured in the absence of C_2Cl_4 injection into the system. Due to the fact that the presence of soot alters the surface temperature and that Cl_2 reacts with the stainless steel sheath of the thermocouples, it became necessary to perform surface temperature measurements in the absence of C_2Cl_4. Thus, the temperatures reported in this chapter correspond to the initial collection temperature during soot production runs.

For the local sampling experiments, samples of soot were collected from eleven zones in the reactor. The data of samples obtained from symmetrical fractions was averaged, resulting in eight fractions, labelled from A to H in Figure 52.

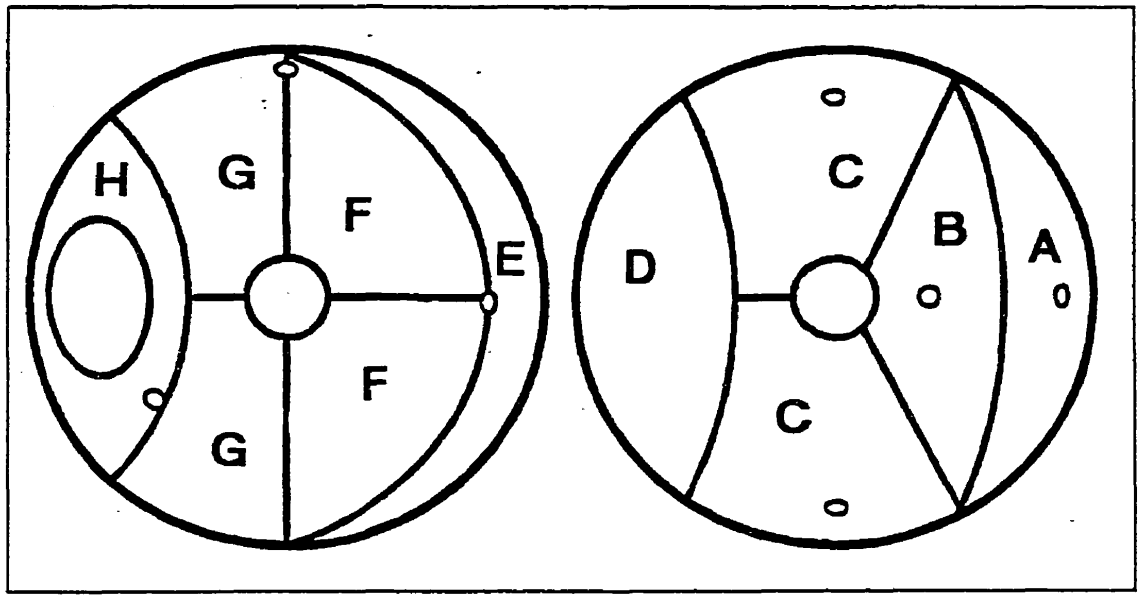

Figure 52: Division of reactor hemispheres in sections, labelled A to H.

The temperatures measured at specific reactor locations are shown in Figure 53, for experiments run at 55 kW and 65 kW. At 55 kW, the surface temperatures ranged from 392 °C to 680 °C, depending on the reactor location, whereas at 65 kW, the temperature range was 450 °C to 715 °C.

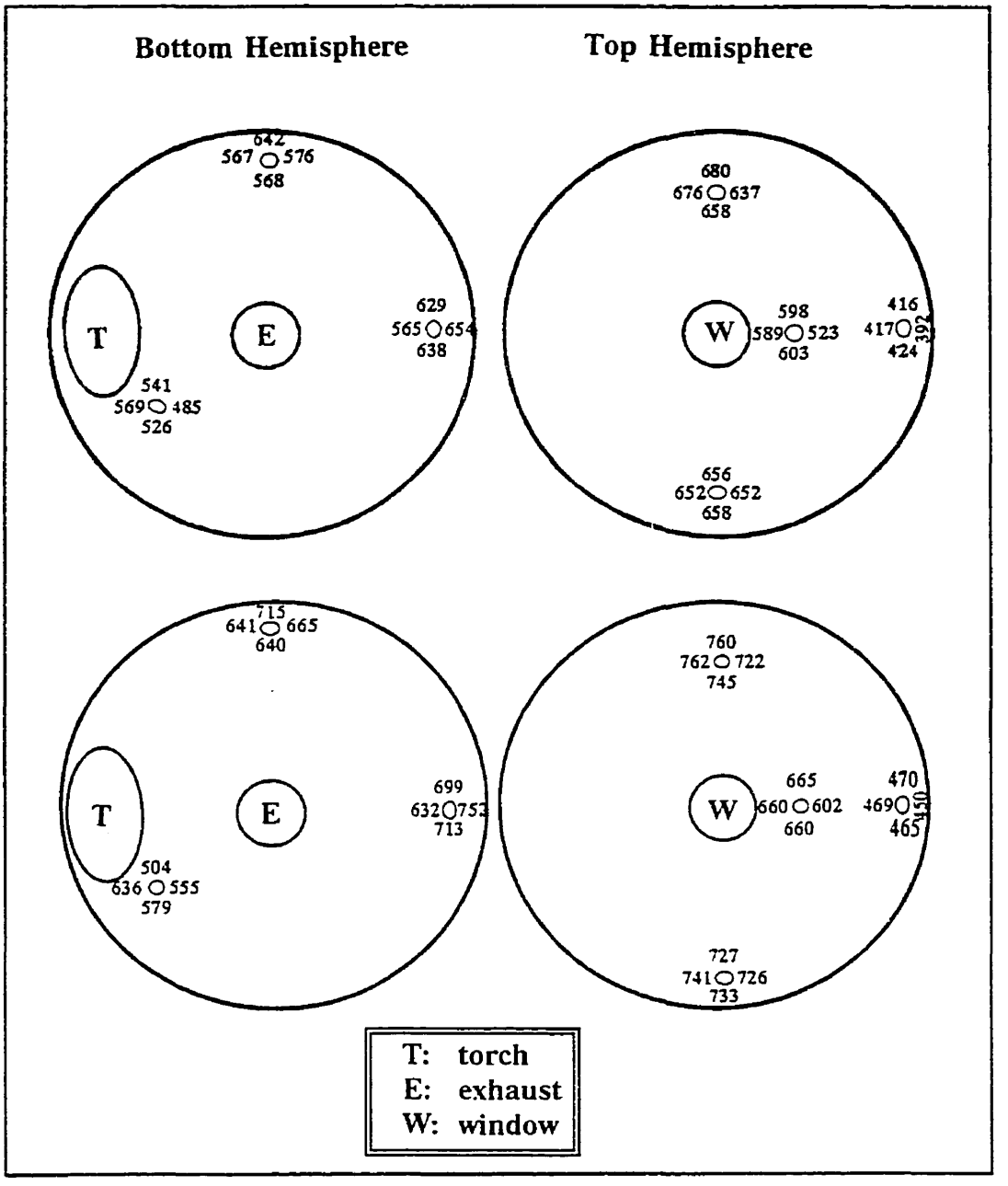

Figure 53: Initial temperatures of various collection sites within the reactor for experiments run at 55 kW (top) and 65 kW (bottom) [300 torr].

Wall temperatures are expected to be highest in Section D, located near the jet impact. However, Section D did not have a port for a thermocouple, so it was not possible to measure the temperature at this location.

An attempt was made by Bilodeau to predict the wall temperatures at different locations through theoretical modelling calculations. The reactor location is expressed as the angle θ, relative to the vertical axis in the computational domain, as shown in Figure 54. Figure 55 shows the calculated and experimental values of the wall temperature as a function of reactor location.

The model predicts extremely high wall temperatures near the jet impact (θ=90°) due to the high temperature of the plasma jet and the strong thermal exchange at this point. It is doubtful whether the predicted temperatures at this location are as high as predicted by the model (up to 1,600 K), since at such high collection site temperatures, fullerenes would not condense. Furthermore, Section D, located at θ=90°, shows a relatively high deposition of fullerenes, as will be seen later in this chapter, in Figures 56 and 57.

The model shows that the temperature decreases as the location near the exhaust tube is reached at θ=-35°. The decrease in temperature along this point may be

due to the enlargement of stream lines, as will be discussed later. There is a temperature increase near the torch neck, θ=-65°, which may also be explained by the narrowing of the streamlines at this point. In general, the values of wall temperature predicted by the model are in good agreement with the experimental values in the range -10°<θ<+40°. The increasing trend of temperature with increasing θ seen in the modelling calculations, however, is not so evident in the experimental data. Since a temperature measurement could not be made in Section D, the elevated temperature predicted by the model at θ=90° could not be confirmed.

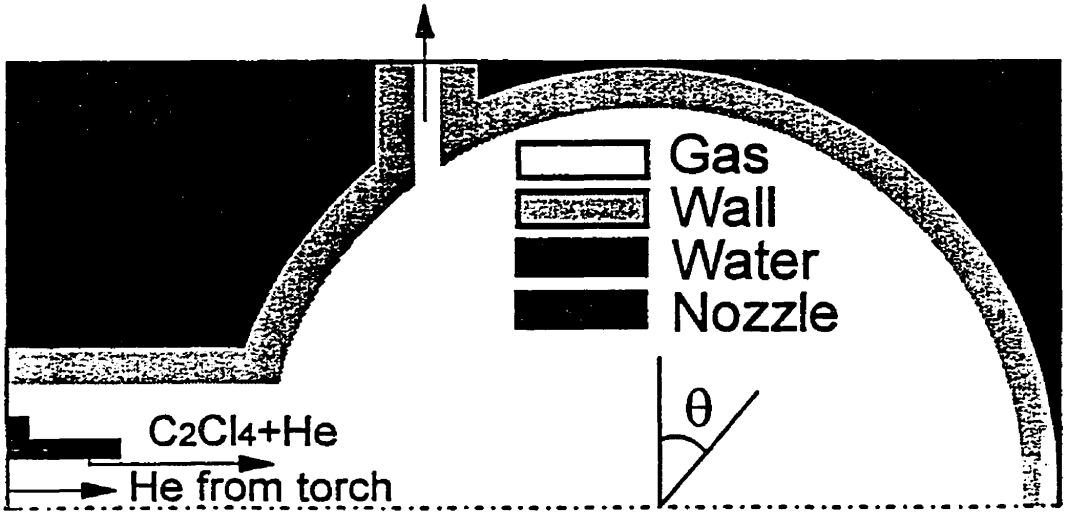

Figure 54: Definition of θ in computational domain [Bilodeau, 1996].

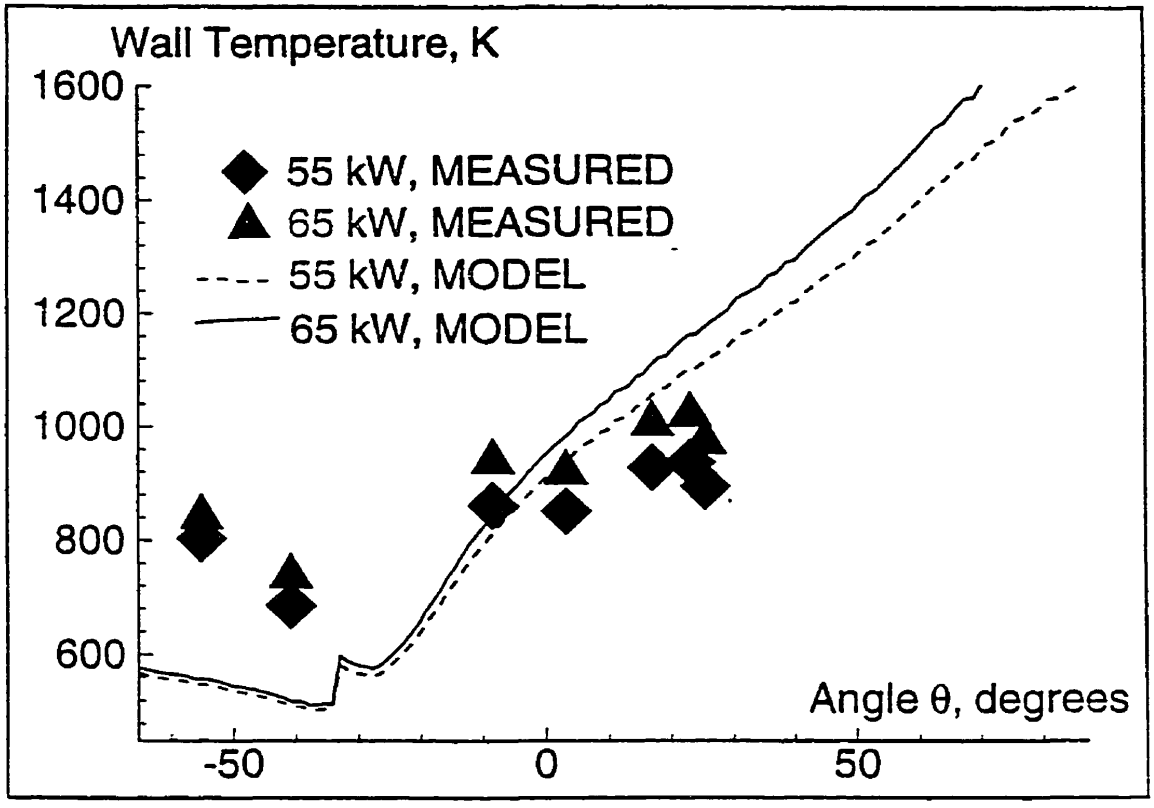

Figure 55: Predicted wall temperatures as a function of angle relative to vertical axis (300 torr) [Bilodeau, 1996].

Figures 56 and 57 show the concentration of insoluble carbon soot, C_{60}, and C_{70} in terms of mass per unit area for experiments run at 55 and 65 kW, respectively. The sections of the reactor labelled A to H may be seen in Figure 52, as well as in Figure 58, which appears later in this chapter. The concentration of higher fullerenes was not taken into account in these measurements. The concentration of insoluble carbon soot was determined by subtracting the concentration of soluble products from the total soot concentration.

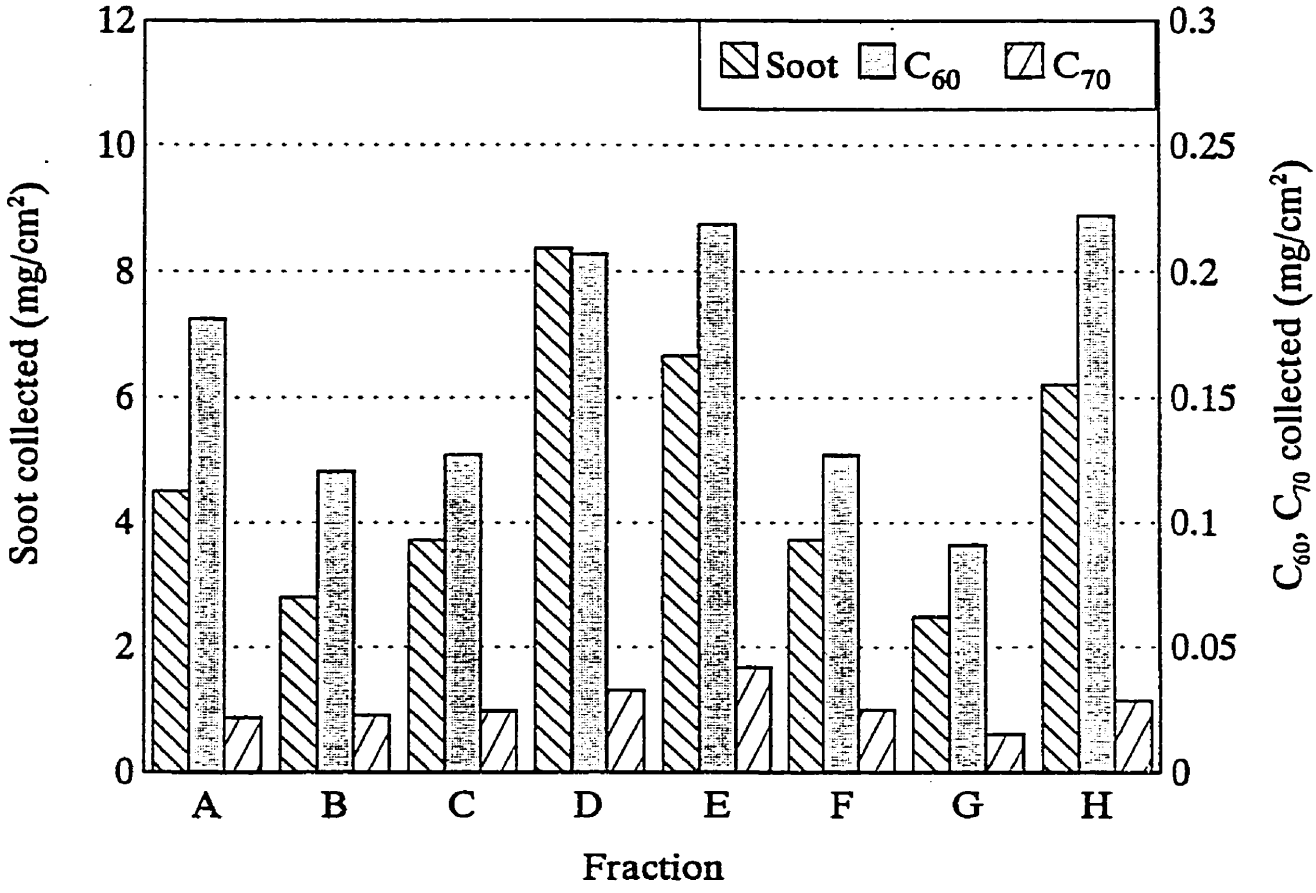

Figure 56: Concentration (mg/cm^2) of insoluble carbon soot, C_{60} and C_{70} as a function of reactor location for experiment run at 55 kW [0.29 mol/min C_2Cl_4, 300 torr].

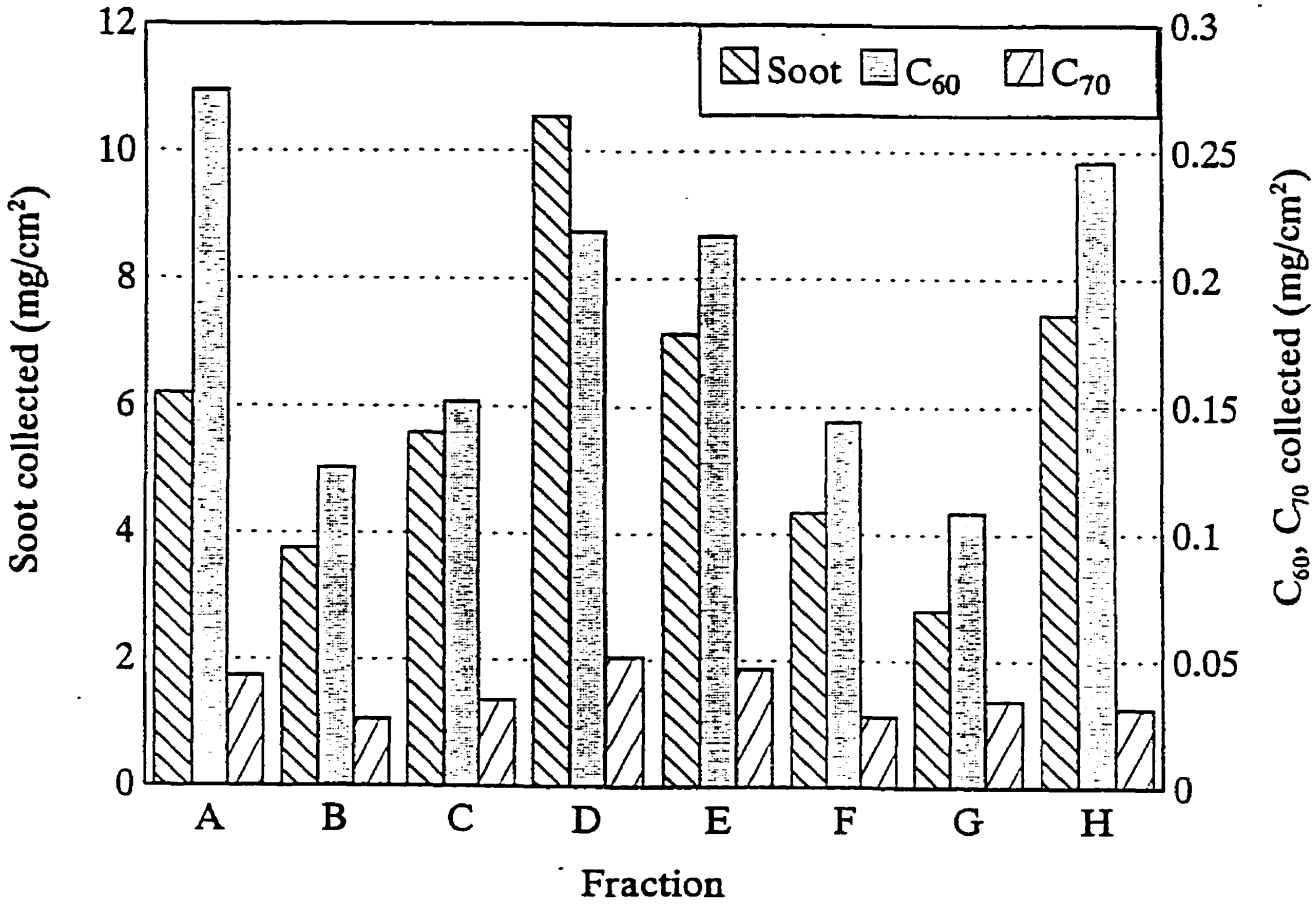

Figure 57: Concentration (mg/cm^2) of insoluble carbon soot, C_{60} and C_{70} as a function of reactor location for experiment run at 65 kW [0.29 mol/min C_2Cl_4, 300 torr].

The deposition pattern of insoluble carbon soot gives a great deal of information on the flow pattern within the reactor. The insoluble carbon soot fraction consists mostly of graphite, with a small amount of large, insoluble, chlorinated, poly-aromatic compounds. Therefore, the collection of this group of products is not expected to be sensitive to temperature, since the sublimation temperature of graphite, which is 3,200 °C (Chapter 5, Figures 23-25), is well above the temperature of the collection site. The largest deposit of insoluble carbon soot per unit area was found in Section D for experiments run at 55 kW and 65 kW. Sections C and E, adjacent to Section D, are expected to show a relatively high concentration of carbon soot. However, only Section E shows a large deposition of insoluble carbon soot, the deposition in Section C being significantly lower. Section H shows a significant deposition of insoluble material, particularly at 65 kW. The lowest concentrations of insoluble carbon soot were found in Fractions B and G. The concentration of carbon soot in fractions H and A, located near the torch neck, showed higher carbon soot deposition than Fractions B and G.

Results of mathematical modelling of the reactor system used in this study provide a great deal of insight on the flow patterns within the reactor. The assumptions, conservation equations and detailed results from the model may be

found in Appendix D.

A plot of the stream functions, as calculated by the model, is shown in Figure 58. The plot shows that the main stream hits the reactor wall facing the plasma jet and then follows the wall until the exit for the exhaust is reached. The entrainment of surrounding gas into the plasma results in a large recirculation around the plasma jet. The flow pattern can also be seen in the plot of velocity profile shown in Figure 59. In Figure 59, a smaller recirculation is also seen near the torch neck. Therefore, from the modelling results, it is expected that the highest deposition of carbon soot would be found in Section D since the main stream hits the reactor wall at this point with the highest loading of products. Sections C and E are adjacent to Section D and thus are also expected to show a high deposition. Experimentally, Section E was found to show a high deposition of carbon soot whereas Section C showed much lower soot deposition, which is not predicted by the model. The high deposition in Section E, located on the bottom hemisphere, as compared to Section C, which is located on the top hemisphere, may be explained by the fact that the exhaust for the reactor was located on the bottom and thus the flow may have not been symmetric. In the 2-D model, the exhaust is represented by a ring, and, thus, the two hemispheres are symmetric.

In the model, Sections A, B, G and F are located at angular positions near the exhaust, and thus, are expected to have lower deposition rates of carbon soot than the other sections. This observation is confirmed experimentally for Sections B, G and F, although Section A showed a relatively large deposition of carbon soot. The failure of the model to predict the high deposition rate in Section A may again be due to the fact that in the model, Section A is very near the exhaust tube, whereas in the real system, the exhaust is located only on the bottom hemisphere.

The deposition of soot in Section H, as seen from the experimental results, was high for experiments run at 55 and 65 kW. Section H is located near the neck of the torch and thus is not impinged by the main stream of the plasma jet. However, diffusion of products from the main stream to adjacent stream lines may result in the transfer of products from the jet to the wall of Section H. The stream lines, as seen in Figure 58 are shown to be compressed near the torch neck, thus leading to efficient mass transfer from the plasma jet to the adjacent reactor wall.

The deposition pattern of C_{60} within the reactor is different than the deposition pattern observed for the insoluble carbon soot. At 65 kW, the highest

concentration of C_{60} was found in Fraction A, followed by Fraction H. This result is quite interesting since the highest deposit of C_{60} did not occur in the same region where the highest deposit of insoluble carbon soot was found (Section D). In Sections D and E, C_{60} deposition may be lower due the elevated wall temperature. The deviation of the C_{60} deposition pattern from the carbon soot deposition pattern is less apparent for the experiment at 55 kW since the temperatures of the wall are lower. At 55 kW, very high concentrations of C_{60} were found in Sections D and E, similar to the deposition pattern of carbon soot.

The deposition of C_{70}, having a higher sublimation temperature than C_{60}, is influenced by the wall temperature to a lesser degree. The highest deposition of C_{70} per unit area was found in Sections D and E for experiments run at 55 kW and 65 kW. However, there was a high deposition of C_{70} in Section A in the experiment at 65 kW, which may also be explained by elevated wall temperatures in locations facing the plasma jets.

Local sampling experiments in conjunction with the mathematical model, developed by Bilodeau [1996], have provided an insight on the flow pattern and temperature profile within the reactor. Such information is expected to be valuable in the design of an optimal reactor for the production of fullerenes via

the *PyroGenesis* process.

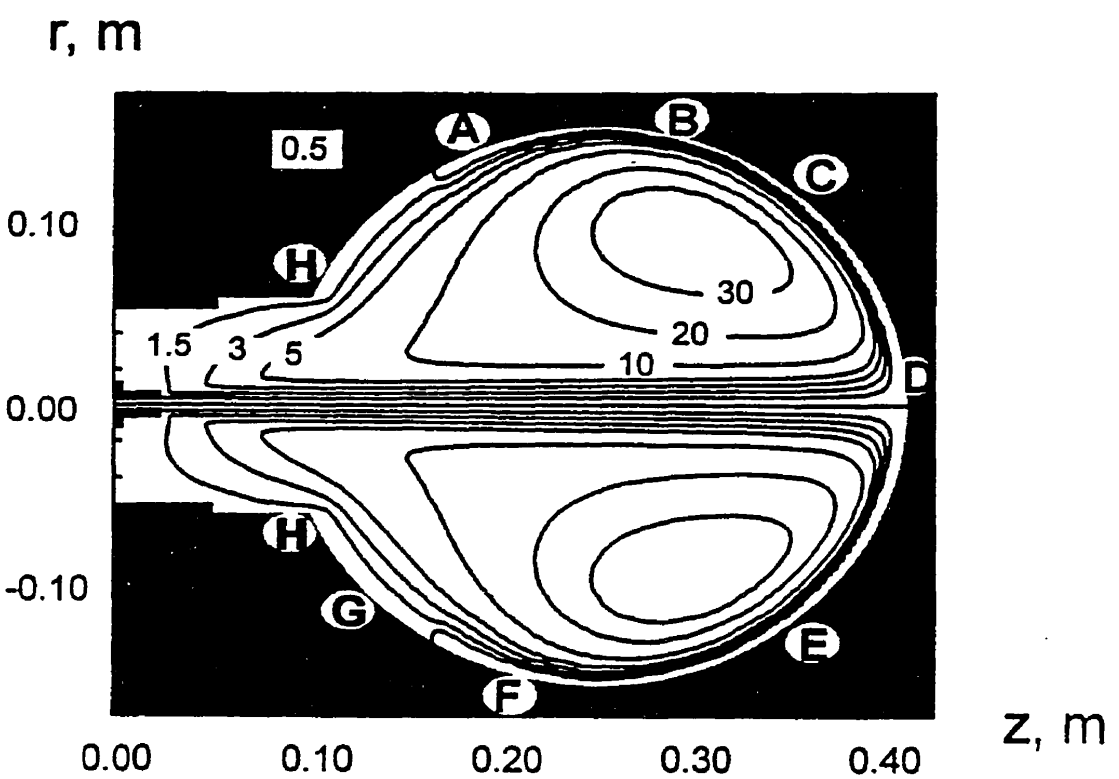

Figure 58: Stream functions predicted by mathematical modelling (65 kW, 0.29 mol/min C_2Cl_4, 300 torr) [Bilodeau, 1996].

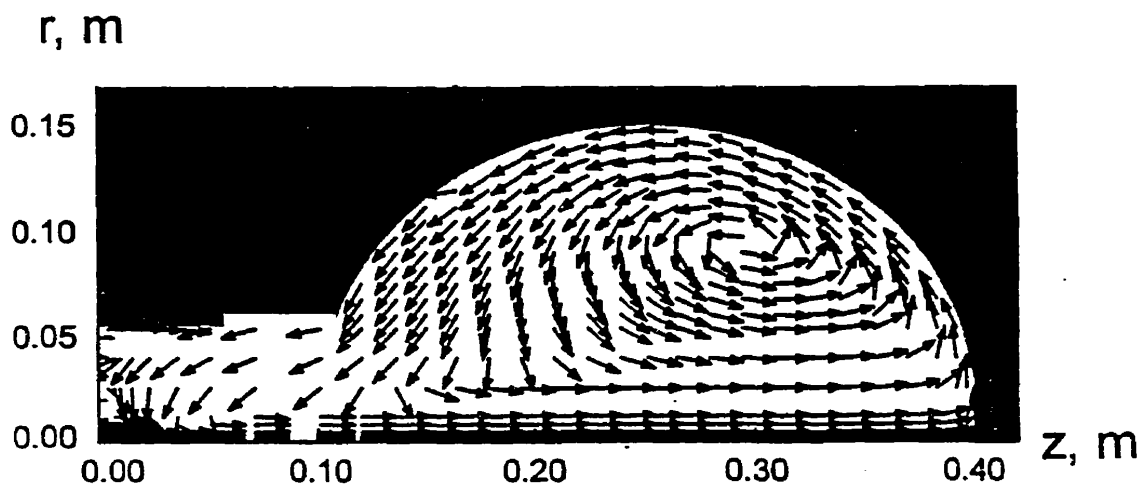

Figure 59: Velocity profile in reactor as predicted by mathematical modelling (65 kW, 0.29 mol/min C_2Cl_4, 300 torr) [Bilodeau, 1996].

CHAPTER 9: IDENTIFICATION OF BY-PRODUCTS AND PURIFICATION OF *PYROGENESIS* SOOT

The work presented in this chapter is focussed on the characterization of the *PyroGenesis* soot in terms of its composition and its ability to be purified by conventional extraction and chromatographic techniques.

9.1 Identification of by-products

The identification of by-products produced by the *PyroGenesis* process was carried out for two reasons. Because the purification of fullerenes by chromatography proved to be difficult due to the presence of by-products, a better understanding of the composition of the crude extract became essential. In addition, the identification of some by-products may give some valuable clues as to the mechanism by which fullerenes form in the *PyroGenesis* process.

A variety of chlorinated compounds were identified by GC-MS. Since the samples of compounds, obtained from HPLC runs as described in Section 4.6, were very small and due to the multitude of components in each sample, no other technique was used for the confirmation of the structure of these compounds. The identification of compounds via GC-MS, alone, does not constitute conclusive

proof of the structure. However, for the purpose of this discussion, these results were deemed satisfactory.

The observed products derived from *PyroGenesis* soot may be classified in two categories: Class I, consisting of chlorinated, non-aromatic compounds and Class II, comprising of perchlorinated aromatic species.

The only compound identified in Class I was tetrachloroethylene (C_2Cl_4), which is also the carbon source for fullerene synthesis in the *PyroGenesis* process. C_2Cl_4 was identified in a sample derived from soot collected in the quench zone. It is difficult to say whether the C_2Cl_4 found in the soot was present due to the incomplete treatment of C_2Cl_4 introduced into the process or whether C_2Cl_4 was reformed after pyrolysis of the starting material. According to Tirey *et al.* [1990], C_2Cl_4 begins to pyrolyse at 800 °C and is completely dissociated at 1,100 °C. Since there seems to be good mixing of the hydrocarbon with the plasma flame, as discussed in Section 7.1, it is unlikely that there was incomplete pyrolysis of C_2Cl_4 by the plasma. C_2Cl_4 presumably formed in a cooler region in the reactor or quench zone. The boiling point of C_2Cl_4 is 121 °C, and thus explains its presence only in the quench zone, since the collection temperatures in the reactor are much higher.

A number of different perchlorinated aromatic species (Class II) were observed in samples collected from the reactor and quench zone. The structures of possible species formed during the *PyroGenesis* process are found in Figure 60. Hexachlorobenzene (C_6Cl_6, MW=284), octachlorostyrene (C_8Cl_8, MW=308), octachloronapthalene ($C_{10}Cl_8$, MW=404), octachloroacenaphthalene ($C_{12}Cl_8$, MW=428), $C_{14}Cl_8$ (MW=452) and $C_{18}Cl_{10}$ (MW=547) were identified in a sample of soot collected in the quench zone. Quantification of these compounds was not possible due to the lack of good separation on the HPLC column which was used to obtain the samples, since this column was primarily purchased for the quantification of C_{60} and C_{70}. The output from the GC-MS scans are included in Appendix D.

The formation of small, chlorinated by-products in the *PyroGenesis* process was found to be promoted in the reactor under low temperature conditions resulting from low input power conditions or in the quench zone where temperatures are low for all operating conditions (Chapter 6, Figure 26). It was also found that shorter experiments resulted in a higher concentration of chlorinated products in the soot (Chapter 7, Figure 41). In addition to low temperatures, surface reactions may also explain the formation of these chlorinated species. Taylor *et al.* [1994] reported that surface catalyzed reactions, of the type shown below,

result in the termination of the free-radical chains, thus inhibiting molecular growth.

$$C_2Cl_3 + Cl + \text{wall} \rightleftharpoons C_2Cl_4 + \text{wall}$$

Tirey *et al.* [1990] have observed that perchlorinated aromatic compounds are more readily formed than non-chlorinated aromatic hydrocarbons from the pyrolysis of chlorinated mixtures. In this work, as shown in Chapter 1, Figure 14, the highest concentration of C_6Cl_6 was found between 850-1,000 °C. $C_{12}Cl_8$ was found in high concentrations between 875-1,050 °C. C_8Cl_8 and $C_{10}Cl_8$ were detected between 750-900 °C, however the concentration of these compounds was significantly lower than C_6Cl_6 and $C_{12}Cl_8$. It should be noted that all of these compounds were also found in the *PyroGenesis* soot collected from the quench zone.

According to Tirey *et al.* [1990], many complex acetylenic and olefinic pathways may be devised to result in the formation of higher molecular weight aromatic species. These pathways, summarized in Figures 61 and 62, show chemically activated chlorine displacement and isomerization reaction channels for the formation of hexachlorobenzene and octaclorostyrene, and octachloronaphthalene and octachloroacenaphthylene, respectively. Octachloroacenaphthylene is an

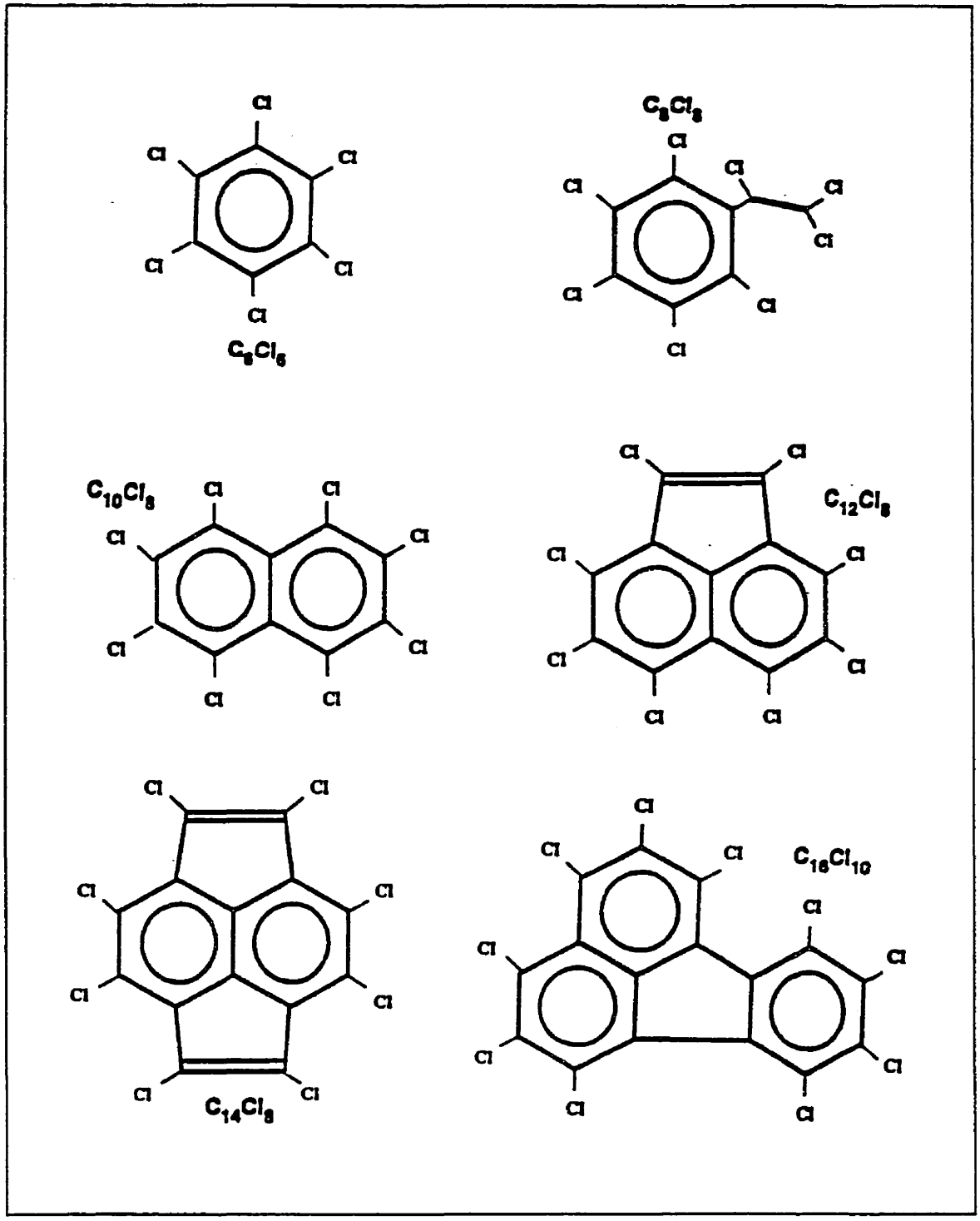

Figure 60: Structure of Class II chlorinated compounds

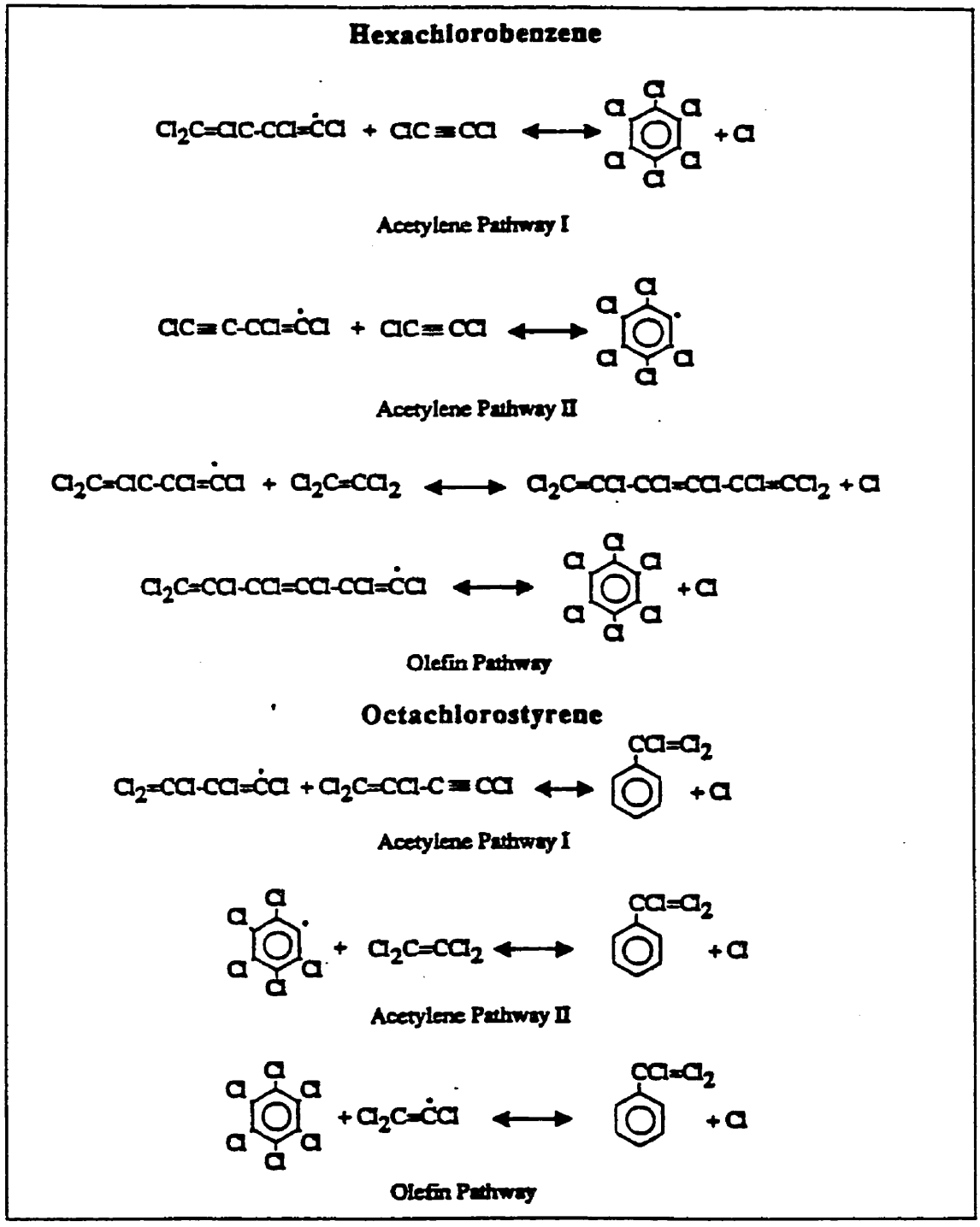

Figure 61: Reaction channel to formation of hexachlorobenzene and octachlorostyrene [Tirey *et al.*, 1990]

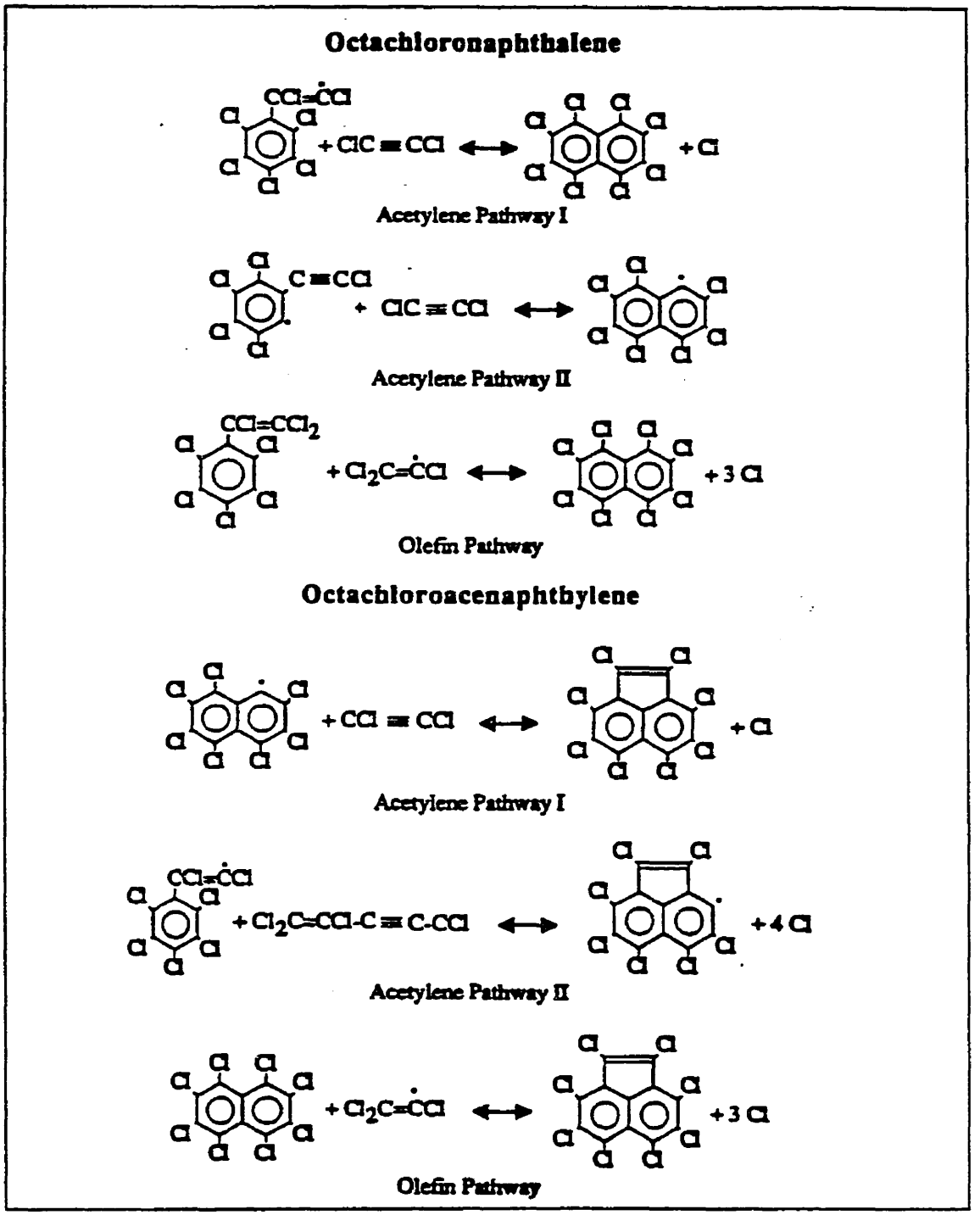

Figure 62: Reaction channel to formation of octachloronaphthalene and octachloroacenaphthylene [Tirey *et al.*, 1990]

interesting compound since it composed of one pentagon and two hexagons, similar to portions of the fullerene molecules.

From the mechanisms shown in Figures 61 and 62 for the formation of large polychlorinated aromatic compounds, the question is raised whether fullerenes may be formed through a series of reactions involving chlorine displacement and isomerization in the various steps. According to Heath [1992], in the fullerene production process based on the arc vaporization of graphite, linear chains of carbon rearrange to form 3-dimensional structures consisting of 6-membered and 5-membered rings which eventually form closed fullerene structures. In the *PyroGenesis* process, the formation of fullerenes may follow a similar mechanism or, alternatively, could the formation of fullerenes produced via the *PyroGenesis* process proceed through a series of reactions involving C_2Cl_2, similar to those shown for the formation of large polyaromatic hydrocarbons? In the thermodynamic study presented in Chapter 5, the presence of C_2Cl_2 was observed when the formation of graphite was inhibited (Figure 26). The presence of C_2Cl_2 in the temperature range where fullerenes are predicted to form may raise the question as to the implication of this intermediate in the fullerene formation process. Although these questions are fascinating, they cannot be conclusively answered based on the work presented herein. One comment that can be made,

however, is that the reactions resulting in the chlorinated PAH's described by Tirey *et al.* occurred in the temperature range of 850-1050 °C, which is significantly lower than the temperature range which has been predicted for fullerene growth, 2,200-2,600 K [McKinnon, 1991]. Therefore, it seems feasible that the formation of fullerenes via the *PyroGenesis* process proceeds through the growth of carbon clusters, similar to the mechanism by which fullerenes form in the vaporization of graphite methods. The presence of the chlorinated aromatic compounds identified in this work may be due to termination of fullerene precursor molecules (C_n), which were not given an adequate residence time in the high temperature fullerene formation zone.

9.2 Purification by Chromatography

Column chromatography is the most widely accepted and used technique for the purification of C_{60} and C_{70}. Various chromatographic methods using a variety of packing materials and solvents have been investigated for the purification of fullerenes. These methods have been described in Section 3.5.2. Two such chromatographic methods have been adopted in this work for the purification of C_{60} and C_{70} from *PyroGenesis* extract. The composition of *PyroGenesis* extract, compared to fullerene extracts produced from different processes, is unique due to the presence of chlorinated by-products. As such, it is expected that the

purification of fullerenes from *PyroGenesis* extract would be more difficult.

Chromatographic processes are typically very slow, require the use of large quantities of solvents and are expensive because the packing material in many cases must be replaced after each run. Furthermore, due to the irreversible adsorption of fullerenes to the packing material, chromatographic techniques result in the loss of fullerenes. For these reasons, column chromatography is only useful in the lab scale, and becomes quite difficult to scale-up for industrial use. Nonetheless, column chromatography was useful in the present work for assessing the ease with which fullerenes could be purified from *PyroGenesis* soot.

9.2.1 Purification of C_{60}

The purification of C_{60} from *PyroGenesis* extract was performed on chromatography columns packed with a mixture of activated carbon (Norit A) and silica gel, according to the procedure of Scrivens *et al.* [1992], using toluene as the mobile phase. This method has been shown to offer significant improvements over purification on alumina, with hexane as the mobile phase, since the time required for purification is greatly reduced due to the higher solubility of fullerenes in toluene. Furthermore, the packing material is much less expensive than alumina. To further improve the elution rate, the columns may be run

under a pressure of air or inert gas.

Using a mixture of activated carbon and silica gel as the stationary phase and toluene as the mobile phase, the purification of C_{60} was investigated. A column with an internal diameter of 3.8 cm was used for the study. An argon pressure of 10 psi was used above the mobile phase to provide a flow equivalent to 1.4 cm/min. The crude extract used for all experiments was first washed with ether according to the procedure described in Appendix B prior to being introduced onto the column.

Two factors are considered to be very important in purification via chromatography, namely:

(i) the purity of a compound in a particular fraction, and,

(ii) the recovery of a compound in a high purity fraction.

For example, a sample of C_{60} which is 99% pure, but only accounted for 50% of the C_{60} originally present in the extract is considered unacceptable. Similarly, a sample having a C_{60} recovery of 99% and a purity of 50% is also considered unacceptable.

The height of the packing material plays a key role in the operation of the chromatography column. When a column is too short, insufficient separation of C_{60} from the by-products and C_{70} may occur. On the other hand, longer columns may result in a lower recovery of C_{60} and C_{70} due to irreversible adsorption to the packing material. Results from two chromatographic runs in which the column height was 21 and 25 cm are shown in Table 7. There was no significant difference in the purity nor the recovery of C_{60} obtained from the chromatographic runs in Table 7. It is highly likely that if the column height was varied below 21 cm or above 25 cm, the chromatographic separation of C_{60} would have been affected. However, since the results obtained in the chromatographic runs shown in Table 7 were considered to be satisfactory, no other experiments were performed to optimize the height of the column. Since crude extracts

Table 7: Effect of column height on C_{60} purity and recovery

Column height (cm)	**Purity of C_{60} in C_{60}-rich fraction**	**Recovery of C_{60} in C_{60}-rich fraction**
21	98.8%	75%
25	98.0%	74%

derived from *PyroGenesis* soot may vary greatly in composition, in subsequent chromatography experiments, the column height was fixed at 25 cm in order to ensure proper purification of C_{60}.

The amount of material which is loaded onto a column, referred to as column loading, is known to have an effect on the operation of the column. The loading of the column has been defined as follows:

$$Column\ Loading = \frac{mass\ of\ crude\ extract}{cross\text{-}sectional\ area\ of\ column}$$

The loading of ether-washed extract per cross sectional area was varied from 0.3 g/cm^2 to 0.5 g/cm^2. in an attempt to increase the throughput through the chromatography column. The purity and recovery of C_{60} in the C_{60}-rich fraction are shown graphically in Figure 63, as a function of column loading. It should be noted that each point on these graphs corresponds to an extract derived from soot obtained under different operating conditions. However, the fullerene content of the extracts used for this study was equivalent. The extracts contained 31.0% - 37.2% C_{60} and 9% - 11.7% C_{70}.

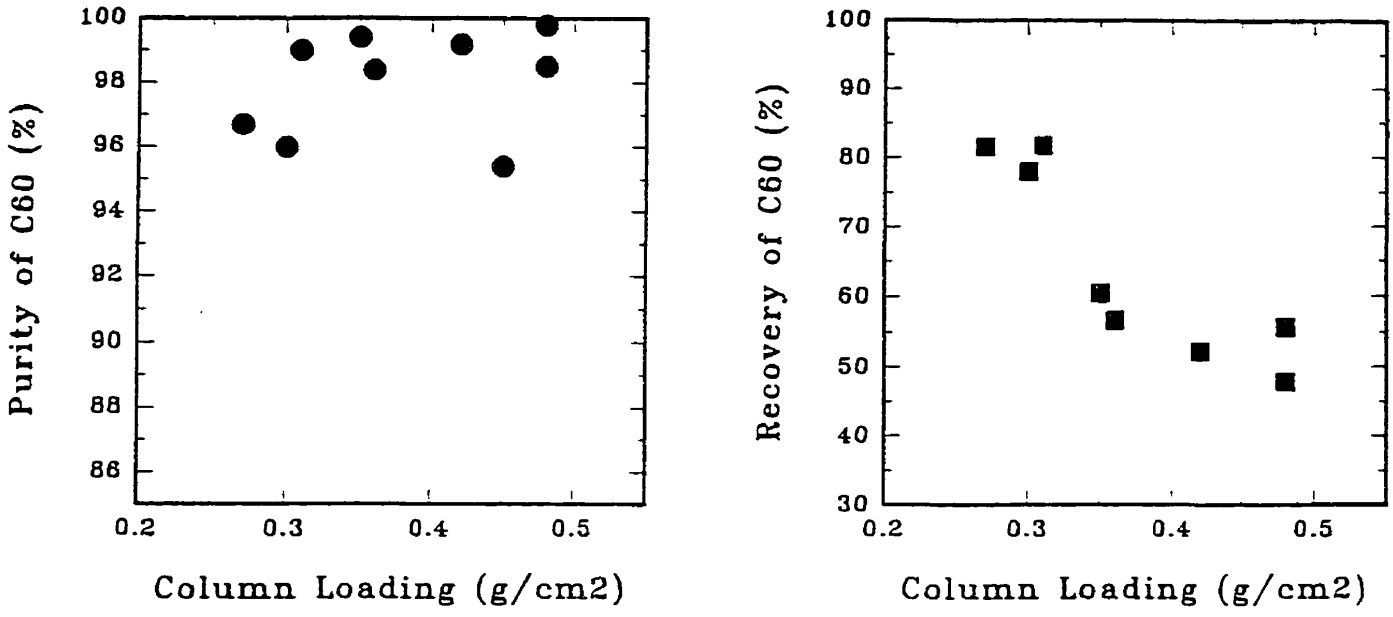

Figure 63: Purity (left) and recovery (right) of C_{60} in C_{60}-rich fraction as a function of column loading

Within the range of column loadings used, the purity of C_{60} was not sensitive to the column loading. The colour of the effluent from the column was monitored visually and only solutions which were purple in colour were collected in the C_{60}-rich fractions. Once the colour of the effluent solution changed, the flask was changed to collect subsequent fractions. Furthermore, since the composition of each extract differed slightly due to the fact that the extracts were obtained from different soot production experiments, it is likely that the purity in the C_{60} fraction would also depend on the by-products present in the extract. As a result,

the purity of the samples relates more to the rapidity with which the flask was changed during the operation of the column and to the initial composition of the extract, and does not, in this case, relate to the column loading. However, if the column loading was increased above 0.5 g/cm^2, it is likely that at some point, the purity would be compromised.

The recovery of C_{60} in the C_{60}-rich fraction seems to show a strong decreasing trend when the column loading is increased. A column loading of approximately 0.3 g/cm^2 resulted in a C_{60} recovery of 80% in the pure fraction, whereas column loadings approaching 0.5 g/cm^2 resulted in a C_{60} recovery of only 50%.

The composition of the extract loaded onto the column has a significant effect of on the purification process. When the crude extract consists of a high concentration of C_{60}, high purity and high recovery of C_{60} can be obtained. However, when the extract contains a relatively low concentration of C_{60}, a lower purity and recovery is expected, irrespective of the length of the column and sample loading. For example, when an extract containing 18% C_{60} (loading = 0.3 g/cm^2) was used for purification, the C_{60} fraction was 95% pure, with a recovery of only 60%. A similar loading of extract having 32% C_{60}, resulted in an 80% recovery of C_{60} in a fraction which is 99% pure. For this reason, the partial

removal of by-products by solvent extraction with diethyl ether, as described in Appendix B (Section B.3) is an essential step for the purification of fullerenes from *PyroGenesis* soot. Under the best operating conditions, using a column 3.8 cm in diameter, approximately 1 gram of pure C_{60} is eluted in 2 hours.

During the C_{60} purification process, two red fractions were collected after the elution of C_{60} from the column. The first fraction typically consists of 50-75% C_{60} and 14-25% C_{70}. This fraction was further purified on an activated carbon / silica gel column. The second red fraction, consisting of 18-35% C_{60} and 45-67% C_{70}, was purified using a modified alumina column, as described below.

9.2.2 Purification of C_{70}

An alternative chromatographic technique is a SOXHLET type chromatographic column in which the solvent is recirculated by evaporation and condensation [Khemani *et al.*, 1992]. This method is similar to that used for extracting the mixed fullerenes from the soot (Section 3.2.1). Although this type of column requires minimal supervision, it takes several days for purification. For example, this technique takes 20 to 30 hours to elute pure C_{60} and an additional 50-70 hours to elute C_{70}.

C_{70} rich fractions were obtained by loading the red fractions obtained from the Norit A/Silica Gel column onto a SOXHLET chromatography column packed with neutral alumina. The typical composition of the red fraction was 18-35% C_{60} and 45-67% C_{70}. The internal diameter of the SOXHLET alumina column was 5.8 cm. Hexane was used as the mobile phase. The column loading of the red fraction varied from 1.05/cm^2 to 1.12/cm^2. The highest purity of C_{70} obtained from this column was 84% with a C_{70} recovery of 81% in the C_{70}-rich fraction. A C_{70} fraction which was 92% pure was obtained, however, the C_{70} rich-fraction from the first alumina column was further purified on a second alumina column.

It is quite clear than the purification of C_{70} from *PyroGenesis* extract is difficult, requiring at least three chromatographic steps. Many chromatographic steps are undesired because of the cost associated with chromatography, as well as the loss of material in each step. The low yield of C_{70} in soot coupled with the difficulty in purifying C_{70} explains the elevated price for pure C_{70}, as compared to C_{60} in the marketplace.

It is evident that although the extract produced via the *PyroGenesis* process, using the present reactor configuration, contains a variety of by-products, conventional purification techniques may be used to isolate C_{60} and C_{70}. The purification of

PyroGenesis soot, however, is more difficult than the purification of soot produced via the arc vaporization of graphite which does not contain any by-products, other than graphite.

CHAPTER 10: COMPARATIVE STUDY OF FULLERENE PRODUCTION METHODS

The development of the *PyroGenesis* process was greatly influenced by the low scale-up capability of existing fullerene production technologies. Currently, commercial production of fullerenes by companies such as MER Corp. [Tuscon, Arizona] and SES Inc. [Houston, Texas] is realized by methods based on the arc vaporization of graphite electrodes. In addition to the arc vaporization of graphite rods, other fullerene production technologies are based on the vaporization of carbon powder in thermal plasmas and the combustion of benzene or other hydrocarbons. The *PyroGenesis* process, in its present reactor configuration, is compared to these fullerene production technologies in Table 8. The various production technologies have been compared based on the quantity of fullerenes produced per kilowatt-hour or per mole of carbon fed into the process.

According to the Table 8, the production of fullerenes per kilowatt-hour of energy via the *PyroGenesis* process, in its present reactor configuration, was found to be 0.28 g/kWh. This yield based on energy input seems to be much higher compared to the vaporization of carbon powder [Yoshie *et al.*, 1992], yet

Table 8: Comparison of various fullerene production processes

Process	Soot g/h	$C_{60}+C_{70}$ g/h	$C_{60}+C_{70}$ per energy (g/kWh)	$C_{60}+C_{70}$ per carbon input (%)	Concentration of $C_{60}+C_{70}$ in soot	Difficulty in purification	Difficulty in scale-up
PyroGenesis	440 264	15.5 10.7	0.28 0.19	2% 2.8%	5.6%	yes	no
Carbon arc [Smalley, 1993]	30	3.6	0.92	<20%	13%	no	yes
Carbon powder in plasma [Yoshie *et al.*, 1992]	30	2.1	0.08	7%	7%	no	yes
Combustion of benzene [Howard *et al.*, 1992]	3.7	0.45	___	0.5%	<20%	yes	no

significantly lower that the arc vaporization of graphite method [Smalley, 1993].

When comparing the production of fullerenes per unit mole of carbon fed, the carbon arc method seems to show a higher conversion from carbon to fullerenes as compared to the *PyroGenesis* process. The vaporization of carbon powder also results in a higher conversion of carbon to fullerenes as compared to the *PyroGenesis* process. In an atmosphere where only carbon atoms are present in an inert gas, a high conversion of carbon to fullerenes may be expected. In the *PyroGenesis* process, competing reactions of carbon with halogen atoms may result in a lower conversion of carbon to fullerenes. Competing reactions may also explain the low conversion of carbon to fullerenes in the combustion synthesis of fullerenes, where hydrogen and oxygen are present, along with the carbon atoms. The *PyroGenesis* process, however, results in a much higher carbon conversion when compared to the combustion synthesis method.

A comparison of the concentration of fullerenes in the soot produced by various methods is often cited by authors. The *PyroGenesis* process, in the reactor configuration used in this study, produces a soot which contains up to 5.3% fullerenes, while the arc vaporization method has been reported to yield up to 30% fullerenes [Koch *et al.*, 1991]. However, commercial soot by the carbon arc

method only yields 8-10% fullerenes. The combustion synthesis of fullerenes is reported to yield 0.0026-20% fullerenes in soot. Although the various technologies are often compared by the concentration of fullerenes in soot achieved, this point of comparison is not very useful in evaluating technologies, since the concentration of fullerenes in soot does not give an indication of the production rate of fullerenes or the scale up-potential of the technology.

The production of fullerenes via the vaporization of graphite or carbon powder is advantageous since no soluble by-products are formed during the process, thus rendering a more facile purification of C_{60} and C_{70}. The *PyroGenesis* process, as well as the combustion synthesis process, both involve competing reactions which result in the formation of undesired by-products. Process optimization should however lead to the reduction of by-products formation.

As has been seen repeatedly throughout this thesis, the *PyroGenesis* process, in its present configuration, is far from optimal. It has been shown that in the present reactor, fullerene synthesis is affected by the cooling effects of the surrounding water-cooled wall, which is in close proximity to the high temperature zone. This factor alone accounts for the relatively low yield of fullerenes per kWh and per mole of carbon fed. In an optimized reactor configuration, heat

losses can also be minimized through the use of a refractory lined reactor, as opposed to a water-cooled reactor. Furthermore, proper design of the high temperature reaction zone and low temperature condensation zone would lead to maximum fullerene production and minimum by-product formation.

Clearly, the main advantage of the *PyroGenesis* process is that it can be scaled up to produce industrial quantities of fullerenes. Even in the lab-scale unit presented in this work, an equivalent of 15 g/h of fullerenes were produced, a factor of 4 higher than the arc vaporization of graphite method. This work has resulted in a better understanding of conditions under which fullerene synthesis is promoted in the *PyroGenesis* process and therefore, may be used as starting point from which the process can be scaled up and optimized.

CONCLUSIONS

A technology, based on the thermal plasma dissociation of halogenated hydrocarbons, was developed as part of this work. Chlorinated hydrocarbons, in particular tetrachloroethylene (C_2Cl_4), resulted in higher fullerene yields when compared to hydrogenated and fluorinated hydrocarbons, due mostly to the instability of C-Cl bonds at high temperatures.

In the present reactor configuration, the temperature of the collection site was strongly affected by the deposit of soot during the production run. The deposit of soot on the reactor surface acted as a thermally insulating layer, thus, reducing the heat losses to the cooling water. As a result, the temperature rise in the reactor affected the rate of fullerene deposition on the wall. The temperature of the collection site also influences the rate of by-product formation and collection.

An adequate residence time in a high temperature zone is required for fullerene formation. The operating parameters, such as input electrical power, C_2Cl_4 feed rate and reactor pressure, influence the residence time in a high temperature zone and thus affect fullerene formation. In the present reactor, an input power in excess of 55 kW was required for the treatment of up to 0.54 mol/min of

C_2Cl_4. High C_2Cl_4 feed rates resulted in a lower conversion of C_2Cl_4 to fullerenes. Lower reactor pressures (200 and 300 torr) resulted in higher fullerene yields, as compared to results obtained at 400 torr. Local sampling experiments, in conjunction with the mathematical model developed by Bilodeau [1996], provided an insight on the flow pattern and temperature profile within the reactor.

Various perchlorinated aromatic compounds present in the *PyroGenesis* soot were identified. The structure of these compounds is reminiscent of the fullerene structure, which may offer some insights as to how fullerenes form via the *PyroGenesis* process. Due to the low temperature of formation of these compounds, it is believed, however, that fullerenes form through a series of C-C reactions, similar to those proposed for the formation of fullerenes via the arc vaporization of graphite method.

C_{60} and C_{70} were purified by conventional chromatographic techniques, however the presence of by-products resulted in a longer and multi-step purification process.

In summary, the work undertaken as part of this PhD thesis, has led to the

successful development of a technology which can potentially be used for the large scale synthesis of fullerenes. The work, therefore, serves as a basis on which an optimal reactor configuration can be designed for fullerene production via the thermal plasma dissociation of halogenated hydrocarbons. It is clear that the reactor used in this study did not offer optimum conditions for the production and collection of fullerenes. The residence time of reacting species in the fullerene formation zone was difficult to control due to the proximity of the surrounding water-cooled walls to the hot reaction zone. Furthermore, fullerene collection was also inadequate due to the increase in the collection temperature with time, caused by the deposition of the insulating soot layer. An improved reactor would be characterized by an optimum residence time of reactive species in the high temperature formation zone and by a controlled temperature collection zone.

FUTURE WORK

In order to optimize the *PyroGenesis* process, a new reactor must be designed and fabricated in which the fullerene formation and fullerene collection zones can be controlled effectively. Future developmental work may include the following:

- Argon should be investigated as the plasma-forming gas, due its significantly lower cost over helium.
- The design of a new nozzle for the injection of C_2Cl_4 into the plasma is required in order to enable continuous operation over several hours.
- The formation of larger fullerenes and other molecules, such as endohedral fullerenes and derivatized fullerenes, should be investigated.
- Alternative purification techniques should be investigated for the purification of C_{60}, C_{70} and potentially other fullerene compounds from the *PyroGenesis* soot.

CONTRIBUTION TO KNOWLEDGE

A novel method for the production of fullerenes was developed in which halogenated hydrocarbons may used as starting materials for fullerene synthesis. Such a process may be scaled up to produce industrial quantities of fullerenes.

The effect of the process parameters on the residence time of carbon species in the high temperature zone required for fullerene formation was understood. This body of information, contained in this thesis, forms a basis on which an optimized reactor configuration can be designed for the large scale synthesis of fullerenes via the *PyroGenesis* process. It is believed by the author that in the future, should a commercial market for fullerenes develop, the world's supply of fullerenes will be produced via the thermal plasma dissociation of halogenated hydrocarbons.

REFERENCES

Ajayan, P.M., Iijima, S. 1992, Smallest Carbon Nanotube, *Nature*, **358(6381)**, 23-23.

Ajie, H., Alvarez, M.M., Anz, S.J., Beck, R.D., Diederich, F.N., Fostiropoulos, K., Huffman, D.R., Kraetschmer, W., Rubin, Y., Schriver, K.E., Sensharma, D., Whetten, R.L. 1990, Characterization of the All Carbon Molecules C_{60} and C_{70}, *J. Phys. Chem.* **94(24)**, 8630.

Aldersey-Williams, H. 1994, The Most Beautiful Molecule, Aurum Press, London.

Atwood, R.D., Koutsantonis, G.A., Raston, C.L. 1994, Purification of C_{60} and C_{70} by Selective Comlexation with Calixarenes, *Nature*, **368(6468)**, 229.

Averitt, R.D., Alford, J.M., Halas, N.J. 1994, High purity vapour phase purification of C_{60}, *Appl. Phys. Lett.*, **65(3)**, 374.

Bacon, R. 1960, Growth, Structure and Properties of Graphite Whiskers, *J. Appl.*

Phys., **31(2)**, 283.

Ballschmiter, K., Kirschmer, P., Zoller, W. 1986, Experiments in High Temperature Chemistry of Organohalogens, *Chemosphere*, **15(9-12)**, 1369.

Barton, J., Howlet, K.E. 1951, The Kinetics of the Dehydrochlorination of Substituted Hydrocarbons. Part VIII. The Mechanism of the Thermal Decomposition of 1:1:2:2- and 1:1:1:2- Tetrachloroethane, *J. Chem. Soc.*, 2033.

Bilodeau, J.F., Alexakis, T., Meunier, J.L., Tsantrizos, P.G. 1996, Modeling of the Synthesis of Fullerenes by the Plasma Torch Dissociation of C_2Cl_4, *J. Phys. D: Appl. Phys.*, (submitted Nov. 5, 1996).

Boulos, M., Fauchais, P., Gauvin, W.H., Pfender, E. 1983, Plasma Technology Fundamentals and Applications, Thermal Plasmas: Technology and Applications, 1.

Brabec, C.J., Anderson, E.B., Davidson, B.N., Kajihara, S.A., Zhang, Q.-M, Bernholc, J. 1992, Precursors to C_{60} fullerene formation, *Phys. Rev. B, Rapid Commun.* **46(11)** 7326.

Calestani, G. 1994, Chemical and Structural Aspects of High T_c Superconductors, Proc. of 1994 GNSM School, ed. M. Acquarone, 2.

Chang, T.M., Naim, A., Ahmed, S.N., Goodloe, G., Shevlin, P.B. 1992, On the Mechanism of Fullerene Formation. Trapping of Some Possible Intermediates, *J. Am. Chem. Soc.*, **114**, 7603.

Chen, H.S., Kortan, A.R., Haddon, R.C., Koplan, M.L., Chen, C.H., Mujsce, A.M., Chou, H., Fleming, D.A. 1991, Reactivity of C_{60} in pure oxygen, *Appl. Phys. Lett.*, **59(23)**, 2956.

Chibante, L.P.F., Thess, A., Alford, J.M., Deiner, M.D., Smalley, R.E. 1993, Solar Generation of the Fullerenes, *J. Phys. Chem.*, **97**, 8696.

Diederich, F., Whetten R.L. 1992, Beyond C_{60}, The Higher Fullerenes, *Acc. Chem. Res.*, **25**, 119.

Diehl, M., Degen, J., Schmidtke, H.H. 1993, Nonlinear Behavior in the Optical Spectra of Solid Fullerene C_{60}, *Ber. Bunsenges. Phys. Chem.*, **97**(7), 908.

Duclos, S.J., Brister K., Haddon, R.C., Kortan, A.R., Thiel, F.A. 1991, Effects of Pressure and Stress on C_{60} Fullerite To 20 GPa, *Nature (London)*, **351**, 380.

Ebbesen, T.W., Tabuchi, J., Tanigaki, K. 1992, The mechanistics of fullerene formation, *Chem. Phys. Lett.*, **191**, 336.

Elzey, F.F. 1965, A Programmed Introduction to Statistics, Wadsworth Publishing Company, Inc., Belmont, CA., 363.

Fischer, J.E., Heiney, P.A., McGhie, A.R., Romanow, W.J., Denenstein, A. M., McCauley, J.P., Jr., Smith, A.B. 1991, III Compressibility of Solid C_{60}, *Science*, **252**, 1288.

Friedman, S.H., DeCamp, D.L., Sijbesma, R.P., Srdanov, G., Wudl, F., Kenyon, G.L. 1993, Inhibition of the HIV-1 Protease by Fullerene Derivatives: Model Building Studies and Experimental Verification, *J. Am., Chem., Soc.*, **115**, 6506.

Gillot, J., Goldberger, W.M.. Separation by Thin-Film Fractional Sublimation 1969, *Chem. Eng. Progr. Symp. Series*, **65(91)**, 36.

Gladisch, H. 1962, Hydrocarbon Process, *Petroleum Refiner*, **41(6)**, 159.

Goeres, A., Sedlmayr, E. 1991, On the Nucleation Mechanism of Effective Fullerite Condensation, *Chem. Phys. Letts.*, **184**, 310.

Hamilton, R.J., Sewell, P.A. 1977, Introduction to High Performance Liquid Chromatography, Chapman & Hall, London.

Haufler, R.E., Conccicao, J., Chibante, L.P.F., Chai, Y., Byrne, N.E., Flanagan, S., Haley, M.M., O'Brian, S.C., Pan, C., Ziao, Z., Billups, W.E., Cinufolini, M.A., Hauge, R.H., Margrave, J.L., Wilson, L.J., Curl, R.F., Smalley, R.E. 1990, Efficient production of C_{60} (Buckminsterfullerene), $C_{60}H_{36}$ and the solvated buckide ion, *J. Phys. Chem.*, **94**, 8634.

Haufler, R.E., Chai, Y., Chibante, L.P.F., Conceicao, J., Jin, C., Wang, L.S., Maruyama, S., Smalley, R.E. 1991, Carbon Arc Generation of C_{60}. *Mat. Res. Soc. Proc.* Eds. R.S. Averback, J. Bernholc, D.L. Nelson, Materials Research Society, Boston, MA., **206**, 627.

Haufler, R.E. 1994, Techniques of Fullerene Production, Fullerenes: Recent

Advances in the Chemistry and Physics of Fullerenes and Related materials, *Proc. of 185th Meeting of the Electrochemical Society*, San Fransisco, Eds. Kadish, K.M., Ruoff, R.S., **94-24**, 50.

Heath, J.R. 1992, Synthesis of C_{60} from Small Carbon Clusters, in Fullerenes: Synthesis, Properties and Chemistry of Large Carbon Clusters, Hammond, G.S., Kuck, V.J., ACS, Washington DC, 1.

Hebard, A.F. 1992, Superconductivity in doped fullerenes, *Physics Today*, Nov. 1992, 26.

Heflin, J.R., Garito, A.F. 1992, Optics beyond the limits, *Nature*, **356**, 192.

Howard, J.B., Lafleur, A.L., Makarovsky, Y., Mitra, S., Pope, C.J., Yadav, T.K. 1992, Fullerenes Synthesis in Combustion, *Carbon*, **30(8)**, 1183.

Huang, C.H., Gan, L.B., Luo, C.P., Jhou, D.J., Xu, G.X. 1993, A Novel Chemical Method for Preparation of 99% Pure C_{60}, *Poster abstract from the First International Interdisciplinary Colloquium on the Science and Technology of the Fullerenes*, 172.

Huczko, A., Lange, H., Resztak, A., Byszewski, P. 1995, Carbon Arc Plasma Synthesis of Fullerenes, *J. High Temp. Chem. Proc.*, **4(4)**, 125.

Iijima S. 1991, Helical Microtubules of Graphitic Carbon, *Nature*, **354**, 56.

Inomata, K., Aoki, N., Koinuma, H. 1994, Production of Fullerenes by Low Temperature Plasma Chemical Vapour Deposition under Atmospheric Pressure, *Jpn. J. Appl. Phys.*, **33**, L197.

Khemani, K.C., Prato, M., Wudl, F. 1992, A simple Soxhlet method for the isolation of pure C_{60} and C_{70}, *J. Org. Chem.*, **57**, 3254.

Kikuchi, K., Nakahara, N., Wakabayashi, T., Honda, M., Matsumiya, H., Moriwaki, T., Suzuki, S., Shiromaru, H., Saito, K., Yamauchi, K., Ikemoto, I., Achiba, Y. 1992, Isolation and identification of fullerene family: C_{76}, C_{78}, C_{82}, C_{84}, C_{90} and C_{96}, *Chem. Phys. Letts.*, **188(3,4)**, 177.

Koch, A., Khemani, K.C., Wudl, F. 1991, Preparation of fullerenes with a simple benchtop reactor, *J. Org. Chem.*, **56**, 4543.

Koruga, D., Hamefoff, SW., Withers, J., Loufty, R., Sundareshan, M. 1993, Fullerene C_{60}, Elsevier Science Publishers B.V., 281.

Kratschmer, W., Lamb, L.D., Fostiropoulos, K., Huffman, D.R. 1990, Solid C_{60}: A New Form of Carbon, *Nature*, **347**, 354.

Kroto, H.W., Heath, J.R., O'Brien, S.C., Curl, R.F., Smalley, R.E. 1985, Buckminsterfullerene, *Nature (London)*, **318**, 162.

Lafleur, A.L., Howard, J.B., Marr, J.A., Yadav, T. 1993, Proposed Fullerene Precursor Corannulene Identified in Flames both in the Presence and Absence of Fullerene Production, *J. Phys. Chem.*, **97**, 13539.

Li, J., Komiya, S., Tamura, T., Nagasaki, C., Kihara, J., Kishio, K., Kitazawa, K. 1992, Growth and properties of pure C_{60} single crystals from vapor, *Physica C*, **195(1-2)**, 205.

Manoliadis, P. 1995, Purifiaction of fullerenes via thin film fractional sublimation, M. Eng. Thesis, McGill University, Montreal.

Martin, L.B. 1992, Diamond Film Growth: What is Really Happening?, *Am. Cer. Soc. Bull.*, **71(9)**, 1419.

Maruyama, S., Lee, M.Y., Haufler, R.E., Chai, Y., Smalley, R.E. 1991, Thermionic Emission from Giant Fullerenes, *Zeitschrift Fur Physik D - Atoms, Molecules and Clusters*, **19(1-4)**, 409.

Mathews, C.K., Sai Baba, M., Lakshmi Narasimhan, T.S., Balasubramanian, R., Sivaramman, N., Srinivasan, N.G., Vasudeva Rao, P.R. 1992, Vaporization Studies of Buckminsterfullerene, *J. Phys. Chem.*, **96**, 3566.

McKinnon, T.J. 1991, Calculated Equilibrium Yields of C_{60} from Hydrocarbon Pyrolysis, *J. Phys. Chem.*, **95(22)**, 8941.

Meijer, G., Bethune, D.S. 1990, Laser Deposition of Carbon Clusters on Surfaces - A New Approach to the Study of Fullerenes, *J. Chem. Phys.*, **93(11)**, 7800.

Meilunas, R.J., Chang, R.P.H., Liu, S., Kappes, M.M. 1991, Nucleation of diamond films on surfaces using carbon clusters, *Appl. Phys. Lett.*, **59(26)**, 3461.

Orfeuil, M., Aschard, J.L. *et al.* 1988, The Tioxide Process, in Arc Plasma Processes: A maturing Technology in Industry, International Union for Electroheat, 121.

Palstra, T.T.M., Zhou, O., Iwasa, Y., Sulewski, P.E., Fleming, R.M., Zegarski, B.R. 1995, Superconductivity at 40 K in Cesium doped C_{60}, *Solid State Commun*, **93(4)**, 327.

Pan, C., Chandrasekharaiah, M.S., Agan, D., Hauge, R.H., Margrave, J.L. 1992, Determination of Sublimation Pressures of C_{60}/C_{70} Solid Solution, *J. Phys. Chem.*, **96**, 6752.

Pan, C., Sampson, M.P., Chai, Y., Hauge, R.H., Margrave, J.L. 1991, The heats of Sublimation from a Polycrystalline Mixture of C_{60} and C_{70}, *J. Phys. Chem.*, **95**, 2944.

Pang, L.S.K., Vassallo, A.M., Wilson, M.A. 1991, Fullerenes from Coal, *Nature (London)*, **352(6335)**, 480.

Pateyron, B., Elchinger, M.F., Delluc, G., Fauchais, P. 1992, Thermodynamic and

Transport Properties of Ar-H_2 and Ar-He Plasma Gases Used for Spraying at Atmospheric Pressure. I: Properties of the Mixtures, *Plasma Chem. Plasma Proc.*, **12**(4), 421.

Raghavachari, K., Binkley, J.S. 1987, Structure, Stability and Fragmentation of Small Carbon Clusters, *J. Chem. Phys.*, **87**, 2191.

Regueiro, M.N., Monceau, P.,Rassat, A., Bernier, P., Zahab, A. 1991, Absence of a metallic phase at high pressures in C_{60}, *Nature*, **354**, 289.

Rosseinsky, M.J., Ramirez, A.P., Glarum, S.H., Murphy, D.W., Haddon, R.C., Hebard, A.F., Palstra, T.T.M., Kortan, A.R., Zahurak, S.M., Makhija, A.V. 1991, Superconductivity at 28 K in Rb_xC_{60}, *Phys. Rev. Lett.*, **66**, 2830.

Ruoff, R.S., Tse, D.S., Malhotra, R., Lorents, D.C. 1993, Solubility of C_{60} in a Variety of Solvents, *J. Am. Chem. Soc.*, **97**(13), 3379.

Saxby, J., Chatfield, S.P., Palmisano, A.J., Vassallo, A.M., Wilson, M.A., Pang, L.S.K. 1992, Thermogravimetric Analysis of buckminsterfullerene and Related Materials in Air, *J. Phys. Chem.*, **96**(1), 17.

Scrivens, W.A., Bedworth, P.V., Tour, J.M. 1992, Purification of Gram Quantities of C_{60}. A New Inexpensive and Facile Method, *J. Am. Chem. Soc.*, **114(20)**, 7917.

Sekiguchi, H., Honda, T., Kanzawa, A. 1991, Decomposition of chlorofluorocarbons using a thermal argon plasma, *ISPC -10 Proceedings*, **1.5-2**, 1.

Smalley, R.E. 1992, Self-Assembly of the Fullerenes, *Acc. Chem. Res.*, **25**, 98.

Smalley, R.E., Haufler, R.E. 1993, Electric Arc Process For Making Fullerenes, Patent No. 5,227,038.

Taylor, P.H., Tirey, D.A., Rubey, W.A., Dellinger, B. 1994, Detailed Modeling of the Pyrolysis of Trichloroethene: Formation of Chlorinated Aromatic Species, *Combust. Sci. and Tech.*, **101**, 75.

Taylor, R., Langley, G.J., Kroto, H.W., Walton, D.R.M. 1993, Formation of C_{60} by pyrolysis of naphthalene, *Nature*, **366**, 728.

Taylor, R., Walton, D.R. 1993, The Chemistry of Fullerenes, *Nature*, **363(6431)**,

685.

Tirey, D.A., Taylor, P.H., Kasner, J., Dellinger, B. 1990, Gas Phase Formation of Chlorinated Aromatic Compounds from the Pyrolysis of Tetrachloroethylene, *Combust. Sci. and Tech.*, **74**, 137.

Tohji, K., Saito, K., Matsuoka, I. 1994, The effect of carbon materials on the preparation of fullerenes, Fullerenes: Recent Advances in the Chemistry and Physics of Fullerenes and Related materials, *Proc. of 185th Meeting of the Electrochemical Society*, San Fransisco, Eds. Kadish, K.M., Ruoff, R.S., **94-24**, 132.

Tsantrizos, P.G., Grenier, S. 1995, Process for the Synthesis of Fullerenes, Patent No. 5,395,496.

Tutt, L.W., Kost, A. 1992, Optical Limiting Performance of C_{60} and C_{70} Solutions, *Nature*, **356**, 225.

Vassallo, A.M., Palmisano, A.J., Pang, L.S.K., Wilson, M.A. 1992, Improved Separation of Fullerene-60 and -70, *J. Chem. Soc. Chem. Commun.*, 60.

Wakabayashi, T., Mizuno, K., Imagawa, T., Amono, T., Hirakawa, S., Komaki, H., Kobayashi, S., Kushiyama, S., Aizawa, R., Koinuma, Y., Ohuchi, H. 1989, Decomposition of Halogenated Organic Compounds by r.f. Plasma at Atmospheric Pressure, *ISPC-9 Proceedings*, L111.

Yoshie, K., Kasuya, S., Eguchi, K., Yoshida, T. 1992, Fullerenes Formation in a RF-DC Hybrid Plasma Reactor, *Appl. Phys. Lett.*, **61(23)**, 2782.

Appendix A
Error Analysis

Analytical and Sampling Error Analysis (B50)

(4 min, 65 kW, 0.29 mol/min C2Cl4, 300 torr)

	Soot collected (g/min)	% C60 in soot	% C70 in soot	C60 collected (mg/min)	C70 collected (mg/min)
Sample 1	3.69	3.43%	0.88%	126.57	32.47
		3.32%	0.80%	122.51	29.34
		3.35%	0.85%	123.62	31.37
Sample Mean				**124.23**	**31.06**
Sample 2	3.69	3.51%	0.88%	129.52	32.47
		3.47%	0.83%	128.04	30.63
		3.45%	0.86%	127.31	31.73
Sample Mean				**128.29**	**31.61**
Sample 3	3.69	3.45%	0.85%	127.31	31.29
		3.35%	0.82%	123.62	30.26
		3.31%	0.79%	122.14	29.15
Sample Mean				**124.35**	**30.23**
Sample 4	3.69	3.25%	0.79%	119.93	29.15
		3.32%	0.83%	122.51	30.63
		3.37%	0.87%	124.35	32.10
Sample Mean				**122.26**	**30.63**
Overall Mean				**124.95**	**30.90**
Overall Standard Deviation				**2.65**	**1.08**

Analysis of Variance

Source of Variation	Degrees Freedom	Sum of Squares	Mean Square	F
Between samples	dfb= 3	SSb 19.25	MSb= 6.42	1.45
Within samples	dfw 8	SSw 35.40	MSw 4.43	
Total	dft= 11	SSt= 54.65		

The F values obtained from literature for 0.05 and 0.01 levels of significance at dfb=3 and dfw=8 are 4.07 and 7.57, respectively

Since the calculated F value is less than both the literature values [Elzey, 1965], then we can accept the null hypothesis that there is no sampling error.

Experimental Error

(4 min, 55 kW, .29 mol/min C2Cl4, 200 torr)

Expt No.	Soot Collection (g/min)	% C60 in soot	% C70 in soot	C60 collected (mg/min)	C70 collected (mg/min)
B12	3.09	3.13%	0.66%	96.72	24.35
B15	3.32	3.18%	0.76%	105.58	28.04
B25b	3.43	3.15%	0.66%	108.05	24.35
Mean				103.45	25.58
Standard Deviation				4.86	1.74

Appendix B
Removal of By-Products

APPENDIX B
REMOVAL OF BY-PRODUCTS FROM *PYROGENESIS* EXTRACT

To facilitate purification by chromatography, a number of techniques were investigated for the removal of by-products from the fullerene crude extract prior to column chromatography. From experiments in chromatography, described in Section 9.3, it was found that high purity C_{60} can only be obtained if the extract which is loaded onto the column consists of at least 30% C_{60}. As such, the removal of a portion of by-products became an essential step of the purification process.

B.1 Variation of solvent to soot ratio during extraction process

The first step required for most purification techniques involves the process by which fullerenes are separated from the insoluble carbon soot. The extraction procedure used in this work involved the dispersion of the carbon soot in toluene through the use of a sonication bath. Sonication of the mixture enhances the dissolution of the solute in a solvent, by breaking up the aggregates of solid material via ultrasonic waves.

The volume of toluene used for extraction has a significant effect on the composition of the crude extract. When a small volume of toluene per gram of soot is used, the crude extract is much richer in C_{60} than when a higher ratio of solvent to soot is used. Two examples are shown in Table B.1. In the first example, the C_{60} content in 78C extract was increased from 20.0% to 29.3% by decreasing the solvent to soot ratio from 200 mL/g to 100 mL/g. Similarly, the C_{70} content was increased from 7.3% to 11.3% when the solvent volume was decreased. Even though less solvent was used, the extraction of C_{60} and C_{70} was not affected, as seen in columns 5 and 7 of Table B.1. Similarly, in 78E crude extract, 50 mL/g was sufficient to extract all of the C_{60} and C_{70}, yet increase the concentration of C_{60} in the crude extract from 27.6% to 45.8% and the concentration of C_{70} from 8.3% to 16.3%.

As can be seen in Section 9.1, there is a variety of by-products present in the *PyroGenesis* soot, which have very different solubilities in toluene. By-products having a lower solubility in toluene than fullerenes may not be extracted when a low solvent to soot ratio is used, since the solution becomes saturated with compounds having a high solubility. As such, through the variation of the solvent to soot ratio, it was possible to remove some by-products from the crude extract, thus enriching the extract with fullerenes.

Table B.1: Effect of toluene volume on composition of crude extract

(1)	(2)	(3)	(4)	(5)	(6)	(7)
Extract No.	**Volume toluene per gram soot (mL/g)**	**% extraction**	**% C_{60} in extract**	**% C_{70} in extract**	**C_{60} extracted per gram of soot (mg/g)**	**C_{70} extracted per gram of soot**
78C	200	8.9%	20.0%	7.3%	17.5	6.5
	100	5.6%	29.3%	11.3%	15.6	6.3
78E	200	8.2%	27.6%	8.3%	22.5	6.8
	50	4.8%	45.8%	16.3%	22.0	7.8

B.2 Simple sublimation of fullerene extract

Because fullerenes have a high sublimation temperature relative to other organic compounds, simple sublimation was attempted in order to remove by-products having a lower sublimation temperature from the crude extract. A ceramic vacuum furnace, shown in Figure B.1, was used for this study.

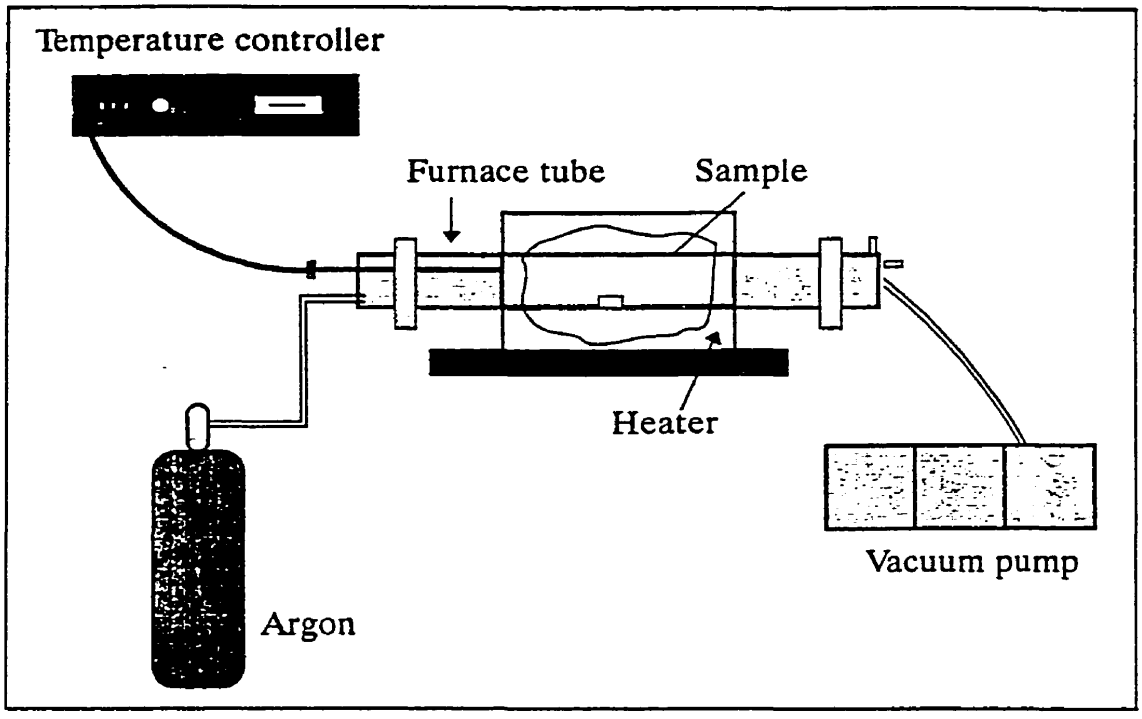

Figure B.1: Schematic of apparatus for simple sublimation experiments.

The sample, placed in a modified glass vial, was introduced into the furnace, the chamber was evacuated and backfilled with argon to a pressure of 7.5 torr. The temperature was varied from 250 °C to 400 °C. Volatile compounds are carried from the vial by argon, to the water-cooled collection finger, where these compounds condense. After each experiment, the vial was weighed to determine weight loss, and all condensed material found inside the alumina tube and on the cold finger was collected and weighed.

The first experiments were run with crude extract derived from commercial soot produced via the arc-vaporization of graphite, which consists only of fullerenes. Three experiments were run in which the temperature of the furnace was 300 °C, 350 °C, and 400 °C. The experiment performed at 300 °C did not result in any loss of material, whereas at 350 °C, sublimation of 15% of the material occurred. At 400 °C, there was a significant weight loss, amounting to 70% of the fullerenes. The total initial weight of fullerenes was accounted for after each experiment, in the vial and as a deposit in the furnace.

When *PyroGenesis* extract, containing 20% C_{60}, was subjected to a temperature of 250°C, the results were surprising. The weight loss in the sample was 27%, however, the material which remained in the vial after the run was no longer completely soluble in toluene. In fact, only 28% of the extract dissolved in toluene. Although the soluble portion of the treated extract was enriched with fullerenes (34% C_{60}), more than 50% of the C_{60} could not be accounted for. C_{60} either reacted with other by-products in the extract, or decomposed during heating. Reaction with other products could lead to polymerization or to the formation of larger fullerene derivatives which may no longer be soluble in toluene. Furthermore, decomposition of C_{60} into graphite would also result in an insoluble end product.

B.3 Solvent extraction of by-products with various solvents

Solvent extraction techniques using different solvents were investigated as another method for removing by-products from *PyroGenesis* extract. Organic solvents investigated for the selective extraction of by-products from the *PyroGenesis* crude extract included tetrahydrofuran, dichloromethane, ethyl acetate, acetone and methanol. Solvents were chosen based on their low affinity for fullerenes since it was necessary to minimize losses of fullerenes. Extraction experiments were performed on commercial soot using a SOXHLET extraction method, as described in Section 3.5.1. For the first set of experiments, the SOXHLET extraction was run for 20-24 hours using different solvents. Results are summarized in Table B.2.

Table B.2: Extraction of C_{60} by various solvents

Solvent	**% of C_{60} extracted**
Tetrahydrofuran	50%
Dichloromethane	28%
Ethyl acetate	17%
Acetone	3%
Methanol	0%

Tetrahydrofuran and dichloromethane were not suitable for selectively extracting by-products, because these solvents dissolved a significant quantity of C_{60} (50% and 28%, respectively). Although, acetone and methanol did not readily C_{60}, they were also undesired since aromatic compounds have a very low solubility in these solvents. This was also confirmed experimentally by the low overall extraction of products, less than 0.5%, using acetone and methanol. Ethyl acetate gave promising results and was therefore considered in subsequent experiments.

In addition to ethyl acetate, diethyl ether was also investigated further for the potential removal of by-products from *PyroGenesis* extract, based on its reported use by Scrivens *et al.* [1992] for the extraction of impurities from commercial fullerene extract prior to column chromatography. Controlled experiments were performed using ethyl acetate and diethyl ether in which a SOXHLET extraction was monitored by changing the flasks at various time intervals. Each fraction was collected and analyzed by HPLC. Results of the test are summarized in Figure B.2.

As seen in Figure B.2, diethyl ether removed 22% of the by-products present in the soot, whereas ethyl acetate only removed 15% of the by-products. The losses of C_{60} after 1.3 hours were 2.5% for diethyl ether and 1.9% with ethyl acetate.

Based on these results, a new procedure was developed, where the crude extract is dispersed in diethyl ether (mL diethyl ether per gram of extract), using an ultrasonic probe, and then filtered over a bed of silica gel. Using this procedure, up to 27% of the by-products were removed from the crude extract. This procedure was adopted as a required step to be performed prior to purification of the crude extract by column chromatography.

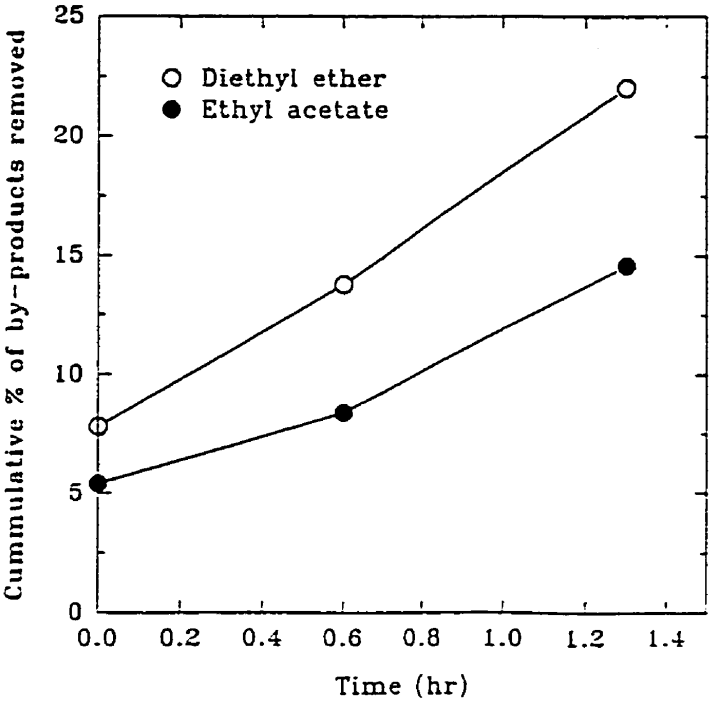

Figure B.2: Cumulative % removal of by-products as a function of time using Soxhlet extraction technique [19% extractable, 21% C_{60}, 7% C_{70}]

Appendix C
Bilodeau *et al.* [1996]

Modeling of the Synthesis of Fullerenes by the Plasma Torch Dissociation of C_2Cl_4

Jean-François Bilodeau[1], Theodora Alexakis[1,2], Jean-Luc Meunier[1], Peter G. Tzantrizos[2]

[1] Plasma Technology Research Center

Dept. of Chemical Engineering, McGill University (Canada)

[2] PERMA, a division of Pyrogenesis, Inc., Montreal (Canada)

Abstract

A mathematical model is developed for the simulation of the *PyroGenesis* thermal plasma reactor used for the synthesis of fullerenes (C_{60}, and others) via the dissociation of C_2Cl_4. The reactor studied is a spherical, water-cooled chamber equipped with a non-transferred d. c. plasma torch. C_2Cl_4 is introduced into the plasma jet. The equation of continuity is solved, along with the equations of conservation of axial and radial momentum and energy. The K-ε model is used for the consideration of the turbulence effects. The radiation term is represented by the net emission coefficient method. The equation of transport for C_2Cl_4 is solved in order to estimate the quality of the mixing with the hot jet, not taking into account chemical reactions. Fields of the flow, temperature and concentration patterns are presented. The deposition rates and wall temperatures obtained experimentally are compared to results of the model.

1. Introduction

The *PyroGenesis* process was recently developed for the potential large scale production of fullerenes [1]. The process is based on the thermal plasma dissociation of halogenated hydrocarbons. Using C_2Cl_4 as the carbon source, a 3% conversion of C_2Cl_4 to fullerenes has been obtained, based on carbon input, and the fullerene yield in soot was 5.3%. The temperature of the collection site, which is itself a function of the power input and reactor geometry, has been shown to play a critical role in fullerene collection. Hence, in order to optimize the process for maximum fullerene production and collection, a better understanding of the flow pattern and temperature gradients within the reactor is essential.

The combination of high temperatures and the presence of chlorine make the in-situ diagnostic of the reactor a difficult task. Also, the presence of high soot concentrations in the gas and the significant wall deposition forbid any spectroscopic temperature and/or concentration measurements. The mathematical modeling of this process is thus performed in order to gain insight on the mechanisms in the reactor. Free and wall confined plasma jet models have been developed in the past for various applications [2-8].

In the present work we will first describe the experimental setup of the *PyroGenesis* process and the assumptions and development of the mathematical model. The wall temperatures calculated by the model are compared with the experimental measurements. The model will also give an estimate of the quality of the mixing of C_2Cl_4 with the hot gas stream. Finally, the

calculated flow pattern, temperatures and mass fraction of C_2Cl_4 will be used to explain the deposition patterns for total soot and for C_{60} and C_{70}.

2. Experimental

A schematic of the overall reactor assembly is shown in Figure 1. The reactor is a spherical, water-cooled vessel (ID=30 cm), equipped with a non-transferred d.c. plasma torch. C_2Cl_4 is introduced into the plasma jet through a nozzle consisting of an annular ring with three openings. C_2Cl_4 is dissociated in the plasma, forming a reactive cloud of C and Cl atoms and molecules. Under controlled operating conditions, some of the carbon atoms recombine to form fullerenes, which condense with soot on the reactor wall. The gas leaving the reactor then enters the quench zone, a stainless steel receptacle containing a water-cooled coil, where the products remaining in the exhaust gas condense. The operating conditions used to produce fullerene-bearing soot for the study reported herein are summarized in Table 1.

Wall temperature measurements were taken by thermocouples located at various positions in the reactor. These measures were made only in runs performed without C_2Cl_4 injection, due to the high corrosivity of this product. Samples of soot were collected from eleven zones in the reactor. The data of samples obtained from symmetrical fractions was averaged, resulting in 8 fractions labeled from A to H. The soot samples were weighed and analyzed for their C_{60} and C_{70} content by High Performance Liquid Chromatography (HPLC). Results are reported as mass per unit area.

3. Mathematical Model

3.1 Assumptions

The major assumptions used in the development of the model are the following:

- The plasma is assumed at LTE and the reactor is operated in steady state conditions.

- The reactor is assumed axisymmetric along the plasma jet. Thus three dimensional effects due to the exhaust pipe and the hydrocarbon injection by the three nozzle holes are neglected, but the momentum of these flows is respected. Viscous dissipation is neglected, as well as gravity effects as justified by the strong forced convection.

- The time averaged effects of the turbulence are considered. The K-ε model is used to calculate the contribution of turbulence in the equations of momentum, energy and hydrocarbon mass conservation.

- The effect of the swirl imparted to the gas upstream of the torch is assumed to be negligible within the reactor.

- Compressibility effects are neglected. In the case analyzed here the flow is subsonic in all the domain except in a small region inside the nozzle, based on sound velocities reported by Pateyron et al. [9]. At an axial position of 4 cm downstream of the nozzle exit, the squared Mach number M^2 is below 0.5. It is thus expected that these effects will not influence significantly the global behavior of the reactor.

- The plasma is optically thin. The radiation term is represented by the net emission coefficient method, with $R_p = 0.5$ mm. The values take into account the proportion of carbon in the gas,

assuming the hydrocarbon in fully dissociated state. This last assumption is quite valid in the regions where radiation is important.

- The effect of the electric field is neglected in the region considered, including the nozzle and the spherical reactor.

3.2 Conservation Equations

To obtain the velocity, temperature and concentration fields in the gas phase we need to solve the equations of continuity and of the conservation of axial and radial momentum, energy and hydrocarbon species, which write in cylindrical coordinates:

- Continuity equation:

$$\frac{\partial \rho}{\partial t} + \frac{1}{r}\frac{\partial}{\partial r}(r\rho v_r) + \frac{\partial}{\partial z}(\rho v_z) = 0 \qquad (1)$$

t is the time, z and r are respectively the axial and radial coordinates, ρ is the density, and v_z and v_r are the axial and radial components of the bulk gas velocity.

- Axial and radial momentum equations:

$$\frac{\partial}{\partial t}(\rho v_z) + \frac{1}{r}\frac{\partial}{\partial r}(r\rho v_r v_z) + \frac{\partial}{\partial z}(\rho v_z v_z) = -\frac{\partial P}{\partial z} + 2\frac{\partial}{\partial z}\left(\eta\frac{\partial v_z}{\partial z}\right) + \frac{1}{r}\frac{\partial}{\partial r}\left[r\eta\left(\frac{\partial v_z}{\partial r} + \frac{\partial v_r}{\partial z}\right)\right] \quad (2)$$

$$\frac{\partial}{\partial t}(\rho v_r) + \frac{1}{r}\frac{\partial}{\partial r}(r\rho v_r v_r) + \frac{\partial}{\partial z}(\rho v_z v_r) = -\frac{\partial P}{\partial r} + \frac{2}{r}\frac{\partial}{\partial r}\left(r\eta\frac{\partial v_r}{\partial r}\right) + \frac{\partial}{\partial z}\left[\eta\left(\frac{\partial v_z}{\partial r} + \frac{\partial v_r}{\partial z}\right)\right] - 2\eta\frac{v_r}{r^2} \quad (3)$$

in which η is the effective viscosity, defined later.

- Energy equation:

$$\frac{\partial}{\partial t}(\rho h)+\frac{1}{r}\frac{\partial}{\partial r}(r\rho v_r h)+\frac{\partial}{\partial z}(\rho v_z h)=\frac{\partial}{\partial z}\left(\frac{k}{C_p}\frac{\partial h}{\partial z}\right)+\frac{1}{r}\frac{\partial}{\partial r}\left(r\frac{k}{C_p}\frac{\partial h}{\partial r}\right)-U \qquad (4)$$

h is the gas specific enthalpy, k the effective thermal conductivity (laminar + turbulent), C_p the specific heat at constant pressure and U is the radiation loss term.

- Hydrocarbon mass conservation:

$$\frac{\partial}{\partial t}(\rho X)+\frac{1}{r}\frac{\partial}{\partial r}(r\rho v_r X)+\frac{\partial}{\partial z}(\rho v_z X)=\frac{\partial}{\partial z}\left(\rho D\frac{\partial X}{\partial z}\right)+\frac{1}{r}\frac{\partial}{\partial r}\left(r\rho D\frac{\partial X}{\partial r}\right)-S_m \qquad (5)$$

X is the mass fraction of hydrocarbon in the gas and D is the effective mass diffusivity. This last equation considers only the transport of the hydrocarbon. Evidently the hydrocarbon will dissociate and react, and thus results presented here can only give estimates of the quality of the mixing between the reactant and the helium plasma jet. S_m is a mass source term that simulates the condensation of the hydrocarbon at around 1600 K. This results in more realistic hydrocarbon concentrations in the jet, since it will eliminate the gaseous hydrocarbon in the surrounding gas that is pumped by the fast flowing gas.

The effect of turbulence on the transport coefficients is considered using the well-known K-ε model as reported by Murphy and Kovitya [4]. The effective transport coefficients mentioned in the previous equations are:

$$\eta=\eta_l+\eta_t \quad , \quad k=k_l+\frac{\eta_t C_p}{\sigma_h} \quad , \quad D=D_l+\frac{\eta_t}{\rho\sigma_x} \quad , \quad \text{with} \quad \eta_t=C_d\rho\frac{K^2}{\varepsilon} \qquad (6)$$

in which η_l , k_l *and* D_l are the molecular viscosity, thermal conductivity and diffusivity.

Two additional equations need to be solved, for the turbulent kinetic energy (K) and its rate of dissipation (ε):

$$\frac{\partial}{\partial t}(\rho K)+\frac{1}{r}\frac{\partial}{\partial r}(r\rho v_r K)+\frac{\partial}{\partial z}(\rho v_z K)=\frac{\partial}{\partial z}\left(\eta_k \frac{\partial K}{\partial z}\right)+\frac{1}{r}\frac{\partial}{\partial r}\left(r\eta_k \frac{\partial K}{\partial r}\right)+G-\rho\varepsilon \qquad (7)$$

$$\frac{\partial}{\partial t}(\rho \varepsilon)+\frac{1}{r}\frac{\partial}{\partial r}(r\rho v_r \varepsilon)+\frac{\partial}{\partial z}(\rho v_z \varepsilon)=\frac{\partial}{\partial z}\left(\eta_\varepsilon \frac{\partial \varepsilon}{\partial z}\right)+\frac{1}{r}\frac{\partial}{\partial r}\left(r\eta_\varepsilon \frac{\partial \varepsilon}{\partial r}\right)+C_1 G\frac{\varepsilon}{K}-C_2\rho\frac{\varepsilon^2}{K} \qquad (8)$$

The effective diffusion coefficients for K and ε are:

$$\eta_k=\eta_l+\frac{\eta_t}{\sigma_k} \quad , \quad \eta_\varepsilon=\eta_l+\frac{\eta_t}{\sigma_\varepsilon} \qquad (9)$$

and G is given by:

$$G=\eta_t\left[2\left(\left(\frac{\partial v_r}{\partial r}\right)^2+\left(\frac{v_r}{r}\right)^2+\left(\frac{\partial v_z}{\partial z}\right)^2\right)+\left(\frac{\partial v_z}{\partial r}+\frac{\partial v_r}{\partial z}\right)^2\right] \qquad (10)$$

Using the constants in Table 2, we thus have a closed system of equations.

However a correction is brought in the region outside the nozzle, as suggested by Rodi [10] for the case of axisymmetric jets:

$$C_d=0.09-0.04f \quad , \quad C_2=1.92-0.0667f \quad , \text{ where } \quad f=\left|\frac{\delta}{2\Delta u}\left(\frac{\partial (v_z)_0}{\partial z}-\left|\frac{\partial (v_z)_0}{\partial z}\right|\right)\right|^{0.2} \qquad (11)$$

In this last definition, δ is the jet diameter (defined by the radius at 1% of the axis velocity), Δu is the velocity difference over the jet radius and $(v_z)_0$ is the axial velocity in the center of the jet.

3.3 Boundary and specific conditions

The computational domain is shown in Figure 2 and consists of the nozzle, the torch tube and the spherical reactor. The axis of symmetry is taken to be in the direction of the plasma jet. The flow in the plasma torch is not solved. The equations presented above are applied to the points in the gas phase that are not on the boundaries of the computational domain or adjacent to solid walls. Specific conditions are applied in the last mentioned locations:

Nozzle entrance: parabolic velocity and temperature profiles are assumed at the nozzle entrance, which is located just at the torch exit:

$$v_z = v_{z,max}\left(1-\left(\frac{r}{r_{noz}}\right)^2\right) \quad , \quad T = T_{wal} + \left(T_{max} - T_{wal}\right)\left(1-\left(\frac{r}{r_{noz}}\right)^2\right) \qquad (12)$$

r_{noz} is the nozzle radius and T_{wal} the temperature set for the torch wall. The values of maximal temperature and velocity (T_{max}, $v_{z,max}$) are calculated in order to satisfy the energy balance and the total flow rate obtained experimentally on the torch. Profiles of other forms satisfying this condition have been tested and generated similar results downstream of the nozzle end. Other conditions at the nozzle entrance are given by:

$$v_r = 0 \quad , \quad X = 0 \quad , \quad K = 0.003 v_z^2 \quad , \quad \varepsilon = 3K^{3/2} / r_{noz} \qquad (13)$$

These initial estimates of the turbulence parameters have been used by Murphy and Kovitya [4].

Axis of symmetry: Radial gradients are null for all variables except for the radial velocity.

$$\frac{\partial v_z}{\partial r} = \frac{\partial h}{\partial r} = \frac{\partial X}{\partial r} = \frac{\partial K}{\partial r} = \frac{\partial \varepsilon}{\partial r} = 0, \quad v_r = 0 \qquad (14)$$

Reactor exhaust: Gradients are assumed to be null in the direction of the flow, and the radial velocity is adjusted to ensure conservation over the reactor.

$$\frac{\partial v_z}{\partial r} = \frac{\partial h}{\partial r} = \frac{\partial X}{\partial r} = \frac{\partial K}{\partial r} = \frac{\partial \varepsilon}{\partial r} = 0 \qquad (15)$$

Turbulence near walls: The conditions on the grid points adjacent to the walls are within the computational domain and are not strictly to speak boundary conditions. However in order to take into account the influence of the walls on the intensity of turbulence, wall functions are used to define the values of K and ε for the adjacent points, as suggested by Murphy and Kovitya [4]:

$$K_p = U_\tau^2 / \sqrt{C_d} \ , \ \varepsilon_p = U_\tau^3 / \left(k_0 y_p\right) \qquad (16)$$

in which k_0 is the von Karman constant, equal to 0.41 and y_p is the distance from the point to the wall. U_τ is the frictional velocity and is calculated by the following expression, in which U_p is the velocity parallel to the wall and E is the roughness parameter, taken to be 9.973 for smooth walls:

$$\frac{U_p}{U_\tau} = \frac{1}{k_0} \ln\left(\frac{E \rho U_\tau y_p}{\eta}\right) \qquad (17)$$

Reactor walls: Special conditions are also fixed for the walls, which lie within the computational domain:

$$v_z = v_r = X = K = \varepsilon = 0 \qquad (18)$$

Heat transfer through the wall occurs by thermal conductivity only. All the region surrounding the reactor wall is assumed composed of water. In this region the temperature is fixed at 350 K and the velocities are not solved. The heat transfer between the wall and water is defined by a convection coefficient.

3.4 Details of the solution

The conservation equations are solved by the SIMPLE method described by Patankar [11]. They are put in the general form proposed by this method:

$$\frac{\partial}{\partial t}(\rho\phi)+\frac{1}{r}\frac{\partial}{\partial r}(r\rho v_r\phi)+\frac{\partial}{\partial z}(\rho v_z\phi)=\frac{\partial}{\partial z}\left(\Gamma_\phi\frac{\partial\phi}{\partial z}\right)+\frac{1}{r}\frac{\partial}{\partial r}\left(r\Gamma_\phi\frac{\partial\phi}{\partial r}\right)+S_\phi \qquad (19)$$

in which ϕ is in turn 1, v_z, v_r, h, X, K and ε. Γ_ϕ and S_ϕ are the diffusion coefficient and source term associated to the variable ϕ. In the general case the equations of continuity (1) and of hydrocarbon conservation (5) have no source term S_ϕ. However since the C_2Cl_4 injection and the simulated condensation occur within the computational domain, they are represented by a term on the right hand side of the corresponding equations, at the concerned locations.

Thermodynamic and transport properties are calculated for pure helium gas at thermodynamic equilibrium, except for the density which is corrected to account for C_2Cl_4. The thermodynamic properties (C_p and enthalpy) are given by the equilibrium composition, which is determined by the internal partition functions of He, He^+ and electrons. The laminar viscosity and thermal conductivity are calculated by the method of Chapman and Enskog [12,13]. The laminar diffusivity of C_2Cl_4 in helium is calculated by the following expression, based on the diffusion of rigid spheres [14]:

$$D_{AB}=\frac{2}{3}\left(\frac{k_B}{\pi}\right)^{3/2}\left(\frac{1}{2m_A}+\frac{1}{2m_B}\right)^{1/2}\frac{4T^{3/2}}{p(d_A+d_B)^2} \qquad (20)$$

In this last equation k_B is Boltzmann's constant, p is the pressure in Pa, m_A and d_A are the mass and equivalent diameter of species A. In order to obtain a conservative estimate of the diffusion of the hydrocarbon, the molecular weight of C_2Cl_4 in non dissociated form was applied in the last equation. Some tests were run with a diffusivity based on the mass of atoms and led to similar results, which is explained by the fact that turbulent diffusion is dominant. The thermal conductivity of the reactor wall is given as 13 W/mK [15] and the thermal conductivity of tungsten is interpolated from values given in [16]. The heat transfer coefficient between the wall and the cooling water is 100 W/(m^{2}K).

An artifice is used in order to obtain a higher number of grid points in the reactor wall without needing an excessive number of grid points in the overall solution. The application of this artifice uses the assumption that the dominant component of the heat transfer at each location of the reactor wall is the radial component, which is verified by the higher thermal gradients in this direction. In this situation, in a spherical shell the heat transfer through a wall of thickness th_1 and thermal conductivity k_1 is equivalent to that of a wall of thickness th_2 and thermal conductivity k_2 if the following expression is satisfied, in which R_r is the reactor radius [14]:

$$\frac{k_2}{\left(\frac{1}{R_r}\right)-\left(\frac{1}{R_r+th_2}\right)}=\frac{k_1}{\left(\frac{1}{R_r}\right)-\left(\frac{1}{R_r+th_1}\right)} \qquad (21)$$

A non-uniform grid of 168 x 118 is used for the results presented here. Trials have shown that the solution shows no significant influence of the grid definition at this level.

4. Results and discussion

The simulations were made with the geometry and operating parameters of the process described above (section 2). Figure 3 shows a contour plot of the stream function of helium, normalized by the torch flow rate

$$\psi_{He} = \frac{\int_0^r J_{He} r dr}{\left(\int_0^{r_{max}} \rho v_z r dr\right)_{z=0}} = \frac{\int_0^r \left(\rho v_z - J_{C_2Cl_4}\right) r dr}{\left(\int_0^{r_{max}} \rho v_z r dr\right)_{z=0}}$$

J_{He} and $J_{C_2Cl_4}$ are the helium and hydrocarbon fluxes in the axial direction. The letters around the reactor in Figure 3 refer to the sections at which deposition rates were measured experimentally, and a discussion of the experimental results is presented later. The figure shows that the main stream hits the reactor wall facing the plasma jet and follows the wall until the exhaust tube is reached. Entrainment of surrounding gas into the plasma jet causes one large recirculation around the jet. A small recirculation, which is not seen on the figure, also occurs at the bottom of the torch tube. The orientation of the gas velocities in the reactor can be seen in Figure 4. It should be noted that the length of the arrows is independent of the intensity. The study of the turbulent viscosity shows its strong effect on transport coefficients in the reactor, except in a high temperature conical zone near the jet axis that does not extend past the nozzle end. Tests without the consideration of turbulence effects have shown results deviating significantly from these.

The temperature field is presented in Figure 5. As can be observed, strong thermal gradients occur on the reactor wall, just in front of the jet. Combined with the local velocity field, the

resulting rate of temperature decrease just upstream of this region reaches 3 10^6 K/s. The temperature field shows less important gradients on the sections of the wall facing the side of the jet. A favorable temperature zone for the formation of fullerenes is expected to lie between 1900 and 2300 K [17]. As can be seen, this region is small in the present configuration.

Figure 6 shows the calculated and experimental values of the wall temperature for cases without injection of hydrocarbon. The temperature is plotted as a function of the angle θ relative to the vertical in the computational domain (see Figure 2). The results are presented for two values of the power (55 and 65 kW), and as expected, the temperatures are slightly higher in the case at higher power. However the trends observed are the same for both cases. Wall temperatures are higher near the jet impact (angle close to +90 degrees), due to the high temperatures in the jet and the strong thermal exchange. The temperature decreases gradually along the wall to reach a minimum near the exhaust tube (angle = - 35 degrees), due to the enlargement of stream lines and hence the reduced heat exchange efficiency. The temperature increases again near the torch neck (angle = - 65 degrees), which is explained by the narrowing of stream lines at that point (see Figure 3) and thus the improved heat exchange. Good agreement is obtained with the experimental values for the points lying in the -10 to +40 degrees range. The temperature drop near the exhaust and increase close to the neck predicted by the simulation are also observed in the experimental measurements, but to a lesser degree. It is to be noted that the radiation absorbed by the walls is not considered.

Figure 7 presents the isocontours of the mass fraction of hydrocarbon (C_2Cl_4) in the jet region, along with the isocontours of temperature for 2000 and 3000 K. The normalized stream

function isocontour limiting the mainstream is that valued at 1.09, due to the addition of 20 slpm of helium with the hydrocarbon injection. This line is also shown on the graph. The values of concentration are calculated using a laminar diffusivity based on C_2Cl_4 in the non dissociated state, and thus give conservative estimates of the importance of molecular diffusion and thus of the quality of the mixing. The observation of the results shows that, for x= 0.08 m, the value of the mass fraction of C_2Cl_4 on the 2000 and 3000 K isocontours are 10% and 30% of the value on the axis, respectively. These results suggest that most of the hydrocarbon is well heated by the plasma jet and thus good mixing occurs between the helium jet and the hydrocarbon, favoring a good dissociation of the reactants. Simulations performed with the diffusivity calculated assuming the C_2Cl_4 in the dissociated form give only slightly differing values, and the qualitative behavior is similar to that of the base case. This is due to the dominance of the turbulent contribution in the diffusion. Also we can note that the load of hydrocarbon spreads radially. Streamlines outside the mainstream carry significant proportions of product, and thus soot and C_{60}, once condensation has occured.

Figure 8 shows isocontours of the hydrocarbon mass fraction over the reactor. As can be noted, the distribution of hydrocarbon proportion in the gaseous phase spreads gradually along the flow, and drops rapidly near the 1600 K isocontour due to the simulated condensation in the model.

Figures 9 and 10 show the experimental results of the concentration of total soot, C_{60} and C_{70} obtained after 4 minutes of operation, as a function of the location. The concentrations are expressed as milligrams per square centimeter, for experiments run at 55 and 65 kW,

respectively. The location of the fractions within the reactor is shown in Figure 3. The largest deposit of total soot per unit area was found in Fraction D, for experiments run at 55 kW and 65 kW. This is expected from the analysis of the flow patterns and mass fraction contours, since the mainstream hits the wall at this location with the highest loading of products and soot. Fraction E is close to the jet impact and also shows high deposition. Fraction C is approximately symmetrical to E, and shows the same tendency for 65 kW, however at 55 kW its yield is smaller. Fractions B, F and G are situated at an angular position near the exhaust tube and have the lowest deposition rates. This can be explained, in a similar way as for the low wall temperatures in the same region, by the enlargement of stream lines. Also, the streamlines following the wall are gradually depleted of soot. The model fails to predict the high soot deposition at A. This can be justified by the fact that the exhaust is actually a tube located below the centerline and not distributed axisymmetrically as is considered by the model. Section A is thus considered by the model as very near the exhaust tube, whereas in the experiment it is not. Section H is close to the torch tube and shows high deposition rates. Although the mainstream (stream function between 0 and 1.09) does not reach this point, the analysis of the concentration patterns (see Figure 7) has shown that the diffusion causes a significant amount of hydrocarbon (and thus soot) to be transported by nearby streamlines. The streamlines tend to compress near the torch tube, as seen on Figure 3, leading to an efficient mass transfer to the walls. Deposition rates of total soot are generally higher at 65 kW than at 55 kW, but the above mentioned tendencies are maintained.

The analysis of the concentration of C_{60} at 65 kW as a function of the angular position shows a different deposition pattern than the total soot. The concentrations of C_{60} are highest near the

torch tube (Sections A and H), due to the combined effect of high total soot deposition and moderate wall temperatures. In front of the jet (Sections C, D, E), the deposition rate is lower due to the high wall temperature that cause its partial sublimation. The rates of deposition are smallest near the exhaust tube (B, F, G), but the concentrations of C_{60} in the soot are higher than in the hot regions. This interpretation seems to be confirmed by the experimental observation that the C_{60} collection rate in the exhaust section increased with operating time. Indeed this is justified by the increased wall temperature [1] that causes C_{60} to stay in vapor in a higher proportion until its exit of the reactor. This deviation to the deposition pattern of C_{60} from the total soot is less important for the experiment at 55 kW, due to the lower wall temperatures. C_{70}, which has a higher sublimation temperature than C_{60}, is less influenced by the wall temperature. Indeed it shows a deposition pattern more similar to that of the total soot, for experiments at 55 and 65 kW.

5. Conclusions

A two-dimensional model is developed to simulate a reactor for the synthesis of fullerenes by the decomposition of C_2Cl_4 in a helium plasma jet. The model solves the equation of continuity, the conservation equations for momentum and energy, and the transport equation for C_2Cl_4. The fields of the stream function, gaseous and wall temperature, and C_2Cl_4 mass fraction are presented. These results, and comparison with experimental measurements, lead to the following conclusions:

- High thermal gradients and velocities occur at the impact point of the jet on the reactor wall. These strong gradients result in limited reaction time for fullerenes to be formed from the

dissociated state that occurs at the high temperatures of the jet. It is expected that the complex chemistry of formation of fullerene molecules requires a significant amount of time to proceed. This suggests that the reduction of these gradients by the increase of the distance between the torch and the wall, or a change to a cylindrical configuration, may be favorable for higher fullerene yields.

- The calculated wall temperatures correlate well with the measured values in the regions located at angles between -10 and +40 degrees relative to the vertical. For regions located outside this range, the prediction of a maximum in wall temperature near the exhaust is also observed experimentally, but to a lesser degree. As is also observed experimentally, the reactor wall temperature then increases near the torch, mainly due to the narrowing of streamlines, and thus more efficient transfer in that region.

- The model predicts that in the present nozzle configuration most of the C_2Cl_4 will be entrained in the high temperature stream (T > 2000 - 3000 K), and that good mixing is achieved.

- The model justifies the high deposition rate of total soot facing the jet by the high product loading of the gas at this point. The deposition rate then decreases along the wall until the exhaust is reached, due to the reduction of the concentrations in the gas stream and the widening of streamlines, reducing the deposition efficiency. The increase of the deposition rate near the torch is explained by the narrowing of the streamlines in that region, which is also responsible of the increase in wall temperature. However, the model does not predict the high deposition rate in section A, which is explained by the importance of non axisymmetric effects at this point. For C_{60} at 65 kW the global deposition pattern is modified by its partial evaporation from regions of high wall temperature. This results in low yields in front of the jet.

For C_{60} at 55 kW, and for C_{70} at both values of the power, the effects of evaporation are less important.

References

[1] Alexakis T, Tzantrizos Y S, Meunier J-L and Tzantrizos P G 1995 Proc. Int. Symp. Plasma Chem. (ISPC-12), Vol. 3, 1177

[2] Chang C H and Ramshaw J D 1993 Plasma Chem. Plasma Proc. **13** 189

[3] Ramshaw J D and Chang C H 1992 Plasma Chem. Plasma Proc. **12** 299

[4] Murphy A B and Kovitya P 1993 J. Appl. Phys. **73** 4759

[5] Huang P C, Heberlein J and Pfender E 1995 Plasma Chem. Plasma Proc. **15** 25

[6] Chyou Y P and Pfender E 1988 Plasma Chem. Plasma Proc. **9** 291

[7] McKelliget J, Szekely J, Vardelle M and Fauchais P 1982 Plasma Chem. Plasma Proc. **2** 317

[8] Dilawari A H, Szekely J and Westhoff R 1990 Plasma Chem. Plasma Proc. **10** 501

[9] Pateyron B, Elchinger M-F, Delluc G and Fauchais P 1996 Plasma Chem. Plasma Proc. **16** 39

[10] Rodi W 1980 in *Turbulence Models and their Applications in Hydraulics*, International Association for Hydraulic Research, Delft, The Netherlands

[11] Patankar S V 1980 Numerical Heat Transfer and Fluid Flow, Hemisphere

[12] Chen W L T, Heberlein J, Pfender E, Pateyron B, Delluc G, Elchinger M-F and Fauchais P 1995 Plasma Chem. Plasma Proc. **15** 559

[13] Pousse J, Chervy B, Bilodeau J-F and Gleizes A 1996, to appear in Plasma Chem. Plasma Proc. vol 13 no. 4

[14] Bird R B, Stewart W E and Lightfoot E N 1960, Transport phenomena, Wiley, New York

[15] Perry R H and Chilton C H 1973 Chemical Engineers' Handbook, McGraw-Hill, New York

[16] Weast R C, editor 1987-88 CRC Handbook of Chemistry and Physics, CRC Press, Boca Raton, Fla

[17] McKinnon J J 1991 J. Phys. Chem. **95** 8941

Table 1: Experimental conditions for fullerene soot production

Torch power	55 kW and 65 kW
Helium flow rate	225 slpm
C_2Cl_4 feed rate	0.29 mol/min
He carrier gas flow rate	20 slpm
Run duration	4 minutes

Table 2: Constants used in the turbulence model

C_1	C_2	σ_k	σ_ε	C_d	σ_h	σ_X
1.44	1.92	1.0	1.3	0.09	0.9	0.9

List of Figures

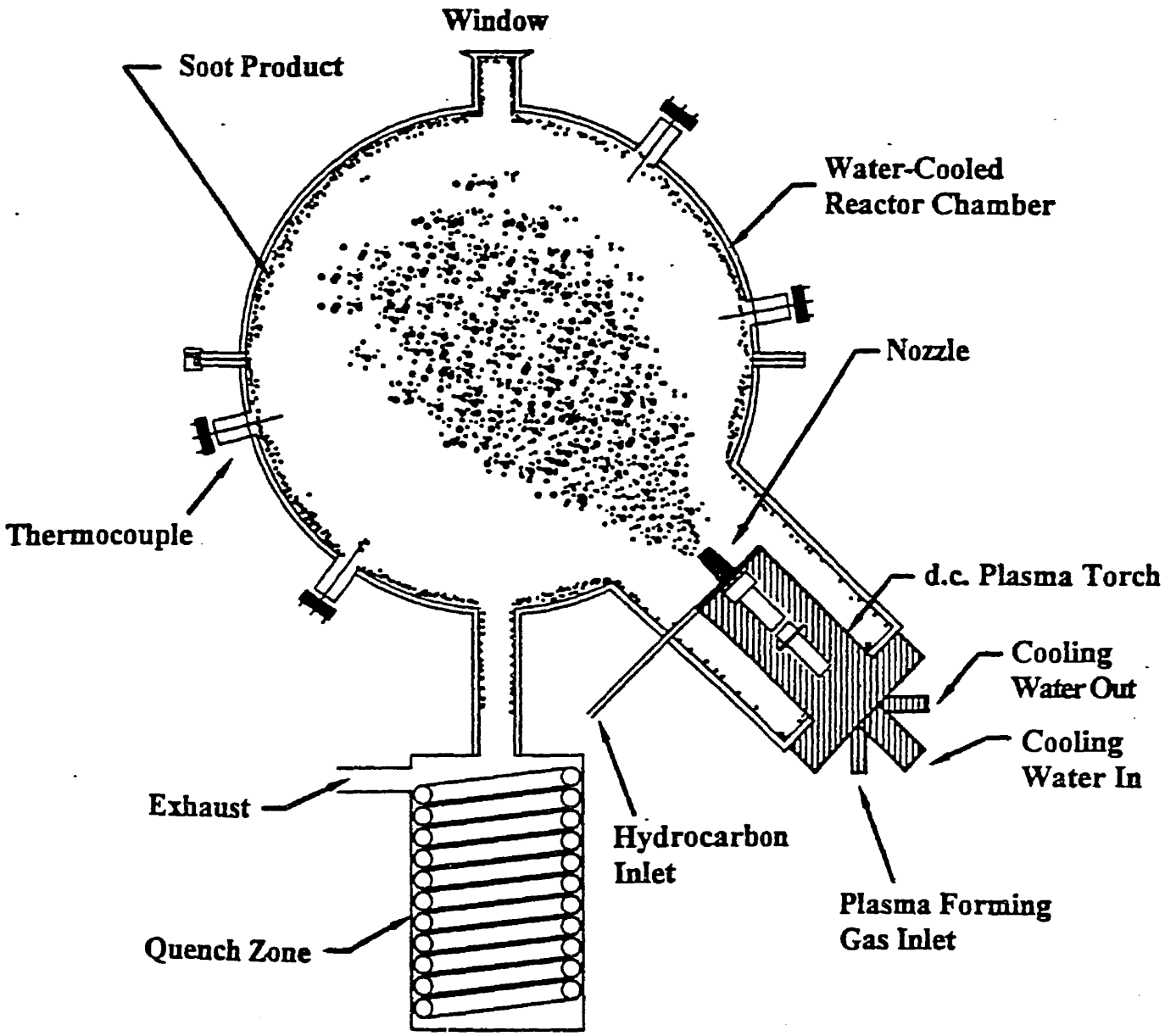

Figure 1 - Bilodeau, Alexakis et al, "Modeling of the Synthesis..."

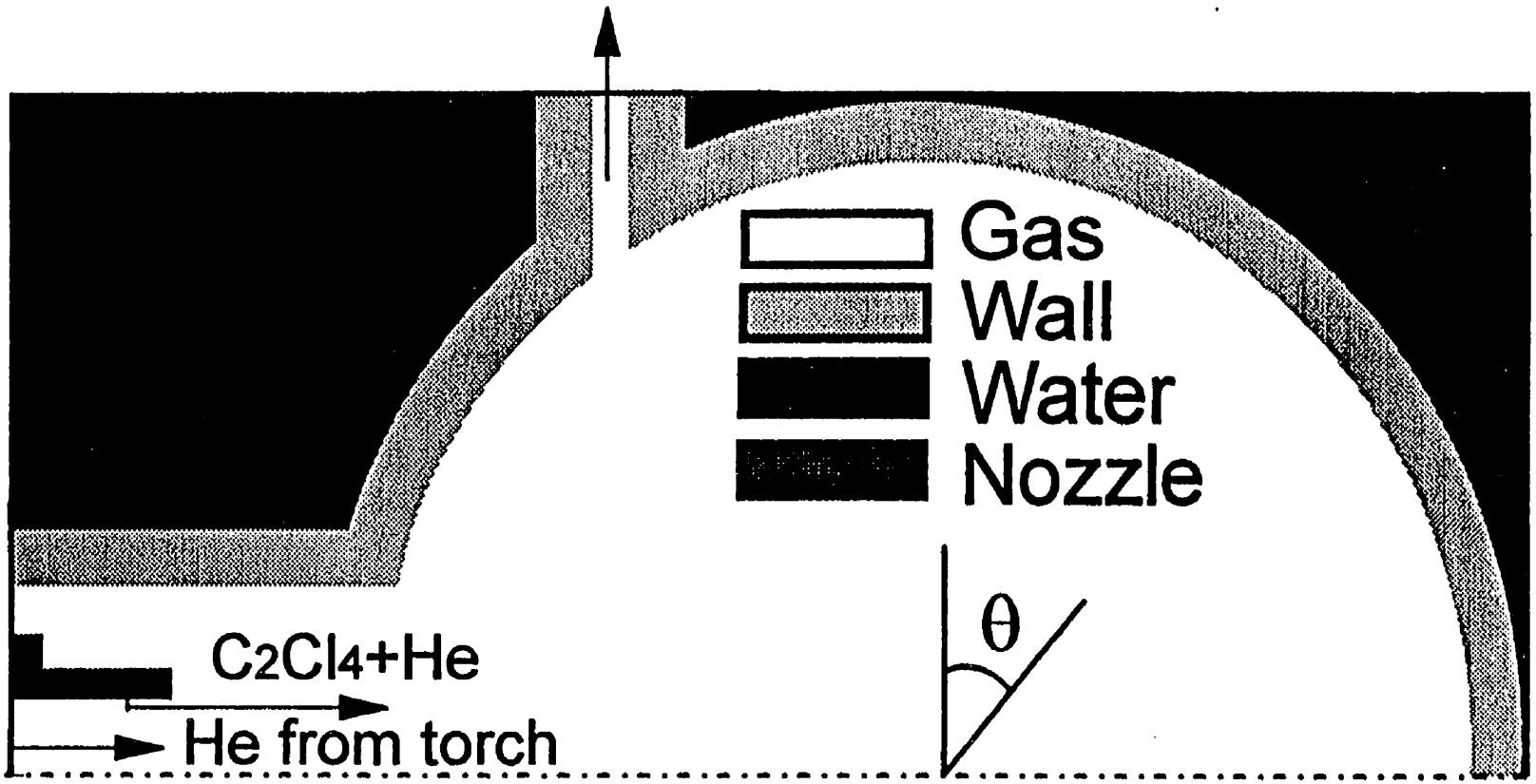

Figure 2 - Bilodeau, Alexakis et al, "Modeling of the Synthesis of Fullerenes..."

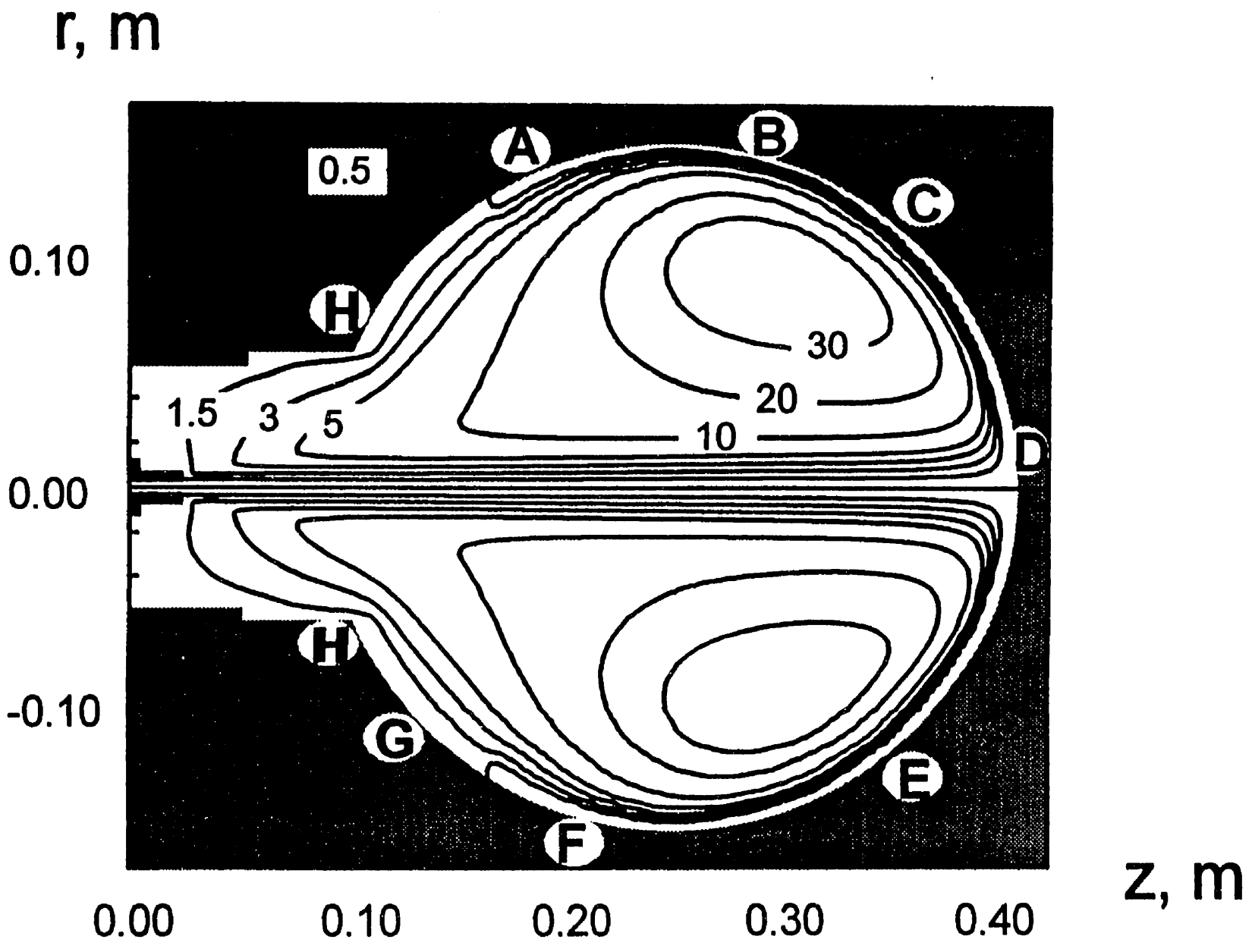

Figure 3 - Bilodeau, Alexakis et al., "Modeling of the Synthesis of Fullerene..."

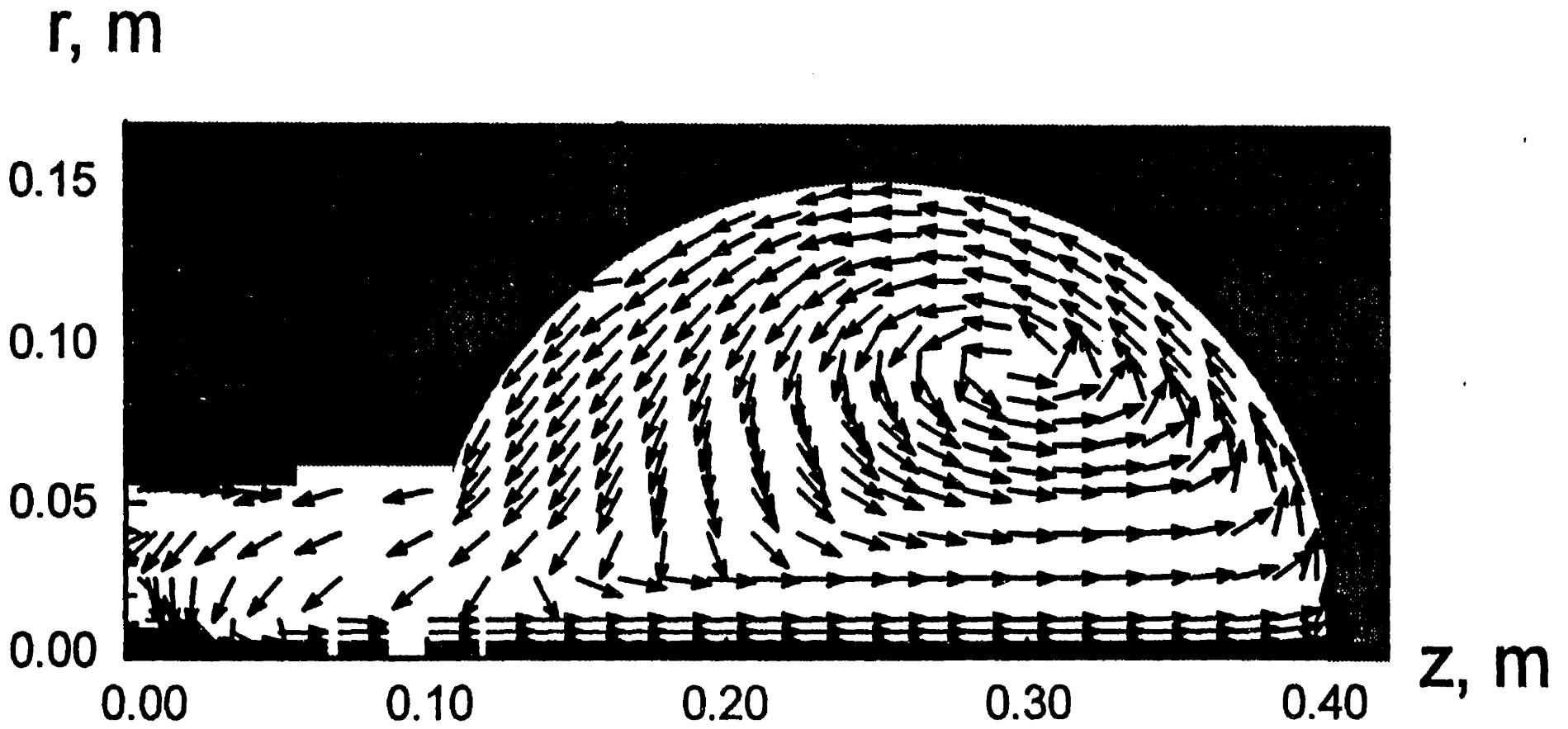

Figure 4 - Bilodeau, Alexakis et al., "Modeling of the Synthesis of Fullerene..."

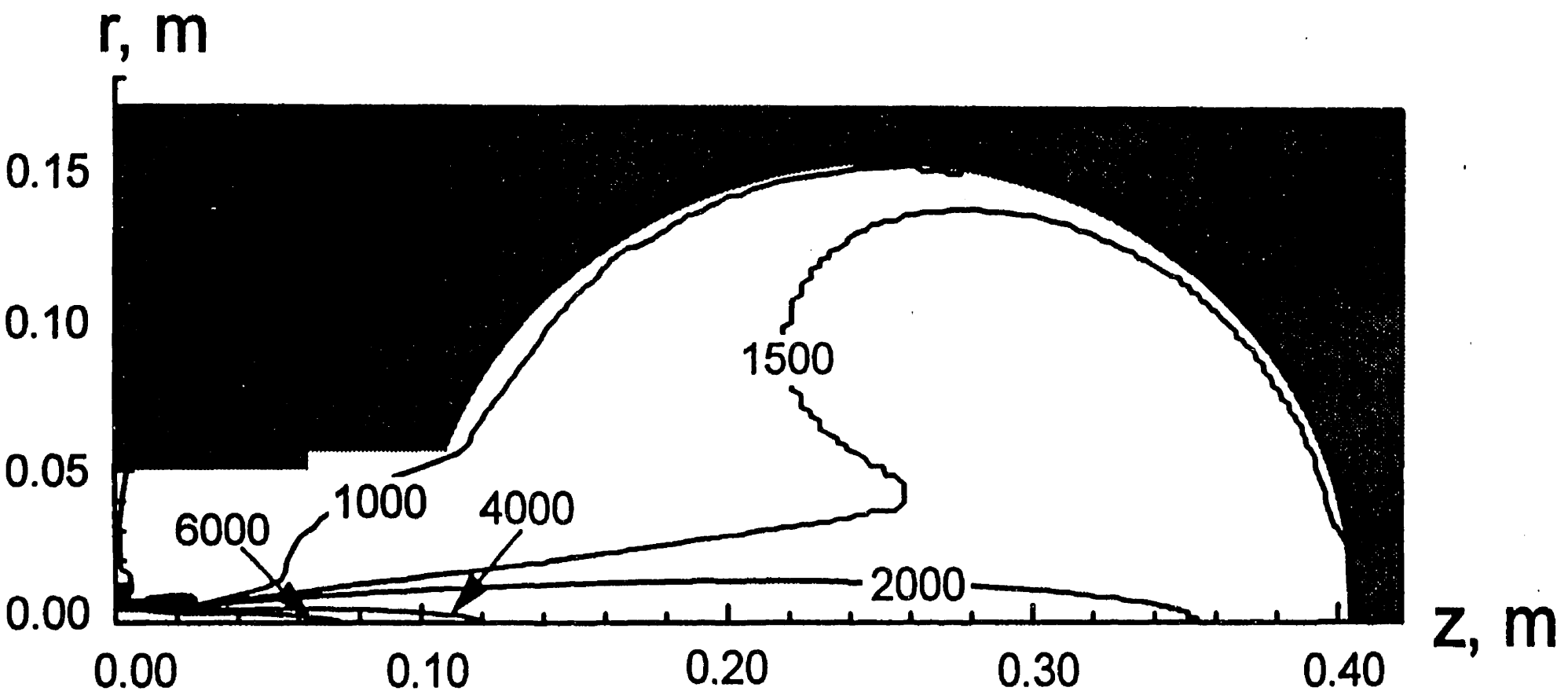

Figure 5 - Bilodeau, Alexakis et al., "Modeling of the Synthesis of Fullerene..."

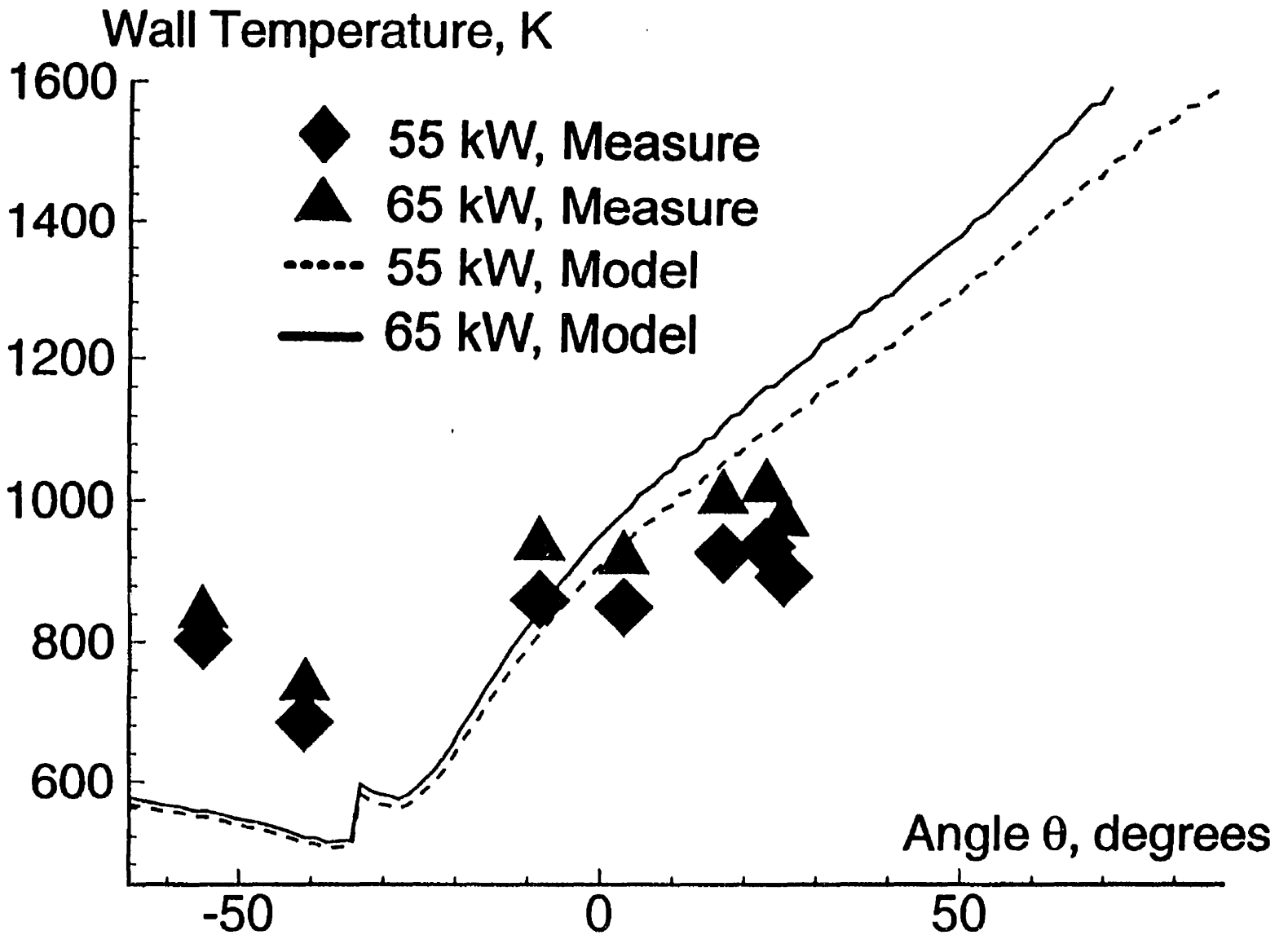

Figure 6 - Bilodeau, Alexakis et al., "Modeling of the Synthesis of Fullerene..."

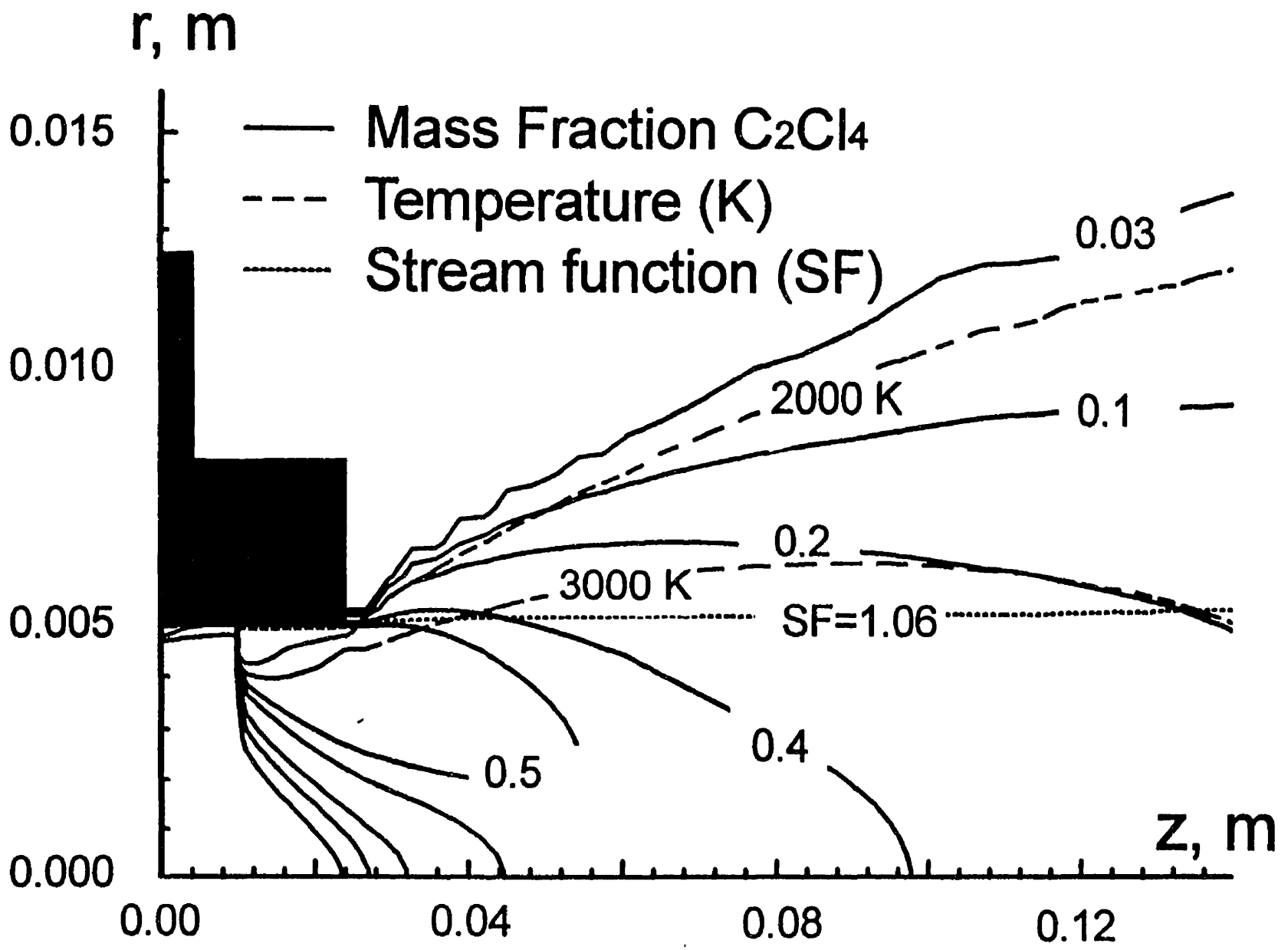

Figure 7 - Bilodeau, Alexakis et al., "Modeling of the Synthesis of Fullerene..."

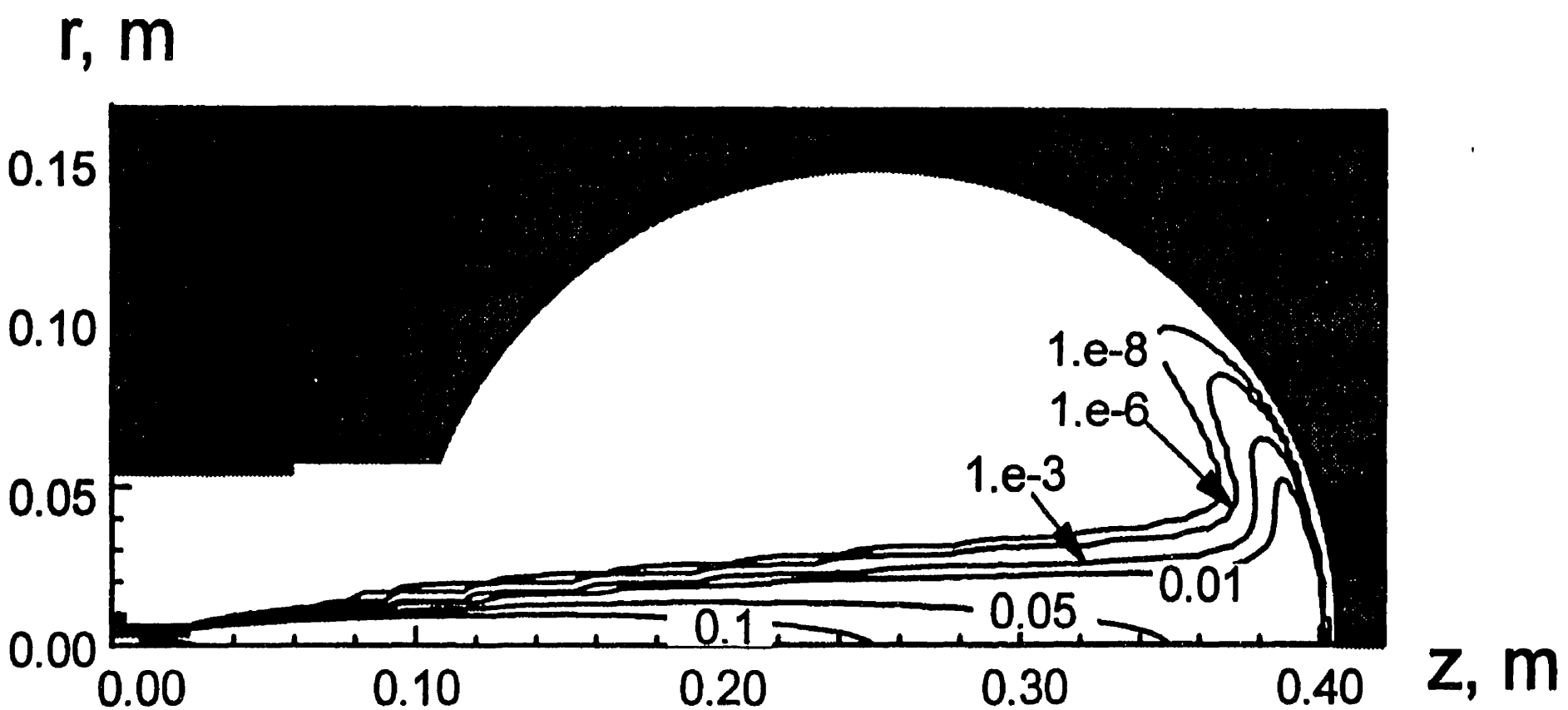

Figure 8 - Bilodeau, Alexakis et al., "Modeling of the Synthesis of Fullerene..."

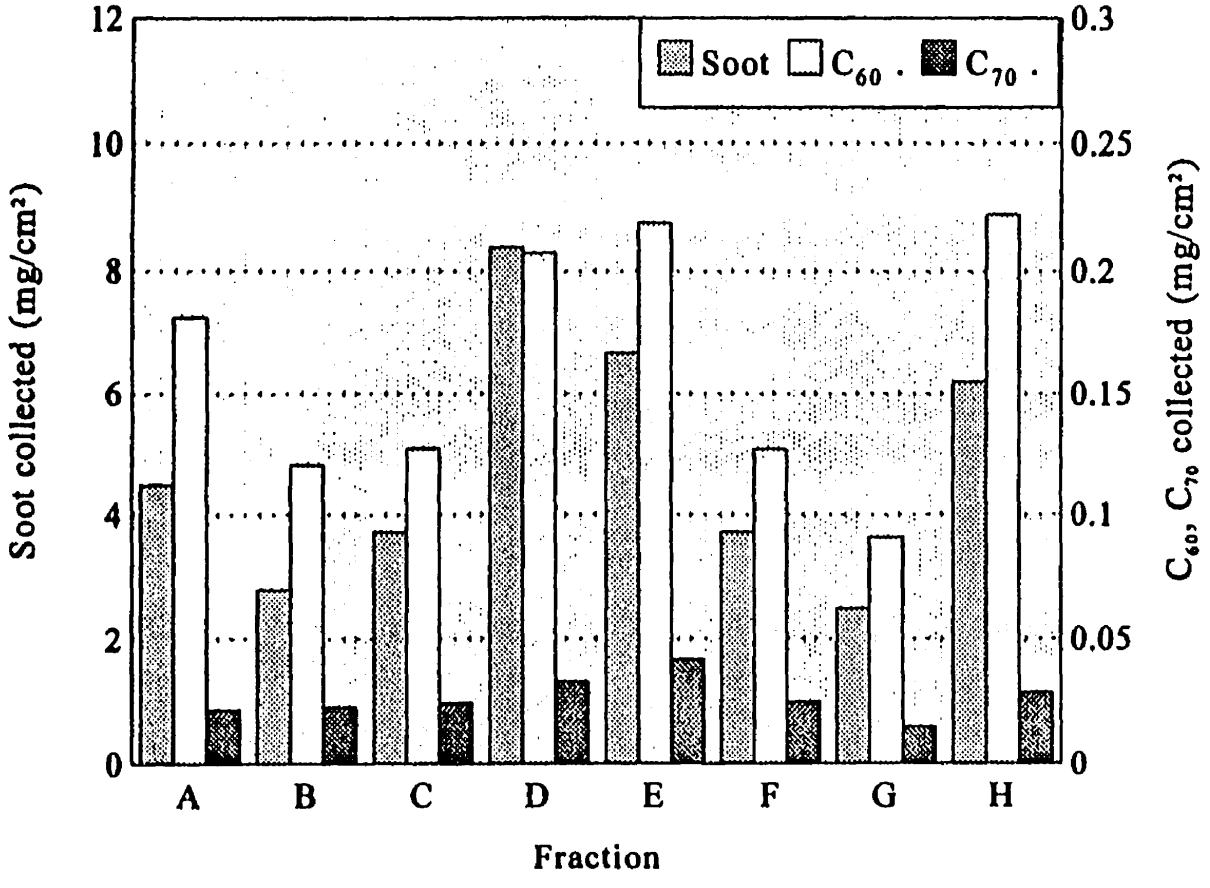

Figure 9 - Bilodeau, Alexakis et al., "Modeling of the Synthesis of Fullerene..."

65 kw

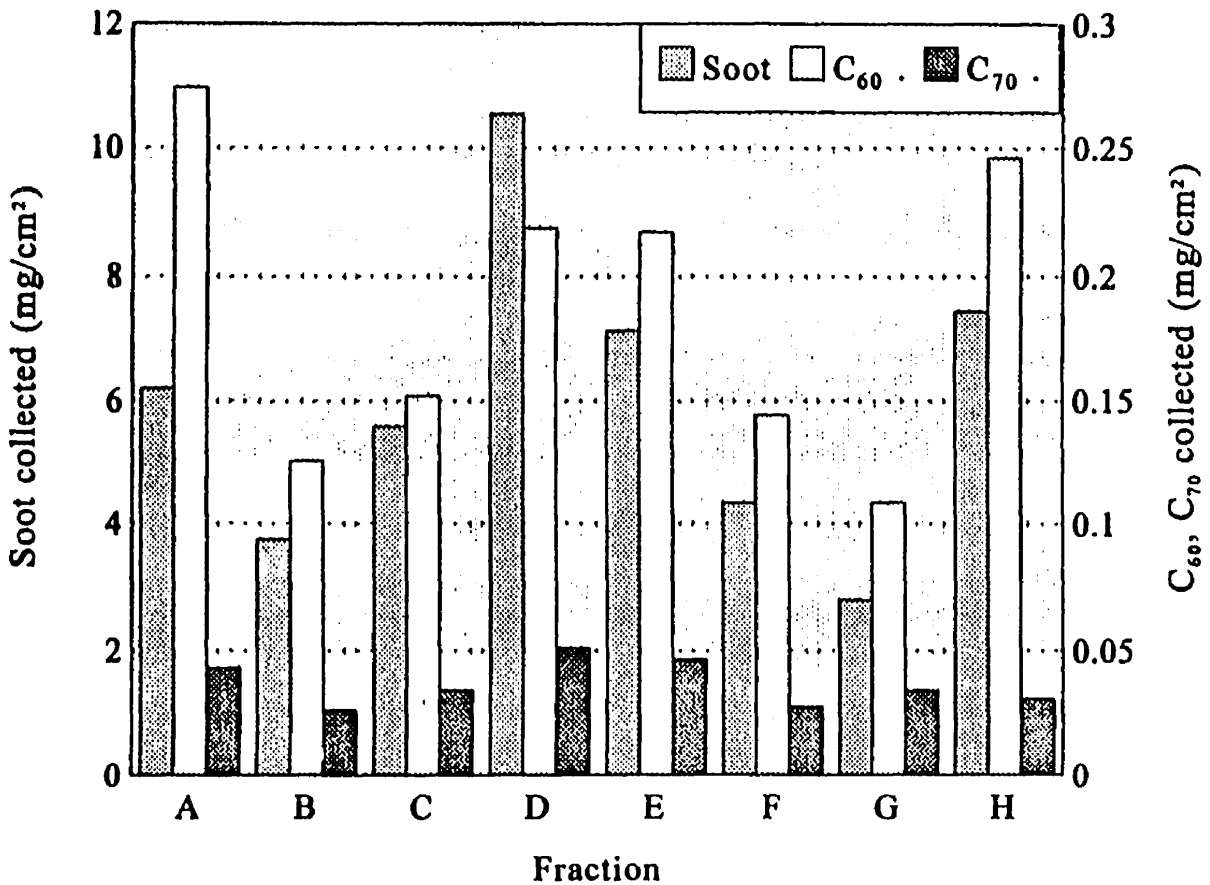

Figure 10 - Bilodeau, Alexakis et al, "Modeling of the Synthesis of Fullerenes..."

Appendix D
GC-MS Output

Quality : 97
ID : Ethene, tetrachloro-

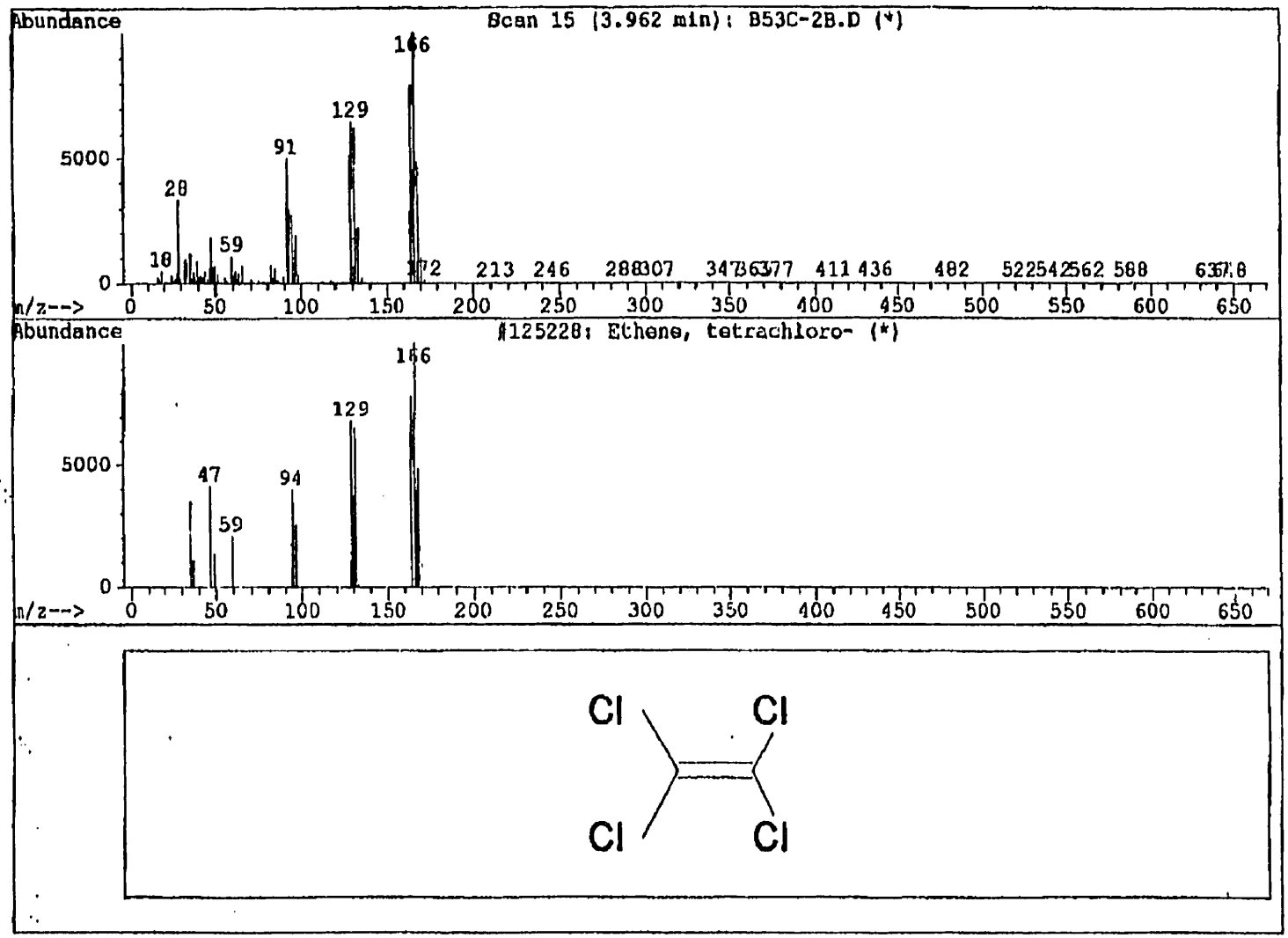

Library Searched : C:\DATABASE\WILEY138.L
Quality : 99
ID : Benzene, hexachloro-

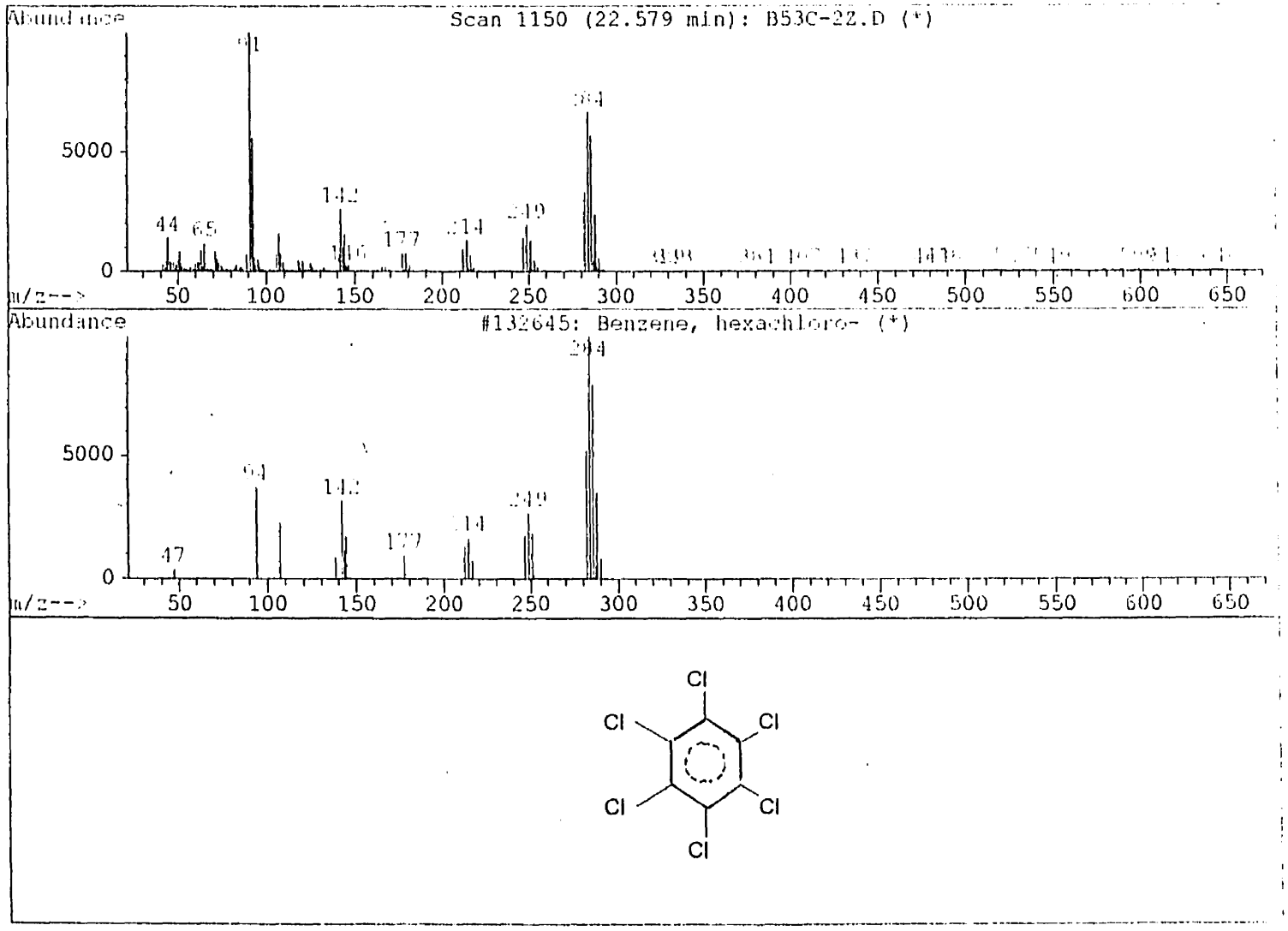

Possible compound

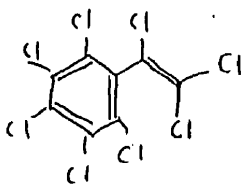

pentachloro(trichloroethenyl)benzene
octachlorostyrene

MW 8Cl 8C 380

Removal of Cl

- -1 345
- -2 309
- -3 273.5
- -4 238
- -5 202.5
- -6 167 → -1C 155
- -7
- -8

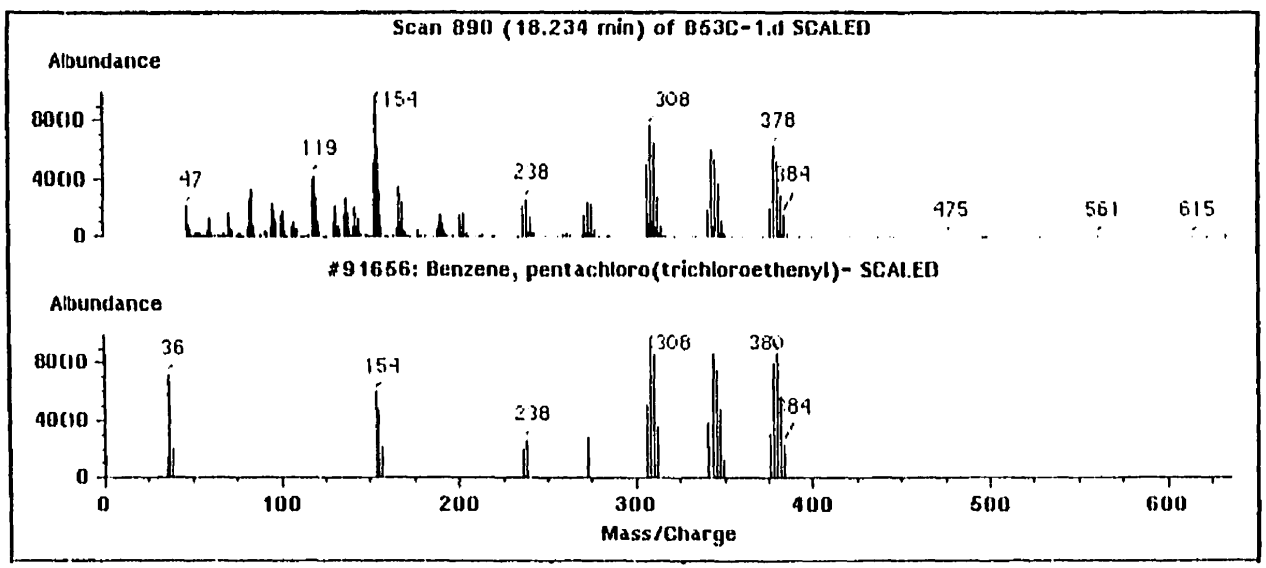

Library Searched : C:\DATABASE\WILEY138.L
Quality : 96
ID : Naphthalene, octachloro-

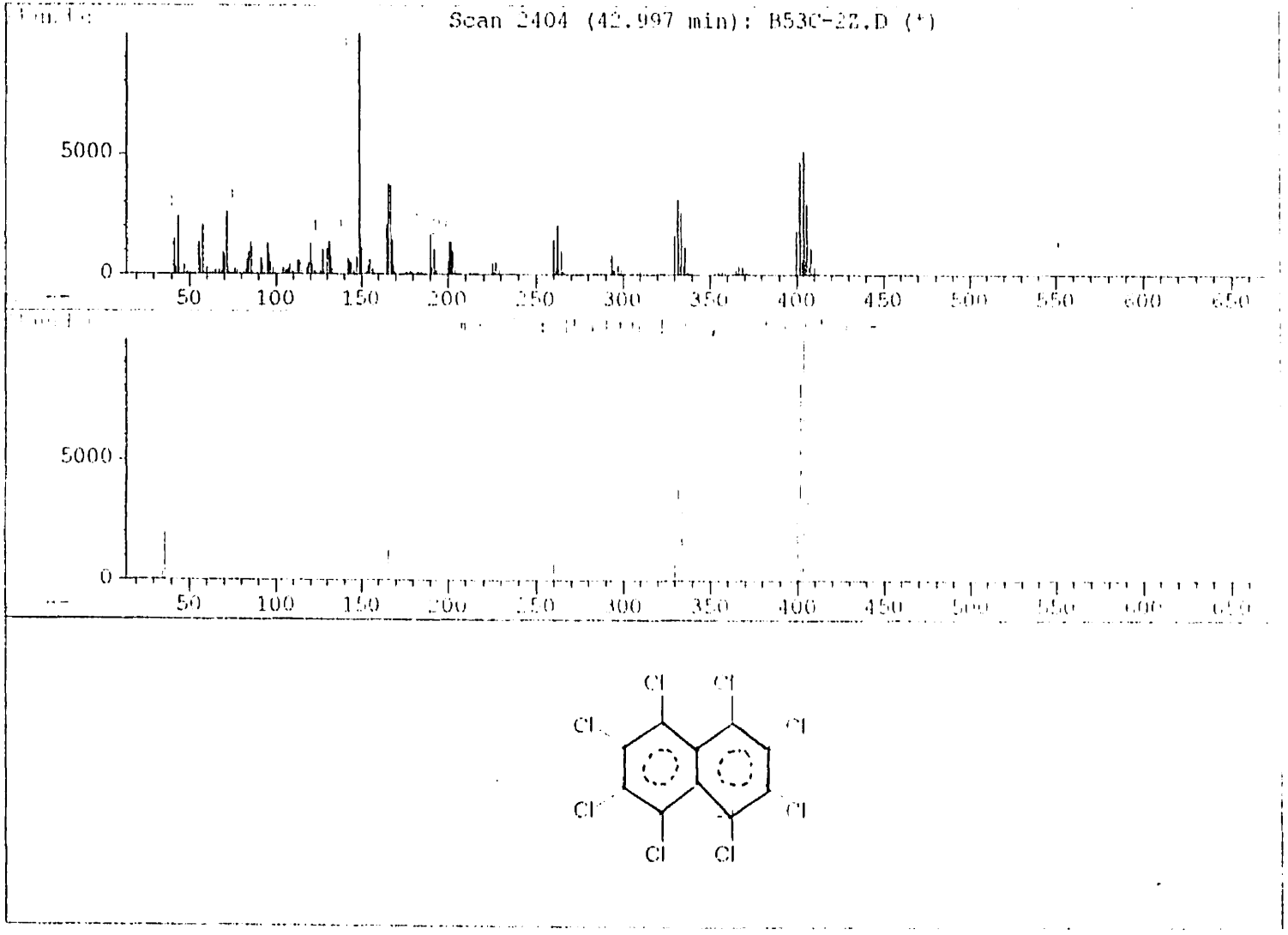

(4) Possible compound

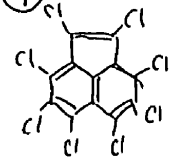

8 Cl
12 C

MW 428

octachloroacenaphthylene

Removal of Cl

-1 392.5
-2 357
-3 321.5
-4 286
-5 250.5
-6 215
-7 179.5
-8 144

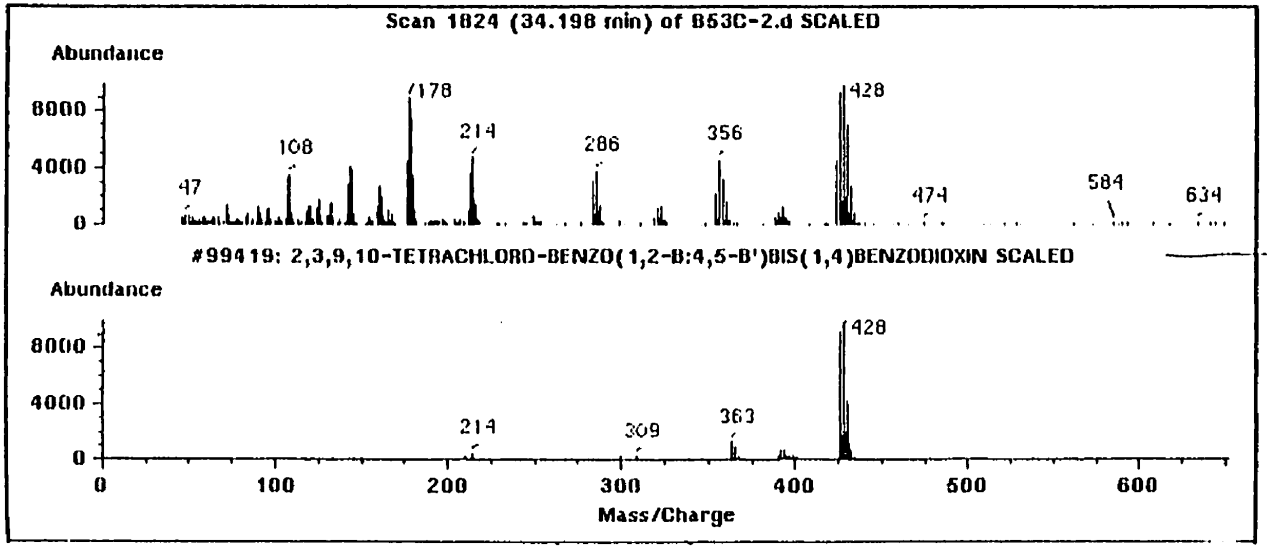

→ This is NO the compound

Possible compound

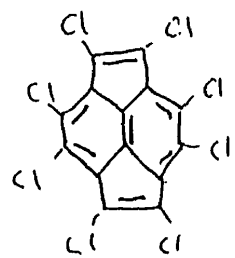

8Cl
14C
MW 452

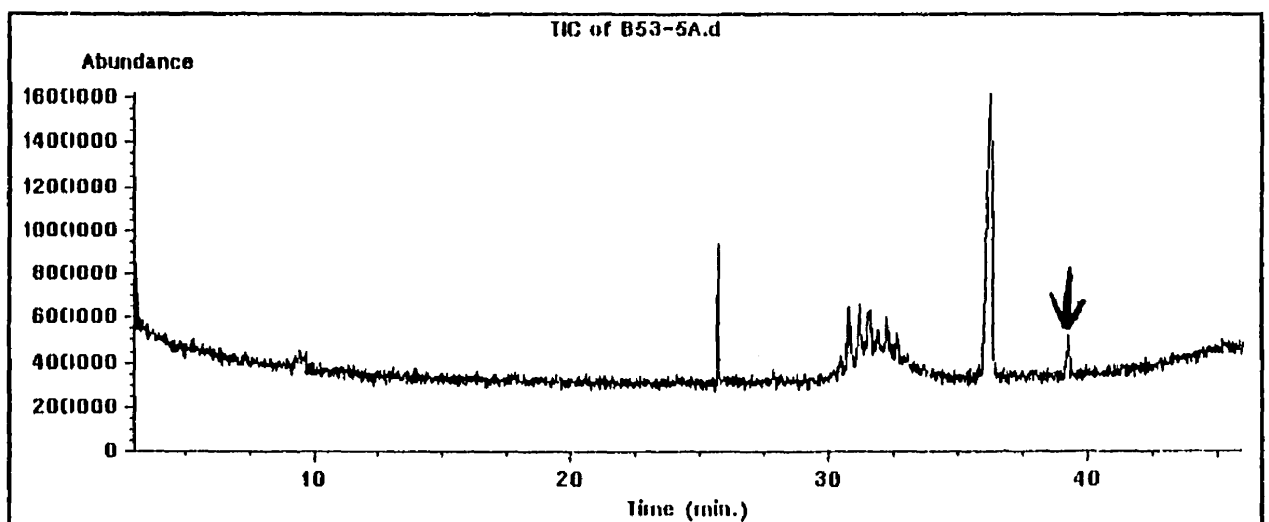

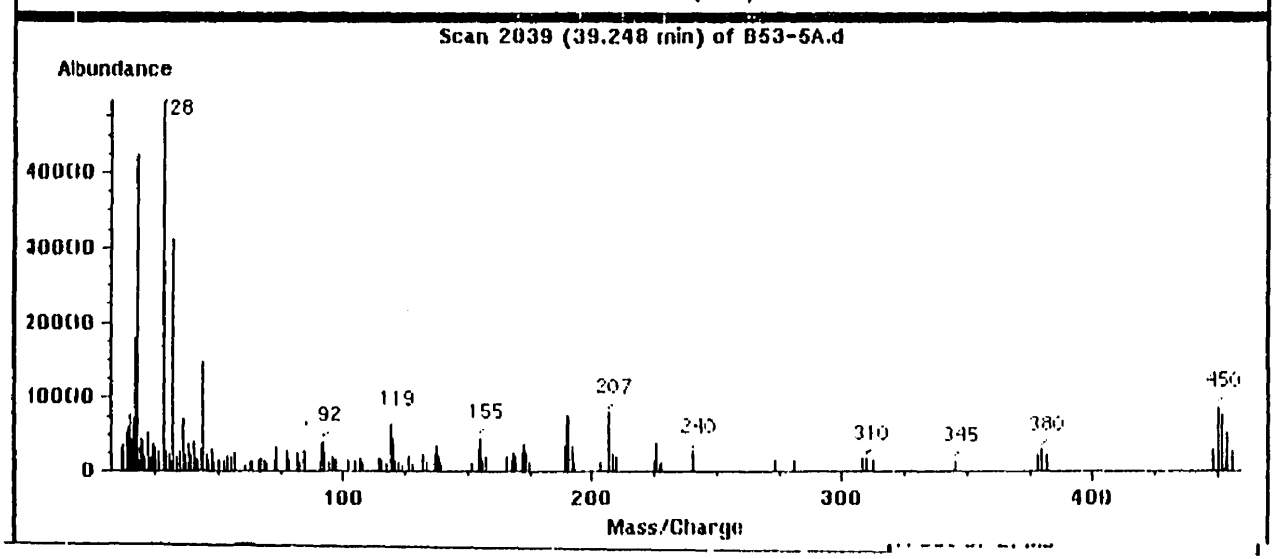

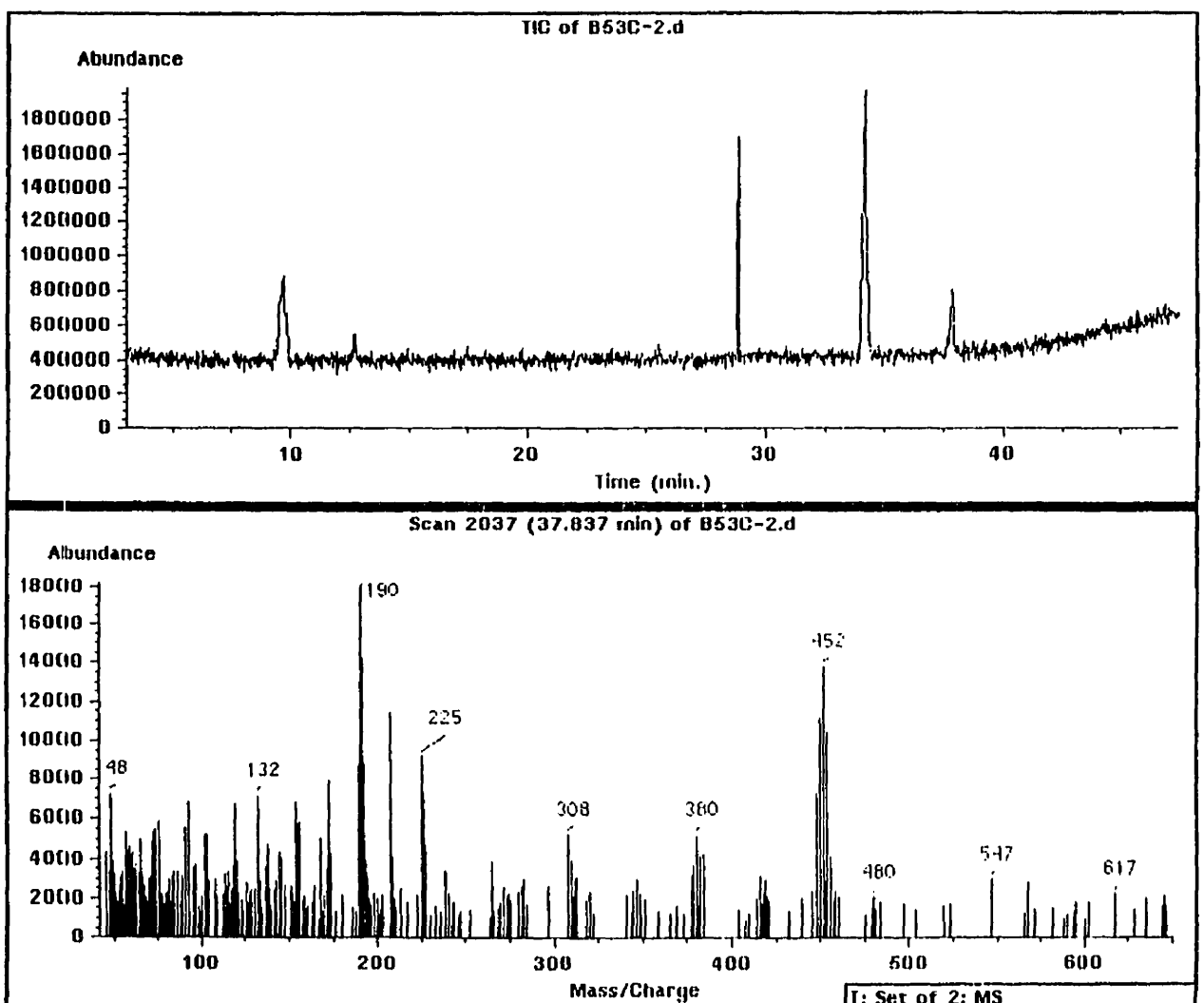
TIC of B53C-2.d
Abundance
1800000
1600000
1400000
1200000
1000000
800000
600000
400000
200000
0
10
20
30
40
Time (min.)
Scan 2037 (37.837 min) of B53C-2.d
Abundance
18000
16000
14000
12000
10000
8000
6000
4000
2000
0
48
132
190
225
308
380
452
480
547
617
100
200
300
400
500
600
Mass/Charge
T: Set of 2: MS

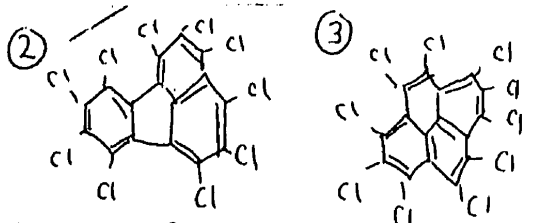

decachlorofluoranthene

MW 547

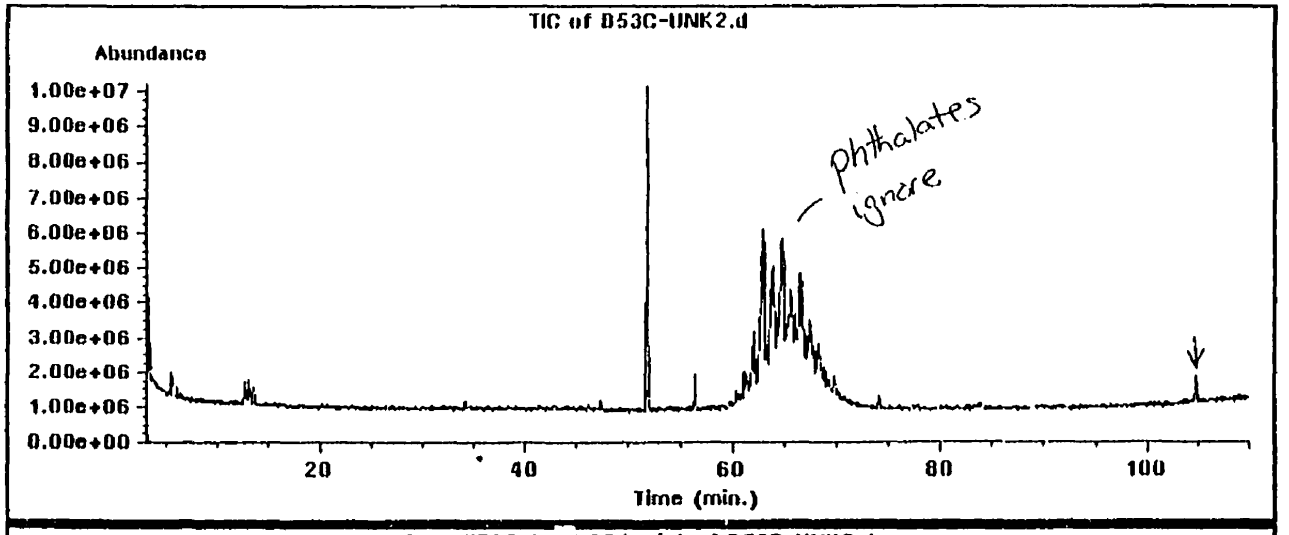

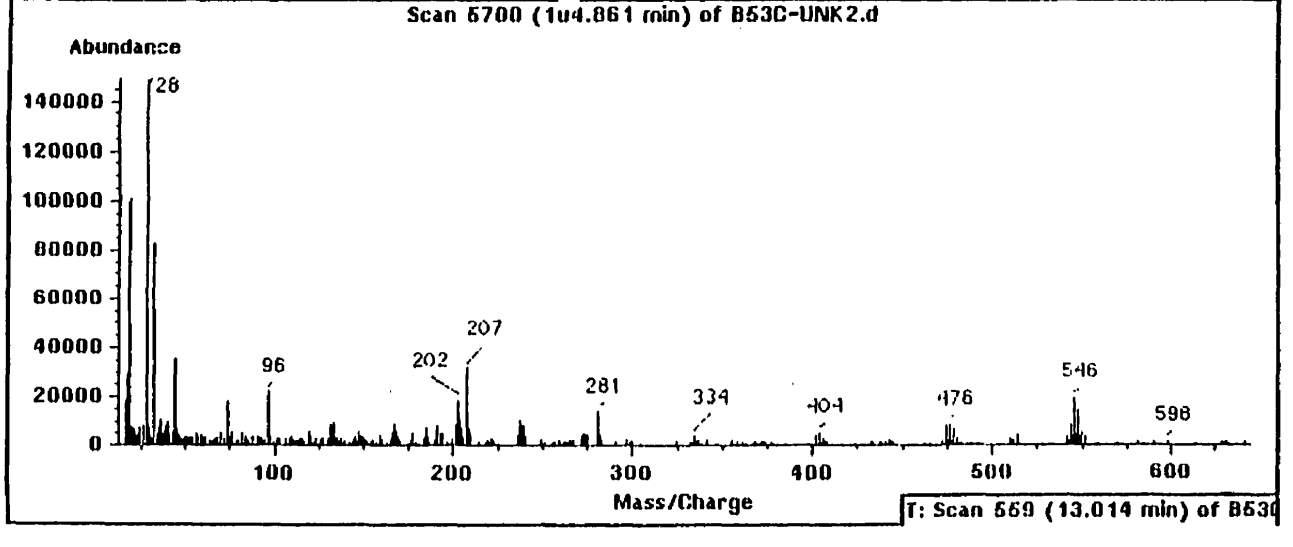

IMAGE EVALUATION TEST TARGET (QA-3)

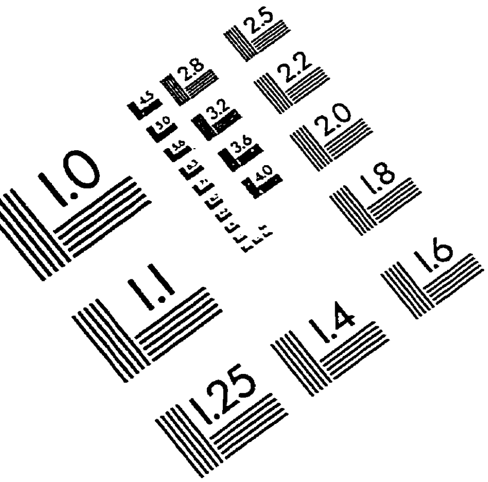

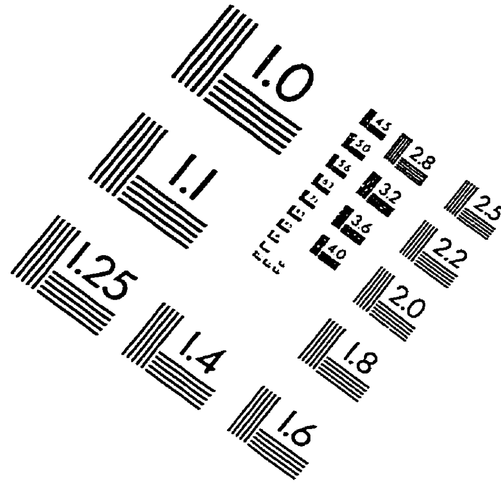

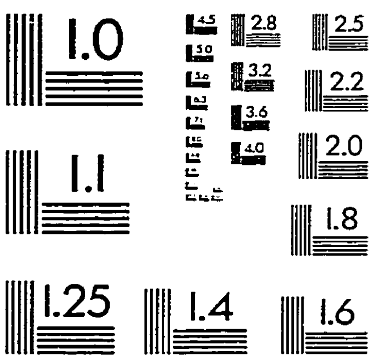

150mm

6″

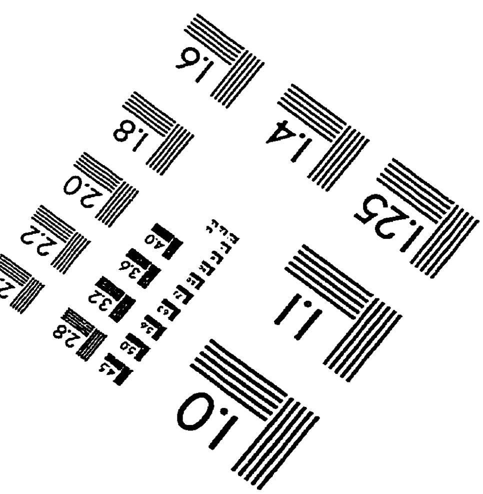

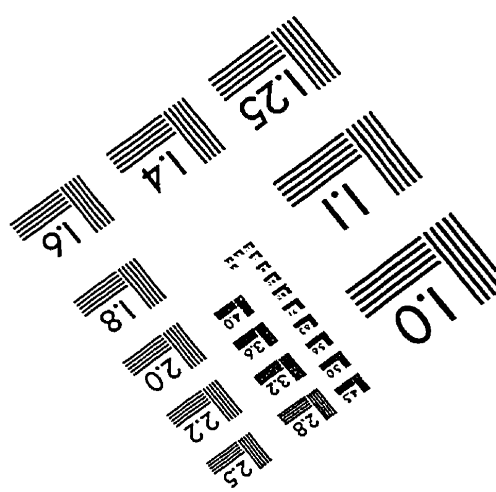

APPLIED IMAGE, Inc
1653 East Main Street
Rochester, NY 14609 USA
Phone: 716/482-0300
Fax: 716/288-5989